Carbon felt modifications for electro-Fenton process towards zero energy depollution

Thi Xuan Huong Le

THÈSE

Pour obtenir le grade de

Docteur

Délivré par **l'Université de Montpellier**

Préparée au sein de l'école doctorale **Sciences Chimiques Balard (ED459)**
Et de l'unité de recherche **Institut Européen des Membranes (IEM)**

Spécialité : **Chimie séparative matériaux et procédés**

Présentée par **Thi Xuan Huong LE**

Carbon felt modifications for electro-Fenton process towards zero energy depollution

Soutenue le 6 mars 2017 devant le jury composé de

M. Frédéric FAVIER, Directeur de Recherche ICGM, CNRS, Montpellier	**Président du jury**
M. Enric BRILLAS, Professeur Université de Barcelona, Espagne	**Rapporteur**
M. Boniface KOKOH, Professeur IC2MP, Université de Poitiers	**Rapporteur**
Mme. Armelle RINGUEDE, Chargée de Recherche IRCP, CNRS – Chimie ParisTech	**Examinatrice**
M. Mehmet Ali OTURAN, Professeur LGE, Université Paris-Est Marne la Vallée	**Examinateur**
Mme. Sophie TINGRY, Chargée de Recherche IEM, CNRS, Montpellier	**Examinatrice**
M. Marc CRETIN, Professeur IEM, Université de Montpellier	**Directeur de thèse**
M. Mikhael BECHELANY, Chargé de Recherche IEM, CNRS, Montpellier	**Co-encadrant de thèse**

Acknowledgments

This thesis was carried out at Department IP2 (Interface, Physic chemistry, Polymer), European Membrane Institute (IEM), Montpellier, France, under support of an excellent team with the participation of many great people who contributed directly and indirectly to this work.

First and foremost, I would like to extend my very deep gratitude to Prof. Marc CRETIN, my main supervisor, and Dr. Mikhael BECHELANY as co-supervisor who always beside to support as well as encourage by their continuous useful advice and immense knowledge that they shared with me throughout the whole period of three years at IEM.

I place my deep thanks to Dr. Sophie TINGRY, Dr. Stella LACOUR for their precious guidance and scientific assistantship to perform the experiment relevant to Fuel-cell and electro-Fenton system.

I would like to show my gratitude to Prof. Mehmet Oturan and Dr. Nihal Oturan. They welcame me with a warm attitude to work at the laboratory Géomatériaux et Environnement, Université de Marne-La-Vallée. The knowledge and experience that I have learned about electro-Fenton treatment at your lab are actually valuable and help me a lot to perform successfully this PhD thesis.

I also thank to Prof. Anne JULBE, Dr. Martin DROBEK, Dr. Cyril VALLICARI for their support during the time I worked on porous carbon material to design Fuel-cell Fenton. Many thanks go to Mrs. Valérie BONNIOL, Mr. Eddy PETIT, Mr. A. EL MANSOURI, and Mrs. Nathalie MASQUELEZ. I am very grateful for your effort to analyze carefully all my results by HPLC, IC, BET, TGA. In addition, Mr. Christophe CHARMETTE is very enthusiastic to help me for all experiments using gas.

I wish to express my sincere thanks to the reviewer of this thesis, Prof. Enric BRILLAS and Prof. Boniface KOKOH for their effort to revise this thesis and give out well-founded opinions.

I give my warm thanks to all my colleagues, whom I had the pleasure to work with during the realization of PhD. Your help and fruitful scientific discussion that we had together will be precious baggage in my future science work.

Thanks to 911 project of Vietnamese government that financed all of living cost during three years in Montpellier. You give me a wonderful chance to effectuate my dream about doing research at a beautiful developed country, France.

The last but not the least, great thankfulness are sent to my family, my dear friends for their love and unconditional motivation throughout good and bad times. All my love and gratitude!

Abstract

This thesis manuscript presents the modification and application of carbon felt material for wastewater treatment accommodating biorefractory pollutants by electro-Fenton (EF) process. First of all, the optimal condition of EF treatment for dye/pharmaceuticals removal using commercial carbon felt (CF) was investigated. From that, the degradation pathways in the relationship with the toxicity of their by-products were built and proposed. Concerning the modification for commercial CF, a new cathode was set up by electrochemical deposition of reduced Graphene Oxide (rGO) on the surface of CF via various reduction ways. The structure property of modified electrode was investigated by Scanning Electron Microscopy (SEM), X-ray Diffraction (XRD), X-ray Photoelectron Spectroscopy (XPS), and Brunauer–Emmett–Teller (BET). The new cathode exhibited good stability and high treatment efficiency when it was applied to decompose Acid Orange 7 (AO7), a model azo dye molecule. The EF treatment was also developed further by contributing a new Fuel-cell Fenton system without any external power supply. In this approach, AO7 was continuously degraded by electro-Fenton process at a carbonaceous micro-porous cathode (CF /porous Carbon (pC)) by direct clean electrical energy supplied from abiotic glucose oxidation at a CF/gold anode (CF@Au). The catalytic properties of both anode and cathode induced a stable output current density of 360.3 ± 51.5 mA m^{-2} at 400 ± 50 mV, maintained for long-term period. As a consequence, 90 % of the initial concentration of the pollutant, identified by High Performance Liquid Chromatography (HPLC) analysis, was eliminated upon extended EF degradation for 10 h, and the cell power output of 170 mW m^{-2} was stable at least for two months. Hence, this first proof of the concept about an abiotic Fuel cell (FC) – Fenton system demonstrated a high efficiency towards pollutant degradation with a huge potential in both energy-related areas and environmental protection.

Table of Contents

Acknowledgments ii

Abstract iv

Table of Contents v

List of figures xii

List of tables xv

List of abbreviations xvi

CHAPTER 1. GENERAL INTRODUCTION 1

1.1. Background 1

1.2. Research objectives 1

1.3. Study plan 2

CHAPTER 2. LITERATURE REVIEW 3

2.1. Abstract 3

2.2. Introduction 3

2.3. Manufacturing method and characterization of CF material 5

2.3.1. Manufacturing method of CF material 5

2.3.2. Characterization of CF electrodes 7

2.3.2.1. Structural properties 7

2.3.2.1.1. Morphology 7

2.3.2.1.2. Porosity 9

2.3.2.1.3. Specific surface area 9

2.3.2.2. Physical properties 11

2.3.2.2.1. Permeability 11

2.3.2.2.2. Mass transfer 12

2.3.2.2.3. Electrical resistivity 13

2.4. Conclusion on the characterization of CF electrodes 14

2.5. Modification of CF electrodes 15

2.5.1. Plasma treatment 15
2.5.2. Thermal treatment 16
2.5.3. Chemical treatment 17
2.5.4. Metallic modification 18
2.5.5. Graphene based modification 20
2.5.6. Carbon nanotube based modification 22
2.5.7. Carbon nanofiber based modification 24
2.5.8. Polymer based modification 26
2.5.9. Zeolites based modification 29
2.5.10. Conclusion on the modification of CF electrodes 31
2.6. Energy applications of CF-based electrodes 32
2.6.1. Introduction 32
2.6.2. Vanadium redox flow batteries 32
2.6.3. Biofuel cells 38
2.6.4. Microbial fuel cells 39
2.6.5. Capacitors - supercapacitors 41
2.6.6. Electrochemical solar cells 41
2.6.7. Lithium ion batteries 42
2.6.8. Conclusion on energy applications of CF-based electrodes 43
2.7. Application of CF-based electrodes for wastewater treatment by EF process 43
2.7.1. Introduction 43
2.7.2. EF process 44
2.7.3. CF for EF process 45
2.7.4. Modified EF systems using CF cathodes 54
2.7.4.1. Modified felts cathodes for homogeneous EF 54
2.7.4.2. Modified felts cathodes for heterogeneous EF 55
2.7.4.3. Hybrid EF system using CF cathodes 56

2.7.4.4. Pilot-scale 60

2.7.5. Conclusion on application of CF-based electrodes for wastewater treatment by EF process 62

2.8. Conclusion 63

CHAPTER 3. COMMERCIAL CARBON FELT FOR REMOVAL OF ACID ORANGE 7 AND ACETAMINOPHEN USING ELECTRO-FENTON PROCESS IN AQUEOUS MEDIA 65

3.1. General introduction 65

3.2. Toxicity removal assessments related to degradation pathways of azo dyes: toward an optimization of EF treatment 65

3.2.1. Abstract 65

3.2.2. Introduction 66

3.2.3. Materials and methods 68

3.2.3.1. Chemicals and bacterial strain 68

3.2.3.2. Degradation of AO7 in EF system 68

3.2.3.3. Analytical methods 69

3.2.3.3.1. UV-Vis spectrophotometry analysis 69

3.2.3.3.2. High-performance liquid chromatography-UV (HPLC-UV) 70

3.2.3.3.3. IC and TOC analysis 71

3.2.3.4. Toxicity tests 71

3.2.4. Results and discussion 73

3.2.4.1. Effect of applied current on the degradation kinetics 73

3.2.4.2. Effect of catalyst concentration on the mineralization efficiency 74

3.2.4.3. Degradation pathway of AO7 during EF process 75

3.2.4.4. Evolution of aromatic compounds 76

3.2.4.5. Evolution of short-chain carboxylic acids 77

3.2.4.6. Evolution of inorganic ions 78

3.2.4.7. Toxicity assessment during AO7 degradation 79

3.2.4.8. Degradation pathway of AO7 solution 84

3.2.5. Conclusions 86

3.3. Correlation between degradation pathway and toxicity of ACE and its by-products, using EF process in aqueous media 87

3.3.1. Abstract 87

3.3.2. Introduction 88

3.3.3. Experimental 90

3.3.3.1. Materials 90

3.3.3.2. Electrochemical system for ACE degradation 90

3.3.3.3. Analytical procedures and toxicity test 91

3.3.4. Results and discussion 91

3.3.4.1. Degradation pathway of ACE during EF process 91

3.3.4.1.1. Evolution of aromatic compounds 91

3.3.4.1.2. Evolution of short-chain carboxylic acids 93

3.3.4.1.3. Evolution of inorganic ions 94

3.3.4.1.4. Degradation pathway of ACE mineralization during EF process 95

3.3.4.2. Toxicity evolution of ACE solution during EF process 97

3.3.4.2.1. Global toxicity 97

3.3.4.2.2. Toxicity of intermediate sub-products 98

3.3.5. Conclusions 102

3.4. General conclusions 103

CHAPTER 4. EFFICIENT REMOVAL OF ACID ORANGE 7 DYE BY ELECTRO-FENTON PROCESS USING GRAPHENE BASED CARBON FELT 104

4.1. General introduction 104

4.2. Abstract 104

4.3. Introduction 105

4.4. Experimental 107

4.4.1. Materials 107

4.4.2. Electrode modification 107

4.4.2.1. Preparation of the dispersion and GO deposition 107
4.4.2.2. GO reduction at CF surface 107
4.4.3. Material characterization 108
4.4.3.1. Physical techniques 108
4.4.3.2. Electrochemical techniques 108
4.4.3.3. Mineralization of azo dye by the EF process 109
4.5. Results and discussion 109
4.5.1. Structural properties of the electrodes 109
4.5.2. Effect of current and time for GO deposition on CF 113
4.5.3. Effect of the electrochemical conditions on the GO reduction 114
4.5.4. Electrochemical behavior of the modified electrodes 115
4.5.4.1. Electroactive surface area characterization 116
4.5.4.2. Charge transfer resistance of the interface 116
4.5.5. Removal of azo dye by electro-Fenton process 117
4.6. Conclusion 119
4.7. General conclusions and perspectives 119
CHAPTER 5. GOLD PARTICLES GROWTH ON CARBON FELT FOR EFFICIENT MICROPOWER GENERATION IN A HYBRID BIOFUEL CELL 121
5.1. General introduction 121
5.2. Abstract 121
5.3. Introduction 122
5.4. Experimental 124
5.4.1. Materials 124
5.4.2. Preparation of gold nanoparticles-modified CF (CF@Au) 124
5.4.3. Preparation of enzyme-immobilized electrode 125
5.4.4. Material characterization 125
5.4.5. Electrochemical characterizations 125
5.5. Results and discussion 126

5.5.1. Characterization of the structural properties of gold particles on CF.... 126

5.5.1.1. Effect of the gold loading quantity 128

5.5.1.2. Effect of the heating temperature 129

5.5.2. CF@Au as support for electrocatalysis 131

5.5.2.1. Enzymatic O_2 reduction on CF@Au 131

5.5.2.2. Glucose electrooxidation on CF@Au..... 132

5.5.3. Glucose/O_2 hybrid BFC..... 133

5.6. Conclusions..... 135

5.7. General conclusions 135

CHAPTER 6. DESIGN OF NOVEL FUEL CELL-FENTON SYSTEM: A SMART APPROACH TO ZERO ENERGY DEPOLLUTION..... 136

6.1. General introduction 136

6.2. Abstract..... 136

6.3. Introduction..... 137

6.4. Experimental..... 138

6.4.1. Materials 138

6.4.2. Fabrication of porous carbon/CF (CF@pC) cathode..... 139

6.4.3. The Fuel Cell – Fenton system 140

6.4.4. Material characterization 141

6.4.5. Electrocatalytic activity measurements 141

6.5. Results and discussion 142

6.5.1. Characterization of the CF@pC cathode..... 142

6.5.2. FC– Fenton system efficiency 145

6.6. Conclusions..... 150

6.7. General conclusion..... 150

CHAPTER 7. CONCLUSION and PERSPECTIVES..... 151

7.1. Conclusion 151

7.2. Perspectives..... 153

SCIENTIFIC CONTRIBUTIONS 154

References 158

Résumé en français..... 185

List of figures

Figure 2-1. Typical shape of commercial (a) CF and (b) GF [31]. 6
Figure 2-2. SEM image of felts. 7
Figure 2-3. Shape of water droplet on GF (*SGL GFD2.5*, thickness 2.8 mm) [14]. 12
Figure 2-4. Schematic diagram of electrochemical cell for the identification of the mass transfer of CF [38]. 13
Figure 2-5. The electrical resistivity device. 14
Figure 2-6. Schematic diagram of atmospheric pressure plasma jet [51]. 16
Figure 2-7. SEM images and contact angles of GF (a, d), GF-ethanol (b, e) and GF-ethanol/hydrazine (c, f) [64]. 18
Figure 2-8. Nyquist plots of CF, CF-Bi, GF and GF-Bi in 0.05 M V^{2+} + 0.05 M V^{3+} + 3 M H_2SO_4 solution at DC voltage -0.55 V [30]. 19
Figure 2-9. (a) SEM image of PbO_2/GF [69] and (b) Reactor of deposition of Fe on GF [71]. 20
Figure 2-10. Characterization of graphene based felts. 21
Figure 2-11. EPD of graphene on positive electrodes [76]. 22
Figure 2-12. SEM images of (a) CNTs grown on GF, (b) N-CNTs grown on GF [79], (c) CNTs on CF by CVD [80], and (d) CNTs on CF by EPD [81]. 23
Figure 2-13. (a, b) SEM images and (c) The high-resolution TEM (HR-TEM) of CNFs on CF [48]. 25
Figure 2-14. Characterization of polymer based felts. 27
Figure 2-15. The schematic diagram illustrating the one-step electrosynthesis of PPy/GO composites on GF working electrode via electropolymerization of pyrrole while using GO as the anionic dopant [105]. 29
Figure 2-16. Characterization of zeolite based felts. 30
Figure 2-17. Components of a vanadium redox flow cell stack using CF [127]. 33
Figure 2-18. Schematic of a VRFB with flow fields using GF electrode [131]. 38
Figure 2-19. MFC configuration [149]. 40
Figure 2-20. Schematic representation of the principle of the photosynthetic bioelectrochemical cell using CF electrodes [160]. 42
Figure 2-21. Schematic presentation of the electrocatalytic production of hydroxyl radicals by the EF process [167]. 45

Figure 2-22. Scheme of the experimental set-up used for the EF treatments using CF cathode. 46
Figure 2-23. General reaction sequence proposed for the mineralization of methyl parathion in aqueous acid medium by hydroxyl radicals following EF process [173]. 53
Figure 2-24. Evolution of the inhibition of marine bacteria, *Vibrio fischeri* luminescence (Microtox method) during EF processes 54
Figure 2-25. The schematic diagram of: (a) the novel vertical-flow EF reactor [205]; and (b) Continuous bubble EF reactor 57
Figure 2-26. Schematic diagram of the MFC-Fenton system using soluble iron catalyst for paracetamol degradation by EF process at cathode chamber 58
Figure 2-27. Schematic diagram of two chamber BEF systems in batch mode using non-catalyzed CF [199]. 59
Figure 2-28. Schematic diagram of the EF system powered by a single-chamber MFC [213]. 60
Figure 2-29. Scheme of the EF pilot plant. 61
Figure 2-30. Sketch of the autonomous solar pre-pilot plant used for the SPEF treatment of 10 dm^3 of Direct Yellow 4 (DY4) solutions. 62
Figure 3-1. Molecular structure of AO7. 66
Figure 3-2. Schematic of the degradation of AO7 by EF process. 69
Figure 3-3. AO7 degradation by EF process on CF cathode (60 cm^2) 74
Figure 3-4. TOC removal after 8h treatment of 200 mL AO7 (0.1 mM). 75
Figure 3-5. Evolution of AO7 by-products. 79
Figure 3-6. Evolution of the inhibition of marine bacteria luminescence after 5 min and 15 min of exposure with a sample taken after different EF treatment duration of AO7 solution. 80
Figure 3-7. Toxicity of AO7 by-products appearing between different time. 81
Figure 3-8. Toxicity of mixtures of AO7 by-products. 83
Figure 3-9. General reaction sequence proposed for AO7 mineralization in acid medium by hydroxyl radicals during EF process. 85
Figure 3-10. Evolution of the concentration of ACE and the aromatic degradation by-products during EF treatment. 92
Figure 3-11. Evolution of the concentration of carboxylic acids during EF degradation of ACE. 93
Figure 3-12. Evolution of the inorganic ions concentration during EF degradation of ACE. . 94
Figure 3-13. TOC removal during EF degradation of ACE. 95

Figure 3-14. General reaction sequence proposed for ACE mineralization in acidic medium by hydroxyl radicals during EF process. 96
Figure 3-15. Inhibition of *Vibrio Fischeri* marine bacteria luminescence during EF treatment. 97
Figure 3-16. Toxicity of standard solutions of ACE and other aromatic compounds. 100
Figure 3-17. Toxicity of ACE by-products. 102
Figure 4-1. SEM images of (a) raw CF, (b) CR-CF, (c) CPR-CF, and (d) TR-CF electrodes. 110
Figure 4-2. (a) XRD of graphite powder and GO; (b) XPS of GO. 111
Figure 4-3. XPS of (a) GO-CF, (b) CR-CF, (c) TR-CF and (d) CPR-CF electrodes..... 112
Figure 4-4. Effect of current and time for GO deposition on CF. 113
Figure 4-5. Effect of the GO reduction conditions. 115
Figure 4-6. Electrochemical characterization of raw_CF, CR-CF, TR-CF and CPR-CF electrode. 117
Figure 4-7. TOC removal following electrolysis time. 118
Figure 5-1. Characterization of CF@Au anode. 127
Figure 5-2. Effect of the gold loading quantity on CF@Au anode. 129
Figure 5-3. Effect of heating temperature on CF@Au anode. 130
Figure 5-4. Enzymatic O_2 reduction on. 132
Figure 5-5. Glucose electrooxidation on CF@Au anode. 133
Figure 5-6. Electrical performance of the hybrid BFC at 30 °C with BOD-immobilized CF@Au cathode in O_2-saturated PBS (0.1 M, pH = 7.0) and CF@Au anode in 0.1 M KOH (pH = 11.0) containing 10 mM glucose. 134
Figure 6-1. Schematic diagram of the FC-Fenton based system. 141
Figure 6-2. Characterization of CF@pC cathode. 143
Figure 6-3. Shapes of water droplets formed on (a) raw CF, and (b) CF@pC surface. 144
Figure 6-4. Acitivity of FC-Fenton system. 146
Figure 6-5. Characterization of electrodes after two months use in FC-Fenton system. 147
Figure 6-6. AO7 degradation by FC-Fenton system. 149

List of tables

Table 2-1. Comparison of manufacturing factors and physical properties between carbon and GF based on rayon or PAN precursor [32]. 6
Table 2-2. Properties of carbon and GF electrodes [33]. 8
Table 2-3. Characteristics comparison of rayon and PAN based GF [29]. 10
Table 2-4. Correlations between the mass transfer coefficient and the solution flow rate [44]. 13
Table 2-5. The activity efficiency of the VRFB using graphite & CF-based electrodes. 34
Table 2-6. Removal of POPs by EF process on graphite & CF-based cathodes in stirred tank reactor at 25 °C. 47
Table 3-1. List of AO7 by-products and their concentrations during EF experiment 77
Table 3-2. HPLC and LC/MS identification parameters (retention times (t_R)), MS mass fragmentation) of aromatic by-products formed during the EF treatment of AO7. 86
Table 3-3. HPLC and LC/MS identification parameters (retention times (t_R) and mass fragmentation) of aromatic by-products formed during EF treatment of 500 mL ACE solution at C_0 = 1.0 mM; pH =3; [Na_2SO_4]=50 mM, I = 500 mA and [Fe^{2+}] = 0.2 mM. 92
Table 3-4. The aromatic by-products and their concentrations (RSD 2% n=3) at several treatment times of ACE solution (1 mM) during EF process. 98
Table 3-5. List of ACE carboxylic acid by-products and their maximum concentrations (RSD 2% n=3) corresponding to treatment time from 40 min to 480 min during EF experiment. . 102
Table 4-1. Apparent first order rate constants and abatements for the degradation kinetics of AO7 on raw CF and CPR-CF. 118

List of abbreviations

ACE	Acetaminophen
AO7	Acid Orange 7
AOPs	Advanced Oxidation Processes
AQDS	Anthraquinone-2,6-disulfonat
ALD	Atomic Layer Deposition
APPJs	Atmospheric Pressure Plasma Jets
BET	Brunauer–Emmett–Teller
BDD	Boron-Doped Diamond
BFC	Bio-fuel Cell
BEF	Bio-electro-Fenton
CF	Carbon Felt
CNTs	Carbon Nanotubes
CVD	Chemical Vapor Deposition
CVs	Cyclic voltammograms
CE	Coulombic efficiency
DCF	Diclofenac
DMF	N,N-dimethyl formamide
DO 61	Direct orange 61
EDX	Energy-dispersive X-ray Spectroscopy
EF	electro-Fenton
EAOPs	electrochemical advanced oxidation processes
EIS	Electrochemical Impedance Spectroscopy
EPD	Electrophoretic Deposition
EE	Energy efficiency
ENXN	Enoxacin
FC	Fuel cell
GF	Graphite Felt
GO	Graphene Oxide
HPLC	High Performance Liquid Chromatography
IC	Inorganic Carbon
FeAB	Iron alginate gel beads
LSV	Linear Scanning Voltammetry

MFC	Microbial Fuel Cell
MWCNTs	Multi-Walled Carbon Nanotubes
OCV	Open Circuit Voltage
ORR	Oxygen Reduction Reaction
POPs	Persistent Organic Pollutants
Pt	Platinum
PAN	Polyacrylonitrile
PANi	Polyaniline
PPy	Polypyrrole
PCOC	4-chloro-2-methylphenol
PB	Prussian blue
SPEF	Solar Photo-electro-Fenton
rGO	Reduced Graphene Oxide
RTD	Residence Time Distribution
RF	Radiofrequency
SCE	Saturated Calomel Electrode
SEM	Scanning Electron Microscopy
SWCNT	Single-Walled Carbon Nanotube
TGA	Thermal Gravimetric Analysis
TOC	Total Organic Carbon
XPS	X-ray Photoelectron Spectroscopy
XRD	X-ray Diffraction
ZIF-8	Zeolitic Imidazolate Framework
ZnO	Zinc Oxide
VE	Voltage efficiency
VRFB	Vanadium Redox Flow Batteries

CHAPTER I

GENERAL INTRODUCTION

CHAPTER 1. GENERAL INTRODUCTION

1.1. Background

Urban industrial operation has long been identified as a major cause of environmental contaminations through atmospheric deposition and wastewater discharge. The wastewater containing persistent organic pollutants (POPs) is always a dangerous threat for living environment because of their high toxicity and difficulty to treat completely by using normal physical chemistry methods. Advanced oxidation processes (AOPs) are widely investigated for the removal of recalcitrant organic pollutants from wastewater. Over the past decade, the AOPs have attracted increasing interest as promising powerful methods for efficiently removing dyes from water. AOPs are environmentally friendly chemical, photochemical, or electrochemical methods sharing the common feature of the *in-situ* production of hydroxyl radicals (•OH) as their main oxidizing agent. One of the most popular chemical AOPs is the Fenton method, where a mixture of Fe^{2+} and H_2O_2 (Fenton's reagent) is used to degrade organic compounds. To avoid using chemical reactants, H_2O_2 can be produced by direct electroreduction of dissolved O_2 on graphite-based electrode. When combined with Fe^{2+} to produce hydroxyl radicals, the method (called electro-Fenton) is more efficient than the basic Fenton process and easier to manage [1]. In this process, carbonaceous materials are usually used as cathode, such as three-dimensional graphite [2], reticulated vitreous carbon (RVC) [3, 4], carbon sponge [5], GF [6] or activated carbon fiber (ACF) [7, 8]. The electro-Fenton (EF) process using carbon & graphite felt cathodes have been applied to remove successfully many different kinds of POPs including dye pollutants [6], pharmaceutical compounds [9], herbicides and pesticides [10-12]. In addition, the friendly environmental feature of EF treatment is also proved when it can degrade efficiently the very toxic initial contaminants to non-toxic compounds like CO_2, H_2O or short-chain carboxylic acids [13]. Because of promising potentials of wastewater treatment by EF process, it will be useful and necessary to improve its efficiency towards a low cost, clean and green technology.

1.2. Research objectives

The objectives of this study are as follows:

- To attain the highest treatment rate by EF process; the important parameters affecting directly the results such as applied current, concentration of catalyst are needful to be well investigated. Moreover, correlation between degradation pathway and toxicity of POPs as

well as their by-compounds is studied carefully to have a comprehensive view about EF treatment using CF cathode.

- To modify successfully CF for upgrading efficiency of EF process; the understanding relevant to their properties, used modification ways or their applications is essential to study.
- To improve the drawback of pristine CF; rGO was deposited on its surface. The upgraded properties of fabricated electrode were proved by physical as well as electrochemical characterizations. For application, the modified felt was used as cathode to remove dye pollutant by EF technology.
- To decrease the cost of EF treatment, design a new EF system without using input power is also important purpose of this study.

1.3. Study plan

To attain the above objectives, the following topics were investigated:

- Overview of the current state of affairs relating to properties of CF -based materials, modification methods and their applications (Chapter 2).
- Toxicity removal assessments related to degradation pathways of azo dyes: toward an optimization of EF treatment (Chapter 3).
- Correlation between degradation pathway and toxicity of acetaminophen (paracetamol, ACE) and its by-products, using EF process in aqueous media (Chapter 3).
- Efficient removal of AO7 dye by electro-Fenton process using graphene based CF (Chapter 4).
- Gold particles growth on CF for efficient micropower generation in a hybrid biofuel cell (BFC) (Chapter 5).
- Design of novel FC-Fenton system: a smart approach to zero energy depollution (Chapter 6).

CHAPTER II

LITERATURE REVIEW

Carbon felt based-electrodes for energy and environmental applications

This chapter is in preparation for publication as:

Thi Xuan Huong Le, Mikhael Bechelany, Marc Cretin, *Carbon felt based-electrodes for energy and environmental applications: A Review*.

CHAPTER 2. LITERATURE REVIEW

2.1. Abstract

Carbonaceous materials are abundantly used for electrochemical applications and especially for energy and environmental purposes. In this review, the CF based-electrodes are discussed in a holistic manner. First of all, the study centers on the issues relevant to pristine felts materials such as manufacturing method and specific properties. The various methods and equations used to identify physical values of felts material are supplied. As main part of the review, the different modification methods for felts electrodes are described. The novel properties of fabricated materials are characterized by physical as well as electrochemical techniques. The strengths of each method are presented in the comparison with raw felts electrodes. The energy applications of CF based-electrodes are figured out in various fields such as vanadium redox flow batteries (VRFB), microbial fuel cell (MFC), BFC capacitors, solar cell and lithium ion batteries. For environmental application, we focus our study on the wastewater treatment containing biorefractory pollutants by EF process. The degradation result by EF technology using felts materials is impressive when most of toxic contaminants are mineralized to non-toxic compounds at the end of the electrolysis. To decrease the cost treatment and upgrade the treatment efficiency, the EF system has been improved by using modified electrodes or new catalyst sources. The felts materials are also investigated to apply in BFC-Fenton in which electrons were produced from FC towards zero-energy depollution. Finally, the sketches about EF pilot open new gates for application of felts materials in industrial areas.

Key words: Carbon felt, modification, energy application, electro-Fenton process, hydrophilicity, conductivity, electroactive surface are, zero energy depollution.

2.2. Introduction

CF is commonly used as electrode due to their good electronic conduction. They have high surface area and porosity able to provide abundant redox reaction sites, excellent electrolytic efficiency, mechanical stability, and relatively low cost [14-17]. They simultaneously have, however, some disadvantages relevant to their inadequate wettability and electrochemical activity in aqueous solutions because of their hydrophobic surface nature and poor kinetics for reduction and oxidation reactions. This partly declines the performance of pristine felts when they are applied at electrodes [18, 19]. In the effort to make the felts electrodes more active, several

modification methods have been adopted at various conditions. After modification process, the electrochemical activity of CF could be remarkably enhanced [19, 20].

CF based-electrodes have been the subject of few reviews relevant to energy and environmental topics. Most reviews focus on redox flow batteries (RFBs) and wastewater treatment by electrochemical advanced oxidation processes (EAOPs). Chakrabarti *et al.* reported some modification methods to improve the catalytic properties and the conductivity of CF electrodes for RFBs such as deposition of metals, addition of functional groups by chemical and thermal treatments on the electrode surface. Several methods to produce vapour grown carbon fibers, carbon nanotubes (CNTs), or nitrogenous groups on the carbon fiber surface of graphite felt (GF) electrodes were discussed [21]. The progress on felt electrodes in RFBs was still a fascinating topic in some recent reviews [22, 23]. Beside that, CF were used widely as cathode materials for removal of POPs in aqueous medium by EF process. According to the review of Brillas *et al.*, carbon electrodes present many advantages like nontoxicity, good stability, conductivity, and chemical resistance [1]. The efficiency of EF system using felt cathodes was summarized in the comparison with other materials like activated carbon fiber, reticulated vitreous carbon, carbon sponge, *etc* [24-26]. Obviously, reviews dedicated to CF based-electrodes have concentrated only a few of their characteristic features or modification methods towards individual applications. From these reviews, it is actually difficult to understand this material in detail or to choose suitable methods of modification for various demands. To surmount this difficulty requires deeper reviews focusing the different aspects of CF materials, which were investigated according to the following scheme:

- First, we discuss the commercial method of producing CF materials and supply the specific properties combining with methods and equations to identify physical values of felt materials.
- The most important part is the modification methods used to improve the properties of felts electrodes relating mainly to hydrophilicity, conductivity, and electroactive activity. Interestingly, the different modification methods induce different performance.
- Both pristine and modified felts electrodes are applied in energy field of VRFB, MFC, BFC, capacitors, electrochemical solar cells and lithium ion batteries. From there, we compare and discuss the upgraded efficiency of modified electrodes.
- Afterwards, we concentrated on using CF cathodes for wastewater treatment by EF technology. Unlike the previous reviews about removal POPs by EF technology, this

study presented a new approach with following structure: First, we present the definition about EF process and the studies using non-modified felts cathode. In the next step, we investigated the modified EF systems on the basis of various aspects: configuration, cathode material, and catalyst. Beside that, we looked at bio-Fenton systems without input power in which clean and green energy from FC is used for EF process. Finally, with an eye towards industrial applications, some EF pilot scales were investigated for the treatment of a large volume of pollutants solution. Using solar radiation as available power for EF pre-pilot plants is also an interesting idea to grow the future research for CF-based electrodes.

- In the last part, some important conclusions and perspectives in this field were presented to open new trends for CF-based electrodes.

2.3. Manufacturing method and characterization of CF material

2.3.1. Manufacturing method of CF material

Generally, there are two types of precursors which are most commonly used for graphite/CF manufacture, including rayon and polyacrylonitrile (PAN) [27]. The manufacturing process for felts material is usually done via needle-punching processing and subsequently graphitization [28]. GF is manufactured by graphitization of CF where the processing temperature for GF is around 2000-2600°C, and 1200-1600°C for CF. Their outward appearances are almost exactly alike Figure 2-1. However, the various precursors and processing parameters used in their manufacture can impact on the graphitization stage of the felt materials, and that can lead to the differences between carbon and GF (Table 2-1). Indeed, there are several hundred grades of carbon/GF available from different sources, and the variation from felt to felt is considerable. Particularly, a study by Zhong *et al.*, found the resistivity of GF based on rayon, 0.023 Ω cm, to be much higher than that of the PAN variety, 0.0038 Ω cm. The specific surface area of this PAN based felt, 266.86 m^2 g^{-1}, is slightly greater than that of the rayon based felt, 238.27 m^2 g^{-1}, and this may partly account for the lower electrical resistivity [29]. A study of Liu *et al*. showed that CF (*Shanghai Q-Carbon Material Co., Ltd., China*) exhibited a much higher electrocatalytic activity than GF (*GFD4.6, SGL Group, Germany*), due to its higher amount of C-OH and quaternary nitrogen groups and the presence of higher amounts of defect sites [30].

Figure 2-1. Typical shape of commercial (a) CF and (b) GF [31].

Table 2-1. Comparison of manufacturing factors and physical properties between carbon and GF based on rayon or PAN precursor [32].

Properties	CF		GF	
	PAN	**Rayon**	**PAN**	**Rayon**
Bulk density (g cm^{-3})	0.14	0.09 - 0.10	0.10	0.08
Carbon content (%)	98.5	≥ 99	> 99.5	≥ 99.9
Ash content (%)	< 0.75	≤ 0.05	0.05	≤ 0.01
Thermal conductivity (at 1500 °C, W/mk)	0.13	0.22	0.08	0.39
Tensile strength (MPa)	0.18	0.13	0.12	0.10
Process Temperature (°C)	1500	1400	2400	2200-2500

In brief, the differences in the precursors and manufacturing factors as well as the processing procedure employed would affect significantly the properties of the produced felts materials.

2.3.2. Characterization of CF electrodes

2.3.2.1. Structural properties

2.3.2.1.1. Morphology

From SEM images, carbon and GF are often observed under long smooth fibres dispersed randomly with homogeneous large void spaces between them (Figure 2-2). Each fibre has cylinder-like shape with shallow grooves along the long axis which was formed by combination of thinner fibres, melted together lengthways as reported by González-García *et al.* [33]. The addition or cutting of thinner sheets from the original can change the thickness of the three-dimensional felts electrode. The geometrical shape of fibers is quite different from other materials, partly leading to various values for structural as well as physical parameters as shown in Table 2-2.

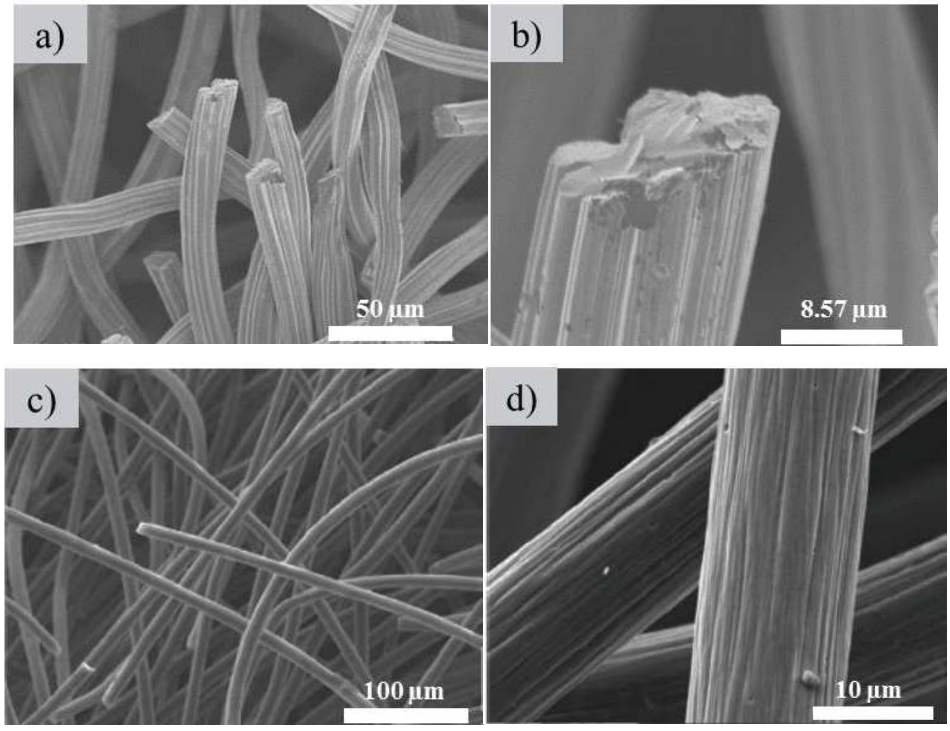

Figure 2-2. SEM image of felts. (a, b) CF (*Johnson Matthey Co., Germany*, thickness 1.27 cm) and (c, d) GF (*GFD 2.5, SGL Group*, thickness 2.8 mm) [14] at various magnifications.

Table 2-2. Properties of carbon and GF electrodes [33].

			Porosity		Mean pore diameter		Specific surface area		Apparent electrical resistivity
Material	Company	Type	Value	Method	Value/m	Method	Value/m^2 m^{-3}	Method	Value/Ω m
GF	Carbone-Lorraine	RVG 2000	0.95	Unknown					3.5×10^{-3}
		RVC 1000			1.19×10^{-4}		31000	Filamentary analogy	
		RVC 2000			2.57×10^{-4}		15000	Filamentary analogy	
		RVC 4000			1.60×10^{-4}		23500	Filamentary analogy	
		RVC 4002	0.84	Apparent and true density	2.94×10^{-4}	Ergun	33684[b] 3369[c]	Filamentary analogy	2.4×10^{-1} [d]
			0.984	Simulation	0.12×10^{-4}	Filamentary analogy	22100-22700	Ergun	2.7×10^{-3} [e]
							$(0.067\text{-}6) \times 10^{7}$ $(0.8\text{-}2.8) \times 10^{6}$	Porosimetry BET	
CF	SiGRI	Sigratherm GFD 5	0.95	Unknown	1.52×10^{-4}		24000-60000	Filamentary analogy-BET	
CF	Fiber Materials	CH (0.175)	0.86	C density	1.56×10^{-4}		11000	Filamentary analogy	
		CH (0.25)	0.90		2.04×10^{-4}		8800	Filamentary analogy	
CF	Amoco Thornel Mat VMA		0.98	Unknown	6.37×10^{-4}				7.14×10^{-3}

[b]Calculated from mercury porosimetry. [c]Calculated from Residence Time Distribution modelling. [d]Value for the short direction. [e]Value for the long direction.

2.3.2.1.2. Porosity

The Table 2-2 reveals that the porosity of CF usually oscillates in a range of 0.8 ÷ 1. To calculate this value, the helium density and mercury porosimetry (density methods) are usually applied because these methods seem suitable for compressible materials such as CF. By this method, both the true dimensions and the fibrous structure of the felts will be modified by the static pressure of mercury and by the mercury intruded. Porosity, ε, can be calculated from the values of apparent and true densities, according to Eq. (2-1):

$$\varepsilon = \frac{(\rho_R - \rho_A)}{\rho_R} \tag{2-1}$$

where the apparent density of the felts, ρ_A, was determined with a dilatometer prepared for mercury porosimetry, and the true density of the sample, ρ_R, was determined by using helium, a monoatomic gas, small enough to be accessible to the lowest size micropores ($\cong 2\text{Å}$) in the material.

2.3.2.1.3. Specific surface area

Different methods for identifying the specific surface area can give out different values, so comparison of this parameter between several studies is difficult. There are three main ways for identification of specific surface areas of felts, including: (i) structural methods: the filamentary analog procedure [34], (ii) physical methods: physical adsorption of gases [35] and the permeametry mercury porosimetry [36] and (iii) electrochemical methods [37]. For example, in filamentary analog method, the specific surface area is calculated by Eq. (2-2) where all fibers are considered fibers as long, smooth and perfect non-porous cylinders.

$$A_e = \frac{4}{d_f}(1 - \varepsilon) \tag{2-2}$$

where A_e ($m^2\ m^{-3}$) is the specific surface area, d_f is the diameter of the fiber, and ε is the porosity of the material.

In the permeametry method performed by using the Ergun equation which describes the dissipation of mechanical energy in the flow through a porous medium, Ae is identified by Eq. (2-3) and (2-4):

$${A_s}^4 = \frac{N^3(0.096L\rho)^2}{M^2(5\gamma\mu L)^3}\frac{\varepsilon^3}{(1-\varepsilon)^4} \tag{2-3}$$

$$A_e = A_s(1 - \varepsilon) \quad (2\text{-}4)$$

where ρ is the fluid density, μ is the dynamic viscosity of the fluid, γ is the circularity factor of the pores, M and N are the empirical constants which depending on geometrical and physical parameters of the using system.

The adsorption isotherms and mercury porosimetry methods are also utilized. For example, by dynamic BET method using the Quantadsorb Model QS-16 (Quantachrome Corp., NY), the specific surface of CF (*SIGRI GmbH, Meitigen*, 5.0 mm thickness) was obtained at 6.0 x 10^4 m^{-1} [38]. The specific surface area of PAN-based CF was identified at 1.0 m^2 g^{-1} using the BET method [39]. Meanwhile, using the mercury-intrusion method (the results were analyzed by a computer system (Malvem Instruments, UK)), the values of two kinds of GF from rayon and PAN precursors were found as 238.27 and 266.86 m^2 g^{-1}, respectively (Table 2-3). Obviously, there was a significant difference in specific surface area between main pores and total measured pores for each felt sample. This illustrated the unique structural characteristics of the GF with the coexistence of macropores (space between fibres of the felt as observed on SEM in part 2.3.2.1.1) and micropores [29].

Table 2-3. Characteristics comparison of rayon and PAN based GF [29].

Felt	Company	Thickness (mm)	Main pore diameter (µm)	Main pore volume/total measured pore volume (%)	Specific surface area for main pores (m^2 g^{-1})	Specific surface area for total measured pores (m^2 g^{-1})
Rayon-GF	Fibre Materials, Inc., Maine, USA	3	188.5-36.5	93.2	0.329	238.27
PAN-GF	Sigri Electrograpit GmbH, Germany	2.5	188.5-13.0	92.8	0.390	266.86

Considering electrochemical applications of felts, the electroactive surface area of cathodes was calculated from voltamperometric measurements according to the Randles-Sevcik formula (2-5) [40, 41].

$$Ip = 2.69 \times 10^5 \times AD^{1/2}n^{3/2}\gamma^{1/2}C \quad (2\text{-}5)$$

where n is the number of electrons participating in the redox reaction, A is the area of the electrode (cm^2), D is the diffusion coefficient of the molecule in solution ($cm^2.s^{-1}$), C is the concentration of the probe molecule in the bulk solution (mol cm^{-3}), and γ is the scan rate of the potential perturbation (V s^{-1}).

For example, Robert *et al.* used simulations method in combination with experimental voltammograms to extract electrochemical properties of the felts electrodes [14]. This experiment was performed in a three electrodes-cell including platinum (Pt) wire mesh (Metrohm, UK) as the counter electrode, a Saturated Calomel Electrode (SCE, IJ Cambria Scientific Ltd) as the reference and GF (*SGL GFD2.5*, thickness 2.8 mm) as a working electrode. By running cyclic voltammograms (CVs) recorded at 0.05 V s^{-1} in an aqueous solution of 0.1 mM ferricyanide and 0.1 M KNO_3, the electrochemical surface area of this felt was identified at 50 cm^2 with geometric surface area of 10 cm^2.

2.3.2.2. Physical properties

2.3.2.2.1. Permeability

The permeability can be changed over a wide range among other materials relying on the hydrophobic nature of felts and their porosity. The value is defined based on the Darcy law in which it is understood as the velocity of a fluid, through a volume unit of a porous medium, per unit of differential pressure. The value of the permeability coefficient is frequently used to give an indication of the ease of passing a fluid through a porous material [42]. The higher the porosity, the easier the fluid flows through a porous material, so that the permeability coefficient will increase with the porosity. Permeability coefficient (PC) is calculated through Eq. (2-6) by the Ergun method:

$$PC = \frac{\varepsilon^3}{K'' {A_e}^2} \quad (2\text{-}6)$$

where ε is the porosity, Ae is the specific surface area, and K'' is the Kozeny constant at 32.824 for media with high porosity (ε >0.98).

The high hydrophobicity of felts materials can reduce simultaneously the permeability. Most of felts are hydrophobic and difficult to wet (Figure 2-3). This phenomenon was found commonly in researches about carbon and GF [14]. The apparent high contact angle suggested a quasi-super-hydrophobic surface similar to that reported by Banks *et al.* for graphene foam [43].

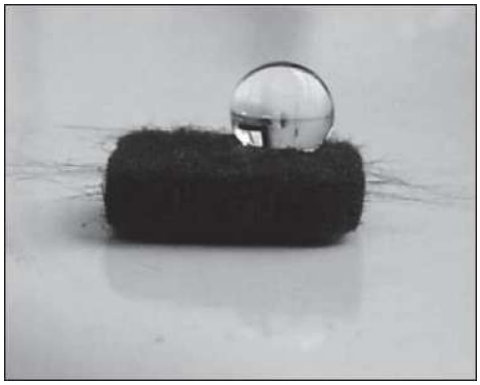

Figure 2-3. Shape of water droplet on GF (*SGL GFD2.5*, thickness 2.8 mm) [14].

2.3.2.2.2. Mass transfer

Study of the mass-transfer characteristics of the CF electrode is performed in an electrochemical flow cell (Figure 2-4) [38]. Mass transfer coefficients have been obtained for a flow-through felts electrode using the limiting-current technique and assuming plug-flow conditions for the range: 25 < Pe < 1700 (Pe = Peclet number relative to felt as a porous material). This value can be calculated by Eq. (2-7):

$$k = -\frac{u}{aL}\ln[1 - \frac{I_l}{FSC_0u}] \quad (2\text{-}7)$$

where k is the mass transfer coefficient, u is the flow velocity of electrolyte (m s^{-1}), a is the specific surface area (m^{-l}), L is the electrode length (m), I_l is the limiting current (A), F is the Faraday constant (96,486 C $equivalent^{-1}$), S is the cross-section of electrode (m^2) and C_0 is the input concentration of electroactive species (mol L^{-1}).

The mass transfer coefficients were identified for some kinds of GF as listed in Table 2-4.

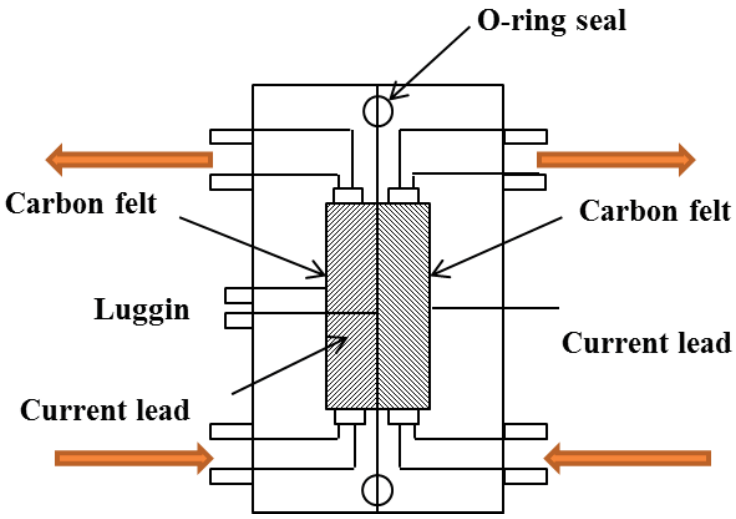

Figure 2-4. Schematic diagram of electrochemical cell for the identification of the mass transfer of CF [38].

Table 2-4. Correlations between the mass transfer coefficient and the solution flow rate [44].

Reaction	Supporting electrolyte	Electrode material	A (cm^{-1})	k ($cm\ s^{-1}$)	Ref.
$Fe(CN)_6^{3-}/Fe(CN)_6^{4-}$	KCl or KOH 0.5 M	GF (thickness 2 mm)	160	$1.9 \times 10^{-2}\ \vartheta^{0.352}$	[45]
Br_2/Br^-	$ZnBr_2$ 2M + $ZnCl_2$ 1M + KCl 3M	GF (thickness 17.5 mm)	110	$1.3 \times 10^{-3}\ \vartheta^{0.72}$	[46]
		(thickness 25 mm)	88	$1.2 \times 10^{-3}\ \vartheta^{0.61}$	
$Fe(CN)_6^{3-}/Fe(CN)_6^{4-}$	KOH 1M	GF (length of 83 mm)	113	$1.6 \times 10^{-2}\ \vartheta^{0.4}$	[47]

A is geometric surface area, ϑ is the fluid flow rate in the reactor

2.3.2.2.3. Electrical resistivity

The electrical resistivity, r_{felts}, of a CF material can be calculated from Eq. (2-8):

$$r_{fet} = \frac{4}{(1-\varepsilon)} r_c \qquad (2\text{-}8)$$

where ε is the porosity, and r_c is the electrical resistivity of the electrode material.

Because of the great number of different felts types and the calculation methods, a wide range of electrical resistivity values for carbon can be found in the literature. As for instance on

RVC 4002 supplied by Carbone-Lorraine, this value altered at least 100 times from 2.4 x 10^{-1} Ω m to 2.7 x 10^{-3} Ω m by using two determination methods for the porosity (ε). Similarly, this value is also variable nearly 100 times between two kinds of GF RVG 2000 and RVC 4002 which are provided from the same company (Table 1).

The value of the electrical conductivity was roughly estimated from the *I*/*V* curves at $V = 0$ V by performing the Eq. (2-9):

$$\sigma = \frac{L}{l*e}\left(\frac{dI}{dU}\right)_{(V=0V)} \quad (2\text{-}9)$$

where *e* and *l* are respectively the thickness and the width of the felts and *L* is the distance between the two silver electrodes (Figure 2-5).

The value of the electrical conductivity of the CF, was found by Wang *et al*. to be approximately 280 S m^{-1} [48], which was in good agreement with the 285 S m^{-1} for the electrical conductivity of RVG 2000-GF [49].

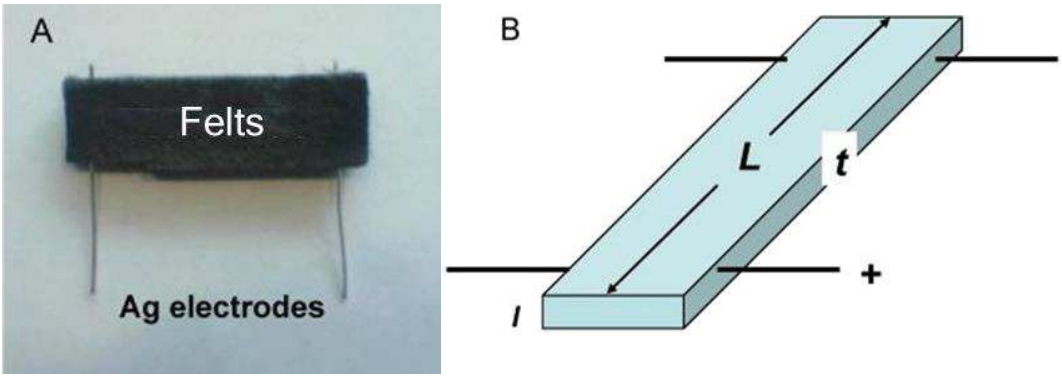

Figure 2-5. The electrical resistivity device. (a) The optical photo of the connecting device used for the electrical conductivity measurements; (b) The scheme of the representative parameters used for the calculation of the electrical conductivity on a rectangular piece of the CF [48].

2.4. Conclusion on the characterization of CF electrodes

In conclusion, although owing interesting characteristics, the studies of intrinsic properties of CF materials has been a hard task because of its hydrophobic nature and its compressibility [33]. Therefore, the choice of suitable methods added to several techniques for calculation of these structural and physical parameters of CF electrodes will still be a fascinating story in the future studies. To improve its performance, especially hydrophobicity and

electrochemical activities for electrodes applications, many modification ways have been applied as discussed in the following section.

2.5. Modification of CF electrodes

2.5.1. Plasma treatment

The purpose of plasma treatment is to improve the wettability of commercial CF due to the growth of oxygen-containing functional groups or/and nitrogen doping on the surface of fibers, and both of which enhanced the electrochemical reactivity. In particularly, oxygen plasma treatment was carried out in a radiofrequency (RF) plasma setup and felts were loaded into the plasma chamber which was filled with oxygen. This process was controlled by the treatment time, the power of the rf generator and the oxygen pressure [50]. In 2015, Chen *et al.* reported the modification of felts (*C0S1011,CeTech, Taiwan*, thickness 6 mm) with atmospheric pressure plasma jets (APPJs) [51]. The APPJs treatment was performed on the felts under the single spot and scanning modes with the presence of N_2 flow rates like in Figure 2-6. The formation of specific oxygen functional groups was observed after the plasma treatment. The elaborated calculation by XPS revealed that this method rather favored the formation of phenolic (C-O) groups than carboxyl (C=O) groups [50]. However, the plasma treatment process only often increases the amount of functional groups on felts and not remarkably the surface area. Apart from oxygen-containing functional groups, nitrogenous groups can also improve electrocatalytic activity of carbon electrode materials for the redox reactions. This is because carbon atoms adjacent to nitrogen dopants possess a substantially high positive charge density to counterbalance the strong electronic affinity of the nitrogen atom. The “positively charged” carbon atoms can work as the active sites for the oxidation reaction, while the five valence electrons of nitrogen atoms contribute extracharge to the bond in graphene layers, which enhances the basicity of carbon and the electrical conductivity of nitrogen doped carbon [52]. Furthermore, nitrogen doping can also make CF materials more hydrophilic to increase the electrochemically active sites [28]. Briefly, the increase amount of surface-active oxygen and nitrogenous groups by plasma treatment can enhance electrochemical performance of the modified material through facilitating charge-transfer between felts electrodes and electrolytes [50, 53].

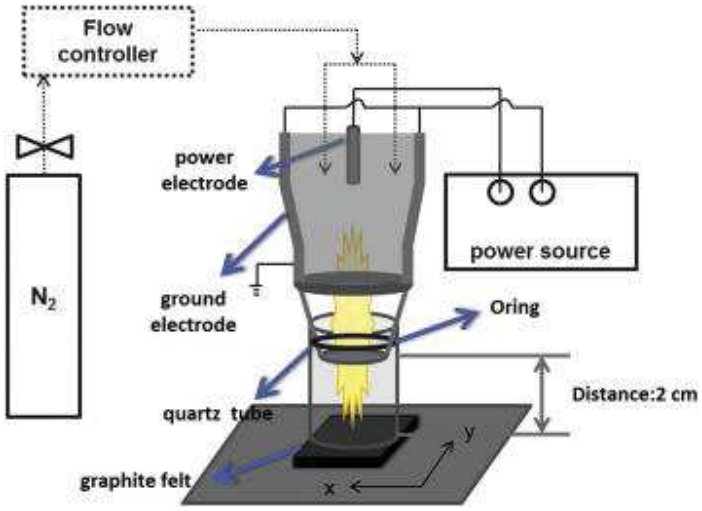

Figure 2-6. Schematic diagram of atmospheric pressure plasma jet [51].

2.5.2. Thermal treatment

The thermal treatment is a simple way for felts modification where samples are annealed in a furnace feeding by gas flow containing oxygen and/or nitrogen. This modification brings to benefits towards upgradation the properties of felts electrodes like plasma treatment in order to improve the electrochemical properties and the hydrophilicity [54]. A significant enhancement of the electrochemical activity was observed in the study of Zhong *et al.* on two kinds of GF, based on rayon or PAN precursors, after thermal treatment [29]. It was found that the electrical conductivity of the PAN based felts was superior to that of its rayon-based counterpart. XPS analysis pointed out that the rayon based felts reacted more easily with oxygen and forms C=O carbon–oxygen groups, while the PAN based felts was more resistant to oxidation and preferentially forms C-O groups. The more extensive oxygen interaction in the rayon felts was thought to be due to its microcrystalline structure. By heat-treating under NH_3 atmosphere at 600 °C and 900 °C in a tubular furnace, the nitrogen-doped (N-doped) GF electrodes was fabricated with high electrochemical performance. The enhanced electrochemical properties of the modified electrodes are attributed to the increased electrical conductivity, the increase of active sites amount, and the improved wettability provided by the introduction of the nitrogenous groups on the surface of GF [28, 55]. Interestingly, the heat treatment can also improve the surface area of the pristine electrodes. After the heat treatment in air at 400 °C, the surface area of the modified felts increased by more than ten times in comparison to the pristine one based on rayon (*SGL*,

thickness 3 mm) [50]. This value was 1344 % higher than bare PAN-CF (*Nippon Chem. GF-3F*, thickness 3mm) [18].

2.5.3. Chemical treatment

Chemical treatment of CF mainly involves the use of strong oxide chemicals in order to activate the surface of felt materials. The surface of the felts can be etched by KOH at high temperature (~ 800 °C) to generate micropores and attain oxygen-containing functional groups. Due to the abundant exposed edge carbon sites and the oxygen-containing functional groups introduced by KOH activation, electrochemical activity of the treated electrode is remarkably improved comparing with bare PAN- GF (*Gansu Haoshi Carbon Fiber Co., Ltd.*) [56]. The samples can be chemically treated by refluxing/boiling in sulphuric acid, nitric acid or by their mixture in order to fabricate felts with a large amount of chemisorbed oxygen on the surface [57, 58]. After treatment procedure, the felts must be washed thoroughly with distilled water and then vacuum dried prior to use as electrodes. The electrochemical activity of the GF was found to increase with increasing acid concentration [59]. The increased electrocatalytic activity of the treated GF was thus attributed to the increased concentration of C−O and C=O functional groups on the surface. The role of oxygen groups towards properties of felts electrodes was well discussed in section 2.5.1. The combination between thermal and chemical treatments sometimes is necessary to improve the electrochemical behavior of the felts [60]. The growth up of functional group on felts electrodes can be done via another method called electrochemical oxidization, which requires the application of constant current or potential in acidic solutions like 1M H_2SO_4. The modification following the electrochemical oxidation way was successfully applied to improve the properties of different felts like GF (*Shanghai Energy Carbon Limited Co., China*) [61] or GF (*Sanye Carbon Co., Ltd.*) [62]. Low-cost chemical reagents like ethanol and hydrazine hydrate were applied for chemically modified the graphite as well. Interestingly, after modification, some carbon nanoparticles (Figure 2-7 c) and oxygen/ nitrogen-containing functional groups appeared simultaneously on the cathode surface, which greatly improved the surface hydrophilic property and the electrocatalytic activity. The contact angles were reduced gradually from 141°, 123° to 110° for bare GF (*Shanghai Qijie Carbon Material Co., LTD*), GF-ethanol and GF-ethanol/hydrazine, respectively (Figure 2-7 d, e, f) [63, 64].

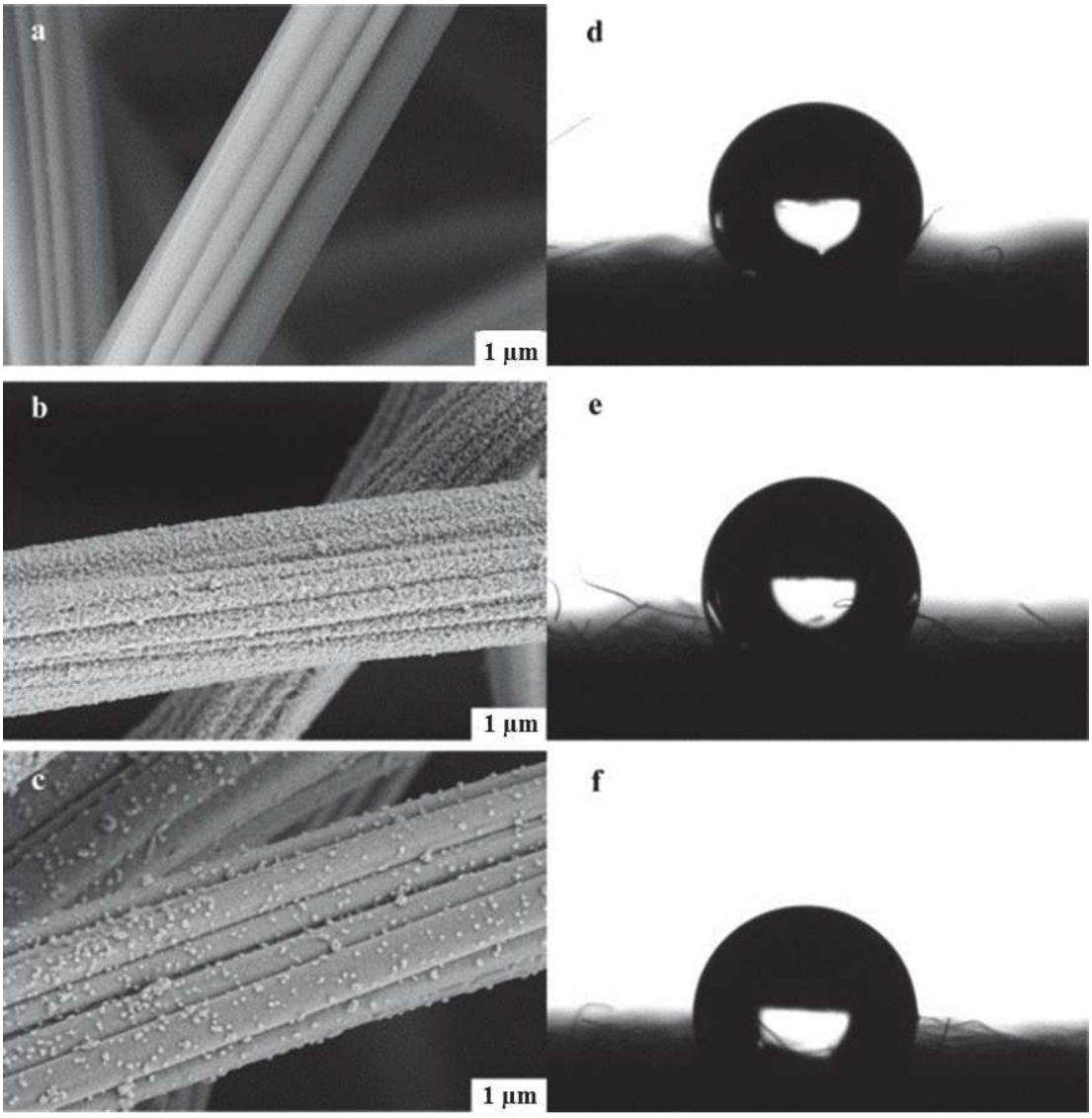

Figure 2-7. SEM images and contact angles of GF (a, d), GF-ethanol (b, e) and GF-ethanol/hydrazine (c, f) [64].

2.5.4. Metallic modification

The metallic modification is towards enhancement of the electro-conductivity of felts electrode materials. Coating metal on the felts fibres can be performed through a simple way of impregnation with solutions containing metallic ions like Pt^{4+}, Pd^{2+}, Au^{4+}, Mn^{2+}, Te^{4+}, In^{3+}, Ir^{3+}, *etc.* In few cases, the CF was thermally treated at high temperatures [57, 65]. The amount of metal on the fibre surface can change depending on the used method and the treatment time. For example, there was 99.77% (wt.%) of Ir loaded on CF (*Shanghai carbon works*) by Energy-

dispersive X-ray Spectroscopy (EDX) analysis after immersing sample into a solution of H_2IrCl_6 for 2 min. The heat treatment in the air at 450 °C for 15 min was performed before and after Ir coating. These steps were repeated eight times. The mechanism of this procedure could be explained by H_2IrCl_6 reduction reaction at 450 °C to form IrO_2 under atmospheric conditions, and the IrO_2 reduction reaction also proceeded on the graphite fibres through Eq. (2-10) [66]:

$$C + IrO_2 = Ir + CO_2 \quad (2\text{-}10)$$

The Ir-material, when coated on the GF surface, could offer a better conductive and catalytic interface between the solution state and the solid state of the electrode, lowering the charge transfer overpotential. Much of the Ir metal was still covered with graphite fibres after 50 charge–discharge cycles in a vanadium redox cell, proving the high stability of the modified electrodes [66]. Similarly, bismuth nanoparticles were deposited on the felt by immersion in a Bi_2O_3 solution followed also by thermal reduction at 450 °C in air. Despite the low metal content (1 at.%) on the surface of the fibers, the Bi-modified felt showed an excellent electrochemical improvement when an electrode was applied for vanadium redox flow battery [19]. The charge transfer resistances for V^{2+}/V^{3+} redox reaction on CF (*Shanghai Q-Carbon Material Co., Ltd., China*) and GF (*GFD4.6, SGL Group, Germany*) electrodes after decoration with Bi were effectively reduced to 0.9 and 1.6 Ω (Figure 2-8), indicating that the presence of Bi nanoparticles accelerate the electron transfer between electrolytes and the felts electrodes [30].

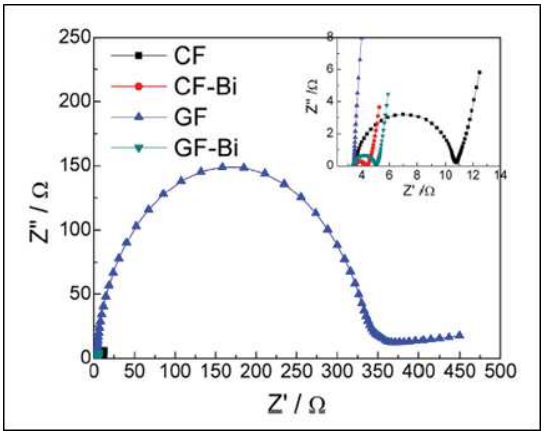

Figure 2-8. Nyquist plots of CF, CF-Bi, GF and GF-Bi in 0.05 M V^{2+} + 0.05 M V^{3+} + 3 M H_2SO_4 solution at DC voltage -0.55 V [30].

Furthermore, the growth up of metal materials on the surface of felts electrodes is performed by other treatments such as electrodeposition and thermal reduction. The

electrodeposition of ruthenium oxide (RuO_2) films on the CF was conducted from a $RuCl_3$ (0.05 M) solution by applying a constant current density of 5 mA cm^{-2} at room temperature [67]. By the same method, Pt particles were successfully coated on CF (*10 × 10 × 5 mm*) [68] or GF (*1 × 2 × 0.15 cm*) [17].

The high cost of noble metal catalysts limited their commercial application. To address this issue, studies focusing on less expensive metals have been performed as well. The electrochemical deposition of PbO_2 on GF was carried out under an applied current of 50 mA cm^{-2} in cell containing 0.5 M $Pb(NO_3)_2$ in 0.1 M HNO_3 solution. After 30 min, β- PbO_2 with a tetragonal structure at the average crystal size of 0.5 µm were compactly covered on felts fibres (Figure 2-9 a) [69]. Similarly, the electrodeposition of MnO_2 on the CF surface was also conducted in a two-electrode electro-chemical cell in 0.25 M manganese acetate ($MnAc_2$) solution under applying a constant current of 8 mA for 10min [70]. Alternatively, thermal deposition of $Fe(CO)_5$ was utilized to load Fe directly on GF *(Sanye Carbon Co., Ltd., Beijing*) in a sealed reactor made of glass (Figure 2-9 b). The temperature was controlled between 165 and 175 °C for 3 min to completely decompose the $Fe(CO)_5$. The generated Fe on the felt was composed of Fe_2O_3, FeOOH and Fe(III) oxides acting as catalysts in order to improve the electrochemical activity of the modified electrode [71].

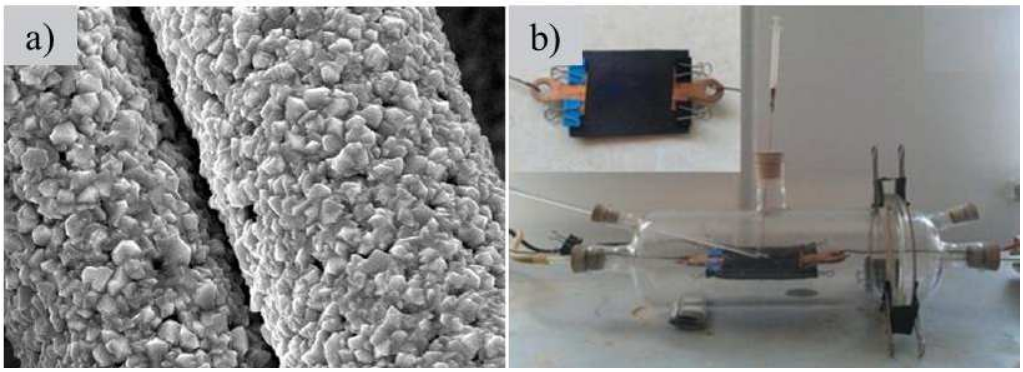

Figure 2-9. (a) SEM image of PbO_2/GF [69] and (b) Reactor of deposition of Fe on GF [71].

2.5.5. Graphene based modification

In recent years, graphene has emerged as an exciting topic of research in materials science and condensed matter physics research. It has received extensive attention due to its remarkable electrical, physical, thermal, optical, high specific surface area and mechanical properties [72, 73]. Therefore, graphene was widely applicable for electrochemical activity of electrodes [74].

Different methods as dip-coating, constant potential technique and electrophoretic deposition (EPD) were used separately or combined together for the coating of graphene based materials on felts electrodes. For example, the coating of rGO on CF (*Shanghai Qijie Carbon Co., Ltd.*) was performed using different steps: (1) Graphene oxide (GO) suspension was prepared by using the sonication for 1h to exfoliate the graphite oxide in water medium. (2) GO was loaded on the CF surface by the dipping-drying process in the prepared GO suspension. (3) The GO was then electrochemically reduced by applying a constant voltage of −1.2 V in 0.5 M Na_2SO_4 electrolyte for 10 min. By comparing the response of CVs curves in 0.5 M Na_2SO_4 solution, the rGO/CF electrode (Figure 2-10 a, d) has overall a higher current density than the bare CF over the scanned voltage range (-0.6 ~ 0.6 V), suggesting a larger electrode surface area and better conductivity after modification [70].

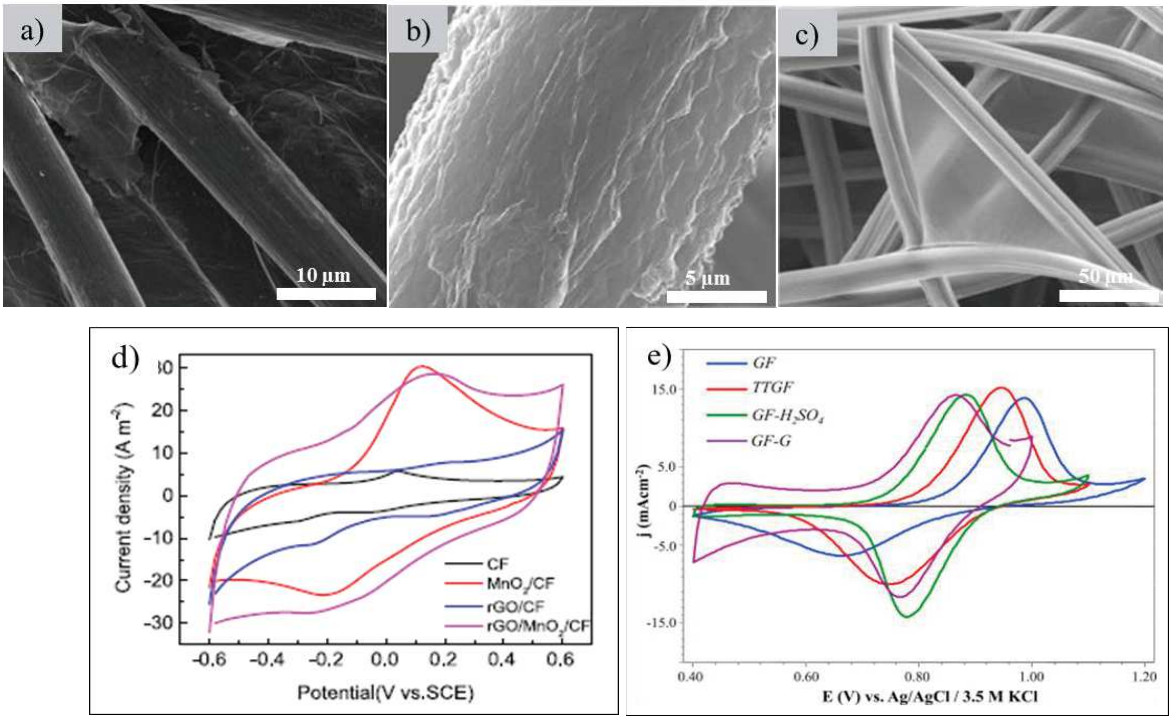

Figure 2-10. Characterization of graphene based felts. SEM images of rGO coated on (a) CF (*Shanghai Qijie Carbon Co., Ltd.*); (b,c) GF (*RVG-2000, Carbon-Lorraine* company); (d) CVs curves of the CF in 0.5M Na_2SO_4 solution at a scan rate of 10 mV s^{-1} and (e) CVs recorded in a 0.05 M $VOSO_4$/1.0 M H_2SO_4 solution at a scan rate of 1 mV s^{-1} on the different GF electrodes [70, 75].

In addition, the EPD shows several advantages for obtaining homogeneous film on felts electrode from suspensions containing well-dispersed charged particles like GO solution, with high deposition rates, simple operation, easy scalability and all that by avoiding the use of binders [76]. A graphene-modified GF (GF-G) was synthesized using EPD technology from GO suspensions in two-electrodes cell. By applying a voltage of 10 V for 3 h, the negative GO sheets were moved towards the positive GF electrode. The GF-G showed graphene-like sheets placed on the surface of the fibers either in a wrinkled configuration (Figure 2-10 b) or anchored between them (Figure 2-10 c). These sheets consisted of partially reduced GO, so the oxygen content decreased from 13 at. % in the initial GO to 3.84 at. %. To compare with other modification methods, the chemical treatment by electrochemical oxidation in 1M H_2SO_4 (GF-H_2SO_4) during 3 h or thermal treatment at 450 °C with the same time, 3 h, under an air flow in a tubular furnace (TTGF) were done. As could be seen clearly from Figure 2-10 e, the electrochemical performance of graphene modification was even higher than GF-H_2SO_4 or TTGF. Because of the excellent electrochemical properties of graphene based materials, they are still a promising future for applications in the modification of CF electrode.

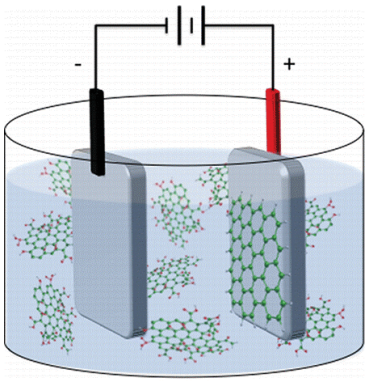

Figure 2-11. EPD of graphene on positive electrodes [76].

2.5.6. Carbon nanotube based modification

CNTs have been attractive for the modification of felts electrodes because of their excellent electrical and thermal conductivities, mechanical flexibility and significantly large surface area [77]. The coating of single-walled carbon nanotube (SWCNT) was performed by simple way where CF was immersed into the SWCNT suspension. The CF was then dried at 80 °C for 5 h. The SWCNT (2 wt% relative to the amount of CF) was ultrasonically dispersed previously in N,N-dimethyl formamide (DMF). The process was repeated until all the SWCNT

suspension adsorbed into the CF. The modified electrode showed a better catalytic performance with higher electron transfer rate [78]. In the other hand, the CNTs could be directly grown on the surface of felts by chemical vapor deposition (CVD) method. This technique does not require a binder. The felts sample was placed in the center of a quartz tube and heated at high temperature (around 800 °C) under Ar gas flow, followed by the injection of the carbon precursor source. Toluene or ethylenediamine was applied as source solution for growth of CNTs or nitrogen-CNTs on GF (Figure 2-12 a, b). Thanks to the small size (~30 nm) of CNTs, they created a significant increase of the electrochemical surface area of the felt materials. In addition, the N-doping could further improve the electrode performance because of the modified electronic and surface properties of CNTs on GF [79]. The CNTs/CF electrode was also obtained by growing CNTs via CVD of methanol on cobalt and manganese metallic particles deposited on CF. The specific surface area of CF loaded with 37.8 mg of CNTs was found to be 148 $m^2 g^{-1}$ instead of 1.0 $m^2 g^{-1}$ for non-modified one [39].

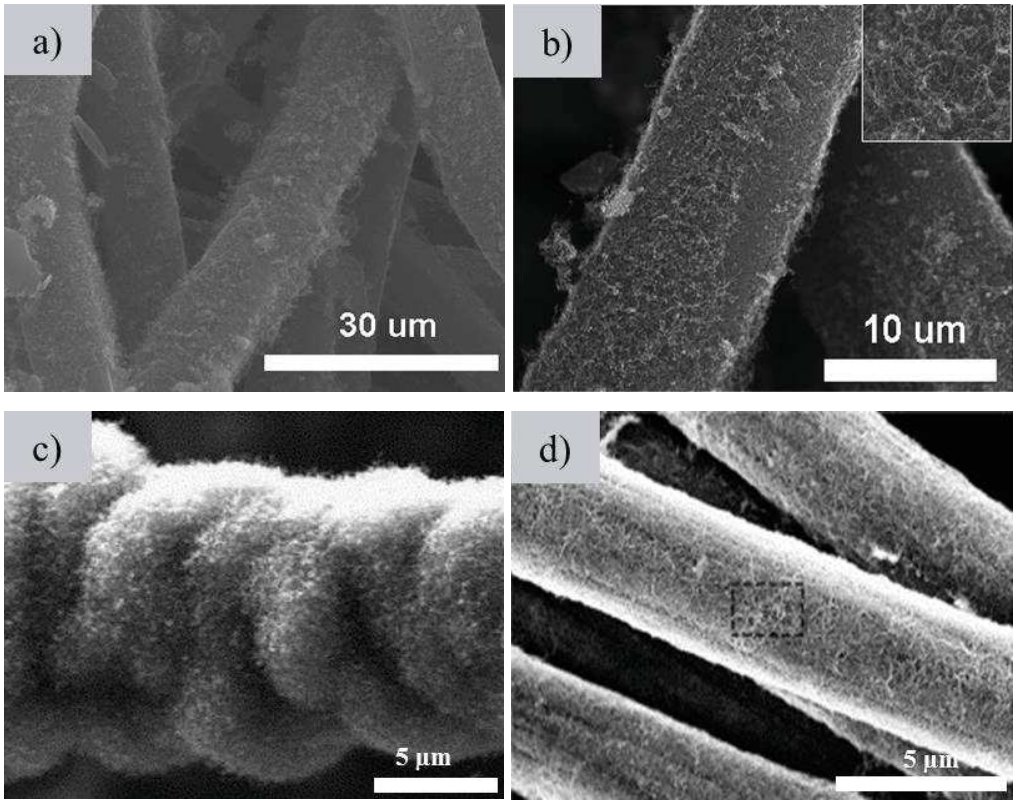

Figure 2-12. SEM images of (a) CNTs grown on GF, (b) N-CNTs grown on GF [79], (c) CNTs on CF by CVD [80], and (d) CNTs on CF by EPD [81].

The CVD is continuously an efficient technique for growth of multi-walled carbon nanotubes on CF. The used precursor was a mixture of $Fe(C_5H_5)_2/C_7H_8$ (with the ferrocene concentration in the toluene solution fixed at 20 g L^{-1}). The CNTs with high aspect ratio were grown from the iron sites, generated by the decomposition and the subsequence nucleation of the iron species from the ferrocene precursor deposited on the CF substrate. The modified CF displayed a significant enhancement of mechanical strength and electrical conductivity along with the effective surface area. The specific surface area successively increases with increasing the CNTs loading and reaches 150 m^2 g^{-1} for a CNTs weight intake of 98%. The residual iron catalyst present on the surface of the vertically aligned CNTs and the felt was removed by an acid treatment (HNO_3, 65%, at 80 °C for 2 h). Thanks to the acidic treatment step, many oxygenated functional groups were contemporaneously formed [48]. Other CNTs/CF electrodes were prepared using the decomposition of methanol on different metallic catalysts, including cobalt, manganese and lithium, supported on CF [80]. The SEM revealed that the CNTs on the CF electrode have a structure that could be recognized as bamboo-like (Figure 2-12 c), which was independent of the diameter in good agreement with the study of Rosolen *et al.* [82].

Beside CVD, EPD shows noticeable advantages as a low-cost and simple method [83, 84]. Before doing EPD, CNTs were dispersed in isopropyl alcohol for 3 h in ultrasonic bath in order to obtain dispersions of 1.6 g/L. Applying a constant voltage of 40 V for 60s, 1.05 wt% CNTs were deposited uniformly on CF with no obvious agglomeration or acutely curly body (Figure 2-12 d) [81]. The studies have been enlarged to utilize as well CNTs anchoring functional groups like carboxyl and hydroxyl. The carboxyl MWCNTs were adhered onto the CF (*Shenhe Carbon Fibre Materials Co. Ltd*, thickness 4 mm) by immersing in a mixture solution of COOH-MWCNTs and 0.02 wt.% Nafion under ultrasonication for 10 min. In this case, using Nafion as a binder guarantees the stability of the MWCNTs/CF electrode. Due to the carboxyl groups on the MWCNTs, the hydrophilic ability of the CF was improved and more active sites were introduced [85]. Similarly, the COOH-MWCNTs were ultrasonically dispersed in dimethyl formamide and then the CF was immersed in this solution. COOH- MWCNTs/CF was obtained by drying the electrode in the oven at 100 °C for 24 h [86].

2.5.7. Carbon nanofiber based modification

Among modifications performed by carbon nanomaterials, carbon nanofibers (CNFs) appear to be a promising candidate, owing to their unique electrical, physico-chemical and

mechanical properties [87, 88]. Using the catalytic chemical vapor deposition (CCVD) technique of carbon-containing gases, CNFs can be produced on a large scale and at a low cost. The growth of CNFs on CF (Figure 2-13) was conducted by support of nickel (Ni) catalyst. Firstly, Ni was deposited onto the CF surface via an incipient wetness impregnation of a solution of nickel nitrate. The calcination and reduction was necessary afterward to change nickel salt to nickel metal. The CNFs was grown on CF by CVD under flow of a mixture C_2H_6/H_2 (40:60, v/v %) from 400 °C to 680 °C. CNFs modification showed a lower surface area for the same weight of carbon intake at 98 wt.%, with 80 $m^2 g^{-1}$ instead of 150 $m^2 g^{-1}$ for CNTs. However, this value was significant in comparison to pristine electrode (1 $m^2 g^{-1}$) [48]. Moreover, Ni catalyst on GF (GF, *Shanghai Xinxing Carbon Co.*) was formed from reduction of nickel nitrate by a mixture of H_2/Ar (1:3 (v/v), flow rate 160 mL min^{-1}) at 600 °C for 3 h. After that, a growth of CNFs on the GF was accomplished at the same temperature in a flow of C_2H_4/H_2 (2:1 (v/v), flow rate 60 mL min^{-1}). The compressive strength of CNFs/GF increased with the increase of the CNFs amount from 5% to 50% [89]. This method was utilized for the CNFs modification of both GF provided by *Shanghai Qijie Carbon Material Co., Ltd.* [90] or GF provided by *Carbone Lorraine Co* [91].

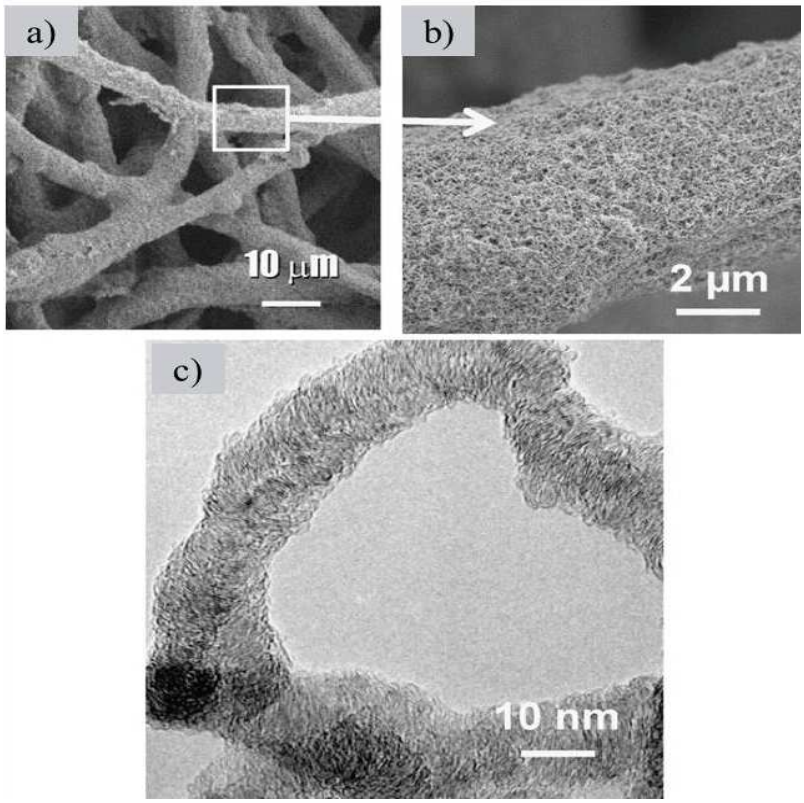

Figure 2-13. (a, b) SEM images and (c) The high-resolution TEM (HR-TEM) of CNFs on CF [48].

Microwave-assisted method is a simple and fast technique for the CNFs modification on CF. This method depends on the usage of microwave irradiation which can heat carbon-based substrates to several hundred degree Celsius within a short time scale of a few minutes or even of just seconds [92]. The synthesis approaches are similar to the CVD method for synthesis of CNFs, but it can decrease the processing times remarkably [93, 94]. The modification process on GF (*GFA6, SGL Carbon*, thickness 6 mm) was performed in subsequent steps like CVD. The full power (1400 W) of the microwave was applied for five to 10 min and repeated two more times to enable further CNFs growth. By the *in-situ* growth of CNFs, the active surface of the electrodes was increased by a factor of 50, which was determined by the electrochemical double layer capacities of the obtained materials [95].

2.5.8. Polymer based modification

Polyaniline (PANi) and polypyrrole (PPy) are the most common conducting polymers for electrode modification because of their high electrical conductivity, ease of preparation, and environmental stability [96, 97]. The coating of conductive polymer film on the surface of CF is usually conducted by the electropolymerization process in solution containing monomers. Interestingly, electropolymerized materials have unique properties which are not peculiar to the corresponding monomers [98, 99]. The pyrrole (PPy)/ anthraquinone-2,6-disulfonat (AQDS) conductive film was coated on CF (*Liaoyang Jingu Carbon Fiber Sci-Tech Co., Ltd., China*) (Figure 2-14 c) in a three electrodes electrochemical cell. A SCE and a Pt mesh were used as the reference electrode and the counter electrode, respectively. The polymer film was formed on the CF surface by applying a constant potential of 0.8V *vs* SCE and its thickness was controlled by the charge passed to the working electrode. The modified electrode resulted in larger current responses when compared to the unmodified electrode in the scan range between -1V to 0.6 V on CVs (Figure 2-14 e). This is the result of the enhanced surface area and conductivity of the PPy/AQDS-modified electrode [100]. Beside that, three kinds of phenothiazies including Thionine (TN), Toluidine Blue (TB) and Methylene Blue (MB) were investigated in order to deposit poly(pheniothiazine) films on CF (*Nihon Carbon Co., Ltd., Japan*, thickness 3mm) electrode surface. The results indicated that the poly(TB) film-modified CF exhibited an excellent electrocatalytic activity where the largest peak currents of polymer type redox activity occurred after the 25th cycle on the electropolymerization CVs. Beside electropolymerization method, the polymer modified-felts could be prepared in a simple way by submerging CF in HCl solution

adding aniline monomer and ammonium persulfate. The polymerization was conducted during 8h by continuously stirring in order to coat PANi on the surface of CF [101].

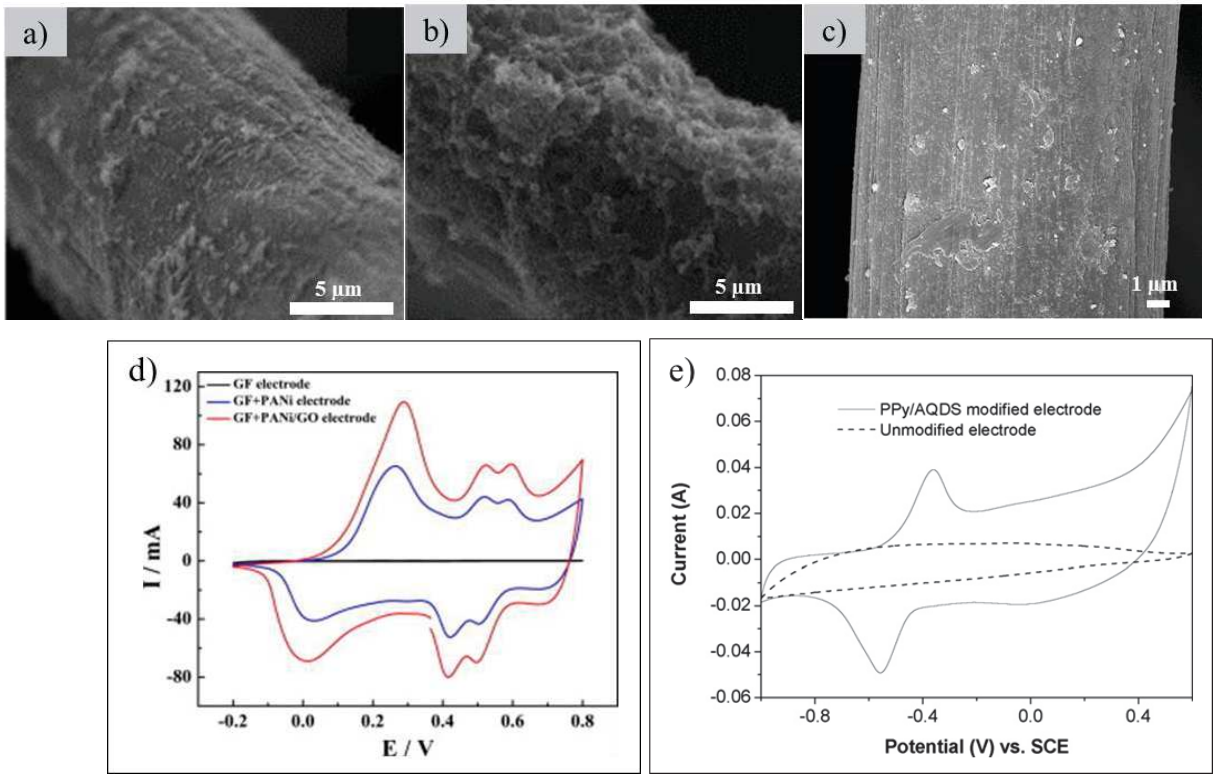

Figure 2-14. Characterization of polymer based felts. SEM images of (a) PANi/GF; (b) PANi/GO-GF, (c) PPy/AQDS-CF; CVs of the modified electrodes in (d) 1.0 M H_2SO_4 solution (Scan rate of 5 mV s^{-1}), and (e) 0.1 M phosphate buffered solution (pH 7.0) (Scan rate of 10 mV s^{-1}) [100, 102].

In order to improve the physicochemical and electrochemical properties of the conducting polymers, many copolymers were prepared and investigated. The electrochemical activity of poly(aniline-co-*o*-aminophenol) was about four times as high as that of PANi in 0.3M Na_2SO_4 solution of pH 5. The copolymer had a good stability and a high reversibility [103]. A poly(aniline-co-o-aminophenol) film with average mass at 1.17±0.1 g was deposited on CF by Cui *et al.* through electrochemical synthesis in solution containing simultaneously aniline and *o*-aminophenol [104]. What's more, the biocompatibility of felts electrodes was increased significantly when they were coated by the co-polymers containing nitrogen/oxygen functional groups. The hydrophilic conductive co-polymers like poly (aniline-co-o-aminophenol), poly

(aniline-co-2, 4-diaminophenol), poly (aniline-1, 8-diaminonaphthalene) acted as the bridge or mediator, playing the role of bonding bacteria and CF cathode more tightly, and facilitated or improved the electron transfer process from cathode to bacteria which is discussed later in MFC application [101]. In terms of the increase of surface area, electronic conductivity, biocompatibility and stability, PPy was simultaneously covered on the GF (*Beijing Sanye Co.Ltd*, thickness 5mm) with GO. One-step electrosynthesis of PPy/GO-GF was performed via in situ electropolymerization of pyrrole in the presence of GO, which contains many functional groups such as –OH and –COOH and thus can act as external dopant of PPy (Figure 2-15). The new electrode exhibited improved performance compared with PPy alone when it could increase significantly the power density of MFC [105]. In order to overcome the unsatisfactory stability of PANi modified GF electrode, GO was introduced into PANi/GO composite for the modification of graphite (*Chemshine Carbon CO., China*) by on electrochemical approach [106]. The PANi/GO-GF (Figure 2-14 b, d) enhanced outstandingly the electrochemical activity as well as the hydrophilicity of GF electrode. The stability of new electrode was actually noticeable when after 1000 s, the oxidation current of the PANi/GO modified GF electrode was still higher than that of the PANi modified GF electrode (Figure 2-14 a) because of the synergistic effect of PANi and GO [102]. Moreover, conductive polymers have been combined with CNTs to increase the effective surface area and the electrical conductivity of the resulting material. The PANi was electropolymerized on the surface of GF (*Beijing Sanye Carbon, China*, thickness 4 mm) followed by the EPD of CNTs [107]. Using polymer for the modification of GF electrode is convenient and effective method because it is low-cost approach and improves the electrochemical performance. Modifications such as the above have been extensively used to prepare composite electrodes for capacitive systems for the improvement of capacity storage which makes them promising routes for energy applications.

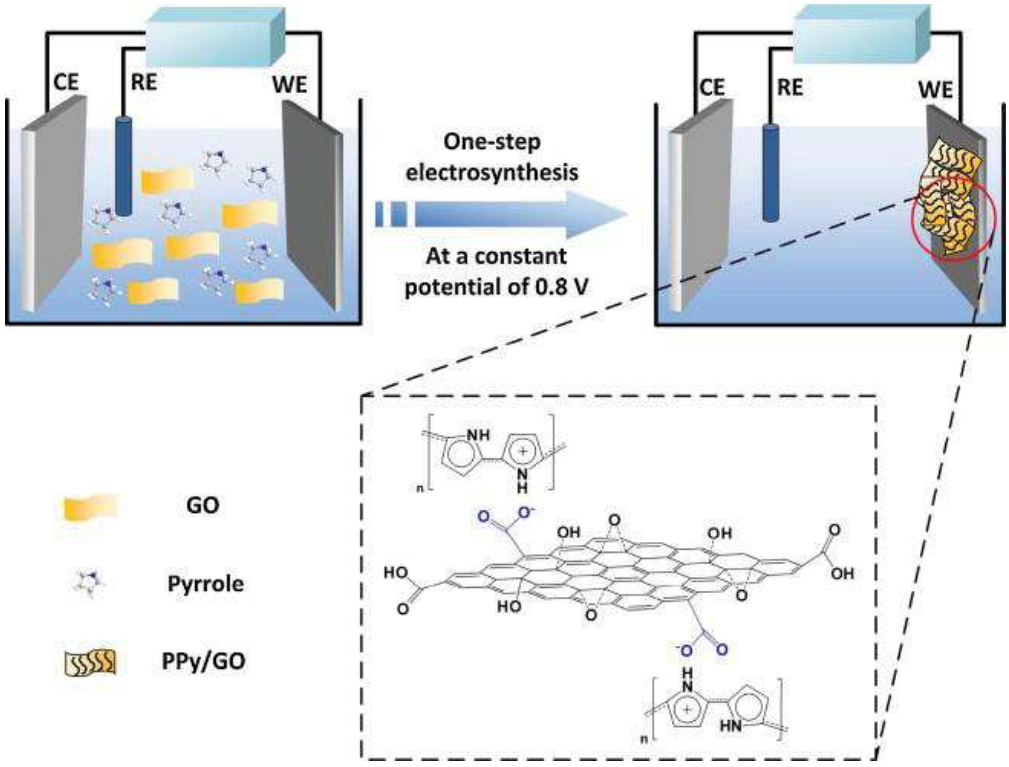

Figure 2-15. The schematic diagram illustrating the one-step electrosynthesis of PPy/GO composites on GF working electrode via electropolymerization of pyrrole while using GO as the anionic dopant [105].

2.5.9. Zeolites based modification

Zeolites are porous crystalline aluminosilicates of SiO_4^{4-} and AlO_4^{5-} tetrahedra connected by oxygen bridges. Zeolite-modified electrodes have numerous applications in various fields especially in electroanalytical chemistry because of the unique molecular sieving properties of zeolites [108]. NaX zeolite was grown up on GF (Figure 2-16 a) during hydrothermal synthesis at 100 °C for 3 h in solution containing sodium silicate, sodium aluminate, and sodium hydroxide with a molar composition of 3.5 Na_2O: 1 Al_2O_3: 2.1 SiO_2: 1000 H_2O. It could been seen clearly from Figure 2-16 d that the GF modified with NaX showed a higher electrochemical activity after ex-situ acclimatization in presence of bacterial in comparison to bare electrodes which proved the interest of the approach for bio-electrodes preparation and used in MFC [109, 110].

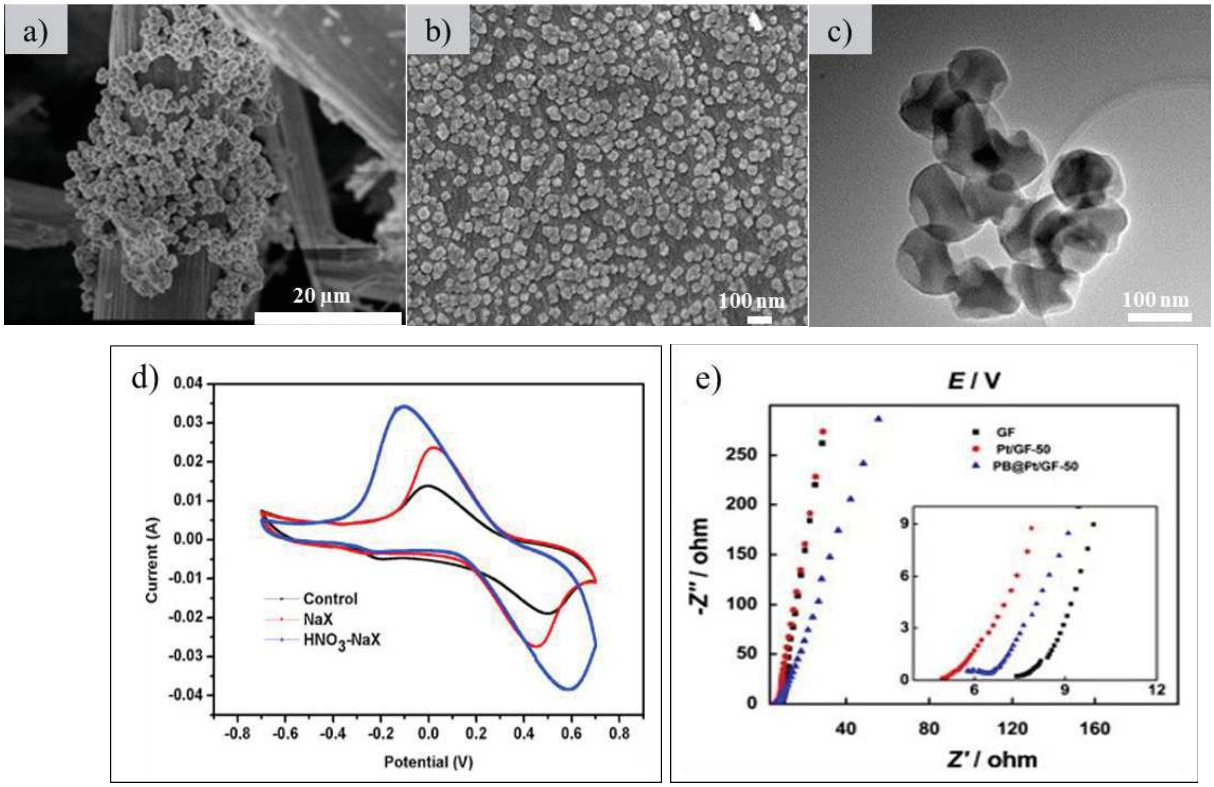

Figure 2-16. Characterization of zeolite based felts. SEM images of (a) HNO_3-NaX/GF, (b) PB@Pt/GF, (c) TEM image of PB nanoparticles, (d) CVs of the three GF electrodes at the end of the ex-situ acclimatization (vs. Ag/AgCl, scan rate of 5 mV/s ranging from −700 mV to +700 mV), and (e) Nyquist plots of GF, Pt/GF-50 and PB@Pt/GF electrodes in 0.5 M KCl aqueous solution [17, 109].

Another kind of zeolite named as Prussian blue (PB, ferric hexacyanoferrate) is also of interest for electrode modification [111, 112]. PB and its analogues are the prototype of a number of polynuclear transition-metal hexacyanometalates, which have an open, zeolite-like structure [112-114]. Its electrochemical behavior was reported for the first time in 1978 by Neff *et al.* [115]. Some years later the PB has attracted extensive attention due to its features relevant to inherent electrochromic [116], electrochemical [117], photophysical [118], as well as molecular magnetic properties [119]. The PB modification on felts electrodes was conducted via the chemical deposition process. Pt was first electrodeposited on GF to increase the conductivity and to render the catalysts for PB growth. Secondly, the Pt/GF electrode was immersed for 60 min into 20 mL of a solution containing 1.0 mM $FeCl_3$, 1.0 mM $K_3Fe(CN)_6$, 0.1 M KCl and 0.025 M HCl. Afterward, the electrode was copiously washed with distilled water and dried at 90 °C for

2 h. This sample was noted as PB@Pt/GF. The SEM images of PB@Pt/GF (Figure 2-16 b) showed clearly the three-dimensional hierarchical macroporous open-pore structure, proving the successful deposition of PB (Figure 2-16 c) on the GF. The magnitude of solution resistance (Rs) obtained for GF, Pt/GF and PB@Pt/GF electrodes are 7.38 Ω, 4.94 Ω and 5.72 Ω, respectively (Figure 2-16 e). The electrochemical stability of the PB@Pt/GF was investigated by submitting each electrode to 150 consecutive voltammetric cycles in 0.5 M KCl solution. PB@Pt/GF electrode showed excellent stability, as no decrease of the current was observed during the 150 cycles [17]. In the other hand, GF electrode was modified by a novel PB and ionic liquid 1-butyl-3-methylimidazolium tetrafluoroborate ([Bmim][BF_4]) via simple method involving GF placed in a ultrasound bath of [Bmim][BF_4] and then in a PB precursor solution. In this case, the immobilization of [Bmim][BF_4] supported the anchoring PB nanoparticles on the surface of the GF [120].

2.5.10. Conclusion on the modification of CF electrodes

It is actually difficult to give a certain answer about the best modification method for felts electrodes. Which method is most suitable depends on the purpose of the fabricated electrodes. For example, for Li-ion battery (LIBs) applications, the CNTs modification is necessary, because the LIBs demand nanostructured electrodes support for the high reversible Li intercalation capacity. CNTs have displayed great potential owing to their novel structural, electrical and mechanical properties [77]. For MFC applications, the biocompatibility is an important key for growing up of bacteria on felts electrode, so the polymer modification will be a wise choice. On the other hand, to create low cost electrodes, we can use simple methods with little need for expensive chemicals like chemical treatment in acid medium. In addition, the different modification methods can be combined to improve the performance of felts materials. Nowadays, this trend of combining methods attracts a lot of attention, especially methods like deposition of both gold particles and graphene [121, 122], polymer with graphene [105] and CNTs with polymer [107]. Briefly, CF electrodes will become more useful with interesting properties depending on various modification methods which can be applied in a wide panel of applications.

2.6. Energy applications of CF-based electrodes

2.6.1. Introduction

In this section, the application of CF – based electrodes in energy field will be discussed, consisting of VRFB, BFC, MFC, capacitors, electrochemical solar energy and Li-ion batteries. The operability of modified electrodes is evident through the comparison with bare electrodes in each issue. Additionally, the felts electrodes produced by different companies or modification methods will be collated and collected for a multidimensional overview about this material.

2.6.2. Vanadium redox flow batteries

VRFB has been considered to be one of the most promising candidates for large scale stationary energy storage applications. VRFB consists of two electrolyte tanks with the electrolytes of V(IV)/V(V) (positive half-cell) and V(II)/V(III) (negative half cell) in acid solution, carbon fabric materials as electrodes and membranes as separators [123, 124]. Carbon and GF-based materials were selected as the most suitable electrodes for both the positive and negative half-cells in the VRFB because of their three-dimensional network structures and specific surface area, as well as high conductivity and chemical and electrochemical stability [23, 125, 126]. Figure 2-17 shows the components of a half-cell in a stack where the electrochemical reaction of vanadium ions occurs on the fiber surface. Multiple cells can be stacked together in series to produce the desired voltage, while current output is determined by the area of the electrodes and membranes. To upgrade the power density and to decrease the size and the cost of a VRFB, it is necessary to develop high-performance of felts electrodes relevant to the electrocatalytic activity, the conductivity, the hydrophilicity and the pore structure [57]. The modified felts can increase the electrochemical activity towards the VO_2^+ /VO^{2+} redox couple by facilitating the electron transfer through the electrode/electrolyte interface for both oxidation and reduction processes [60]. Table 2-5 summarizes activity efficiency of the VRFB using non-modified and modified felts electrodes.

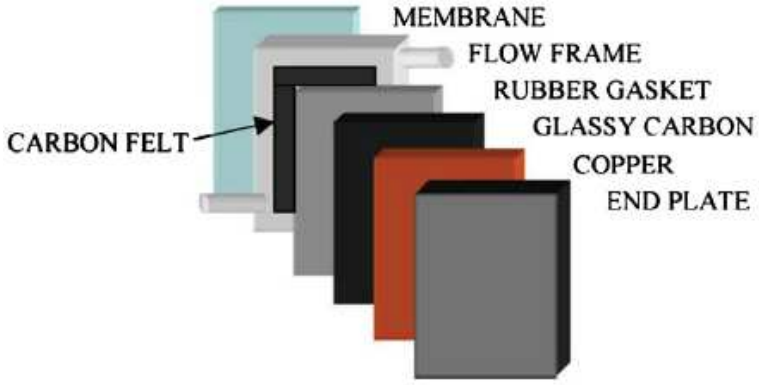

Figure 2-17. Components of a vanadium redox flow cell stack using CF [127].

Table 2-5. The activity efficiency of the VRFB using graphite & CF-based electrodes.

Electrode material		Electrode area (cm^2)	Membrane material	Employed solutions	Current density ($mA\ cm^{-2}$)	Coulombic efficiency (%)	Voltage efficiency (%)	Energy efficiency (%)	Ref.
Rayon- GF [a] (thick 3mm)	The pristine	25 cm^2	CMV (*Asahi Glass Co., Japan*)	2 M V(V) in 4 M H_2S0_4 and 2 M V(II) in *3* M H_2SO_4 for the positive and negative half-cells	40	96.0	77.3	74.2	1993 [29]
	Thermal treatment (400 °C, Air)					98.2	87.2	86.0	
PAN- GF [b] (thick 2.5mm)	The pristine					94.0	80.9	76.2	1993 [29]
	Thermal treatment (400 °C, Air)					94.0	89.3	83.9	
PAN- GF [c]	Electrochemical oxidation in 1.0 M H_2S0_4	12 cm x 18 cm	PE-0 1 cation exchange membrane (*Hangzhou Qianqiu Water Treatment Co., China*)	1.6 M V(III) in 3 M H_2S0_4 at anode 1.6 M V(IV) in 3 M H_2S0_4 at cathode	50	96.48	79.85	77.04	2007 [61]
PAN - CF [c]	The pristine	10 cm^2	Nafion 117 (*DuPont, USA*)	0.5M $VOSO_4$/0.25M $(VO_2)_2SO_4$ as positive electrolyte, and 0.5M VSO_4/0.5M $V_2(SO_4)_3$ in 2M H_2SO_4 as negative electrolyte	20	79.7	80.6	65.0	2007 [66]
	Metalic modification (Ir)					80.6	87.5	69.7	
CF (thick 5 mm)	The pristine	2.5 cm x 2.5 cm	Proton exchange membrane (Nafion 212)	1.5 M VO^{2+} + 2 M H_2SO_4 and 1.5 V^{3+} + 2 M H_2SO_4	20	89.5	87.2		2012 [78]
	CNTs/CF					91.5	90.5		

PAN- CF [d] (thick 4 mm)	The pristine	28 cm^2	Nafion 212 (*DuPont*)	1.5 M $VOSO_4$ + 2 M H_2SO_4	50	90.5	85.2	77.1	2012 [85]
PAN- GF [e], (thick 5 mm)	The pristine	5 cm x 5 cm	Nafion 117 ion exchange	2 M VO^{2+} in 3 M H_2SO_4 at cathode 2 M V^{3+} in 3 M H_2SO_4 at anode	80	90	77	70	2013 [128]
	Electrochemical oxidation in H_2SO_4					91.5	82.5	75	
PAN- GF [d] (thick 6 mm)	The pristine	5 cm × 6 cm	Membrane (*Nepem-1110, Best Industry & Trade Co., Ltd*)	1.5 M V(IV)/3.0 M H_2SO_4 at cathode 1.5 M V(III)/3.0 M H_2SO_4 at anode	60	93.9	72.1	67.7	2013 [129]
	Fenton's Reagent/GF					98.8	75.1	74.2	
PAN- GF	The pristine	25 cm^2	Nafion 117 ®	1 M $VOSO_4$ in 3 M H_2SO_4	20	85	55	47	2013 [130]
	$CuPt_3$ nanoparticles/ GF					99	85	84	
PAN- GF [d] (thick 5mm)	The pristine	3 cm x3 cm	Perfluorinated ion-exchange (*Best Industrial & Trade Co., Ltd., China*)	VO^{2+} (1.2 M)	20	95.18	-	81.03	2015 [28]
	N-dopping					93.50		86.47	
PAN - CF [f] (thick 3mm)	The pristine	5.5cm×6.0 cm	Nafion (*Dupont, N117*)	2M $VOSO_4$ in 2.5M H_2SO_4	40	80.0	85.5	68	2016 [18]
	Thermal treatment (500 °C, Air)					80.0	93.5	75	
PAN- GF [g]	Chemical treatment (KOH)	7 cm × 7 cm	Nafion 115	2 M $V^{3.5+}$ (VO^{2+}/V^{3+} = 1:1) with 2 M H_2SO_4	250	93	69	64	2016 [56]
	0.94 wt.% MWCNTs/CF					93.9	87.3	82.0	
Rayon- GF [h]	The pristine	4 cm^2	Nafion 117 ®	1.0 M $VOSO_4$ in 3.0 M H_2SO_4	25	91.1	91.5	83.3	2016 [75]
	Graphene/GF					99.5	96.3	95.8	

a: Fibre Materials, Inc., Maine, USA;
b: Sigri Electrographit GmbH, Germany;
c: Shanghai Energy Carbon Limited Co., China;

d: Shenhe Carbon Fiber Materials, Co. Ltd., Liaoning China;
e: Shanghai Qijie Limited Co., China;
f: Nippon Chem. GF-3F;
g: Gansu Haoshi Carbon Fiber Co., Ltd.;
h: RVG-2000, Societe Carbon-Lorraine

- Coulombic efficiency (CE):

$$CE = \frac{\int i_{discharge}(t)dt}{\int i_{charge}(t)dt}$$

- Voltage efficiency (VE):

$$VE = \frac{\int V_{average\ discharge}}{\int i_{average\ charge}}$$

- Energy efficiency (EE):

$$EE = CE \times VE$$

Table 2-5 confirms that the battery performance was improved significantly by surface modifications compared with the untreated carbon materials. In a VRFB system where the electrolyte was charged at 1.8 V with a cut-off current inferior to 100mA, using CF (*PAN, Nippon Chem. GF-3F*, thickness 3mm) electrode modified by oxygen plasma treatment could improve both the energy efficiency and discharge capacity. The columbic efficiency (CE) for plasma treated electrodes remained almost constant throughout the galvanostatic cycling (98-100%) [3]. The energy efficiency of a VRFB was also ameliorated by 14% at a current density of 80 mA cm^{-2}, by using treated GF (*C0S1011,CeTech, Taiwan*, thickness 6mm) with APPJs [51]. In another study by Wang *et al.*, the energy efficiency of the as-assembled VRFB was 8.8% higher compared to that on pristine GF with excellent cycling stability by using nitrogen-doped CNTs due to the enhancement of interaction of felts and electrolyte during the battery operation [79]. Significant improvement in energy efficiencies were well observed in cell charge−discharge cycling tests after thermal or acid treatment of the GF (*Fibre, Material Inc., U.S.A*., thickness 3mm). The cell resistance apparently dropped after treatment, leading to a higher average coulombic efficiency at 95.6% instead of 91.6% for untreated felts at a current density of 25 mA cm^{-2}. Furthermore, the voltage efficiency still remained high at a value of 83.0% even at a current density of 60 mA cm^{-2} and after a total of 90 cycles on modified electrodes [54]. The electrocatalyst introduction of noble metals on the surface of felts enhances the electro-conductivity of electrode materials, which reduces the reaction over potential of vanadium ion redox couples. The resistance of the cell using Ir-modified CF (*Shanghai carbon works*) decreased by 25% compared to the cell using non-modified felt [66]. Besides that, the performance of a VRFB with flow fields (Figure 2-18) was improved in comparison with the VRFB without flow fields using GF (*SGL GmbH, Germany*, 3 mm thickness). It was demonstrated that the battery with flow fields has a higher discharge voltage at higher flow rates, but exhibits a larger pressure drop. The energy efficiency for the VRFB with the flow fields was better than that without the flow fields, implying that the inclusion of flow fields in a VRFB could be an effective approach for improving the system efficiency [131]. Actually, upgrading the power density of VRFB using CF electrodes is still a fascinating topic for VRFB in the future.

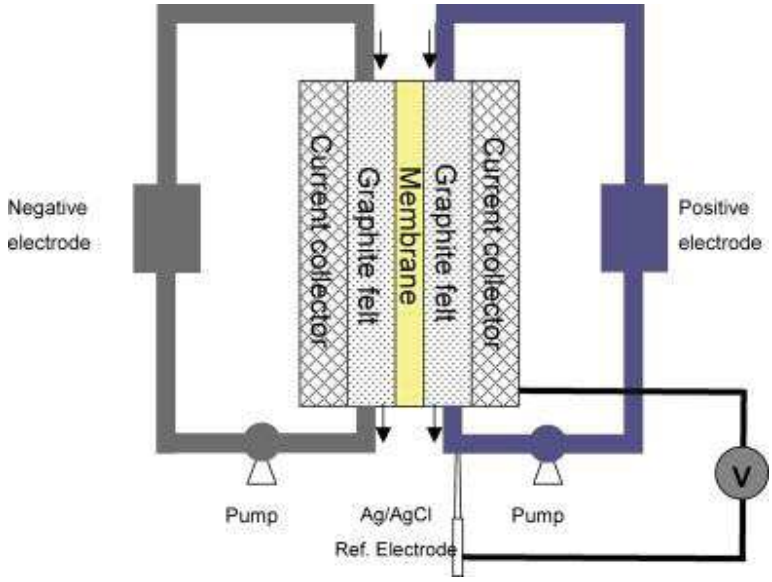

Figure 2-18. Schematic of a VRFB with flow fields using GF electrode [131].

2.6.3. Biofuel cells

BFC is a device which converts the energy conserved in organic and inorganic materials into electrical energy with the help of enzymes or living cells [132, 133] . To develop the power density of BFCs, it is very important to improve direct electron transfer (DET) between the redox enzymes and electrodes [134]. Therefore, the choice of suitable electrodes to meet electronic properties as well as high loading of redox enzymes is essential [135, 136]. Laccase enzyme was adsorbed on three-dimensional GF (*Alfa Aesar, Karlsruhe, Germany*) for the oxygen reduction activity in BFC [137]. The NAD^+-dependent alcohol dehydrogenase and laccase were electrochemically deposited onto the CF, to form the anode and cathode for single-chamber ethanol/O_2 BFC. The open-circuit voltage of this BFC was 860 mV. The maximum power density of the BFC was 1.56 mW cm^{-2}. Specially, this BFC was able to work when the alcoholic beverage acted as the fuel [138]. Moreover, the CF was employed as electrodes for a sucrose/O_2 BFC. Bio-anodes were fabricated by immobilization of four kinds of enzymes namely, invertase, mutarotase, glucose oxidase, and fructose dehydrogenase through cross-linking by glutaraldehyde. Multi-copper oxidase enzyme, BOD, with entrapment of 2,2'-azino-bis(3-ethylbenzothiazoline-6-sulphonic acid) (ABTS), an efficient mediator, coated on CF was applied as bio-cathode for the oxygen reduction. This BFC showed a maximum power density of 2.90 mW cm^{-2} recorded at 0.30 V. The electrochemical performance of bio-anodes was also compared to electrodes on substrates using glassy carbon disk and CF, modified with an adequate amount

of CNTs. Thanks to the good conductivity of the obtained CNTs/CF bioanode, it shows a remarkable enhancement of anodic current on CVs curve [139]. A H_2/O_2 BFC was constructed by using CF (*Toray B0050 carbon felt mat,Toray Co.*) as an electrode material for both the anode and the cathode. The electro-enzymatic reactions at the felt electrodes were stable for both the oxidation of dihydrogen at anode and the reduction of dioxygen at the cathode, generating a cell voltage around 1.17 V at open circuit [140].

Polymer-modified felts were also employed in BFCs. Poly(methylene green) was coated on CF (Alfa Aesar) by electropolymerization applying a potential from −0.3 to 1.3 V for 12 sweep segments at a scan rate of 0.05 V/s in a solution containing 0.4 mM methylene green and 0.1 M sodium nitrate in 10 mM sodium tetraborate. Bio-anode was fabricated by immobilization a layer of tetrabutylammonium bromide salt-treated Nafion with dehydrogenase enzymes on the modified CF. A power density of 1.16 mW cm^{-2} was monitored by using this bio-anode and gas diffusion cathode in an ethanol/O_2 BFC. The bio-anode could operate continuously for more than 30 days, proving the good capacity of felts material for loading of enzyme to produce the energy in the BFCs system [141].

2.6.4. Microbial fuel cells

MFC has been considered as a renewable energy source where the chemical energy can be transferred directly into electrical energy though oxidization of organic substrates by electroactive bacteria. The configurations of MFCs are built up from two-chamber reactors which are separated by the proton exchange membrane (Figure 2-19). The MFCs's power can be generated from the oxidation of organic matter by bacteria at the anode for oxygen reduction at the cathode [142]. CF based electrodes are commonly used in MFCs because they are inexpensive. The electrogenic bacteria can readily attach to the felts anchoring functional groups on the surface like carboxylic acids, alcohols, and quinones because of their similarity with the natural habitat of bacteria [143]. The high conductivity of felts allows the bacteria to dispose of their waste electrons more easily [62]. The felts electrodes used in this field can be listed as CF (*Alfa Aesar*, thickness 3.18 mm) [144], GF (*Xuesheng Technology Co. Ltd., China*, thickness 2 mm) [145], GF (*Hunan Jiuhua Carbon Hi-Tech Co., Ltd., China*, thickness 5 mm) [109, 110], GF (*RVG, Carbone Loraine, France*) [146], GF (*Sanye Carbon Co., Ltd.)* [62], CF (*US Morgan*, thickness 2 mm) [147], CF (*Soft felt SIGRATHERM GFA5, SGL Carbon, Germany*) [58], GF

(*Beijing Sanye Co., Ltd.*, thickness 5 mm) [71, 107, 148] and CF (*Shanghai Qijie Carbon Co., Ltd.*) [70].

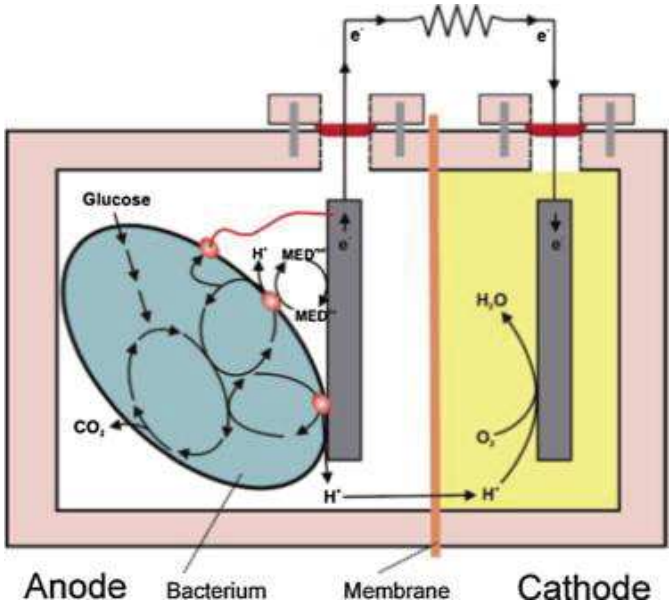

Figure 2-19. MFC configuration [149].

The high electrical generation and good stability are two important keys for MFCs. In terms of these points, different kinds of modified felts were applied for both cathode and anode. For example, the power densities for both abiotic cathodes increased by 300% and biocathodes increased by 180% in MFC using CF (*4 cm × 3 cm × 0.3 cm*) modified by poly (aniline-1, 8-diaminonaphthalene). With the help of conductive polymer coating, the cathode biofilm became thicker and less sensitive to the dissolved oxygen as well as pH change in cathodic compartment, and provided better attachment condition for biofilm which endowed them higher power output [101]. With the aim to improve electron transfer between the microorganisms and the anodes, felts materials owning good biocompatibility have been investigated. The MFC equipped with the PPy/GO modified GF (*Beijing Sanye Co.Ltd*) anode showed a maximum power density of 1326 mW m^{-2} which was significantly larger than that associated with the unmodified GF anode (166 mW m^{-2}). After 120 cycles of lactate feeding, the PPy/GO-GF anode exhibited good stability without noticeable performance degradation [105]. CF (*Liaoyang Jingu Carbon Fiber Sci-Tech Co., Ltd., China*, thickness 5 mm) anode was renovated by immobilization of PPy/anthraquinone-2,6-disulphonic disodium salt (PPy/AQDS) on its surface. The MFC operated with this modified anode showed the maximum power density of 1303 mW m^{-2}, which was 13 times larger than that obtained from the MFC equipped with an unmodified anode [150]. The

coating of CNTs/PANi film on GF electrode (*Beijing Sanye Co.Ltd*, thickness 4 mm) attained an output voltage of 342 mV across an external resistor of 1.96 kΩ constant load, and a maximum power density of 257 mW m^{-2}, increased by 343% compared to that of the pristine GF MFC [107]. Finding cathode and anode materials that exhibit enhancement properties for MFCs is a crucial problem, and is attracting a lot of attention in research and development fields.

2.6.5. Capacitors - supercapacitors

The excellent electronic performance of the modified CF makes them interesting for capacitor and supercapacitor. An electric double-layer capacitor was fabricated from growth nanocrystalline diamond (NCD) film on CF using a hot-filament CVD method. In this case, CF became an innovative material to create porous diamond electrode with large surface area that helped to increase the capacitive response. The NCD/CF composite treated at 1300 K presented around 8 % of oxygen on the surface which improved the wettability and made it easier for the electrolyte ion to access the micropores of electrodes material. This led to a decrease of the internal resistance and an increase in the useable surface area increasing the specific capacitance and energy availability. Therefore, the highest specific capacity was identified at 2.6 mF cm^{-2} for the NCD/CF-1300 K [151]. A new supercapacitor electrode was fabricated by introducing graphene/MnO_2 composites into activated carbon fiber felt (*Shenzhou Carbon Fiber Co., Ltd, China.*, thickness 3 mm). It showed a high specific capacitance up to 1516 mF cm^{-2} in neutral electrolytes and excellent cycling stability with no capacitance decay after 5000 charge - discharge cycles [152]. The GF modified by PPy/MnO_2 composites could be also used as a free-standing electrode for supercapacitors. This electrode displayed specific capacitance as high as 821.3 F g^{-1} at the current density of 0.5 A g^{-1}. The PPy/MnO_2 composites deposited on GF constructed a unique three-dimensional network structure that facilitated the easy access of electrolyte to the composites and leading to enhancement of the capacitive performance [153]. Another flexible supercapacitor electrode was produced through the synthesis of tubular MnOOH on GF. The MnOOH/GF revealed an outstanding energy-storage behavior with a high energy density of 1125 W h kg^{-1} and a power density of 5.05 kW kg^{-1} [154].

2.6.6. Electrochemical solar cells

Solar energy plays a vital type of renewable energy because of its inexhaustible nature, environmental friendliness, and the potential for high power conversion efficiency in solar energy

harvesting devices [155, 156]. Some photosynthetic microorganisms like cyanobacteria have been used to convert directly solar energy into electric energy in an electrochemical cell [157-159]. In a photosynthetic bio-electrochemical cell (Figure 2-20), at the anode, cyanobacteria, *Synechococcus* sp. PCC7942, were used as a photosystem. The electrons were produced from photo-oxidation of water under support of the cyanobacteria catalyst. After that, the electron was transferred to a CF (CF, *Toray Co., Tokyo, Japan*, thickness 1 mm) anode through the mediator, 2,6-dimethyl-1,4-benzoquinone (DMBQ) or diaminodurene (DAD). At the CF cathode, water was regenerated from dioxygen reduction through 2,2′-azinobis(3-ethylbenzothiazolin-6-sulfonate) ($ABTS^{2-}$) as a mediator and bilirubin oxidase (BOD) as a biocatalyst. The maximum electric power was about 0.3–0.4 W m^{-2} for the projective electrode surface area at an apparent efficiency of the light energy conversion of 2–2.5% [160].

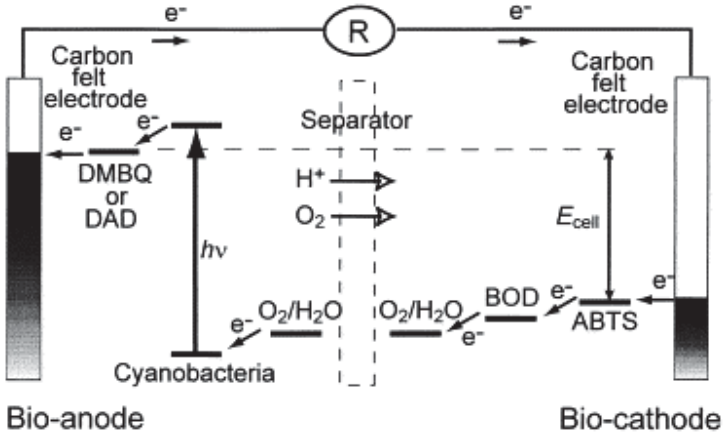

Figure 2-20. Schematic representation of the principle of the photosynthetic bioelectrochemical cell using CF electrodes [160].

2.6.7. Lithium ion batteries

Discovered in 1990s by Sony Corporation, Li-ion batteries (LIBs) have become the leading batteries in category of energy storage owing to their high power and energy density [161]. The behavior of CF electrode modified by CNTs (CNT/CF) for energy storage was analyzed on the basis of lithium intercalation. The CNT/CF could be defined as a three-dimensional web of electronic conductive carbon fiber with excellent mechanical properties. The double-layer capacitance for CNT/CF was 40.3 μF cm^2 at 10 mA of polarization current using 1 mol L^{-1} $LiPF_6$ in mixtures of ethylene carbonate and dimethyl carbonate. The reversible specific capacity was found to remain stable over 50 cycles of discharge/charge [39], proving that

the modified felts electrodes will be promising material for electrochemical devices. In addition, the CF cathode after borax treatment was used in lithium-air batteries [162].

2.6.8. Conclusion on energy applications of CF-based electrodes

CF-based electrodes were popular for vanadium redox flow batteries from the early years of VRFB (1993). The aim of these studies was to lower the cost of VRFB, so cheaper modification methods like chemical treatments were often chosen. Recently, some other modification methods that use graphene or CNTs have been developed and the results are impressive. We also observed similar developments in the field of MFC. However, for capacitors, supercapacitors, electrochemical solar cells or Li-ion batteries, felts electrodes have seen little exploitation yet. For application of felts electrodes in these fields, the choice of modification is highly important, because these applications demand nanostructured electrodes with considerable conductivity. Therefore, these new fields will be a fertile ground for future studies to develop new applications of CF-based electrodes.

2.7. Application of CF-based electrodes for wastewater treatment by EF process

2.7.1. Introduction

For environmental application, CF-based electrodes were used for different purposes like electrochemical reduction of heavy metals [163, 164], electrically swift ion exchange (ESIX) [104], electrosorption desalination [165], *etc*. In this study, we will focus on the application of felts electrodes for the wastewater treatment containing POPs by EF process. The CF-based electrodes once again proved their benefits when they were applied as cathodes during EF process to eliminate POPs in aqueous medium. First of all, an overview about EF process was understood to highlight the advantages of this technology for wastewater treatment. After that, the felts cathodes were applied to remove different kinds of POPs. In this part, we summarized the treatment efficiency by EF method using various CF-based cathodes since the year 2000. At the same time, the mineralization current efficiency (MCE), the degradation pathway, and the toxicity of treated solutions were discussed in detail. Finally, new EF systems that improve treatment efficiency and decrease the consumption costs were selected. Towards these targets, we focused both on modified cathodes to upgrade the hydrogen peroxide production and on new catalysts. Importantly, novel EF configurations in which electrons were driven by a FC using

modified CF will be presented as a clean and green route for the mineralization of biorefractory pollutants.

2.7.2. EF process

Electrochemical advanced oxidation processes (EAOPs) based on Fenton's reaction chemistry are emerging technologies for water remediation. The Fenton reaction has some limitations in application such as the use of a large quantity of chemical reagents, a large production of ferric hydroxide sludge, and a very slow catalysis of the ferrous ions generation. Therefore, it was suggested that the Fenton reaction can be performed catalytically via electrochemistry [26]. Over the past decade, EAOPs have experienced significant developments, showing great efficiency for the decontamination of wastewater polluted with toxic and persistent pesticides, organic synthetic dyes, pharmaceuticals and personal care products, and a great deal of industrial pollutants. The most popular technique among them is the EF process (Figure 2-21), in which H_2O_2 is generated continuously at the cathode with O_2 or air feeding through oxygen reduction reaction (ORR) (Eq. (2-11)) while an iron catalyst (Fe^{2+}, Fe^{3+}, or iron oxides) is added to the effluent. Both iron and hydrogen peroxide react together to generate hydroxyl radicals, mainly oxidant for the treated solution, as shown in the following equations:

$$O_2 + 2H^+ + 2e^- \rightarrow H_2O_2 \quad E^0 = 0.695 \text{ V / SHE} \qquad (2\text{-}11)$$

$$Fe^{2+} + H_2O_2 \rightarrow Fe^{3+} + \bullet OH + OH^- \qquad (2\text{-}12)$$

Since this reaction takes place in acidic medium, it can alternatively be written as:

$$Fe^{2+} + H_2O_2 + H^+ \rightarrow Fe^{3+} + \bullet OH + H_2O \qquad (2\text{-}13)$$

Simultaneously, the Fe^{2+} ions were generated by reduction of ferric ions possibly introduced initially as catalyst to the solution to be treated [166]:

$$Fe^{3+} + e^- \rightarrow Fe^{2+} \quad E^0 = 0.77 \text{ V / SHE} \qquad (2\text{-}14)$$

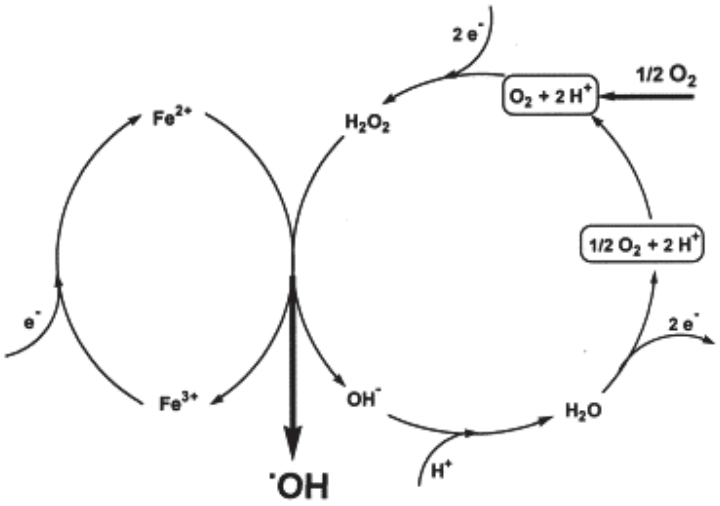

Figure 2-21. Schematic presentation of the electrocatalytic production of hydroxyl radicals by the EF process [167].

The major advantages of this indirect electro-oxidation method compared with the chemical Fenton process are as follows: (i) the on-site production of H_2O_2 because it avoids the risks related to its transport, storage, and handling, (ii) the possibility of controlling the degradation kinetics to allow mechanistic studies, (iii) the higher degradation rate of organic pollutants because of the continuous regeneration of Fe^{2+} at the cathode, which also minimizes sludge production, and (iv) the feasibility of overall mineralization at a relatively low cost if the operation parameters are optimized [1].

2.7.3. CF for EF process

CF are the electrode material of choice for EF process (Figure 2-22). Used as electrode in EF technology, they exhibit outstanding properties like: (i) high specific surface area, good mechanical integrity, commercial availability, and efficient cathodic regeneration of Fe^{2+} ($Fe^{3+} + e^- \rightarrow Fe^{2+}$, Eq. (2-14)), which make them an attractive cathode material for EF process [64, 168]; (ii) Adaptable to many various EF systems with different shapes as well as areas of electrodes from small (2 cm^2) to large size (60 cm^2) [166, 169]; and (iii) its physico-chemical stability allows to decline significantly the cost for the EF technology, since it can be continuously used for many cycles (at least 10 cycles) without any decrease of the treatment efficiency.

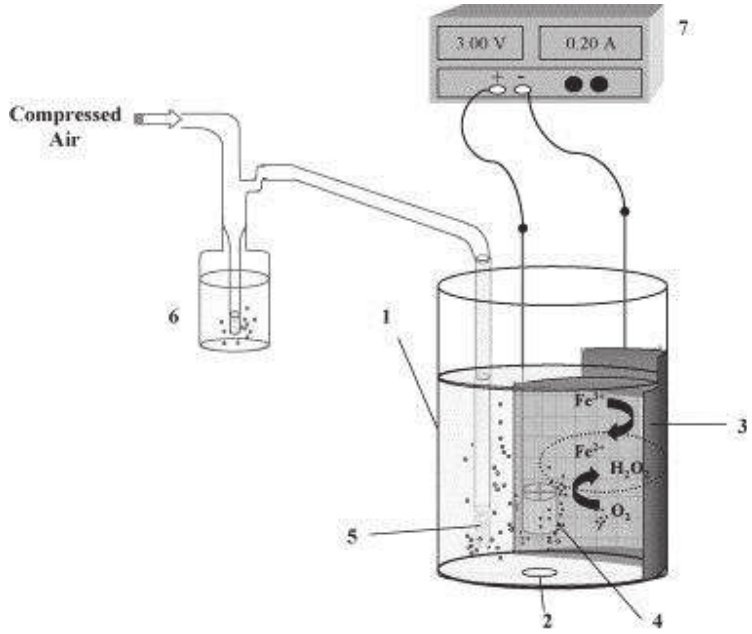

Figure 2-22. Scheme of the experimental set-up used for the EF treatments using CF cathode. (1) Open undivided electrolytic cell containing the treated malachite green solution, (2) magnetic stir bar, ***(3)*** CF cathode, (4) anode (Pt, Ti, *etc*), (5) compressed air diffuser, (6) air drying solution and (7) potentiostat–galvanostat [170].

Table 2-6. Removal of POPs by EF process on graphite & CF-based cathodes in stirred tank reactor at 25 °C.

Cathode material	Geometric surface dimension (cm x cm)	Anode material	Pollutants	Solution	Applied current (mA) or potential (V)	Electrolysis time	Oxidation rate constant	% TOC removal	Ref.
CF lt[a] as working electrode (three-electrode cell)	10 cm^2	1 cm^2 Pt as counter electrode and saturated calomel electrode (SCE) as reference electrode	2,4-dichlorophenoxyacetic acid	125 mL solution with 1 mM of pollutant, 1 mM Fe^{3+}, pH 2.	60 mA	550 min	10^{10} M^{-1} s^{-1}	95	2000 [11]
CF [a] as working electrode (three-electrode cell)	10 cm^2	1 cm^2 Pt as counter electrode, and saturated calomel electrode (SCE) as reference electrode	Pentachlorophenol	125 mL solution with 0.03 mM of pollutant, Mohr salt, pH 3.	50 mA	500 min	3.6 x 10^9 M^{-1} s^{-1}	82	2001 [167]
CF	Pt		Diuron	125 mL solution of 40 mg L^{-1} pollutant with 0.5 mM Fe^{3+} in H_2SO_4 of pH 3.0	100 mA	3 h	4.8 x 10^9 M^{-1} s^{-1}	93	2003 [171]
CF [a]	10 cm^2	1 cm^2 Pt	Pentachlorophenol	125 mL solution with 0.21 mM of pollutant, 0.5 mM Fe^{2+}, pH 3.	200 mA	7 h	3.6 x 10^9 M^{-1} s^{-1}	95	2005 [172]
CF [a]	17 cm × 3.5 cm	4.5 cm^2 Pt	methyl parathion	150 mL solution with 0.20 mM of pollutant in 0.05 M Na_2SO_4 and 0.1 mM Fe^{2+}, pH 3.	150 mA	9 h	(4.20 ± 0.11) x 10^9 M^{-1} s^{-1}	~ 100	2007 [173]
CF [a]	17 cm × 4.1 cm	3 cm^2 BDD	chlorophene	250 mL solution with 84 mg L^{-1} of pollutant in 0.05 M Na_2SO_4 and 0.2 mM Fe^{3+}, pH 3.	300 mA	6 h	(1.00 ± 0.01) x 10^{10} M^{-1} s^{-1}	~ 100	2007 [174]

CF [a]	60 cm^2	5.5 cm^2 Pt	Direct orange 61 (DO 61)	500 mL solution with 0.53 mM of pollutant in 0.05 M Na_2SO_4 and 0.1 mM Fe^{2+}, pH 3.	250 mA	6 h	$(2.06 \pm 0.14) \times 10^{10}$ M^{-1} s^{-1}	98	2007 [169]
CF (thick 0.6 cm)	6 cm × 8 cm	Pt grid	Phenol	150 mL solution with 1.0 mM of pollutant in 0.05 M Na_2SO_4 and 0.1 mM Fe^{2+}, pH 3.	300 mA	7 h	$(2.62 \pm 0.23) \times 10^{9}$ M^{-1} s^{-1}	100	2008 [175]
CF [a]	60 cm^2	35 cm^2 BDD	AO7	500 mL solution with 0.53 mM of pollutant in 0.05 M Na_2SO_4 and 0.1 mM Fe^{2+}, pH 3.	250 mA	9 h	$(1.10 \pm 0.04) \times 10^{10}$ M^{-1} s^{-1}	98	2008 [176]
CF [a]	60 cm^2	Pt 4.5 cm height cylindrical grid (i.d. = 3.1 cm)	Herbicide chlortoluron	500 mL solution with 0.125 mM of pollutant in 0.05 M Na_2SO_4 and 0.1 mM Fe^{3+}, pH 2.8–3.	300 mA	8 h	$(4.8 \pm 0.2) \times 10^{9}$ M^{-1} s^{-1}	98	2008 [166]
CF [a]	15 cm × 4 cm	4.5 cm^2 Pt	Malachite green	250 mL solution with 0.5 mM of pollutant in 0.05 M Na_2SO_4 and 0.2 mM Fe^{3+}, pH 3.	200 mA	540 min	0.244 min^{-1}	~ 100	2008 [170]
CF [a]	15 cm × 4 cm	4.5 cm^2 Pt	Triphenylmethane dyes (malachite green, crystal violet, methyl green, fast green FCF)	250 mL solution with 0.5 mM of pollutant in 0.05 M Na_2SO_4 and 0.2 mM Fe^{3+}, pH 3.0	400 mA	> 25 h	$(1.31\text{-}2.65) \times 10^{9}$ M^{-1} s^{-1}	~ 100	2008 [177]
CF	17 cm×3.5 cm	Pt gauze	AO7	225 mL solution with 0.1 mM of pollutant in 0.05 M Na_2SO_4 and 0.1 mM Fe^{3+}, pH 3.	300 mA	8 h	$(1.20 \pm 0.17) \times 10^{10}$ M^{-1} s^{-1}	92	2009 [178]
GF [a] (thick 0.5 cm)	15 cm × 4 cm	BDD 4.5 cm height cylindrical grid (i.d. = 3.1 cm)	Alizarin Red S	250 mL solution with 200 mg L^{-1} of pollutant in 0.05 M Na_2SO_4 and 0.2 mM Fe^{2+}, pH 3.0	300 mA	210 min	4.92×10^{-4} s^{-1}	95	2011 [6]

Graphite sheet[a]	15 cm^2	Graphite sheet (Carbon Lorraine, France)	Azure B	150 mL solution with 4.83 mg L^{-1} of pollutant in 0.05 M Na_2SO_4 and 8.69 g iron alginate gelbeads (FeAB), pH 2.0	14.19 V	30 min	0 .1865 min^{-1}	89	2012 [179]
GF [a] (thick 0.5 cm)	10 cm x 7 cm	Ti/RuO_2 net 4.5 cm height cylindrical grid (i.d = 3.1 cm)	p-coumaric acid	300 mL solution with 1 mM of pollutant in 0.05 M Na_2SO_4 and 0.3 mM Fe^{2+}, pH 3.0	300 mA	360 min	0.0833 min^{-1}	95	2012 [180]
CF [b]	16 cm × 7 cm	RuO_2–IrO_2	Orange II	200 mL solution with 50 mg L^{-1} of pollutant in 0.05 M Na_2SO_4 and 0.2 mM Fe^{3+}, pH 3.0	1.78 mA/cm2	90 min	0.568 mg L^{-1} min^{-1} for H_2O_2 production	94.3	2014 [13]
GF [c] (thick 0.5 cm)	5 cm × 2 cm (undivided three-electrode cell)	Pt wire as counter electrode and a SCE as reference electrode (undivided three-electrode cell	p-nitrophenol	130 mL solution with 50 mg L^{-1} of pollutant in 0.05 M Na_2SO_4 and 0.2 mM Fe^{3+}, pH 3.	0.65 V	2 h	-	22.2	2014 [64]
Graphite sheet[a]	11 cm^2	BDD (DiaChem, Germany)	Imidacloprid	150 mL solution with 100 mg L^{-1} of pollutant in 0.05 M Na_2SO_4 and 4.27 g iron alginate gelbeads (FeAB), pH 2.0	5 V	4	0.0445 min^{-1}	90 (Imidacloprid removal)	2014 [181]
GF [a] (thick 0.5 cm)	60 cm^2	6cm^2 BDD	4-amino-3-hydroxy-2-p-tolylazo-naphthalene-1-sulfonic acid) (AHPS)	200 mL solution with 175 mg L^{-1} of pollutant in 0.05 M Na_2SO_4 and 2 g L^{-1} pyrite pH 3.0	300 mA	8	0.33 min^{-1}	~100	2015 [182]
CF [a]	60 cm^2	6 cm^2 BDD	Tyrosol	200 mL solution with 0.30 mM (41 mg L^{-1})	300 mA	6	3.57 x 10^9 M^{-1} s^{-1}	90	2015 [183]

				of pollutant in 0.05 M Na_2SO_4 and 1.0 g L^{-1} pyrite pH 3.0					
CF [a]	60 cm^2	6 cm^2 BDD	Levofloxacin	200 mL solution with 0.23 mM of pollutant in 0.05 M Na_2SO_4 and 1.0 g L^{-1} pyrite pH 3.0	300 mA	8	2.5 x 10^{-4} s^{-1}	95	2015 [184]
GF [a] (thick 0.5 cm)	17.5 cm × 5 cm	24 cm^2 BDD (CONDIAS GmbH, Germany)	Sul-famethazine	solution with 0.25 mM of pollutant in 0.05 M Na_2SO_4 and 0.2 mM Fe^{2+}, pH 3.0	1000 mA	6	2.9 x 10^9 M^{-1} s^{-1}	98.5	2016 [185]
CF [a] (thick 0.5 cm)	14 cm x 5 cm	BDD (5 x 4 cm, DIACHEM®)	Norfloxacin	175 mL solution with 0.25 mM of pollutant in 0.05 M Na_2SO_4 and 0.1 mM Fe^{3+}, pH 3.0	300 mA	5	(1.34 ± 0.03) x 10^9 M^{-1} s^{-1}	97.7	2016 [186]
CF [a]	17.5 × 6 cm	25 cm^2 BDD	Sucralose	220 mL solution with 0.2 mM of pollutant in 0.05 M Na_2SO_4 and 0.2 mM Fe^{2+}, pH 3.	200 mA	2 h	-	96.1	2017 [187]
CF	70 cm^2	BDD (5 x 4 cm, DIACHEM®)	Enoxacin (ENXN)	175 mL solution with 0.25 mM of pollutant in 0.05 M Na_2SO_4 and 0.3 g Fe_2O_3-KLN (kaolin), pH 3.0	300 mA	7	1.24 (±0.04) x 10^9 M^{-1} s^{-1}	98	2017 [188]

a: Carbone- Lorraine;
b: Jilin Zhongxin Carbon Fiber,Co., Ltd. China;
c: Shang-hai Qijie Carbon material Co.,Ltd;
TOC: Total Organic Carbon

The review for the mineralization of biorefractory pollutants by EF process using felts cathodes is summarized in Table 2-6. From statistical results, we can see that application of EF technology for elimination of POPs on CF cathodes has been preceded very early by Oturan and co-workers. One of their first papers in 2000s described the EF process in divided cell. The working electrode was a 10 cm^2 piece of CF (*Carbone-Lorraine*). A SCE (E = 0.242 V *vs* NHE) from Radiometer was used as reference electrode. The counter electrode was a 1 cm^2 Pt sheet (Radiometer) which was placed in a cylindrical anodic compartment separated from the cathodic compartment by a glass frit. By this system, almost total mineralization (>95% TOC decay) of 1 mM of the phenoxyacetic herbicide 2,4-D after consuming 2000 C was observed [11]. Afterward, they continued developing their research using an undivided cell with two electrodes by combination of CF cathode and Pt anode for the degradation of the herbicide diuron. A very high efficiency attainted 93 % TOC removal at 1000 C for 125 mL solution containing 40 mg L^{-1} diuron has been reported [171]. From that, a series of studies using EF technology for water treatment on felts cathodes have been conducted to eliminate many different kinds of POPs in aqueous medium, including:

(1) Dye pollutants: 95% TOC of the anthraquinone dye Alizarin Red S was removed in 210 min of electrolysis on GF (*Carbone-Loraine*, thickness 0.5 cm)/Boron-Doped Diamond (BDD) [6]. A mixture containing four triphenylmethane dyes, namely malachite green, crystal violet, methyl green and fast green FCF, with initial COD ca. 1000 mg L^{-1} was totally depolluted with efficiency near 100% at the beginning of the treatment on CF (*Carbone-Lorraine*) [177]. Other dyes were also investigated like malachite green [170], DO 61 [169] and AO7 [176, 178].

(2) For phenolic type compounds: 100% of TOC of aqueous phenol solutions was eliminated by EF process using CF cathode [175]. After 360 min of electrolysis, 95% TOC of the p-coumaric acid (4-hydroxycinnamic acid) was removed on GF (*Carbone-Loraine*, thick 0.5 cm)/Ti-RuO_2 [180]. Pentachlorophenol [167, 172], Bisphenol A [189] are also in this group.

(3) The EF treatment has also been successfully applied to mineralize the herbicides and pesticides such as chlortoluron [166], 4-chloro-2-methylphenol (PCOC) [190], chlorophenoxy acid [10-12] and methyl parathion [173].

(4) Chlorophene [174], triclosan and triclocarban [9] were examples for pharmaceuticals pollutants which have been degraded efficiently by EF process using felts materials.

In 2016, Özcan *et al.* reported a very high mineralization ratio (97.7%) for norfloxacin (NFXN) which has been reached after 5 h electrolysis on CF (*Carbone-Lorraine, France*,

thickness 0.5 cm). Oxidation kinetics of NFXN has been evaluated and the second order oxidation rate constant was determined as (1.34 ± 0.03) x 10^9 M^{-1} s^{-1}. A very high formation rate was observed for all carboxylic acids in the case of BDD/CF electrode combination whereas the preliminary formation rates of carboxylic acids were low for Pt (gauze)/CF [186]. In 2017, a study for elimination of artificial sweeteners sucralose (SUC) from water was carried out for the first time by EF treatment using CF (17.5 × 6 cm, *Carbon-Lorraine*, France) cathode. The mineralization current efficiency (MCE) was calculated from Eq. (2-15) [191]. MCE value for total conversion of SUC into CO_2 and inorganic ions were determined at 20.17% after 60 min of electrolysis for BDD/carbon-felt cell with an applied current of 200 mA [187].

$$\text{MCE (\%)} = \frac{nFV_s\Delta(TOC)_{exp}}{4.32\times10^7 mIt} \times 100 \quad (2\text{-}15)$$

where n is the number of electrons consumed in the mineralization of the pollutant, F is the Faraday constant (96487 C mol^{-1}), Vs is the solution volume (L), Δ(TOC)exp is the experimental TOC decay (mg L^{-1}), 4.32 × 10^7 is a conversion factor (3600 s h^{-1} × 12000 mg carbon mol^{-1}), m is the number of carbon atoms in the pollutant molecule, I is the applied current (A), t is the electrolysis time (h), and n is the number of electrons consumed for mineralization For example it is 48 for Sucralose, according to the stoichiometric balance of reaction (2-16):

$$C_{12}H_{19}Cl_3O_8 + 16H_2O \rightarrow 12CO_2 + 51H^+ + 3Cl^- + 48e^- \quad (2\text{-}16)$$

The EF process can degrade and finally mineralize organic pollutants to less toxic and non-toxic compounds. By reacting with hydroxyl radicals, the pollutants are degraded step-by-step, and eventually mineralized. The attack of hydroxyl radicals, a non-selective oxidizing agent, gives the formation of aromatic intermediate compounds at the beginning of electrolysis. The aromatic ring opening reactions in the next step create aliphatic carboxylic acids (oxalic, acetic, formic acid, etc.) and inorganic ions (i.e. ammonium, nitrate, sulfate, phosphate) as final end-products before mineralization [9, 13]. From that, general schemes for the mineralization of POPs have been proposed, as can be seen in Figure 2-23.

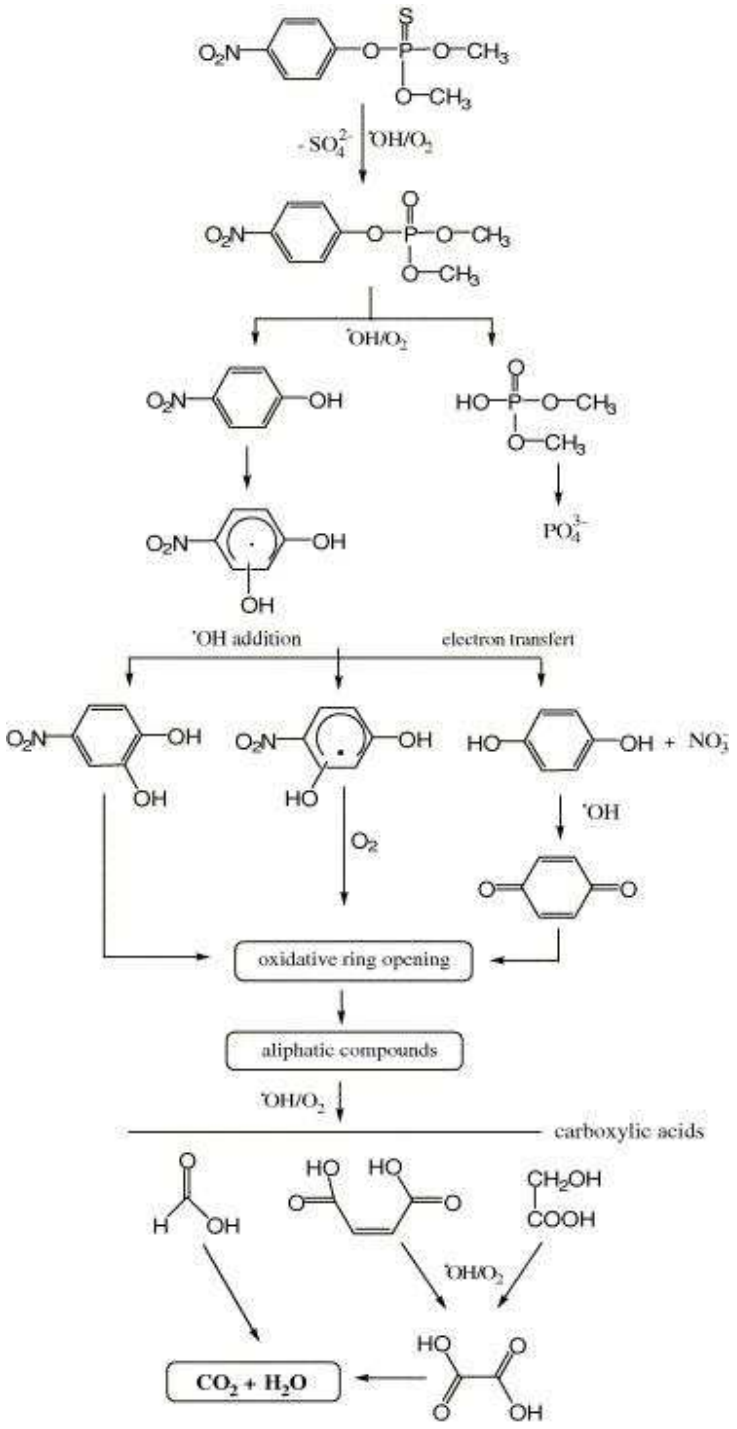

Figure 2-23. General reaction sequence proposed for the mineralization of methyl parathion in aqueous acid medium by hydroxyl radicals following EF process [173].

EF process is an economically and friendly environmentally process to remove the toxicity of the recalcitrant compounds in water. Evolution of solution toxicity during the EF

treatment is often followed by three periods: (i) The formation of significantly high toxic aromatic by-products at the beginning of the treatment as 2-naphtol and 1,2-naphtoquinone, (ii) the toxicity then decreases with disappearance of aromatics, and (iii) at the end of the treatment, this value goes down to zero which shows that the solution toxicity is in relation with aromatic compounds and that the EF mineralization leads to the detoxification of treated solution [172, 176]. In particularly, the toxicity of solutions were disappeared after 240 min for 220 mL solution with 0.2 mM of sucralose (Figure 2-24) [187], and 60 min for 200 mL solution with 50 mg L^{-1} of Orange II [13]. The above results allow proposing EF process on CF cathode as an environmentally friendly method for the treatment of wastewater effluents containing toxic and/or POPs.

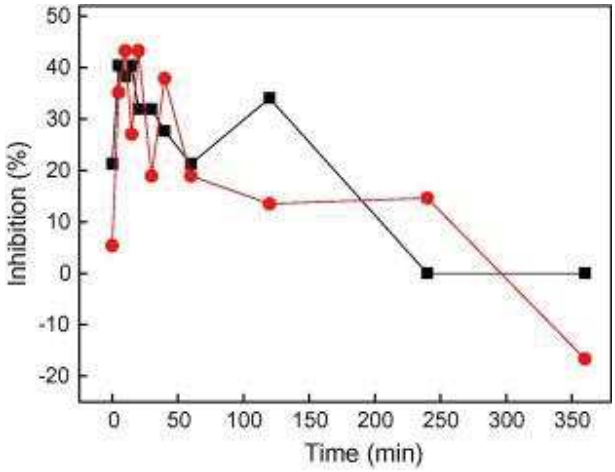

Figure 2-24. Evolution of the inhibition of marine bacteria, *Vibrio fischeri* luminescence (Microtox method) during EF processes with Pt (-■-) and BDD (-●-) anode ($[SUC]_0$ = 0.2 mM, $[Fe^{2+}]$ = 0.2 mM, $[Na_2SO_4]$ = 50 mM, I = 200 mA, pH_0 3.0) [187].

2.7.4. Modified EF systems using CF cathodes

2.7.4.1. Modified felts cathodes for homogeneous EF

The production of hydrogen peroxide and its reaction with catalyst (i.e. iron salt) in solution is a crucial factor for the effective destruction of POPs by homogeneous EF process. Aiming to improve the *in situ* generation of H_2O_2, various attempts have been made to upgrade the electrocatalytic characteristic of CF cathodes. As discussed in section 2.5.3, chemical modification is a simple and efficient way to ameliorate the electrochemical activity of the felt electrodes by changing their surface functional groups. After treatment in a mixture composed of

ethanol and hydrazine hydrate with the volume ratio of 90/10, the concentration of H_2O_2 after 120 min was 175.8 mg L^{-1} on the modified GF (CF-B) (*Shang-hai Qijie Carbon material Co.,Ltd.*) which were nearly three times higher than 67.5 mg L^{-1} for commercial felt (CF). The p-nitrophenol TOC removal ratios were 22.2%, and 51.4% for CF and CF-B, respectively, proving that the treated cathode could efficiently promote the degradation efficiency of the pollutants as compared with the unmodified one. The modified electrode was stable and reusable when the mineralization ratio after 10 cycles was still above 45% [64]. AQDS/PPy composite film was grown on graphite electrodes by electropolymerization of the pyrrole monomer in the presence of anthraquinone-2,6-disulfonic acid. The oxygen reduction potentials shifted to more positive values (-0.65, -0.60, and -0.52 V *vs* SCE for pH 3.0, 4.0, and 6.0, respectively) compared to the bare cathode (-0.85, -0.82, and -0.77 V *vs* SCE), which indicated the stronger electrocatalytic activity of the AQDS/PPy/graphite cathode toward ORR. Therefore, the modified cathode resulted in a large accumulation of electrogenerated H_2O_2 which increase the EF degradation of amaranth azo dye [98]. Additionally, the improvement of the H_2O_2 formation rate was found on felts cathode modified by multi-walled carbon nanotubes [192] and by chemical treatment in H_2SO_4 solution [193].

2.7.4.2. Modified felts cathodes for heterogeneous EF

The EF process suffers from some common drawbacks of Fenton's reaction such as (i) the requirements of strict pH regulation between 2 and 4, (ii) the loss of soluble iron catalyst as hydroxide precipitate [194, 195] and (iii) post-treatment requirements prior to discharge [196]. To overcome these drawbacks in classical EF treatments, many attempts have been performed on the use of heterogeneous catalyst containing iron oxides instead of soluble iron salts. The ability to self-regulate the supply of a constant amount of iron ions all along the reaction time and also the easy recycling of the iron catalyst after treatment are the advantages of using these iron sources in the EF process [197]. Comparing with other heterogeneous iron catalysts, pyrite is a low-cost and abundant natural iron sulfur mineral, which can provide iron ions. It seems to be a good candidate to be employed as heterogeneous catalyst in EF because it self-regulated the Fe^{2+} content and the pH in the solution in the presence of dissolved O_2 through reactions (2-17), (2-18) and (2-19) [184]. Moreover, after the treatment, pyrite can be easily recovered from filtration and reused. Therefore, pyrite has been used widely to remove many biorefractory pollutants in aqueous medium such as azo dye – the (4-amino-3-hydroxy-2-p-tolylazo-

naphthalene-1-sulfonic acid) (AHPS) on GF (*Carbone Lorraine*, thickness 0.5 cm) [182], antibiotic levofloxacin [184] and tyrosol [183] on CF (*Carbone Lorraine*), *etc*.

$$2FeS_2 + 7O_2 + 2H_2O \rightarrow 2Fe^{2+} + 4SO_4^{2-} + 4H^+ \quad (2\text{-}17)$$

$$2FeS_2 + 15H_2O_2 \rightarrow 2Fe^{3+} + 14H_2O + 4SO_4^{2-} + 2H^+ \quad (2\text{-}18)$$

$$FeS_2 + 14Fe^{3+} + 8H_2O \rightarrow 15Fe^{2+} + 2\ SO_4^{2} + 16H^+ \quad (2\text{-}19)$$

Besides the above treatment, iron alginate gel beads (FeAB) was used as the heterogeneous catalyst in the EF treatment in which high imidacloprid removal (90%) was achieved by operating for residence times of 4 h using GF cathode (*Carbon Lorraine, France*) [181]. By using the same catalyst, decolorisation of two typical dyes, Lissamine Green B and Azure B, was attained 87% and 98%, respectively after 30 min, without operational problems and maintaining FeAB particle shapes throughout the oxidation process [179]. In very recent study, Özcan *et al.* prepared a new iron containing Fe_2O_3 modified kaolin (Fe_2O_3-KLN) catalyst, to develop a heterogeneous EF process with three-dimensional CF cathode for the electrochemical oxidation of ENXN. Mineralization efficiency of the EF process increased in the presence of Fe_2O_3-KLN and attained its maximal value in the presence of 0.3 g catalyst at 300 mA. There was a very few amount of leached iron (∼0.006 mM) revealed that hydroxyl radicals were mainly produced by heterogeneous reactions of surface iron species [188]. The performance of the heterogeneous EF treatment for removal pollutants was also improved comparing with that of homogeneous treatment. For example, the pseudo-first-order rate constant of 2.5 x 10^{-4} s^{-1} (R^2 = 0.990) for EF using pyrite catalyst was nearly two times higher than electrochemical oxidation, 1.3 x 10^{-4} s^{-1} (R^2 = 0.992) as determined by Barhoumi *et al.* [184]. In addition, Fe@Fe_2O_3 [198-200], pyrrhotite [201] γ-FeOOH [202, 203] and (γ-Fe_2O_3/F_3O_4 oxides) nanoparticles [204] are interesting iron catalyst sources. The stable performance of these heterogeneous iron catalysts open promising perspectives for fast and economical treatment of wastewater polluted by POPs contaminants using EF treatment on CF cathodes.

2.7.4.3. Hybrid EF system using CF cathodes

To boost the degradation efficiency and reduce the treatment cost, many attempts have been made to change the EF reactor. A novel vertical-flow EF reactor (Figure 2-25 a), composing of 10 cell compartments was designed to degrade tartrazine, a model azo dye. GF cathode

(*Shanghai Qijie carbon material Co., Ltd*) was modified by ultrasonic immersion and coating method, combined with PbO_2/Ti mesh anode. In comparison to the traditional parallel-flow reactor in a single chamber, the new EF system was found to be more complete and efficient. The tartrazine with initial concentration of 100 mg/L could reach near 100% removal. The TOC removal efficiency was 61.64% [205]. This result came from the reason that the mass transfer rate of the target pollutant molecules is accelerated. In addition, the contaminants can be well enriched on the surface in vertical-flow reactor [206].

Rosales *et al.* designed a continuous bubble EF reactor for the degradation of wastewater contaminated with synthetic dyes. This reactor was able to operate without operational problems, and attaining high decoloration percentages of pollutants [207]. The degradation of methyl orange (MO) by the EF process was conducted in a hemisphere-shaped quartz reactor using dual rotating GF disks (*Shanghai Qijie Carbon Material Co., Ltd*) cathode to supply oxygen. The rotation of disk cathode resulted in the efficient production of H_2O_2 without oxygen aeration, offering a potentially cost-effective EF method for degrading organic pollutants (Figure 2-25 b) [208].

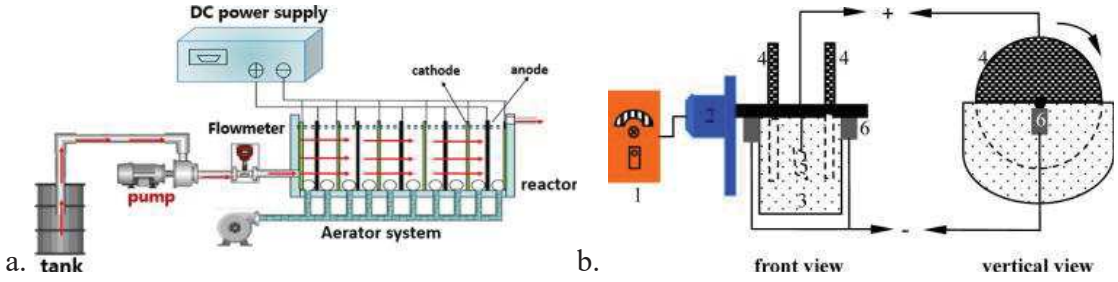

Figure 2-25. The schematic diagram of: (a) the novel vertical-flow EF reactor [205]; and (b) Continuous bubble EF reactor (1) speed controller, (2) motor, (3) electrolytic cell, (4) rotating GF disk cathode, (5) Pt anode, and (6) carbon brush [208].

To further reduce the costs of electricity input for the EF treatment, bio-electro-Fenton (BEF) system has been developed to couple the EF process with MFC which generates electricity directly from organic compounds. Fenton reactions were introduced to MFCs for bio-electrochemical degradation of paracetamol using GF at both cathode and anode without external power supply by Zhang *et al.* (Figure 2-26). Dual-chamber MFC reactors were employed in the anode chambers where bio-electrons were released by oxidizing biodegradable pollutants in low-strength real domestic wastewater. In the cathode chambers, the input fluxes of bio-electrons from the anode could promote the yield of free radical •OH by facilitating the regeneration of

iron source. A Proton Exchange Membrane (PEM, 6.0 cm × 5.5 cm cross-sectional area, *Nafion-117, DuPont, USA*) was installed as a separator to prevent potential diffusion of dissolved oxygen as well as the transfer of iron (III)/iron (II) (Fe^{3+}/Fe^{2+}) ions (sourced from $FeSO_4.7H_2O$ added directly) from cathode to anode chamber [209].

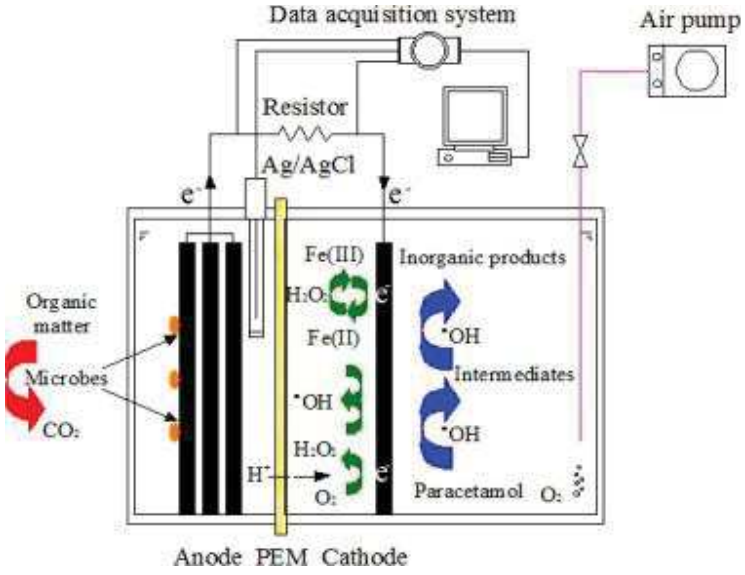

Figure 2-26. Schematic diagram of the MFC-Fenton system using soluble iron catalyst for paracetamol degradation by EF process at cathode chamber (PEM = Proton Exchange Membrane) [209].

The BEF system has been developed towards a clean treatment by using heterogeneous catalysis to avoid iron soluble salts adding. Birjandi *et al.* built up a BEF cell through the combination of a dual-chamber MFC with anaerobic seed sludge as biocatalyst in an anode chamber and an aerobic cathode chamber equipped with a $Fe@Fe_2O_3$/graphite (*Entegris, Inc. FCBLK-508305-00004, USA*) cathode. This cathode served simultaneously as the catalyst iron source instead of directly using Fe^{2+} for the *in situ* EF process (Figure 2-27). The medicinal herbs wastewater was degraded through bio-oxidation by microorganisms at anodic chamber and the EF process at cathodic one [199]. This BEF system was also performed by Zhuang *et al.* on CF (4.5 cm × 4.5 cm, *Liaoyang, China*) [210]. The electricity generated by MFC to *in situ* generate H_2O_2 at a CF cathode for EF process was also investigated to remove p-nitrophenol by Zhu *et al.*. MFC could generate a maximum power density of 143 mW m^{-2} and the p-nitrophenol was completely degraded after 12 h [211]. The similar systems were created to remove biorefractory contaminants in wastewater sources like AO7 dye using CF (5 cm x 3 cm x 0.5 cm, *Xinka Co.,*

Shanghai, China) [212], 17β-estradiol and 17α-ethynyl-estradiol estrogens using Fe@Fe_2O_3/CF (4.5 cm x 4.5 cm, *Liaoyang, China*) [198], azo dye (Orange II) [203] using CF anode and carbon nanotube (CNT)/γ-FeOOH composite cathode, arsenite (As(III)) using γ–FeOOH/CF (4.4 cm × 4.4 cm × 0.5 cm) [202], Rhodamine B using Fe@Fe_2O_3/CF, landfill leachate using CF (5 mm thickness, *Beijing Sanye Carbon Co., Ltd.,China*) anode and pyrrhotite/graphite (5 × 7 cm^2, 5mm thickness) (*grade G10, Hongfeng Carbon Co., Ltd, Shanghai, China*) cathode [200].

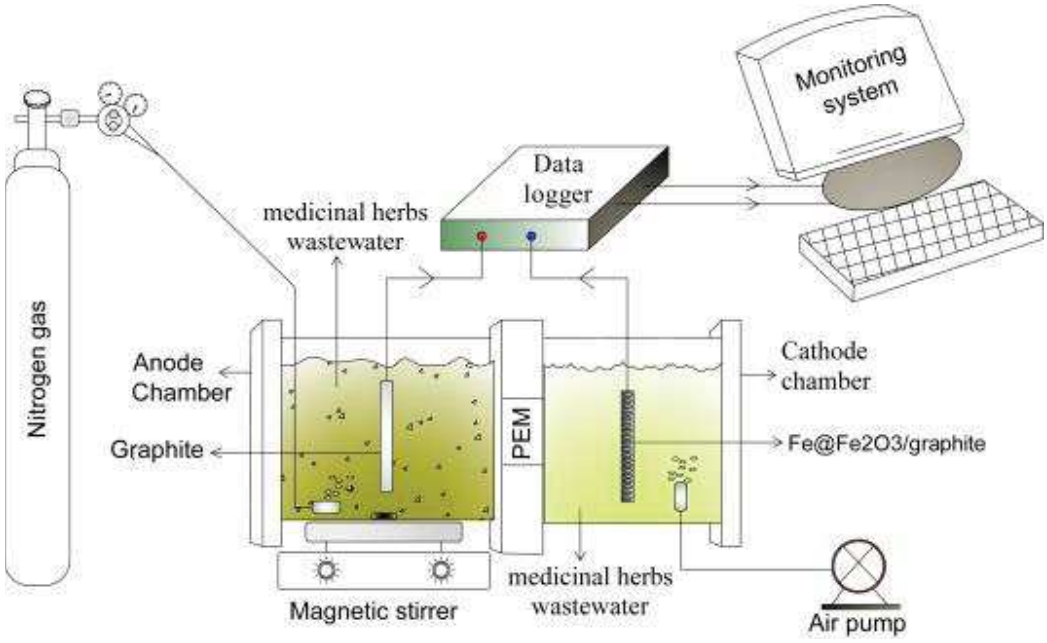

Figure 2-27. Schematic diagram of two chamber BEF systems in batch mode using non-catalyzed CF [199].

Moreover, using modified felts can improve significantly the efficiency of BEF system. The BEF with the modified electrodes, PPy/ AQDS- CF (5.0 cm x 5.0 cm x 0.6 cm, *Liaoyang Jingu Carbon Fiber Sci-Tech Co., Ltd. China*), resulted in the largest rate of H_2O_2 generation in the cathode chamber by the two-electrons reduction of O_2. The increase in the concentration of H_2O_2 was attained on beneficial for the enhancement in the amount of hydroxyl radicals produced by the reaction of H_2O_2 with Fe^{2+}, thus allowing an increased oxidative ability of the EF process towards the decolorization and mineralization of Orange II at neutral pH [100]. In order to avoid the use of expensive membranes in two-chamber MFC and to increase the generated power densities, more efficient dual reactor systems were advanced by using a single-chamber in a modified EF/MFC system (Figure 2-28). The power source from MFC was transferred directly to EF reactors constituted by CF cathode and iron plate anode as catalyst

source. The TOC removal of phenol reached 75 ± 2% in the EF reactor in one cycle after 22 h treatment [213].

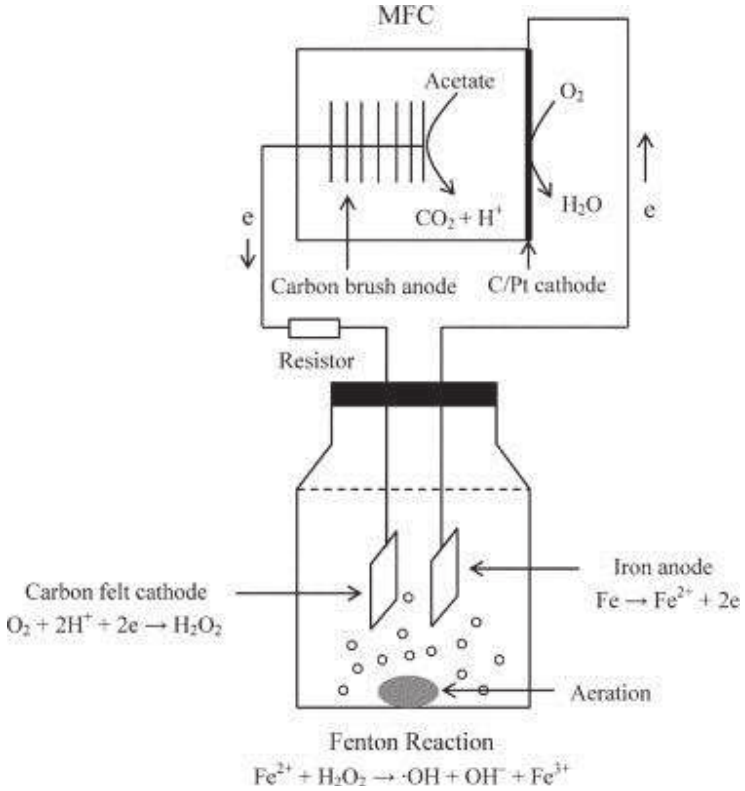

Figure 2-28. Schematic diagram of the EF system powered by a single-chamber MFC [213].

2.7.4.4. Pilot-scale

To assess industrial applications, the EF pilot program was set up to treat large volume of contaminated solutions. An organic micropollutant, diclofenac (DCF), from drinking water was removed by a novel EF filter pilot (Figure 2-29). The CF was used as material for both anode and cathode. The iron nanoparticles (γ-Fe_2O_3/F_3O_4 oxides) was impregnated with cathode and play the role of catalyst. The capacity of feed tank in this EF laboratory-scale pilot plant could attain 200 L. The pilot exhibited satisfactory stability regarding both electrode integrity (no iron leaching) and removal efficiency, even after multiple filtration/oxidation treatment cycles. The degradation of DCF and TOC removal was steadily achieved 85% and 36%, respectively [204].

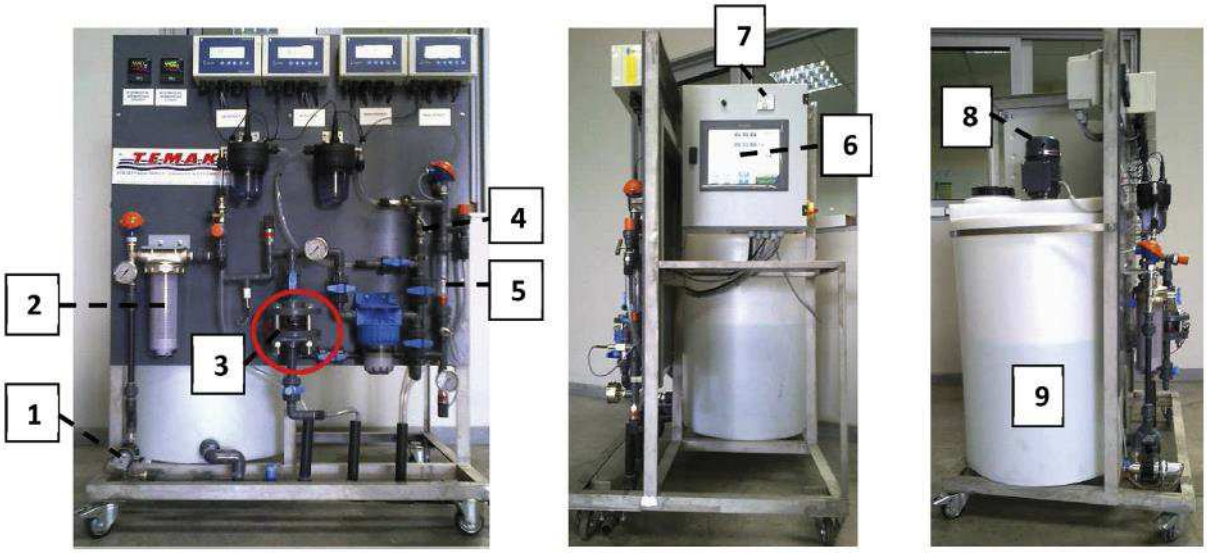

Figure 2-29. Scheme of the EF pilot plant. 1: feed pump, 2: cartridge filter 60 mm, 3: EF 'filter', 4: control valve, 5: flowmeter, 6: PLC (programmable logic controller), 7: voltage regulator, 8: powered agitator, 9: feed tank [204].

By another way, a volume of 8.0 L of textile dye solution, acid yellow 42, was treated efficiently by the advanced Solar Photo-electro-Fenton (SPEF) process in a lab-scale pilot plant. The application of solar radiation in the process (SPEF) created higher current efficiencies and lower energy consumptions than traditional EF process [214]. The usage of sunlight as power source was also found in an autonomous solar pre-pilot plant to mineralize Yellow 4 diazo dye (Figure 2-30). The plant had the capacity of 10 dm^3 and was coupled to a solar compound parabolic collectors which could provide a maximum average current of 5.0 A. At this supplied current, about 96-97 % mineralization was rapidly attained, and a reaction pathway for Direct Yellow 4 was proposed [215]. This solar pre-pilot plant was also contributed to mineralize 89% of the antibiotic chloramphenicol [216], or 94% of sulfanilamide [217].

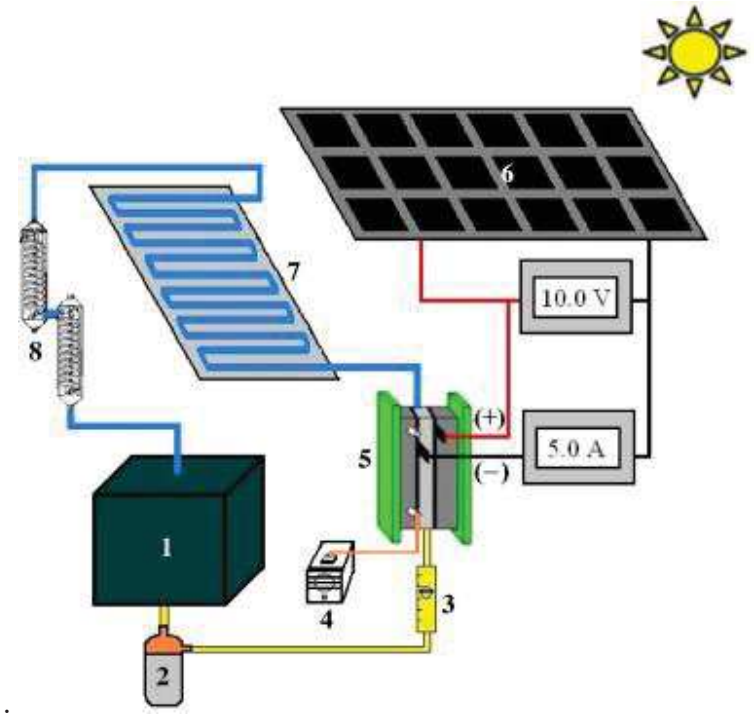

Figure 2-30. Sketch of the autonomous solar pre-pilot plant used for the SPEF treatment of 10 dm^3 of Direct Yellow 4 (DY4) solutions.(1) Reservoir, (2) magnetic drive centrifugal pump, (3) flowmeter, (4) air pump, (5)electrochemical filter-press reactor with a Pt anode and an air-diffusion cathode of 90.2 cm^2 area, (6) solar photovoltaic panel of 50 W maximum power with the corresponding amperemeter and voltmeter, (7) solar compound parabolic components (CPCs) photo reactor of 1.57 dm^3 irradiation volume and (8) heat exchangers [215].

2.7.5. Conclusion on application of CF-based electrodes for wastewater treatment by EF process

Wastewater treatment by EF process, using the CF-based cathodes is a wise and very highly efficient choice. The materials are cheap, non-toxic, and stable. Many toxic biorefractory pollutants were removed completely, creating clean solutions at the end of the electrolysis. Using modified felts cathodes improved hydrogen peroxide generation, an important key of EF process significantly. To overcome the disadvantages of soluble catalyst, other iron sources were successfully applied in EF process. New configurations like vertical-flow EF reactor stacked with 10 cell compartments and continuous bubble EF process continually improved the efficiency of EF treatment. The consumption cost was decreased by zero-energy EF approaches where MFC or abiotic FC supplied clean power. These hybrid EF systems are cost-effective for recalcitrant

contaminants treatment, opening up new development trend for future research in the environmental and energy-related field. The idea from the air-diffusion cathodes used in the solar EF pre-pilot plants is expected to apply for CF-based electrodes in future studies.

2.8. Conclusion

The CF are potential materials which have been widely applied as electrodes in energy and environmental field. Pristine felts have excellent properties with respect to electronic conductivity, chemical stability, light weight, and low cost. However, CF' highly hydrophobic nature make their application in aqueous electrolyte medium difficult. To overcome this drawback, many modification methods have been developed and used resulting in new and various benefits. Plasma, thermal, and chemical treatments change the hydrophobic surface of bare felts to hydrophilic. The enhanced wettability makes it easier for the electrolyte ions to access the active sites of the modified electrodes. Metallic nanoparticles, CNTs, carbon nanofibers, or graphene modification improved significantly the conductivity and the electroactive surface. Besides these modifications, we discussed zeolite material was discussed.

Both pristine and modified felts were employed as electrodes in energy application like VRFB, BFC, MFC, capacitor, solar cell and Li-ion batteries. For environmental applications, we focused in this review on the wastewater treatment containing biorefractory pollutants by EF process. The use of CF as cathode for POPs removal by EF technology attained very high efficiencies where most initial contaminants were mineralized to non-toxic compound at the end of electrolysis. To decrease the cost of treatment and upgrade the efficiency, using modified electrodes and catalysts have improved the EF system. The felts materials were also investigated for applications in BFC-Fenton in which electrons were produced from FC towards zero-energy depollution. The EF pilot program will open doors for new applications of felts materials in industrial areas. The modification and use of carbon based-electrodes for energy and environment applications will be a very interesting topic in the future.

In this thesis, with the aim to improve the performance of EF system using CF cathode towards zero energy depollution, we solved the following issues:

(1) Finding the optimal conditions (applied current and concentration of iron catalyst) for EF process using commercial CF. Investigating the correlation between degradation pathway and toxicity of AO7, ACE as well as their by-compounds.

(2) Modifying the commercial CF by rGO for AO7 mineralization by EF process.

(3) Building up the hybrid BFC from connection of bio-cathode and abiotic anode using CF modified by gold particles both at cathode and anode.

(4) Designing a novel Fuel-cell Fenton, without using input power, from glucose oxidation at abiotic anode (gold particles/CF) and EF process at porous carbon/CF cathode. It is also necessary to monitor cell stability during long period (2 months).

CHAPTER III

COMMERCIAL CARBON FELT FOR REMOVAL OF ACID ORANGE 7 AND ACETAMINOPHEN USING ELECTRO-FENTON PROCESS IN AQUEOUS MEDIA

This chapter has been published in ***Chemosphere*** as:

Thi Xuan Huong Le, Thi Van Nguyen, Amadou Yacouba Zoulkifli, Zoungrana Laetitia, Avril Florent, Eddy Petit, Julie Mendret, Valerie Bonniol, Mikhael Bechelany, Stella Lacour, Geoffroy Lesage, Marc Cretin, *Toxicity removal assessments related to degradation pathways of azo dyes: toward an optimization of electro-Fenton treatment*, Chemosphere, 2016,161, 308–318.

Thi Xuan Huong Le, Thi Van Nguyen, Amadou Yacouba Zoulkifli, Zoungrana Laetitia, Avril Florent, Eddy Petit, Julie Mendret, Valerie Bonniol, Mikhael Bechelany, Duy Linh Nguyen, Stella Lacour, Geoffroy Lesage, Marc Cretin, *Correlation between degradation pathway and toxicity of acetaminophen and its by-products, using electro-Fenton process in aqueous media,* Chemosphere, 2017, 172, 1-9.

CHAPTER 3. COMMERCIAL CARBON FELT FOR REMOVAL OF ACID ORANGE 7 AND ACETAMINOPHEN USING ELECTRO-FENTON PROCESS IN AQUEOUS MEDIA

3.1. General introduction

This chapter focused on using commercial CF as cathode to eliminate AO7 and ACE by EF process. In the AO7 degradation part, we solved some following problems: (1) Finding the optimal conditions (applied current and concentration of iron catalyst) for treatment of 200 mL AO7 (0.1 mM), (2) Using different analytical methods like HPLC-UV and LC-MS, IC to build up a degradation pathway of AO7, and (3) Toxicity of treated solution as well as by-products were measured by monitoring the inhibition of marine bacteria *Vibrio fischeri*. The experiments for degradation pathway and toxicity were done for 500 mL of AO7 (1 mM) at optimal parameters which was found in the first step. Similarly, these optimal conditions about applied current and concentration of iron catalyst were used to treat ACE. The correlation between degradation pathway and toxicity of ACE as well as their by-compounds were also investigated.

3.2. Toxicity removal assessments related to degradation pathways of azo dyes: toward an optimization of EF treatment

3.2.1. Abstract

The degradation pathway of AO7 by EF process using CF cathode was investigated via HPLC-UV and LC-MS, IC, TOC analysis and bioassays (*Vibrio Fischeri* 81.9% Microtox® screening tests). The TOC removal of AO7 reached 96.2% after 8h treatment with the optimal applied current at 500 mA and 0.2 mM catalyst concentration. The toxicity of treated solution increased rapidly to its highest value at the early stage of electrolysis (several minutes), corresponding to the formation of intermediate poisonous aromatic compounds such as 1,2-naphthaquinone (NAPQ) and 1,4-benzoquinone (BZQ). Then, the subsequent formation of aliphatic short-chain carboxylic acids like acetic acid, formic acid, before the complete mineralization, leaded to a non-toxic solution after 270 min for 500 mL of AO7 (1 mM). Moreover, a quantitative analysis of inorganic ions (i.e. ammonium, nitrate, sulfate) produced

during the course of degradation could help to verify molar balance with regard to original nitrogen and sulfur elements. To conclude, a clear degradation pathway of AO7 was proposed, and could further be applied to other persistent pharmaceuticals in aquatic environment.

Keywords: *Carbon felt, Advanced Oxidation Process, Mineralization, Toxicity, Acid Orange 7.*

3.2.2. Introduction

Textile wastewater is still being of great concern from environmental point of view, in terms of toxicity and persistence. Azo dyes, characterized by the presence of azo group (-N=N-), represent approximately 70% in mass of all dyestuffs used worldwide, making them the largest group of synthetic colorants which are released into the environment. Many of them are known or possible toxic, carcinogenic and mutagenic substances that need to be treated before discharge into aqueous medium [218]. AO7, also called Orange II, is a typical azo dye (Figure 3-1).

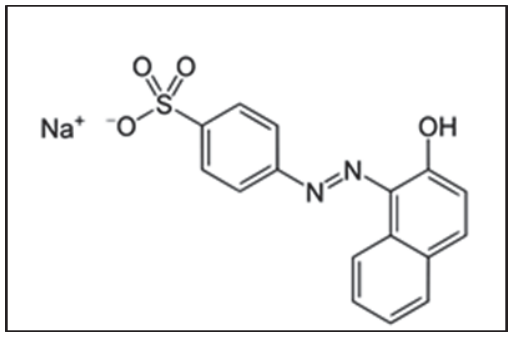

Figure 3-1. Molecular structure of AO7.

EF process has been known as an environmentally friendly electrochemical technology for the degradation of refractory pollutants in aquatic environment [219]. The principal reaction (Eq. (2-12)) of the Fenton oxidation process produces hydroxyl radical through the catalyzed reduction of H_2O_2 by Fe^{2+} in an acidic medium.

$$H_2O_2 + Fe^{2+} + H^+ \rightarrow Fe^{3+} + \bullet OH + H_2O \quad (2\text{-}12)$$

To avoid drawbacks encountered during the Fenton process, mainly H_2O_2 transportation potential risk and activity loss, EF process has been developed. This latter combines the ferrous ion addition with the *in-situ* electro-generation of H_2O_2. The production of H_2O_2 in aqueous solution is obtained by electro-reduction of dissolved oxygen (Eq. (2-11)) under an appropriate

applied current (or cathodic potential) [220]. Cathodic electrodes such as vitreous carbon [221], CF [178], carbon sponge [5], and gas-diffusion electrode [222] are commonly used for this purpose.

$$O_2 + 2H^+ + 2e^- \rightarrow H_2O_2 \qquad E^0 = 0.695 \text{ V / SHE} \qquad (2\text{-}11)$$

Thus, hydroxyl radicals can be generated in the solution by addition of a catalytic quantity of Fe^{2+} ions (Eq. (3-1). •OH can then attack and initiate the oxidation of pollutant (RH) following Eq. (3-1).

$$\bullet OH + RH \rightarrow R\bullet + H_2O \qquad (3\text{-}1)$$

In recent studies, AO7 has been chosen as a model refractory pollutant treated by the Electrochemical Advanced Oxidation Processes (EAOPs), generating •OH radicals in acidic aqueous medium at a BDD or Pt anode. TOC removal could then reach 98% after 9 h of electrolysis [223]. Hydroxyl radicals was also created from Fenton's reagent at the carbon-felt cathode to the removal of nearly 92% TOC from initial AO7 pollutant after 8 h treatment [224]. Besides that, AO7 could be decolorized and degraded by an eco-friendly method through the enzymatic mechanisms involved bacteria [218]. The radiolytic degradation of AO7 in aqueous solutions was also investigated to find by-products concerning N–N and C–N cleavages from mother-molecular [225].

Chemical degradation pathways of dyes by EAOPs have been extensively studied [8, 9]. However the eco-toxicity study of sub-products generated by the process at different times has not been reported yet. The aim of this work is then to acquire both chemical and eco-toxicological information on the degradation mechanisms of AO7 by EF reaction on CF electrode, while proving that hydroxyl radicals (•OH), a highly powerful oxidizing agent, can mineralize toxic and bio-refractory organic pollutants into non or less toxic compounds. To do this, analytical identification and quantification of targeted molecules and their intermediate sub-products will be carried out by HPLC-UV and LC-MS, IC and TOC analysis, together with toxicity assessments performed during the course of EF process.

The results showed that the decomposition of initial pollutants leaded to the appearance of well identified aromatic compounds at the early stage of the process, followed by the formation of several short-chains carboxylic acids before that complete mineralization into carbon dioxide (CO_2) and water (H_2O) was achieved. Thus, a degradation pathway by the advanced oxidation

(EF process) at optimal conditions of oxidant dose or oxidation duration reaching to nontoxic products could be constructed thoroughly and systematically for this model pollutant.

The novelty of this work focuses on the evaluation of the toxicity of by-products related to the degradation pathways of azo dye, AO7. The results were proved tightly via various techniques such as HPLC-UV and LC-MS, IC, TOC analysis and bioassays (Vibrio Fischeri 81.9% Microtox® screening tests). The work one again points out the high efficiency of EF technology for treatment of bio-refractory pollutants where toxic initial compounds are quickly degraded into non-toxic compounds.

3.2.3. Materials and methods

3.2.3.1. Chemicals and bacterial strain

The CF was purchased from A Johnson Matthey Co., Germany. AO7 (Orange II sodium salt), sodium sulphate (anhydrous, 99.0 – 100.5%); sodium hydroxide (99%); sulfuric acid (95-97%); iron (II) sulphate hepta-hydrate (99%); hydroquinone (HQ); 1,4-benzoquinone (BZQ); 2-formyl-benzoic acid (FBA); 1,2-napthoquinone (NAPQ); 2-hydroxyl-1,4-napthalenedione (HNQ); 4-hydroxylbenzenesulphonic acid (HBA); 2-napthol (NOL); oxalic acid (OA); maleic acid (MA); oxamic acid (OMA); fumaric acid (FA) were obtained from Sigma-Aldrich. TOC standard of 1000 mg/L (Sigma-Aldrich Co.) and sodium hydrogen carbonate (99.5%, ACS, Karlsruhe) were used for total organic and inorganic carbon (IC) calibration curves assessments. Bacterial strain of *Vibrio fischeri* NRRL B-11177 involved in toxicity tests came from Hach Lange GmbH, Germany. Osmotic adjusting solution (MilliQ water with 22% NaCl) and diluent (MilliQ water with 2% NaCl) were used for the preparation of bacterial solutions.

3.2.3.2. Degradation of AO7 in EF system

EF experiments were performed at room temperature in a 500 mL undivided cylindrical glass cell with a two-electrodes system (Figure 3-2). The applied current was controlled thanks to a power supply (Lambda Electronic, USA) in galvanostatic mode. The CF cathode (60 cm^2) was used as working electrode and a Pt cylindrical mesh as counter electrode. The anode was centered in the electrolytic cell, surrounded by the cathode, which covered the inner wall of the cell. The distance between the electrodes was 1.5 cm. The aqueous solution of AO7, Na_2SO_4 (50 mM) as supporting electrolyte and $FeSO_4.7H_2O$ as the catalyst were prepared by adjusting pH at 3.0 with sulfuric acid (H_2SO_4). Different conditions of catalyst concentration at 0.05, 0.1, 0.2, 1 and 2 mM

and applied currents at 60, 100, 300, 500 and 700 mA were firstly investigated in order to determine the optimal conditions for the mineralization of 200 mL solutions of AO7 at 0.1 mM.

Then, the monitoring of intermediate compounds was performed in 500 mL solution of AO7 (1 mM), $FeSO_4.7H_2O$ (0.2 mM) and applied current at 500 mA during the experiment. Prior to the electrolysis, oxygen bubbling was done during 5 minutes in order to saturate the solutions and kept during experiment under continuous magnetic stirring at a rate of 800 rpm.

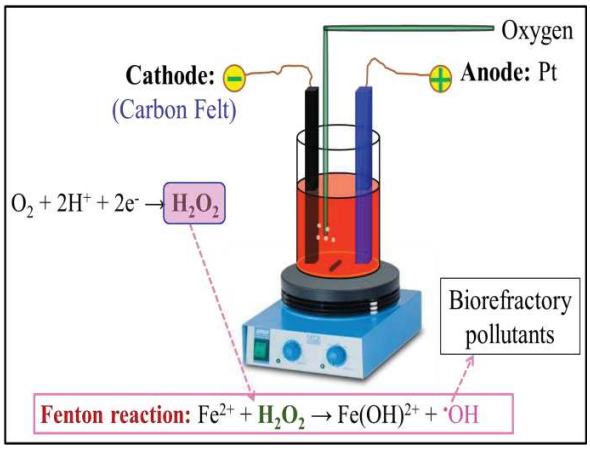

Figure 3-2. Schematic of the degradation of AO7 by EF process.

EF experiments were also performed in a two-separate compartments cell in order to evaluate the influence of anodic oxidation on the degradation of pollutants. Anodic compartment included AO7 (0.1 mM), Na_2SO_4 (50 mM) at pH 3.0 and cathodic one comprised AO7 (0.1 mM), Na_2SO_4 (50 mM), $FeSO_4.7H_2O$ (0.2 mM) at pH 3.0. A proton–exchange membrane (CMX Neosepta from Tokuyama Soda, Japan) was installed as a separator between these two compartments.

3.2.3.3. Analytical methods

3.2.3.3.1. UV-Vis spectrophotometry analysis

The absorption spectrum of AO7 consists in four main bands at λ_{max} of 228, 254, 310 and 485 nm. The decomposition of AO7 was monitored by measuring the dye absorbance at the selected single wavelength λ= 485 nm which is characteristic of azo bond. The absorbance of this bond was proportional to the AO7 concentration, according to the Beer-Lambert law. The

apparatus used was a UV–Visible Spectrophotometer Jenway 6300 (Barioworld Scientific Ltd, Dunmow UK).

3.2.3.3.2. High-performance liquid chromatography-UV (HPLC-UV)

Concentrations of AO7 and their aromatic oxidation by-products were analyzed by a HPLC system (Waters 717 Autosampler and Waters 616 Pump) with a Photodiode Array Detector (Waters 2996 Photodiode Array Detector) fitted with a reverse phase (RP) Thermo Scientific C18 (L=250 mm, I.D=4.6 mm, and 5 µm particles) column. The column temperature was thermostated at 30 ^{o}C. The injection volumes were 20 µL. The mobile phase was a buffer A (HPLC grade water + 0.1 % (v/v) trifluoroacetic acid) and buffer B (HPLC grade acetonitrile + 0.1 % (v/v) trifluoroacetic acid). The flow-rate was 1 mL.min^{-1}. The eluent gradient started with 10% of eluent B, gradually increasing to 70 % in 35 min. Eluent B was elevated to 90 % in 5 min and then the system was kept for 5 min, returning to 10% in 1 min and equilibrating for 9 min (return to initial condition and re-equilibrating the column). UV-Detection was performed at λ=255 nm, for substituted benzene structures monitoring.

The degradation products of AO7 were identified by a LC-MS system. LC-MS system performed with an Alliance e2695 (Waters HPLC pump and autosampler system) and a Quattro-Micro mass spectrometer equipped with an Electrospray probe (Waters Micromass, Wythenshawe, Manchester, UK). The detection conditions were: capillary potential of 3.5 kV, cone voltage of 30 V, source temperature of 120 °C, desolvation temperature of 450 °C, cone gas flow of 50 L h^{-1}, and desolvation gas flow of 450 L h^{-1}. Nitrogen was used as nebulizer gas.

A Waters column HSST3 (L=100 mm, D.I= 2.1 mm, and 5 µm particles) was used for the separation of intermediates. The column was at room temperature (22°C). The injection volumes were 20 µL.

The mobile phase was a buffer A (HPLC grade water + 0.1 % (v/v) formic acid) and buffer B (HPLC grade acetonitrile + 0.1% (v/v) formic acid). The flow rate was 0.25 mL min^{-1}. The eluent gradient started with 10 % of eluent B and was kept for 1 min, gradually increasing to 90 % of B in 2 min and then the system was kept for 1 min, returning to 10 % in 1 min and equilibrating for 2 min (return to initial condition and re-equilibrating the column). The eluent from the chromatographic column successively entered in the UV-Vis diode array detector (Waters PDA996) and the electrospray ionization interface of the mass spectrometer. MS analysis was performed in positive mode. The mass range was 90 to 400 (m/z).

The eluted components having specific retention time and were characterized by their UV-spectra and/or their mass. The quantification using the standard addition method (HPLC-UV) or external calibration against standard (LC-MS) was performed.

Short-chain acids were identified and quantified by using the HPLC-UV system already described, but fitted with a SHODEX KC 811 (D.I=8 mm, L=300 mm, and 7 μm particles) column which was thermostated at 30°C. UV detection was performed at λ=210 nm. The mobile phase was a buffer A (HPLC grade water + 0.1 % (v/v) Pphosphoric acid 85 %). The flow rate was 0.50 mL min^{-1}.

3.2.3.3.3. IC and TOC analysis

Inorganic ions (NO_3^-, NH_4^+, SO_4^{2-}) generated during decomposition of AO7 were identified by an ion chromatography equipment. In the case of anion, Dionex ICS-1000 system was connected with an AS19 column (4 mm × 250 mm) and the eluent was KOH which was applied according to the elution gradient: 10 mM in 10 min then gradient in 20 min to 45 mM. Dionex ICS-900 was used to measure the cation concentration in the treated solution with the column CS12A and eluent of 20 mM methane sulfonic acid. Both columns were thermally controlled at 30 ^{0}C, and DS6 conductivity detector was used.

The TOC of the initial and treated samples was determined with a TOC-L CSH/CSN Shimadzu (Japan) analyzer. Calibration curves for TOC and IC analysis were built up by automatic dilution on the same machine from solutions of TOC standard of 1000 mg/L and sodium hydrogen carbonate.

3.2.3.4. Toxicity tests

The Microtox® bacteria toxicity test was based on the general principles described by ISO (2007) [226]. The toxicity of AO7 and its intermediate by-products formed during its degradation was determined by measuring the effect on the luminescence of marine bacteria. Bacterial luminescence was measured using a Microtox® Model 500 Analyzer (Modern Water Inc.; United Kingdom). The bacteria used in this method was the strain *Vibrio fischeri* NRRL B-11177. This bacterium emitted luminescence during growth relating to cellular respiration which was linked itself to cell activity. As the activity of the cell could be reduced by the presence of toxic elements, bioluminescence is therefore a very good indicator of state of the bacterium and thus of the global toxicity of the sample.

This device allowed for the acute toxicity tests with the help of the software MicrotoxOmni®. To identify the relative toxicity of each sample solution, a 81.9% screening test has been used to characterize the inter-samples toxicity variability: the influence of treatment processes on the effluent toxicity was monitored thanks to a sampling method performed as a function of time. The test performed in this paper is called 81.9% screening test since all samples have been diluted at 81.9% of the initial sample concentration by addition of a 22% NaCl solution to allow *Vibrio fischeri* normal activity and thus luminescence emission. Before measuring the bacteria luminescence, pH of the samples were adjusted between 6.5 and 7.5 by sodium hydroxide or sulfuric acid, then a 0.2 µm-filtration was performed with syringe filters in order to eliminate any precipitate or solid matter in the solution. The inhibition rate at time t: I (t) was calculated thanks to Eq. (3-2):

$$\mathrm{I(t)(\%)} = \left(1 - \frac{\mathrm{LU(t)}}{\mathrm{LU(0)}}\right).100 \qquad (3\text{-}2)$$

where LU(t) is the intensity of luminescence emitted by bacteria after a t=5 min or t=15min of contact with the sample; and LU(0): is the initial intensity of luminescence emitted by bacteria before the addition of the sample.

However, in the absence of toxicity, the luminescence of bacteria decreases over time and under the action of environmental conditions. Thus, it is necessary to compensate the errors due to these factors by taking into account the variability of the luminescence R (t) of the bacteria in a control solution (MilliQ water and NaCl) which gives the LU_0 values. Equation (3-3) gives the corrected term R(t).

$$R(t) = \frac{\mathrm{LU0(t)}}{\mathrm{LU0(0)}} \qquad (3\text{-}3)$$

where LU0(t) is the intensity of luminescence emitted by bacteria after a t=5 min or t=15min of contact with the control solution (MilliQ water and NaCl); and LU0(0): is the initial intensity of luminescence emitted by bacteria before the addition of the control solution (MilliQ water and NaCl).

Then the corrected inhibition rate at time t: Ic(t) intrinsically attributable to the sample toxicity is calculated using equation (6). In the rest of this paper, Ic(t) is called “Inhibition” and is expressed in %.

$$\mathrm{Ic(t)(\%)} = \left(1 - \frac{\mathrm{LU(t)}}{R(t).\mathrm{LU(0)}}\right).100 \qquad (3\text{-}4)$$

Furthermore, eco-toxicity tests were carried out on the commercially available by-products in order to confirm or not the toxicity of the compounds formed during the degradation of the main molecule, AO7. These by-products and their mixtures were prepared with the maximum concentrations detected by HPLC-UV analysis during the eectro-Fenton experiment.

3.2.4. Results and discussion

3.2.4.1. Effect of applied current on the degradation kinetics

In the EF process, the applied current is an important parameter for both operational cost and process efficiency [176]. To evaluate the effect of applied current on the decomposition kinetics of AO7, different currents were investigated as follows: at 60, 100, 300, 500 and 700 mA. Figure 3-3a indicated that the decomposition rate increased rapidly with the rise of cathodic current from 60 mA to 500 mA. However, from applied current values of 500 mA, the degradation nearly kept stable and complete color removal of dye solution could be reached after only 3 min. Therefore this value corresponds to the optimal current density which allows optimal H_2O_2 production and thereby hydroxyl radical generation, while avoiding competitive side-reactions such as H_2O production (Eq. (3-5)), proton reductions or H_2O_2 decomposition at cathode (Eq. (3-6) and (3-7)).

$$O_2 + 4H^+ + 4e^- \rightarrow 2H_2O \quad (3\text{-}5)$$

$$2H^+ + 2e^- \rightarrow H_2 \quad (3\text{-}6)$$

$$H_2O_2 + 2H^+ + 2e^- \rightarrow 2H_2O \quad (3\text{-}7)$$

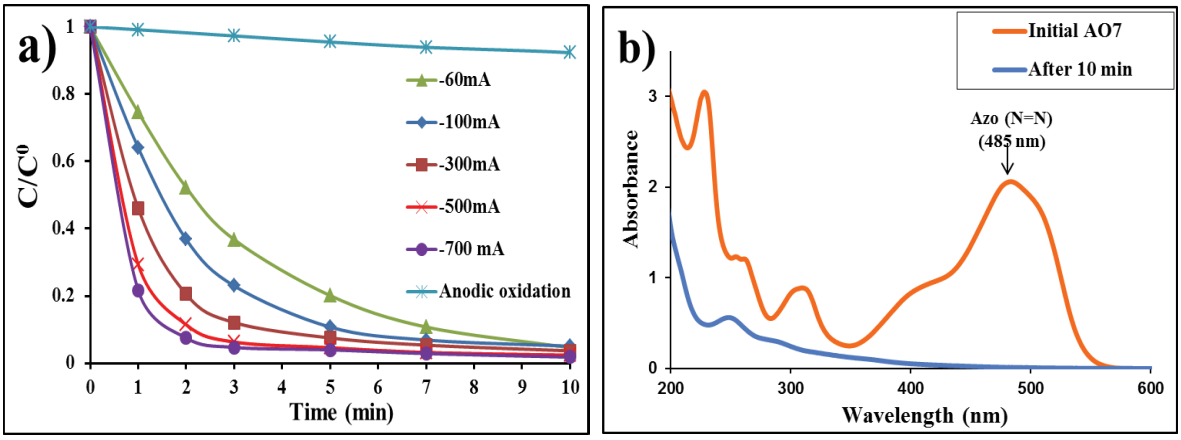

Figure 3-3. AO7 degradation by EF process on CF cathode (60 cm^2).(a) Degradation kinetics of AO7 determined at 485 nm at operating conditions: 200 mL AO7 (0.1 mM) aqueous solution in 50 mM Na_2SO_4 with 0.2 mM Fe^{2+} of pH 3.0, Pt anode, and different constant currents applied. (b) The absorption spectrum of initial AO7 and treated solution after 10 min.

It could be seen from Figure 3-3 b that absorption band related to azo bond (wavelength at 485 nm) disappeared totally after 10 minutes of treatment. The absorption bands at 228, 254 and 310 nm present in the initial solution disappeared rapidly which is characteristics of aromatic ring structure decomposition into various intermediate sub-products before mineralization. As demonstrated in a previous work [224], the hydroxyl radicals could also be created from the oxidation of water on the anode surface according to Eq. (3-8). However, the degradation of AO7 by this anodic oxidation process was very weak, compared to EF process: after 3 min of oxidation process applied, there was only 2.6% of 0.1mM AO7 degradation at anode (Figure 3-3 a) which implies that this process contributed to a very small extent to the overall degradation of AO7 by EF process. In the present study, we will therefore not consider the influence of the anodic oxidation.

$$H_2O \rightarrow Pt(\bullet OH) + H^+ + e^- \quad (3\text{-}8)$$

3.2.4.2. Effect of catalyst concentration on the mineralization efficiency

As it can be seen from Figure 3-4, the mineralization rate increased with increasing Fe^{2+} concentration from 0.05 to 0.2mM, because the higher catalyst concentration, the higher production of hydroxyl radicals at cathode. However, for larger concentrations of catalyst tested (from 1 to 2 mM), a decline in the TOC removal was observed. This is characteristics of a side-

reaction taking place between the excess of hydroxyl radical produced and iron species, as mentioned in previous studies dealing with EF process [227, 228]. Therefore, 0.2 mM of catalyst was chosen as the optimal concentration to be used to degrade AO7. After 120 min treatment, almost 90% of organic compounds in the initial AO7 solution (0.1 mM) were eliminated. The fast degradation of AO7 at the early stage of electrolysis originated from the easy break of azo bond and rapid decomposition of the intermediate naphthalene-type compounds formed, such as 2-naphtol; 2-hydro-1,4 naphthoquinone; and 1,4-benzoquinone (Figure 3-5 a, b).

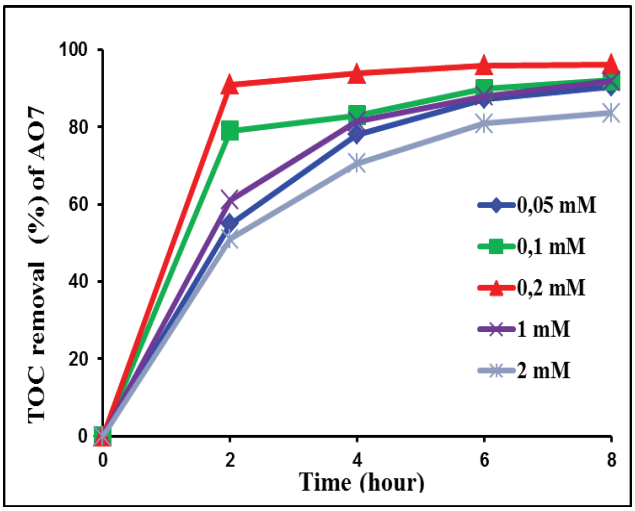

Figure 3-4. TOC removal after 8h treatment of 200 mL AO7 (0.1 mM). pH=3; [Na_2SO_4]=50 mM, I=500 mA for different Fe^{2+} catalyst concentrations between 0.05 mM and 2 mM.

3.2.4.3. Degradation pathway of AO7 during EF process

The construction of the degradation pathways to identify the possible molecular structure of by-products was performed according to the following steps:

(i) Many of AO7 by-products formed in our EF samples had already been identified in previous studies: This was the case of 1,4 benzoquinone (BZQ); 4-hydroxybenzenesulfonic acid (HBA); 2-naphtol (NOL); 2-hydroxy-1,4 naphthoquinone (HNQ); 1,2-naphthoquinone (NAPQ); 2-formyl-benzoic acid (FBA) and hydroquinone (HQ) and other short chain carboxylic acids. For these compounds, we could therefore compare HPLC-UV chromatograms of EF samples with individual chromatograms of the corresponding standard by-products which have been purchased and analyzed in LC-MS and HPLC-UV. The comparison of retention times enabled the by-

product identification in EF samples. Then, standard addition method applied to our EF samples allowed by-product quantitative analyses.

(ii) The other AO7 by-products detected in HPLC-UV chromatograms but that could not be identified in the first step (i) were analysed by LC-MS in order to qualify their molecular structures from the mass spectroscopic signals. They concerned the following molecules: 2,3-Dihydroxy-1,4-naphthalenedione, 1,2-naphthalenediol, 1(3H)-isobenzofuranone, 4-[(2,3-dihydroxy-1-naphthyl)diazenly]-benzenesulfonate, 4-[(2,3,4-trihydroxy-1-naphthyl)diazenly]-benzenesulfonate.

3.2.4.4. Evolution of aromatic compounds

The decomposition of AO7 by EF process led to the formation of various aromatic compounds, short-chain carboxylic acids and inorganic ions, as shown in Figure 5. To identify these products, 500 mL of 1 mM AO7 was electrolyzed with an applied current of 500mA and 0.2 mM of catalyst. Degradation by-products except inorganic ions which were formed during the EF process were analyzed by HPLC-UV and LC/MS (Table 1) as described in section 2.3. It was noticed that aromatic intermediates were already detected at a very short reaction time after only 2 minutes of treatment. AO7 drastically decreased from the first few minutes before complete removal in 20 minutes, while the concentration of 1,4 benzoquinone (BZQ), 4-hydroxybenzenesulfonic acid (HBA), 2-naphtol (NOL), 2-hydro-1,4 naphthoquinone (HNQ) and 1,2-naphthoquinone (NAPQ) increased and reached maximum values of 0.0037 mM, 0.0075 mM, 0.012 mM, 0.17 mM and 0.32 mM, respectively, before being totally degraded after 80 min. The predominant aromatic product from the degradation of AO7 was 2-formyl-benzoic acid (FBA) and hydroquinone (HQ). Their formation was delayed compared to the others and attained the highest concentration at 0.854 mM for HQ and 0.94 mM for FBA in 14 and 40 minutes respectively before completely being removed after 80 and 180 min. From LC/MS analysis, some other aromatic compounds could be identified such as 2,3-Dihydroxy-1,4-naphthalenedione, 1,2-naphthalenediol, 1(3H)-isobenzofuranone, 4-[(2,3-dihydroxy-1-naphthyl)diazenyl]-benzenesulfonate, 4-[(2,3,4-trihydroxy-1-naphthyl)diazenyl]-benzenesulfonate between 10 and 20 min of treatment. The by-products, their occurrence time and their maximum concentrations are listed in

Table 3-1. Also, the evolution of their concentration as a function of time can be shown in Figure 3-5.

Table 3-1. List of AO7 by-products and their concentrations during EF experiment

Aromatic by-products		**Short-chain carboxylic acids**	
By-products and their occurrence period	Maximum concentrations	By-products and their occurrence period	Maximum concentrations
• Hydroquinone (35-60min)	0.854 mM	• Oxalic acid (360-450min)	1.114 mM
• 1,4-Benzoquinone (12-16min)	0.0037 mM	• Maleic acid (450-480min)	0.173 mM
• 2-Formyl-benzoic acid (14-18min)	0.94 mM	• Oxamic acid (450-480min)	0.091 mM
• 1,2-Napthoquinone (6-16min)	0.32 mM	• Fumaric acid (5-30min)	0.254 mM
• 2-Hydroxyl-1,4-napthalenedione (16-28min)	0.17 mM		
• 4-Hydroxylbenzenesulphonic acid (10-16min)	0.0075 mM		
• 2-Napthol (28-35min)	0.12 mM		

3.2.4.5. Evolution of short-chain carboxylic acids

Generation of short-chain carboxylic acids was expected from the oxidative ring opening of aromatic intermediates [229-232]. Actually, during the degradation of AO7 (1mM), the oxalic, the maleic, the oxamic and the fumaric acids could be detected by HPLC at 11.6, 13.59, 15.23 and 23.54 minutes of retention time respectively. Figure 3-5c showed their evolution as a function of EF treatment time during the decomposition of 1mM AO7 aqueous solution at pH 3.0. Generally, these acids were generated in very short time of reaction. In the early period of AO7 decomposition, fumaric acid (FA) was the main short-chain by-product which appeared as soon as the electrolysis started (after 5 minutes of reaction). It was then destroyed quickly into shorter chain acids such as oxalic and maleic acids. Oxalic, maleic and oxamic acids were only

detected after 4h of reaction. This meant that they were typical degradation products from aromatic compounds and fumaric acid. Oxalic acid (OA) was the main final by-product formed before complete mineralization, as also observed during treatments carried out by advanced oxidation techniques [166, 233-235]. Oxamic acid (OMA) could be produced from the degradation of 2-hydroxy-4-(N-acetyl)aminophenol or from the oxidation of acetamide [236]. Maleic acid was detected, but at a very low concentration which is in accordance with what has been reported by Ozcan *et al.* [237]. After 8h treatment, the concentration of oxalic and maleic acids were measured at 0.883 mM and 0.173 mM respectively.

3.2.4.6. Evolution of inorganic ions

The conversion of original nitrogen and sulfur elements from degradation of AO7 dye led to the formation of inorganic ions such as sulfate, nitrate and ammonium which is presented in Figure 3-5 d. Sulfate ion apparition was observed quickly, indeed after 1 h of oxidation treatment its concentration attained around 1 mM which was in good agreement with molar balance with regard to the initial concentration of sulfur elements. In a different way, ammonium ion was generated in small amount during all process. As also seen in Figure 3-5 d, nitrate ion concentration increases linearly with the treatment duration and reached the value of 1.1 mM after 8h. There was no equilibration of the nitrogen molar balance which could be explained by the fact that nitrogen could be transferred to the gas phase via N_2 and NH_3 apparition which have already been observed in previous studies [176].

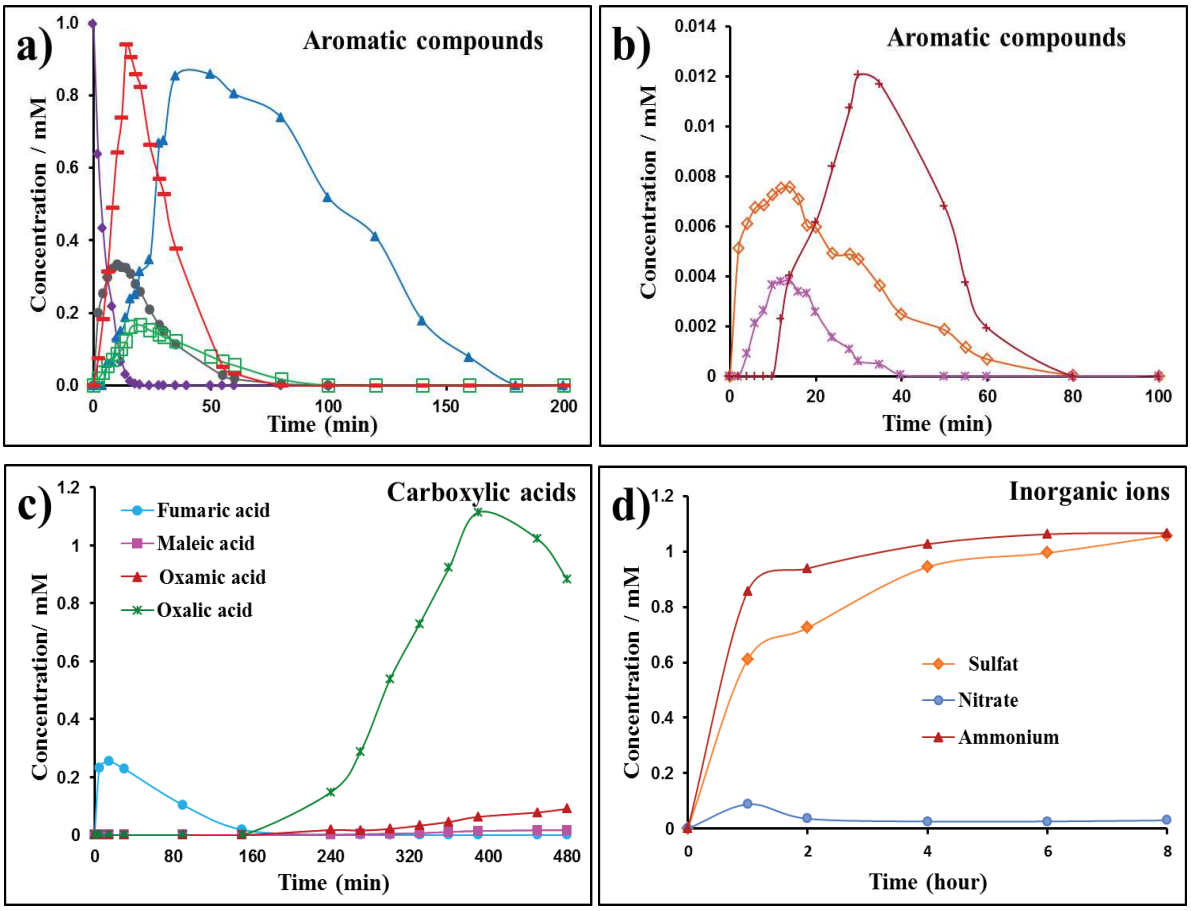

Figure 3-5. Evolution of AO7 by-products. (a, b) Time-course of AO7 and the aromatic degradations: AO7 (◆); 1,2 naphthoquinone (●); Hydroquinone (Δ); 4-hydroxybenzenesulfonic acid (◇); 1,4 benzoquinone (∗); 2-naphtol (+); 2-hydro-1,4 naphthoquinone (□), 2-formyl-benzoic acid (-); (c) Carboxylic acids; (d) Inorganic ions during EF treatment of 500 mL AO7 at C_0 = 1.0 mM; pH =3; $[Na_2SO_4]$=50 mM, I = 500 mA, and $[Fe^{2+}]$ = 0.2 mM.

3.2.4.7. Toxicity assessment during AO7 degradation

Figure 3-6 presented toxicity assessments during AO7 oxidation by EF process (with two different operating conditions: 200 mL of 0.1 mM AO7 in Figure 3-6a and 500 mL of 1 mM AO7 in Figure 3-6b). Toxicity was measured by monitoring the inhibition of marine bacteria *Vibrio fischeri* after 5 min and 15 min of exposure. When the EF process started, luminescence inhibition which reflects solution toxicity immediately increased up to 100% and remained at this value during 20 minutes for 200 mL of 0.1 mM AO7 and 100 minutes for 500 mL of 1 mM AO7. This could be linked to the formation of very toxic compounds like 2-naphtol (NOL); 2-hydro-

1,4 naphthoquinone (HNQ); 1,2-naphthoquinone (NAPQ) and 1,4-benzoquinone (BZQ) (Figure 5a), as already shown by other studies [238-242]. After that, the decomposition of these products and the emergence of short-chain carboxylic acids led to the detoxification of the solution, as confirmed by the inhibition ratio evolution, which decreased quickly to zero after 80 min and 270 min for 200 mL of 0.1 mM AO7 and 500 mL of 1 mM AO7 respectively. These results demonstrated that the solution toxicity is closely linked to the presence of aromatic compounds (AO7 and its by-products) at the early stage of EF process, unlike short-chain carboxylic acids found at the end of electrolysis (such as maleic acid) which have a very low toxicity.

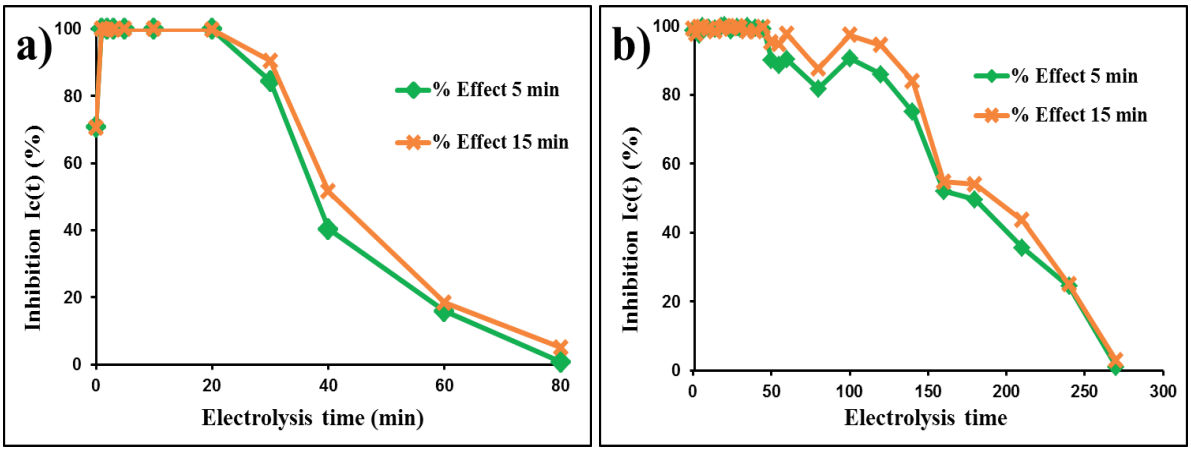

Figure 3-6. Evolution of the inhibition of marine bacteria luminescence after 5 min and 15 min of exposure with a sample taken after different EF treatment duration of AO7 solution. (a) 200 mL of 0.1 mM AO7 and (b) 500 mL of 1 mM AO7 at pH = 3; $[Na_2SO_4]$ = 50 mM, I= 500 mA, and $[Fe^{2+}]$ = 0.2 mM.

After that, the toxicity of each by-product was measured individually at the maximum concentration using HPLC analysis (

Table 3-1). It can be seen from Figure 3-7a that during the analysis time from of 5 to 30 min, 1,4-benzoquinone (BZQ) and 1,2-napthoquinone (NAPQ) had the highest toxicity around 100% compared to 70.43% for 2-formyl-benzoic acid (FBA) or 45.56% for 2-hydroxyl-1,4-naphthalenedione (HNQ). This observation confirms the results found in literature about the toxicity of aromatic hydrocarbons [243]. This result also proved that 1,4-benzoquinone has a strong eco-toxicological impact. Indeed, a small amount formed of only 0.0037 mM caused a noticeable toxic virulence on the selected strain of bacteria. On the opposite, 4-

hydroxylbenzenesulfonic acid (HBA) did not contribute for the toxicity of the oxidized solution when its value was less than 5%. In the following period between 30 and 60 min (Figure 3-7 b), the appearance of hydroquinone (HQ) with the maximum concentration of 0.9 mM led to very high toxicity for the solution. Although, remaining at a low amount, around 0.012 mM, 2-napthol (NOL) presented a remarkable toxicity of 86%. At the end of the experiment, between 6h and 8h (Figure 3-7 c), almost all aromatic compounds were transformed into carboxylic acids like oxalic acid (OA), oxamic acid (OMA) which present a relatively low toxicity.

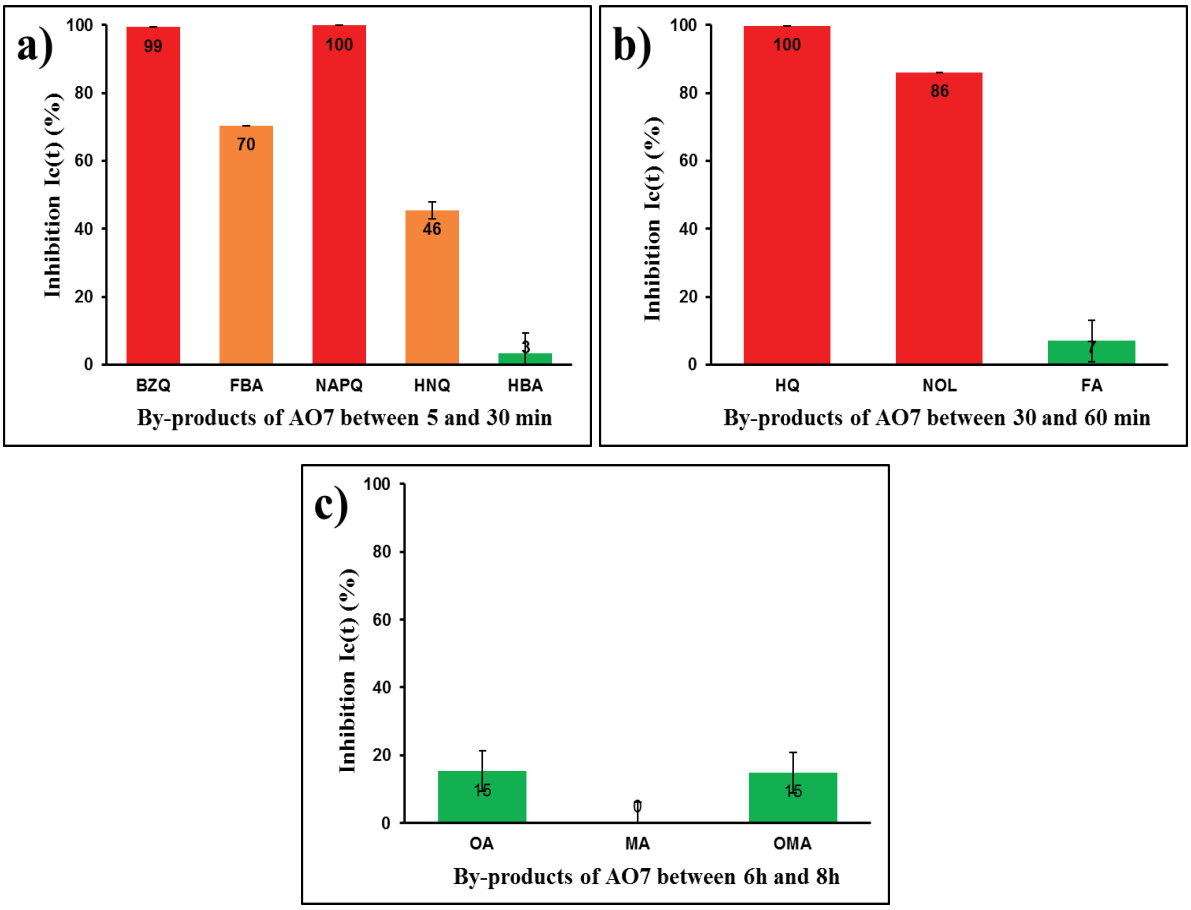

Figure 3-7. Toxicity of AO7 by-products appearing between different time. (a) 5 and 30 min with BZQ = 1,4-benzoquinone, FBA = 2-formyl-benzoic acid, NAPQ = 1,2-napthoquinone, HNQ = 2-hydroxyl-1,4-naphthalenedione, HBA = 4-hydroxylbenzenesulfonic acid; (b) 30 and 60 min with HQ = hydroquinone, NOL = 2-naphthol, FA = fumaric acid, OA = oxalic acid, MA = maleic acid, OMA = Oxamic acid and (c) 6h and 8h of EF treatment of 500 mL (1 mM AO7) at pH =3; $[Na_2SO_4]$ = 50 mM, I = 500 mA, and $[Fe^{2+}]$= 0.2 mM.

To understand well about the toxicity of oxidized solution, AO7 by-products were mixed together at their highest concentrations and the resulting toxicity of the different combinations was measured. Figure 3-8 a, b, c and d shows the toxicity of by-products between 5 and 30 min of EF process which corresponds to the combination of 2, 3, 4, 5 or 6 kinds of compounds identified during this period. Because of high toxicity of 1,4-benzoquinone (BZQ), most of its mixtures with the five other compounds were found to be highly toxic for the marine bacteria. Therefore, the toxicity of these groups was huge, around 100%, while the mixtures which included 2-hydroxyl-1,4-napthalenedione (HNQ), 4-hydroxylbenzenesulphonic acid (HBA) or fumaric acid (FA) did not induce a significant increase of the solution toxicity. The second set of mixtures for AO7 by-products observed between 30 and 60 min of EF process (Figure 3-8 e) were also found to be toxic, except the one with 2-naphthol and fumaric acid as its value was approximately 40%. In agreement with the assessments of individual compounds toxicity and mixture tests, the last mixtures done with compounds observed between 6h and 8h of EF process (Figure 3-8 f) did not show a valuable toxicity. As a result, it could be concluded that the oxidized AO7 solution toxicity was mainly caused by aromatic compounds which appeared during the first minutes of the degradation process. Then, the attack of hydroxyl radical •OH produced by electro-Fenton reaction produced short-chain carboxylic acids which declined importantly the toxicity and lead to a less harmful solution for marine bacteria. These results give out a full picture about toxic combined interactions of AO7 by-products formed during EF oxidation in aqueous medium which could be very useful and interesting for environmental applications of this advanced oxidation process.

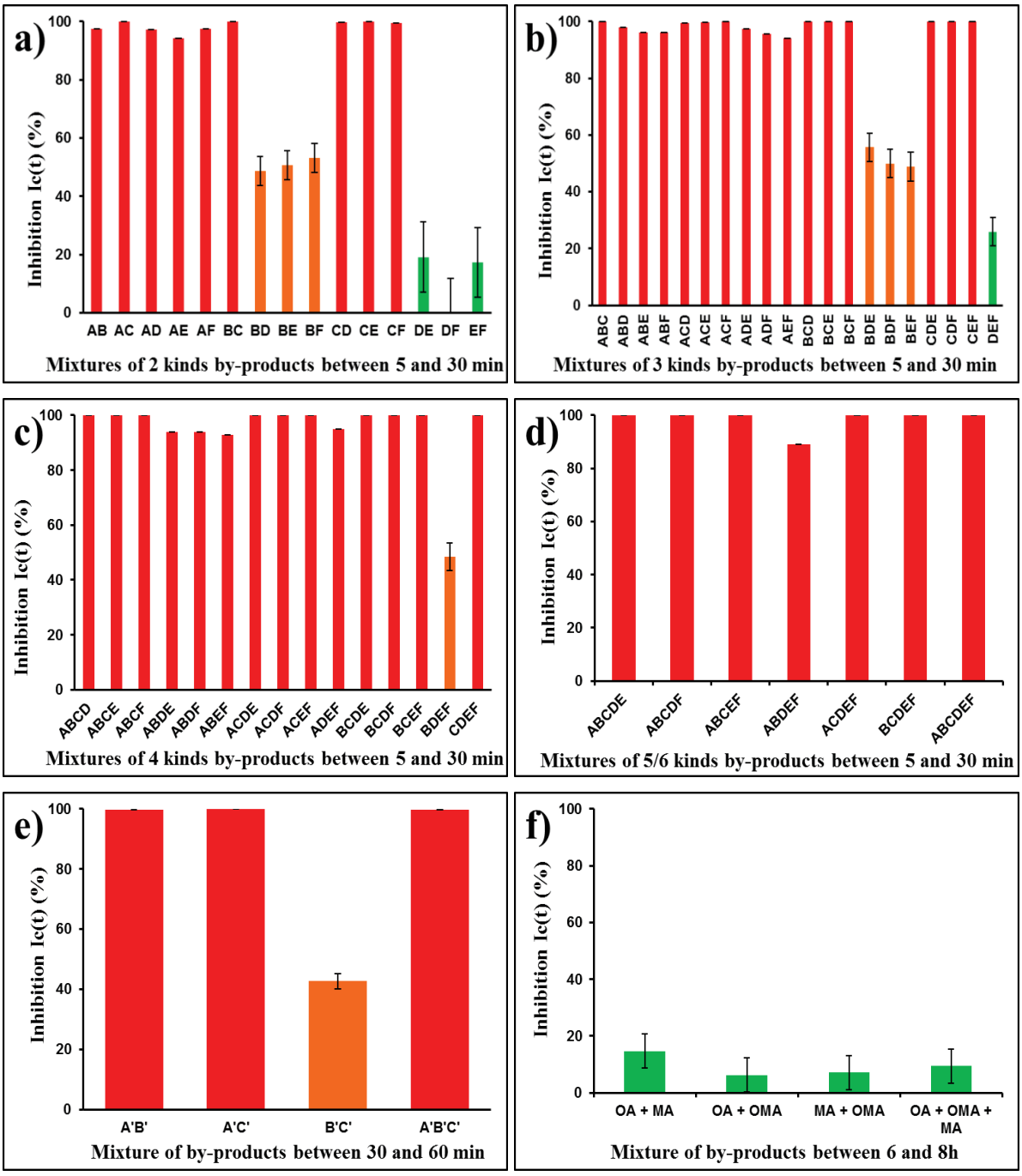

Figure 3-8. Toxicity of mixtures of AO7 by-products. (a) 2 kinds, (b) 3 kinds, (c) 4 kinds, (d) 5 or 6 kinds of by-products found between 5 and 30 min; (e) between 30 and 60 min and (f) for 6h and 8h of EF process of AO7 at following operating conditions: 500 mL (1 mM AO7) at pH =3; $[Na_2SO_4]$=50 mM, I = 500 mA, $[Fe^{2+}]$ = 0.2 mM. A = BZQ, B = FBA, C = NAPQ, D = HNQ, E = HBA, F = FA; A' = HQ, B' = NOL, and C' = FA.

3.2.4.8. Degradation pathway of AO7 solution

From the identification of by-products by HPLC-UV and LC-MS methods (Table 3-2), a possible pathway for AO7 dye degradation by the EF process is proposed in Figure 3-9. The process was initiated by •OH radical attack resulting in the formation of two hydroxylated AO7 molecules, *i.e.* 4-[(2,3-dihydroxy-1-naphthyl)diazenly]-benzenesulfonate (m/z = 346) (XI) and 4-[(2,3,4-trihydroxy-1-naphthyl)diazenly]-benzenesulfonate (m/z = 362) (XII) which were identified within the first minutes of the EF reaction. These hydroxylated intermediates were rarely seen in other previous study dealing with the degradation of AO7 dye. The formation of those intermediates has however been reported during the photocatalytic degradation of azo dye in aqueous TiO_2 solution [244]. Then, the process continued with the •OH radical attack of azo bond to form the following intermediates: 1,2-naphthoquinone (IV) and 4-hydroxybenzensulfonic acid (VI). Afterwards, 4-hydroxylbenzenesulfonic acid underwent further desulfonation to form 1,4-benzoquinone (II) that was then oxidized to hydroxylated hydroquinone (I) and suggested 1,2,4-benzentriol. Actually, the latter product could be hardly identified because it was unstable and quickly transformed into carboxylic acids by oxidative ring opening reactions. Intermediate (IV) was oxidized to form well identified naphthalene-type compounds, such as 2-hydroxy-1,4-naphthalenedione (V), 2,3-dihydroxy-1,4-naphthalenedione (VIII), 1,2-naphthalenediol (IX) and 2-naphthol (VII). The formation of these naphthalene-type products was also been reported in several previous studies dealing with AO7 degradation [245, 246]. By continuous •OH radical action, naphthalene by-products were decomposed into 1(3H)-isobenzofuranone (X) and 2-formyl-benzoic acid (III). These last aromatic by-products were further degraded to generate short-chain carboxylic acids including fumaric acid, maleic acid, oxalic acid and oxamic acid. Finally, these organic acids were decomposed into CO_2, H_2O and inorganic ions.

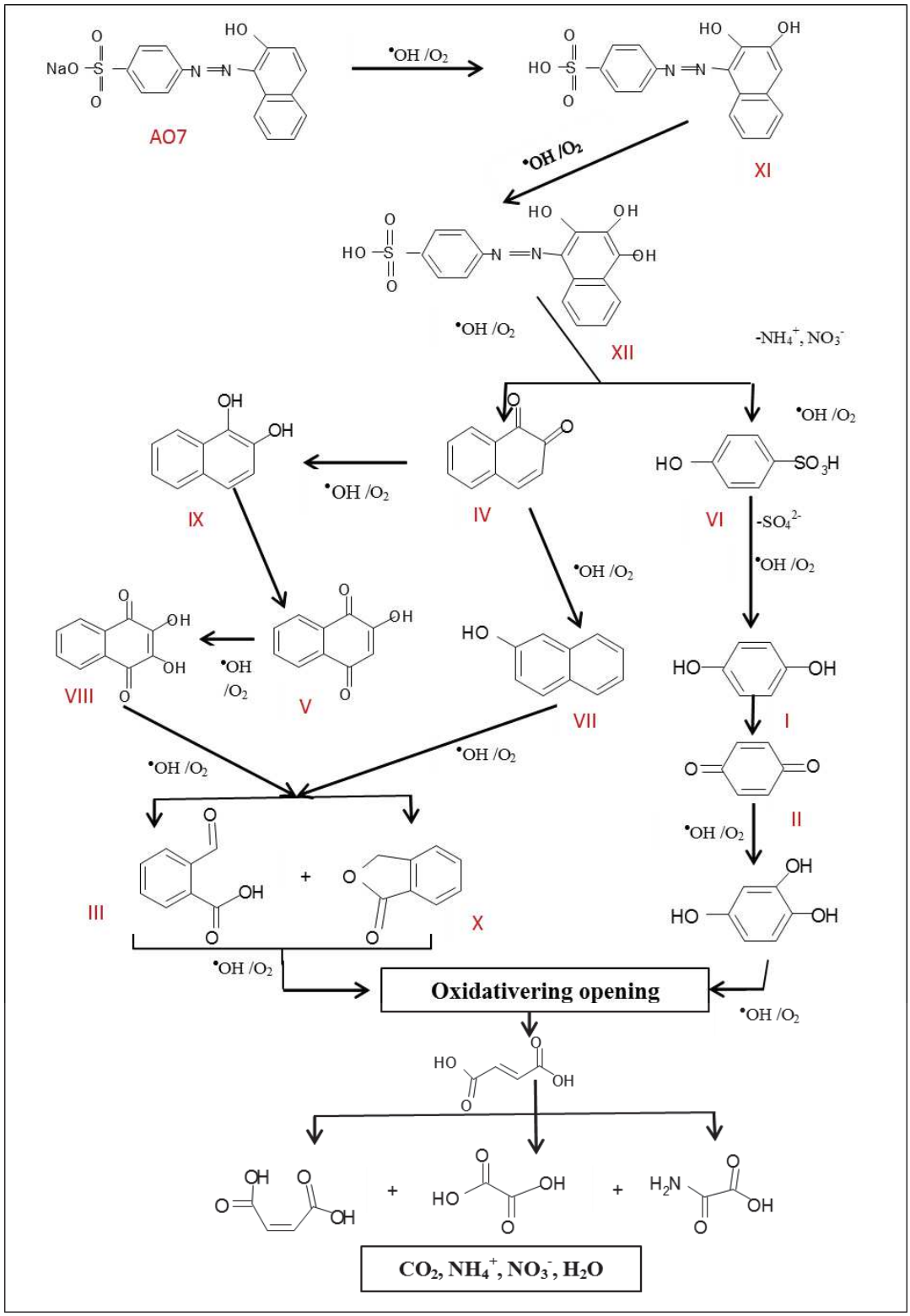

Figure 3-9. General reaction sequence proposed for AO7 mineralization in acid medium by hydroxyl radicals during EF process.

Table 3-2. HPLC and LC/MS identification parameters (retention times (t_R)), MS mass fragmentation) of aromatic by-products formed during the EF treatment of AO7.

No	Compound name	HPLC-UV	LC-MS	
		t_R(min)	t_R(min)	Molecular mass (MH^+) and fragments
I	Hydroquinone	5.08		
II	1,4-Benzoquinone	6.52		
III	2-Formyl-benzoic acid	9.44	1.87	149,118,96
IV	1,2-Naphthoquinone	17.39		
V	2-Hydroxyl-1,4-naphthalenedione	18.71	3.82	175,147,118
VI	4-Hydroxylbenzenesulfonic acid	19.33	4.09	174,158,130,7
VII	2-Naphthol	27.11	4.64	147,91
VIII	2,3-Dihydroxy-1,4-naphthalenedione		2.26	191,163,131,96
IX	1,2-naphthalenediol		2.44	163, 135,118,96
X	1(3H)-isobenzofuranone		3.59	133,128,118,96
XI	4-[(2,3-dihydroxy-1-naphthyl)diazenyl]-benzenesulfonate		4.71	346,329,130,98
XII	4-[(2,3,4-trihydroxy-1-naphthyl)diazenyl]-benzenesulfonate		5.37	362,346,173,128,118

3.2.5. Conclusions

This study focused on using commercial CF (60 cm^2) for the removal of a dye AO7 taken as a pollutant model, by EF process. In a first step, the operating parameters affecting the EF reaction (*i.e.* applied current density and catalyst concentration) were investigated in acidic medium (pH 3.0) and optimized with regards to degradation kinetic and TOC removal results. The operating conditions to get optimal degradations were 500 mA and 0.2 mM for applied current density and catalyst concentration, respectively. At these values, the mineralization of 200 mL of AO7 was 96.2% after 8h treatment. The identification and the evolution of intermediate compounds, as well as the toxicity of the solution, were also examined carefully along the EF

process. In order to characterize and to quantify as accurately as possible the formation of by-products, both the volume of solutions (500mL) and initial concentrations of pollutant (1 mM) were extended. Twelve aromatic by-products could be revealed by HPLC and LC-MS techniques during the decomposition of AO7. The early formation of toxic aromatic products like 1,2-naphtoquinone or 1,4-benzoquinone was correlated to the increase in solution toxicity reaching 100% for 100 first minutes of the EF treatment. The subsequent decomposition of these intermediates led to the formation of short-chain carboxylic acids and thereby to a drastic decrease of the bacteria luminescence inhibition ratio. Consequently the total detoxification of the solution was accomplished after 270 minutes for AO7. The sequential degradation of pollutants and their intermediates produced inorganic ions such as ammonium, nitrate and sulfate which could be quantified at the end of the electrolysis. Finally two complete pathways of AO7 degradation by the EF process could be built and proposed.

3.3. Correlation between degradation pathway and toxicity of ACE and its by-products, using EF process in aqueous media

3.3.1. Abstract

The evolution of the degradation by-products of an ACE solution was monitored by HPLC-UV/MS and IC in parallel with its ecotoxicity (*Vibrio Fischeri* 81.9% Microtox® screening tests) during EF oxidation performed on CF. The aromatic compounds 2-hydroxy-4-(N-acetyl) aminophenol, 1,4-benzoquinone, benzaldehyde and benzoic acid were identified as toxic sub-products during the first stage of the electrochemical treatment whereas aliphatic short-chain carboxylic acids (oxalic, maleic, oxamic, formic, acetic, fumaric acids) and inorganic ions (ammonium, nitrate) were well identified as non-toxic terminal sub-products. Electrogenerated hydroxyl radicals turned then the eco-toxic and bio-refractory of initial ACE molecule (500 mL, 1 mM) and subsequent aromatic sub-products, into non-toxic compounds after 2 hours of EF treatment. The toxicity of every intermediate produced during the mineralization of ACE was quantified and a relationship was established between the degradation pathway of ACE and the global toxicity evolution of the solution. After 8 hours of treatment, a TOC removal of 86.9 % could be reached for 0.1mM ACE at applied current of 500 mA with 0.2 mM of Fe^{2+} used as catalyst.

Key words: *Carbon felt, Advanced Oxidation Process, TOC, Mineralization, By-products, Toxicity*

3.3.2. Introduction

Over the past few years, pharmaceutical drugs have become a severe problematic for the domestic wastewater treatment [247]. Pharmaceuticals such as anti-inflammatories, analgesics, lipid regulators, antibiotics, anti-epileptics, betablockers or oestrogens are used extensively for both human use and livestock. When consumed, 10 to 90% of these drugs are metabolized. A significant quantity of the active ingredients is therefore excreted, mainly with urine and feces, and collected in urban sewer systems or discharged directly into the environment by livestock. Many studies have confirmed the presence of a large number of medicinal substances in all compartments: ground and surface water [248, 249], drinking water [250], tap water [251], ocean water, sediment and soil [252], pointing out the inefficiency of conventional water treatment processes to remove these kinds of micro-pollutants. Even if the amount of these pharmaceuticals in aquatic media is low, usually with concentrations lower than 10 $\mu g\ L^{-1}$ [253-255], its continuous input constitutes at long term a real risk for aquatic and terrestrial organisms [63, 256]. Some pharmaceuticals are indeed suspected to affect the endocrine system of fishes and available data on antibiotics indicate that they can exert toxic effects on algae and invertebrates and may favor the development of antibiotic multi-resistant microorganism strains [257, 258]. Among pharmaceuticals, ACE is an analgesic molecule worldwide consumed, usually selected by researchers as a model emerging contaminant [259]. ACE is also called paracetamol and its chemically name is N-acetyl-p-aminophenol. This drug has been detected in European Wastewater Treatment Plant (WWTP) with a concentration of 6 $\mu g\ L^{-1}$ [253], up to 10 $\mu g\ L^{-1}$ in natural water resource in USA [260] and over than 65 $\mu g\ L^{-1}$ in the Tyne River, UK [261, 262].

Because of the toxicity and persistency of pharmaceuticals, it is necessary to develop powerful methods to ensure the total destruction of pharmaceutical pollutants as well as their potentially toxic degradation by-products. Conventional technologies currently used such as activated carbon adsorption, flocculation, biological degradation, and chemical process like chlorination, have the disadvantages to be poorly efficient for non-biodegradable compounds or to transfer the pollutants into the solid phase (sludge or sorbent). Pollution is, in this case, only displaced and not solved at all. AOPs (Ozonation, UV/H_2O_2, electro- and photo-Fenton) can be

easily incorporated to pre-existing treatment plants and were found to achieve efficient reduction of micropollutant discharge in the aquatic environment [263-267]. Based on the generation of non-selective radicals, such as the hydroxyl radicals (OH), AOPs are considered as a competitive water treatment technology for the degradation of these refractory organic micropollutants and the improvement of effluent quality from treatment plants [268, 269]. A great number of publications have highlighted the potentialities of AOPs, such as UV/H_2O_2 [270, 271]; ozonation [264, 269, 272-274], Fenton and photo-Fenton [275, 276], semiconductor photocatalysis [277, 278], and electrochemical separation and degradation technologies [279] in order to eliminate biorefractory pharmaceuticals. Derived Fenton processes have also already proved to be efficient methods to degrade ACE from water: combined EF and photo-Fenton using a double cathode electrochemical cell [280], coupling adsorption and photo-Fenton using nano-zeolites and cobalt ferrite nanoparticles [281], bio-electrochemical degradation in a MFC-Fenton system [209], or other methods relevant to the photo-Fenton process [282-285]. As a more detailed example, Sirés *et al.* could totally mineralized ACE in CO_2 after 6h of treatment, using the catalytic action of Fe^{2+}, Cu^{2+}, and UVA light to generate hydroxyl radicals. During the electrolysis, several by-products were detected such as hydroquinone, p-benzoquinone, or short chain carboxylic acids [286]. In addition, the combination of adsorption and photo-Fenton method by Irani *et al.* could lead to 99.80 % of the paracetamol removal in 30 min [281].

Depending on the AOPs technique used, several degradation pathways of ACE have been identified and already published [287-290]. All authors observed the formation of reactive by-products due to partial oxidation of the initial molecule and reaction with matrix components [291]. It is important to track the intermediates generated through degradation reactions and to know their eco-toxicity, with the view to verify the safety of the water treatment process. Unfortunately, very few works were aimed at combining analytical chemistry to individual and global toxicity measurement of both products and solution, during AOPs treatment [292] as presented in this study.

Research at laboratory and pilot scale clearly demonstrated that AOPs can be applied to improve the quality of effluents from municipal and industrial wastewater treatment plants by attenuating trace organic contaminants (micropollutants) [268, 269] . However, a potential disadvantage of these processes is the formation of unknown reactive by-products due to partial oxidation of the targeted compounds and reaction with matrix components [291]. Thus the final toxicity of treated effluent should be determined as well as the quantity of targeted compounds

with regard to the detection limits of the analytical protocols. In this study, EF reaction was applied to ACE solution. ACE and its by-products generated during the degradation were monitored by HPLC-UV/MS, IC and TOC analysis. Furthermore, acute toxicity of the ACE solution under EF treatment, as well as individual and mixed intermediate standards has been assessed through Microtox® toxicity test with *Vibrio Fischeri* marine bacteria. Through this study, the relationship between the ACE degradation pathway, the individual by-product toxicity and the global toxicity of the solution could be newly and clearly established, thus building up a more comprehensive understanding and safety control of the mineralization process of ACE by EF process.

3.3.3. Experimental

3.3.3.1. Materials

ACE, sodium sulphate (anhydrous, 99.0 – 100.5%), sodium hydroxide (99%), sulfuric acid (95-97%), iron (II) sulphate hepta-hydrate (99%), benzoquinone, benzaldehyde, benzoic acid, oxalic acid, maleic acid, oxamic acid, formic acid, fumaric acid and acetic acid were obtained from Sigma-Aldrich, USA. Bacterial strain of *Vibrio Fischeri* NRRL B-11177 involved in toxicity tests came from Hach Lange GmbH, Germany. Osmotic adjusting solution (MilliQ water with 22% NaCl) and diluent (MilliQ water with 2% NaCl) were used for the preparation of bacteria solution. The CF was purchased from A Johnson Matthey Co., Germany. TOC standard of 1000 mg L^{-1} (Sigma-Aldrich, USA) and sodium hydrogen carbonate (≥. 99.5%, ACS, Karlsruhe, Germany) were used for total organic and IC calibration curves assessments.

3.3.3.2. Electrochemical system for ACE degradation

EF experiments were performed at room temperature in a 500 mL undivided cylindrical glass cell with a two-electrodes system. The applied current was controlled using a power supply (Lambda Electronic, USA) in galvanostatic mode. The CF cathode (60 cm^2) was used as working electrode and a Pt cylindrical mesh as counter electrode. The anode was centered in the electrolytic cell, surrounded by the cathode, which covered the inner wall of the cell. The distance between the electrodes was 1.5 cm. The aqueous solution of ACE, Na_2SO_4 (50 mM) as supporting electrolyte and $FeSO_4.7H_2O$ as the catalyst were prepared by adjusting the pH at 3.0 with sulphuric acid (H_2SO_4). The intermediate compounds monitoring experiment was performed in 500mL solution of ACE 1 mM and/or 200 mL solution of ACE 0.1 mM with $FeSO_4.7H_2O$ (0.2

mM) at an applied current of 500 mA. Prior to the electrolysis, oxygen bubbling was performed for 5 minutes to saturate the solutions and kept during experiment under continuous magnetic stirring at a rate of 800 rpm.

3.3.3.3. Analytical procedures and toxicity test

The analytical procedures as well as toxicity tests were performed according to the procedures that were well presented in section 3.2.3.3 and 3.2.3.4.

3.3.4. Results and discussion

3.3.4.1. Degradation pathway of ACE during EF process

3.3.4.1.1. Evolution of aromatic compounds

The degradation of ACE by EF process formed some aromatic compounds such as 1,4-benzoquinone, benzaldehyde and benzoic acid identified by HPLC (Figure 3-10) and 2-hydroxy-4-(N-acetyl) aminophenol identified by LC/MS (Table 3-3). It could be noticed that at the beginning of the ACE degradation, 1,4-benzoquinone was the main aromatic by-product identified. Its highest concentration reached 0.23 mM after 10 minutes of the degradation process, then its concentration decreased and this product disappeared totally after 120 minutes. The other identified aromatic intermediates are also detected at a very short time of decomposition process with a concentration peak of 0.09 mM and 0.039 mM at 14 and 10 min for benzoic acid and benzaldehyde respectively. These aromatic compounds were totally decomposed after 120 min of electrolysis and were converted into other aliphatic carboxylic acids and inorganic ions with the right mass balance.

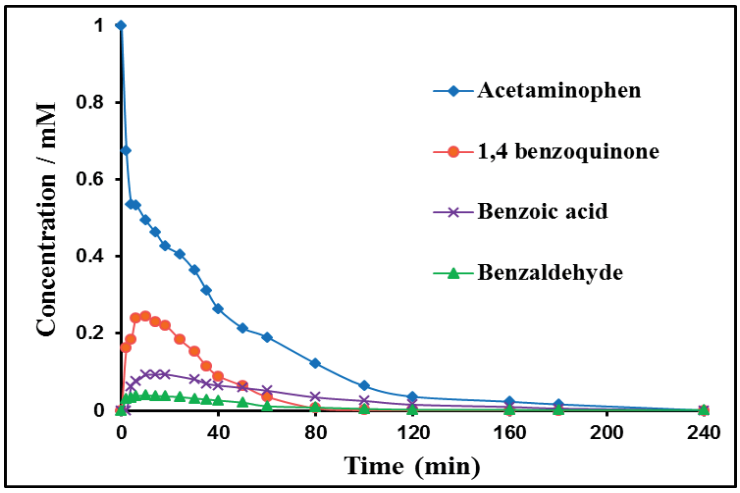

Figure 3-10. Evolution of the concentration of ACE and the aromatic degradation by-products during EF treatment. Condition: 500 mL ACE solution at C_0 = 1.0 mM; pH =3; [Na_2SO_4]=50 mM, I = 500 mA and [Fe^{2+}] = 0.2 mM.

Table 3-3. HPLC and LC/MS identification parameters (retention times (t_R) and mass fragmentation) of aromatic by-products formed during EF treatment of 500 mL ACE solution at C_0 = 1.0 mM; pH =3; [Na_2SO_4]=50 mM, I = 500 mA and [Fe^{2+}] = 0.2 mM.

No	Compound name	HPLC	LC/MS	
		t_R/min	t_R/min	Mass fragmentation (M^+)
I	ACE ($C_8H_9NO_2$)	4.37	2.64	152,110, 93, 82, 65
II	2-hydroxy-4-(N-acetyl)aminophenol ($C_8H_9NO_3$)	-	2.15	168, 126, 108, 80
III	1,4-Benzoquinone ($C_6H_4O_2$)	6.52	-	
IV	Benzaldehyde (C_7H_6O)	9.44	-	
V	Benzoic acid ($C_7H_6O_2$)	18.19	-	

- : Not analysed

3.3.4.1.2. Evolution of short-chain carboxylic acids

The evolution of carboxylic acids concentration during the electrolysis treatment of a 1.0 mM ACE aqueous solution at pH 3.0 is reported in Figure 3-11. These by-products are usually found in ACE degradation by AOPs such as ozonation [289] or electrogenerated hydrogen peroxide process [263]. Oxalic, maleic, oxamic, formic, acetic and fumaric acids were detected at 11.6, 13.59, 15.23, 20.59, 22.25, and 22.89 min of retention time during the degradation experiment. It could be observed from Figure 3-11 that fumaric and oxamic acids were generated after around 20 minutes of electrolysis while other by-products such as maleic, acetic, formic and oxalic acids were detected only after 3h. The accumulation of oxalic acid is well-known in Fenton related processes because of the formation of iron-oxalate complexes that are slowly removed by $^{\bullet}OH$. At the end of the EF treatment (8h), fumaric, acetic and formic acids were completely removed from solution while oxalic and maleic acid were still present in the solution. Singularly, oxamic acid concentration was kept high (around 0.52 mM) after 8h of treatment, with a TOC removal of 51%. This indicated that oxamic acid remained stable under our experimental conditions.

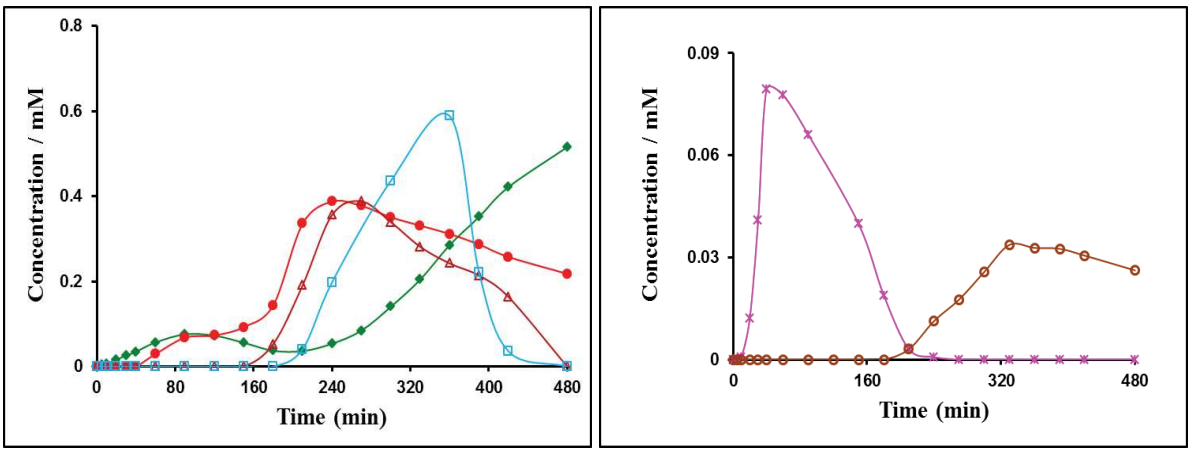

Figure 3-11. Evolution of the concentration of carboxylic acids during EF degradation of ACE. Oxalic acid (●), Acetic acid (□), Formic acid (Δ), Oxamic acid (◆), Fumaric acid (∗), Maleic x 10 (○). Conditions: 500 mL ACE solution at C_0 = 1.0 mM; pH =3; $[Na_2SO_4]$=50 mM, I = 500 mA and $[Fe^{2+}]$ = 0.2 mM.

3.3.4.1.3. Evolution of inorganic ions

The mineralization of ACE and their intermediates also produced inorganic ions. Ammonium and nitrate concentrations have then been monitored during the 8 hours of treatment (Figure 3-12). Nitrate was measured at very low concentrations, compared to ammonium. As noticed by E. Brillas *et al.* [293], the first limiting step of ACE degradation is the hydroxylation reaction leading to 2-hydroxy-4-(N-acetyl) aminophenol (Table 3-3) which is then converted into oxamic acid. The presence of Fe^{2+} in the solution as catalyst could lead to the concomitant production of persistent iron-oxamate complexes which are very difficult to mineralize by •OH, thus limiting the oxidation ability of the EF process. Therefore, nitrate was clearly detected and quantified only after 2h treatment and reached 0.02 mM in 8h while ammonium reached up to 0.38 mM at the same time (Figure 3-12). As shown in Figure 3-11 and Figure 3-12, at the end of the treatment process, the initial nitrogen-containing compound (1mM) was converted into oxamic acid (0.52 mM), ammonium (0.38 mM) and trace of nitrate (0.02 mM). Therefore, a total of 0.92 mM of N in by-products was quantified, which means that the nitrogen mass balance is confirmed, taking into account that around 8 % of nitrogen lost during the EF process could be explained by the fact that nitrogen could be transferred to the volatile phase via N_2 and NH_3 apparition [176].

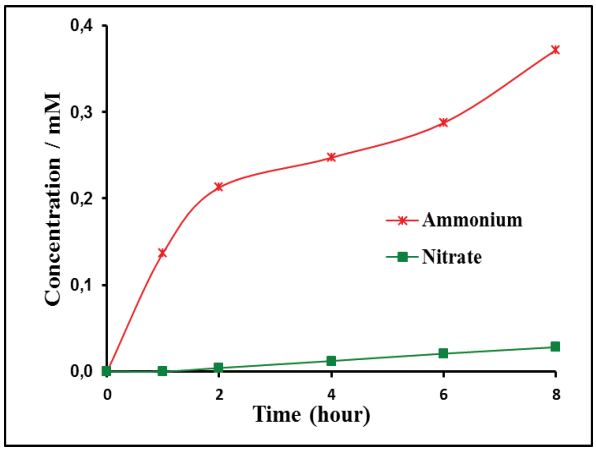

Figure 3-12. Evolution of the inorganic ions concentration during EF degradation of ACE. Conditions: 500 mL ACE solution at C_0 = 1.0 mM; pH =3; [Na_2SO_4]=50 mM, I = 500 mA and [Fe^{2+}] = 0.2 mM.

3.3.4.1.4. Degradation pathway of ACE mineralization during EF process

After 8h treatment, almost 90% of organic compounds in the initial ACE solution (200 mL at 0.1mM) were mineralized, proving the efficiency of the EF process for removing the pharmaceutical pollutants (Figure 3-13).

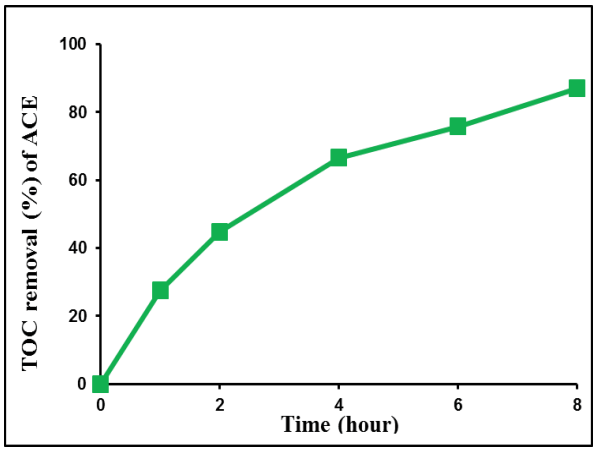

Figure 3-13. TOC removal during EF degradation of ACE. Conditions: 200 mL ACE solution at C_0 = 0.1 mM; pH =3; [Na_2SO_4]=50 mM, I = 500 mA and [Fe^{2+}] = 0.2 mM.

A general reaction sequence for the EF degradation of ACE in acidic medium is proposed in Figure 3-14. The process was initiated by $^{\bullet}OH$ radical attack either on the C(2) position of ACE (I) which led to the formation of 2-hydroxy-4-(N-acetyl)aminophenol (II), or on its C(4)-position which led to 1,4-benzoquinone (III). The formation of these intermediate products could also be proposed in other AOP processes during degradation of ACE [294]. 2-hydroxy-4-(N-acetyl) aminophenol (II) was then degraded into benzoic acid (V), benzaldehyde (IV) and acetamide. Afterwards, all aromatic by-products were further oxidized to produce aliphatic organic acids such as fumaric, oxalic, acetic, formic and maleic acids. On the other way, oxamic acid was generated from the oxidation of acetamide [289]. At the end of the degradation process, unlike oxamic and oxalic acids which persisted under our experimental conditions, all of these last by-products were transformed into CO_2, H_2O and inorganic ions.

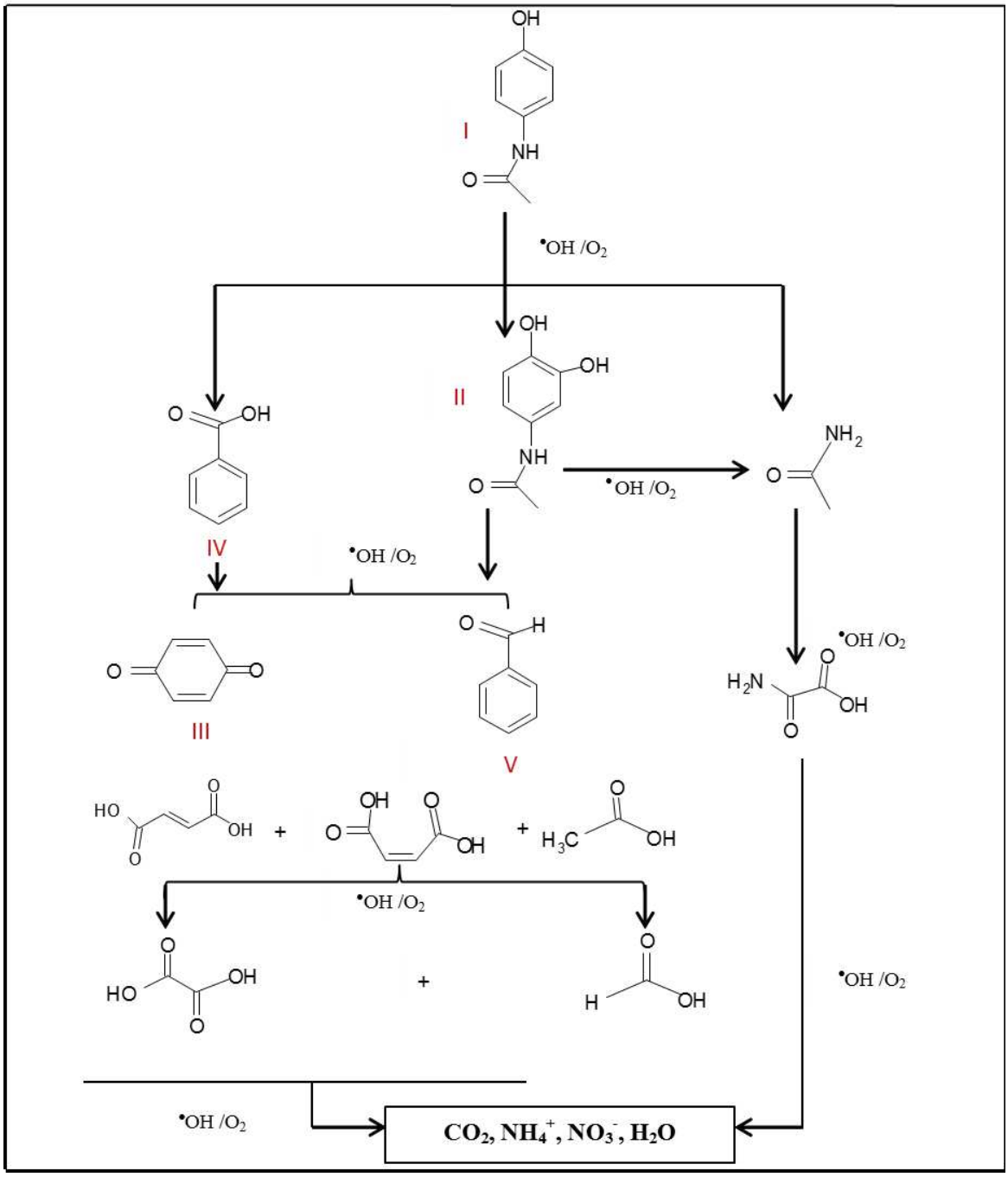

Figure 3-14. General reaction sequence proposed for ACE mineralization in acidic medium by hydroxyl radicals during EF process.

3.3.4.2. Toxicity evolution of ACE solution during EF process

3.3.4.2.1. Global toxicity

The global toxicity evolution of 500 mL of 1.0 mM ACE solution during 8h of EF treatment is shown in Figure 3-15. The acute toxicity of the treated solution after 5 and 15 min time contact with *Vibrio Fischeri* bacteria strains increased rapidly at the early stage of the treatment and reached 100% between 2 min and 55 min. This result is relevant and consistent with regards to the previously proved formation of toxic aromatic by-products like 1,4-benzoquinone, benzoic acid and benzaldehyde [239, 295, 296]. After 60 min, the toxicity markedly declined which well agreed with aromatic compounds found only at trace levels at this stage of the EF reaction (see part 3.3.4.1.1 and Figure 3-10). The predominance of very low toxic short-chain carboxylic acids in this period did not significantly contribute to the inhibition of the bacteria luminescence; consequently, the solution toxicity came to zero at about 120 minutes. After that, the value of the inhibition was continuously kept around zero until 8h where short-chain carboxylic acids were continuously transformed under •OH attack during EF process. The two exposure times measured gave identical inhibition (%) results.

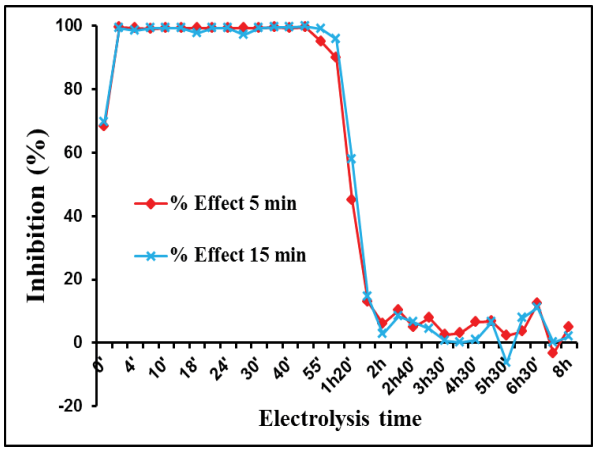

Figure 3-15. Inhibition of *Vibrio Fischeri* marine bacteria luminescence during EF treatment. Condition: 500 mL of 1 mM ACE at pH=3.0; [Na_2SO_4]=50mM, I=500 mA, [Fe^{2+}]=0.2mM. Two exposure time of bacteria to treated solution were used (5 min and 15 min).

3.3.4.2.2. Toxicity of intermediate sub-products

The toxicity of individual and mixed aromatic by-products taken as standard solutions was investigated by the ecotoxicity assays. Their concentration was selected with regard to those analysed during the ACE degradation. For this purpose and according to by-products formation shown Fig. 2, specific times of EF treatment were considered: 10 min, 60 min, 80 min and 120 min corresponding to different mixture solutions and concentrations of by-products (Table 3-4).

Table 3-4. The aromatic by-products and their concentrations (RSD 2% n=3) at several treatment times of ACE solution (1 mM) during EF process.

Time treatment	**Aromatic by-products**	**Concentration measured in ACE solution under EF treatment**
10 min	ACE	0.500 mM
	1,4-Benzoquinone	0.240 mM
	Benzaldehyde	0.039 mM
	Benzoic acid	0.090 mM
60 min	ACE	0.200 mM
	1,4-Benzoquinone	0.040 mM
	Benzaldehyde	0.011 mM
	Benzoic acid	0.050 mM
80 min	ACE	0.120 mM
	1,4-Benzoquinone	0.010 mM
	Benzaldehyde	0.007 mM
	Benzoic acid	0.030 mM
120 min	ACE	0.035 mM
	1,4-Benzoquinone	traces mM
	Benzaldehyde	0.002 mM
	Benzoic acid	0.010 mM

As seen in Figure 3-16 a, b, c and d, ACE itself is not a hazardous pollutant for this strain of bacteria since its toxicity was very low even at the high concentration (0.5 mM) found after

10 min of treatment. Similarly, benzoic acid was also a low toxic by-product, since its negative toxicity values toward bacteria during degradation process significates a positive effect on bacteria growth and activity [297]. On the contrary, 1,4-Benzoquinone presented a noticed important toxicity as the inhibition ratio was around 100% even at very low amount, 0.04 mM (60 min degradation), compared to other formed aromatic intermediates. Although benzaldehyde was not as toxic as 1,4-benzoquinone, this compound still affected badly bacteria luminescence [298]. It caused an acute toxicity between about 50% and 20% at the concentration of 0.039 mM (10 min.) and 0.002 mM (120 min.) respectively. Besides, the mixtures of these aromatic compounds at four periods from 10 min, 60 min, 80 min to 120 min was ecotoxically assessed (Figure 3-16 e). The inhibition ratio reached 100% at the early stage of the treatment (10 min and 60 min), again proving the high toxicity of 1,4-benzoquinone. This is in a good agreement with previous published results [299]. Afterward, a remarkable detoxification was observed after 80 min and 120 min due to the decline of the corresponding toxic aromatics.

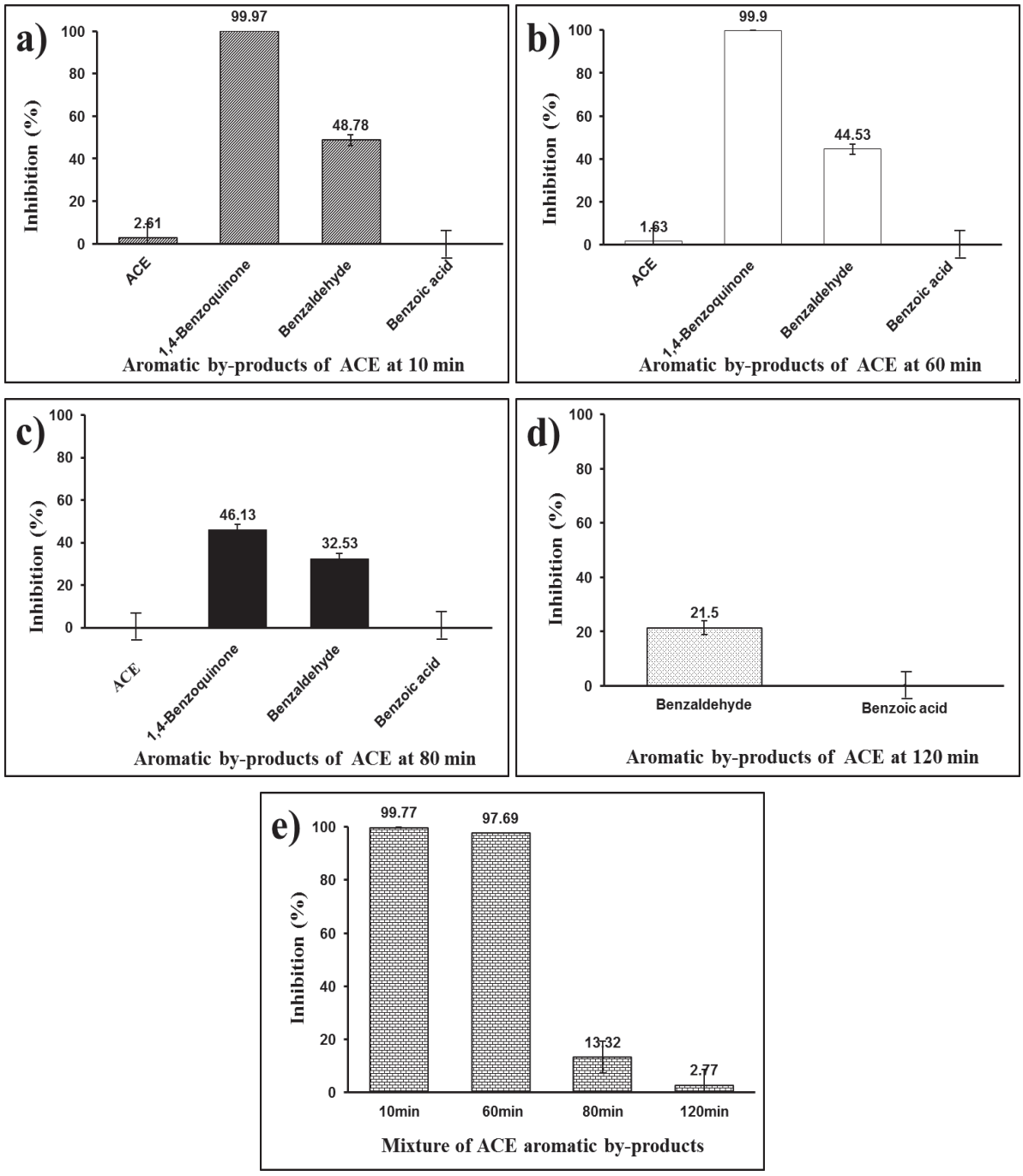

Figure 3-16. Toxicity of standard solutions of ACE and other aromatic compounds. Taken alone (a,b,c,d) or in mixture (e), under identical concentration, during EF process on 500 mL (1 mM ACE) and for different treatment times: (a) 10 min, (b) 60 min, (c) 80 min, (d) 120 min. (e) Mixture solutions of standard ACE and aromatic compounds at different treatment times.

At the end of electrolysis, the oxidation by •OH generated during EF process in solution led to the production of ring opened products such as aliphatic carboxylic acids. These acids, such as formic acid or acetic acid are known to be low or non-toxic compounds [300]. This suggestion was confirmed by their toxicity measurement presented in Figure 3-17 in two ways: individual test on each single standard compound in MilliQ water at its maximum concentration measured during EF process (Figure 3-17 a) and the combination (mixture) of all carboxylic by-products at their maximal concentrations measured during three periods of the electrolysis (Figure 3-17 b): 210 - 270 min (Mix 1); 270 - 330 min (Mix 2) and 330 - 480 min (Mix 3) (Table 3-5). Acetic and oxamic acids toxicity have been measured for similar maximum concentration of about 0.5 mM, but oxamic acid seemed to promote higher toxicity than acetic acid with individual toxicity values of 25.7 % and 7 %, respectively. The toxicity of maleic, oxalic and fumaric acids were around 15%. In comparison with other intermediates, formic acid contributed negligibly to the toxicity of the solution. Interestingly, cocktail effect has been observed: synergistic (Mix 1) as well as antagonist effects (Mix 3) were observed during the comparative study on single and mixture of standard compounds. As observed in other studies with pesticides or antioxidants, the combinations of ACE carboxylic acid by-products did not induce an additive increase of individual toxicity [300]. The toxicity of three mixtures decreased gradually as a function of treatment time, 18.7 %; 18.1 %; and 0 %, from 210 min to 480 min. These results confirmed that EF process is an environmentally friendly technology which can efficiently degrade toxic pollutants into non-toxic compounds.

Table 3-5. List of ACE carboxylic acid by-products and their maximum concentrations (RSD 2% n=3) corresponding to treatment time from 40 min to 480 min during EF experiment. Condition: 500 mL (1 mM ACE) at pH =3; [Na_2SO_4]=50 mM, I= 500 mA, [Fe^{2+}]=0.2mM.

Time treatment	Carboxylic by-products	Maximum concentrations
40 min	Fumaric acid	0.079 mM
240 min	Oxalic acid	0.388 mM
270 min	Formic acid	0.388 mM
330 min	Maleic acid	0.0035 mM
360 min	Acetic acid	0.588 mM
480 min	Oxamic acid	0.516 mM

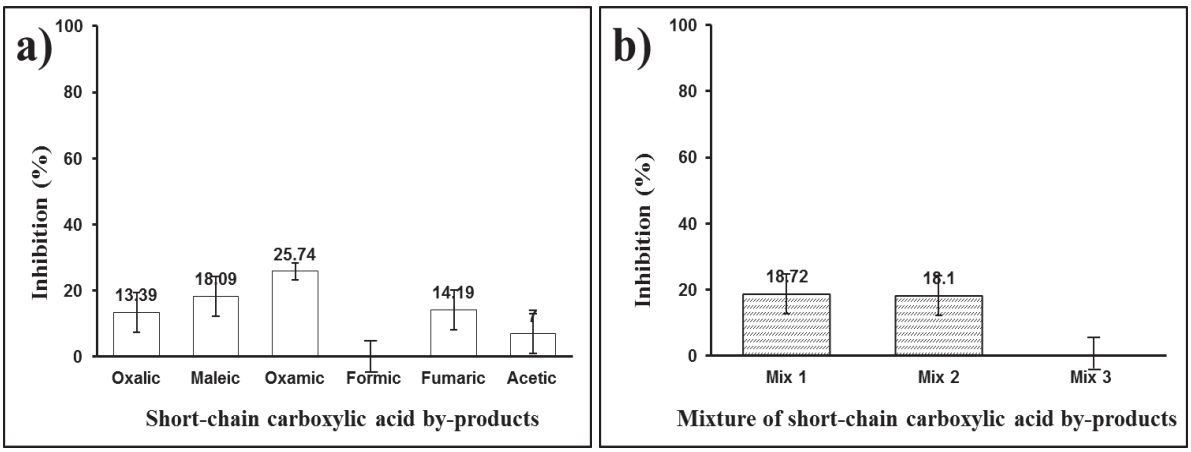

Figure 3-17. Toxicity of ACE by-products. (a) Short-chain carboxylic acid by-products at their maximum concentrations (Table 3-5), and (b) Mixture of the short-chain carboxylic acid by-products corresponding to three periods: 210 - 270 min (Mix 1); 270 - 330 min (Mix 2) and 330 - 480 min (Mix 3) during EF treatment of 500 mL (1 mM ACE) at pH = 3; [Na_2SO_4] = 50 mM, I = 500 mA, [Fe^{2+}] = 0.2mM.

3.3.5. Conclusions

The evolution of TOC, intermediate compound concentrations and acute toxicity of ACE solution in aqueous medium during EF mineralization process have been monitored through

HPLC-UV/MS, IC, TOC analysis and Microtox® toxicity tests. During the first 60 minutes of treatment, the acute toxicity of treated solution reached 100% which was identified to be due to the formation of toxic aromatic products like 1,4-benzoquinone, benzoic acid and benzaldehyde. A total detoxification of the solution was then accomplished after 120 minutes, due to the decomposition of ring-compounds into short-chain carboxylic acids. The mineralization of ACE by hydroxyl radicals (•OH) formed through EF process also produced inorganic ions such as ammonium or nitrate through the bond break between nitrogen and carbon in the initial molecule. The mineralization of 200 mL of 0.1 mM ACE was 86.9% using an applied current of 500 mA and a catalyst concentration of 0.2 mM. The relationship between the decomposition pathway and the evolution of the ACE solution toxicity as a function of EF treatment time was clarified thanks to the toxicity measurement of both individual and mixture of standard compounds (ACE and sub-products).This comprehensive degradation pathway of ACE can further be applied to other persistent pharmaceuticals in aquatic environment.

3.4. General conclusions

The treatment efficiency of 200 mL of both AO7 (0.1 mM) and ACE (0.1 mM) by EF process using commercial CF (60 cm^2) was very impressive. Nearly 96.2% TOC removal of AO7 and 86.9% of ACE were achieved after 8 h electrolysis at applied current of 500 mA with 0.2 mM of Fe^{2+} used as catalyst. The total detoxification of the solution was accomplished after 270 minutes and 120 minutes for AO7 and ACE, respectively. Moreover the innovative point of this approach was to identify sub-products at the different stages of the EF treatment and more especially to link sub-products formation with effluent toxicity toward *Vibria Fischeri* bacteria strain. We have then identified the most toxic sub-products of AO7 and ACE degradation and shown the possibility to control treatment duration thank to the monitoring of effluents toxicity. These results confirmed that EF process is a friendly environmental technology. It will be more useful if we can improve the treatment efficiency by the modification of cathode material. This was the reason for the next chapter where graphene was utilized to modify the commercial CF.

CHAPTER IV

EFFICIENT REMOVAL OF ACID ORANGE 7 DYE BY ELECTRO-FENTON PROCESS USING GRAPHENE BASED CARBON FELT

This chapter has been published in ***RSC Advances*** and ***Carbon*** as:

Thi Xuan Huong Le, Mikhael Bechelany, Joffrey Champavert and Marc Cretin, *A Highly Active Based Graphene Cathode for Electro-Fenton Reaction*, RSC Advances, 2015, 5, 42536 – 42539.

Thi Xuan Huong Le, Mikhael Bechelany, Stella Lacour, Nihal Oturan, Mehmet A. Oturan, Marc Cretin, *High removal efficiency of dye pollutants by electro-Fenton process using a graphene based cathode*, Carbon, 2015, 94, 1003–1011.

CHAPTER 4. EFFICIENT REMOVAL OF ACID ORANGE 7 DYE BY ELECTRO-FENTON PROCESS USING GRAPHENE BASED CARBON FELT

4.1. General introduction

The aim of this chapter was the modification of commercial CF by deposition of rGO to increase the hydrogen peroxide production (H_2O_2). In EF process, H_2O_2 plays an important role for hydroxyl radicals (•OH) generation which is the main oxidizing agent to attack POPs. There were two principle missions in this chapter: (1) The modification of CF was done via different reduction methods of GO. The properties of modified CF were characterized by various physical as well as electrochemical techniques and (2) For application, the fabricated felt (2 cm^2) was applied as cathode to remove AO7 in acidic medium. For environmental applications in the future, the long-term stability of cathode materials is also a key property. Therefore, the EF experiments were repeated after ten cycles, and degradation efficiency was identified by TOC measurement after 2 h electrolysis.

4.2. Abstract

A new cathode for EF process was set up by electrochemical deposition of rGO on the surface of CF. The structure property of modified electrode was investigated. Among the different reduction methods used, the constant potential technique demonstrated a considerable performance. The parameters affecting the conversion of GO to rGO, such as pH, applied potential and duration of the reduction process, were investigated. The rGO modified cathode presents enhanced electrochemical properties like an increase of the redox current and a decrease of the charge transfer resistance in presence of the redox probe $[Fe(CN)_6]^{3-}/[Fe(CN)_6]^{4-}$ showing better kinetic properties compared to raw CF. This improvement enhanced significantly the production of hydrogen peroxide, a key parameter in EF process, which was confirmed by linear scanning voltammetry (LSV) analysis. Therefore, the use of graphene modified cathode could decolorize efficiently AO7, a model azo dye molecule, within only 5 min and almost completely mineralized (94.3 %) it in 8 h treatment under optimal current density applied. The new cathode

exhibited good stability as the mineralization ratio in 2 h that was still above 64% after 10 cycles' degradation, showing that this rGO-CF is a powerful and promising electrode for improving the removal efficiency of dye pollutants using EF technology.

Keywords: *Constant potential reduction, water treatment, reduced graphene oxide, mineralization, hydrogen peroxide production, electro-Fenton reaction.*

4.3. Introduction

Urban industrial operation has long been identified as a major cause of environmental contaminations through atmospheric deposition and wastewater discharge. Textile factories discharge large amounts of wastewater containing a high concentration of dyes that needs to be treated. The wastewater of textile factories is very complex and difficult to treat completely by using conventional physical chemistry methods [301]. AOPs were widely investigated for the removal of recalcitrant organic pollutants from wastewater [228]. Over the past decade, AOPs have attracted increasing interest as promising powerful methods for efficiently removing dyes in aqueous medium [302-304]. AOPs are environmentally friendly chemical [305], photochemical [306], or electrochemical [307] methods sharing the common feature of the in-situ production of hydroxyl radicals (•OH) as their main oxidizing agent. One of the most popular chemical AOPs is the Fenton method, where a mixture of Fe^{2+} and H_2O_2, so-called "Fenton's reagent" is used to produce hydroxyl radicals (Eq. (2-12)) and degrade organic compounds [308].

$$Fe^{2+} + H_2O_2 \rightarrow Fe^{3+} + {}^{\bullet}OH + OH^- \quad (2\text{-}12)$$

To avoid using chemical reagents, H_2O_2 can be produced by the direct electroreduction of dissolved O_2 at the cathode according to Eq. (2-11). When combined with externally added Fe^{2+} as catalyst to produce hydroxyl radicals, the method (called EF) is more efficient than the basic Fenton process and easier to manage.

$$O_2 + 2H^+ + 2e^- \rightarrow H_2O_2 \quad (2\text{-}11)$$

The production of hydrogen peroxide is a crucial factor for the effective destruction of POPs by EF processes. Therefore, there are many studies focused on the modification of carbon based cathode materials to increase the electrogeneration of H_2O_2 such as electrode modification by PAN [220], ethanol/hydrazine hydrate [63], nitrogen functionalized carbon nanotube [309], multi-walled carbon nanotubes/surfactant [192], and PPy/AQDS composite film [310].

In recent years, graphene has been emerged as exciting topics of research in materials science and condensed matter physics research. It has received extensive attention for its

remarkable electrical, physical, thermal, optical, high specific surface area and mechanical properties [72, 73]. Graphene can be prepared by a large variety of routes such as mechanical cleavage [311], epitaxial growth [312], chemical vapour deposition growth [313-315], electrochemical exfoliation of graphite [316-318] and reduction of GO [319]. In all cases, the reduction of GO is regarded as one of the most promising routes for the mass production of graphene and restore well the properties of pristine graphene [320]. GO can be prepared from graphite by oxidization to graphite oxide and subsequent exfoliation. There are a number of methods for the reduction of GO, such as chemical reduction [321], thermal reduction [322], photocatalytic reduction [323] and electrochemical reduction [324]. The properties of graphene strongly depend on the method used for the reduction of GO. The rGO often contains large numbers of defects, such as nano-holes and Stone–Wales defects (heptagon/pentagon bonded carbon atom network). These defects play a significant role to enhance the physical and chemical properties of graphene-based nanomaterials [325].

These outstanding advantages have made graphene highly attractive materials for developing the efficiency of cathode materials applied in EF process. A very recent studies investigated this approach: An *et al.* prepared graphene-$BiFeO_3$ nanoscaled composites as a photo-Fenton catalyst under visible light irradiation [63]. In addition, graphene and polytetrafluoroethylene (PTFE) were also used to prepare a graphene/cathode in EF process by Xu *et al.* [326] or magnetic Fe_3O_4/rGO by Yang *et al.* [327]. However, the use of additional binder like polytetrafluoroethylene (PTFE) or Nafion may result in low conductivity of the composite, poor adhesion to the electrode surface and low graphene loading, as reported by Lv *et al.* [105]. Therefore, in the present study, we investigated different methods for GO reduction (i.e. electrochemical, chemical and thermal modes). Among them, we suggest a simple, low cost and friendly environmental method without adding any toxic reductant or binder to improve electrocatalytic behavior of CF cathode: this method used a constant potential technique to reduce GO deposited on the surface of CF. The graphene modified cathodes was tested for the first time to mineralize azo dye AO7.

4.4. Experimental

4.4.1. Materials

The CF was purchased from A Johnson Matthey Co., Germany. Hydrazine (Sigma-Aldrich, 35 wt% in water) and ammonia solution (Crown Scientific, 28 wt% in water) were used to chemically reduce GO. AO7 (Orange II sodium salt), sodium sulphate (anhydrous, 99.0 – 100.5%), graphite powder and iron (II) sulphate hepta-hydrate (99%), were obtained from Sigma-Aldrich. TOC standard of 1000 mg/L (Sigma-Aldrich. Co) and sodium hydrogen carbonate (≥. 99.5%, ACS, Karlsruhe) were used for calibration.

4.4.2. Electrode modification

4.4.2.1. Preparation of the dispersion and GO deposition

GO was synthesized from graphite powder according to modified Hummers method [328]. The synthesized GO was then prepared by adding it in water at a concentration of 1.5 mg/ml, followed by ultrasonication for 5 h under ambient condition (Bransonic 3510E-MT, 130 W), in order to obtain an homogeneous dispersion of GO (GO).

The pretreatment of CF was carried out by cleaning it in an ultrasonic bath with acetone for 2 h, followed by a rinsing step with deionized water and finally a drying step at 60^0 C for 24 h. This pretreated CF was denoted as raw CF.

GO was deposited on the raw CF surface via the EPD in a two-electrodes cell composed of a Pt foil cathode and raw CF anode. (). Under the electrical field, negative particles of GO were pushed to adhere on the surface of CF. This material was marked as GO-CF. After that in the same cell, the reduction was conducted by reversing electrodes, so GO was reduced by cathodic current on CF at a constant current density of 1.5 mA cm^{-2} for 10 min. The sample fabricated by this method was noted as ECR-CF. To find out the best condition for GO deposition on CF, the experiments was performed at different current densities (0.75; 1.5, 3; and 6 mA cm^{-2}) as well as various times (5, 10, 20, 30 and 40 min).

4.4.2.2. GO reduction at CF surface

After deposition at the optimal condition, GO was reduced by three different methods. The first one was chronoamperometry (Interval time > 0.1s), performed in a N_2 saturated Na_2SO_4

solution (0.1 M) carried out on a μ3AUT70466 Autolab system (Eco Chemie BV, Netherlands) with a three-electrodes system (working electrode: GO-CF with $2cm^2$) ECS reference electrode, auxiliary electrode: Pt foil). Different parameters affecting the reduction were investigated: solution pH, potential and time. The second method was reported by Gordon *et al.* [329] and used a reducing agent (hydrazine) to chemically reduce GO. In this case, the GO-CF electrode was immersed in a solution obtained by mixing 50 mL of MilliQ water, 50 mL of 35 wt% hydrazine and 350 μL of 28 wt% ammonia for few minutes followed by thermal reduction in a hot water bath (~95^0) for 1 h. These modified electrodes were carefully rinsed with deionized water, and then air-dried at room temperature. The third method applied was a thermal reduction conducted in a tubular furnace at high temperature (1000^0C) for 1 h, and under nitrogen atmosphere to remove any oxygen functionalities. For convenience, the three electrodes synthesized by either constant potential reduction, chemical reduction or thermal reduction was denoted as CPR-CF, CR-CF and TR-CF respectively.

4.4.3. Material characterization

4.4.3.1. Physical techniques

Chemical and structural characterizations have been performed using SEM (Hitachi S-4800), a homemade contact angle meter, and XPS (ESCALAB 250 Thermal Electron) with AlKα (1486.6 eV). Binding energies were calibrated by using the containment carbon (C1s = 284.4 eV).

4.4.3.2. Electrochemical techniques

CVs and electrochemical impedance spectroscopy (EIS) experiments were conducted in solution of 10 mM $K_3[Fe(CN)_6]$ and 1.0 M KNO_3 by using the μ3AUT70466 Autolab system (Eco Chemie BV, Netherlands) and Bio-Logic SP-150 in a three-electrodes cell including a working electrode (modified and unmodified CF), a counter electrode (Pt foil), and a reference electrode (Saturated Calomel Electrode, SCE). EIS was used to determine the electrode interfacial charge-transfer resistance (R_{ct}). The impedance spectra were recorded at the open circuit voltage (OCV) with frequency range from 50 kHz to 100 mHz and a voltage amplitude of 10 mV ($2cm^2$ of the working electrode). The LSV was employed to observe the H_2O_2 electrogeneration at the modified electrode with the same surface area. This experiment was carried out with the μ3AUT70466 Autolab device at a scan rate of 5 mV s^{-1} from the open circuit

potential to -1.2 V *vs.* Ag/AgCl in the three-electrodes system. For this measurement, an aqueous solution of Na_2SO_4 (50 mM) was acidified at pH 3.0 and saturated by oxygen for 10 min by compressed air, at a constant magnetic stirring of 800 rpm. The oxygen bubbling was kept constant during the experiment. All the potentials reported in this paper were referred to SCE and all experiments were performed at room temperature, unless stated otherwise.

4.4.3.3. Mineralization of azo dye by the EF process

Mineralization experiments were performed at room temperature in a 75 mL undivided cylindrical glass cell equipped with two electrodes. Galvanostatic mode was applied with a power supply (Lambda Electronique, USA). The prepared cathode (2 cm^2) was used as working electrode and a Pt sheet as auxiliary electrode. The distance between working and auxiliary electrodes was 3 cm. The 30 mL aqueous solution of AO7 (0.1 mM), Na_2SO_4 (50 mM) as supporting electrolyte and $FeSO_4.7H_2O$ (0.2 mM) as the catalyst were prepared by adjusting pH at 3 and magnetically stirred at 800 rpm. Prior to electrolysis, the solution was saturated by O_2 bubbling. The TOC of the initial and treated samples was measured with a TOC-L CSH/CSN Shimadzu (Japan) analyzer. Calibration curves for total carbon (TC) and IC analysis were built up by automatic dilution of standards solutions of TOC (potassium hydrogenophtalate) and IC (sodium hydrogen carbonate).

4.5. Results and discussion

4.5.1. Structural properties of the electrodes

The SEM images of the electrodes resulting from various modifications were given in Figure 4-1 a, b, c, and d. From this analysis, it can be observed that the surface morphology of electrodes was changeable depending on the reduction conditions. The raw CF (Figure 4-1 a) showed smooth surface corresponding to a very low surface area [105, 330]. Some large rGO flakes with wrinkled structure were stuck loosely on the CR-CF (Figure 4-1 b), proving a poor adhesion. As far as the TR-CF (Figure 4-1 d) is concerned, the surface was very rough and presented with many open pores as the result of high temperature treatment. Compared to the other electrodes, CPR-CF expressed a huge quantity of rGO which was randomly deposited on the electrode to form a homogeneous surface.

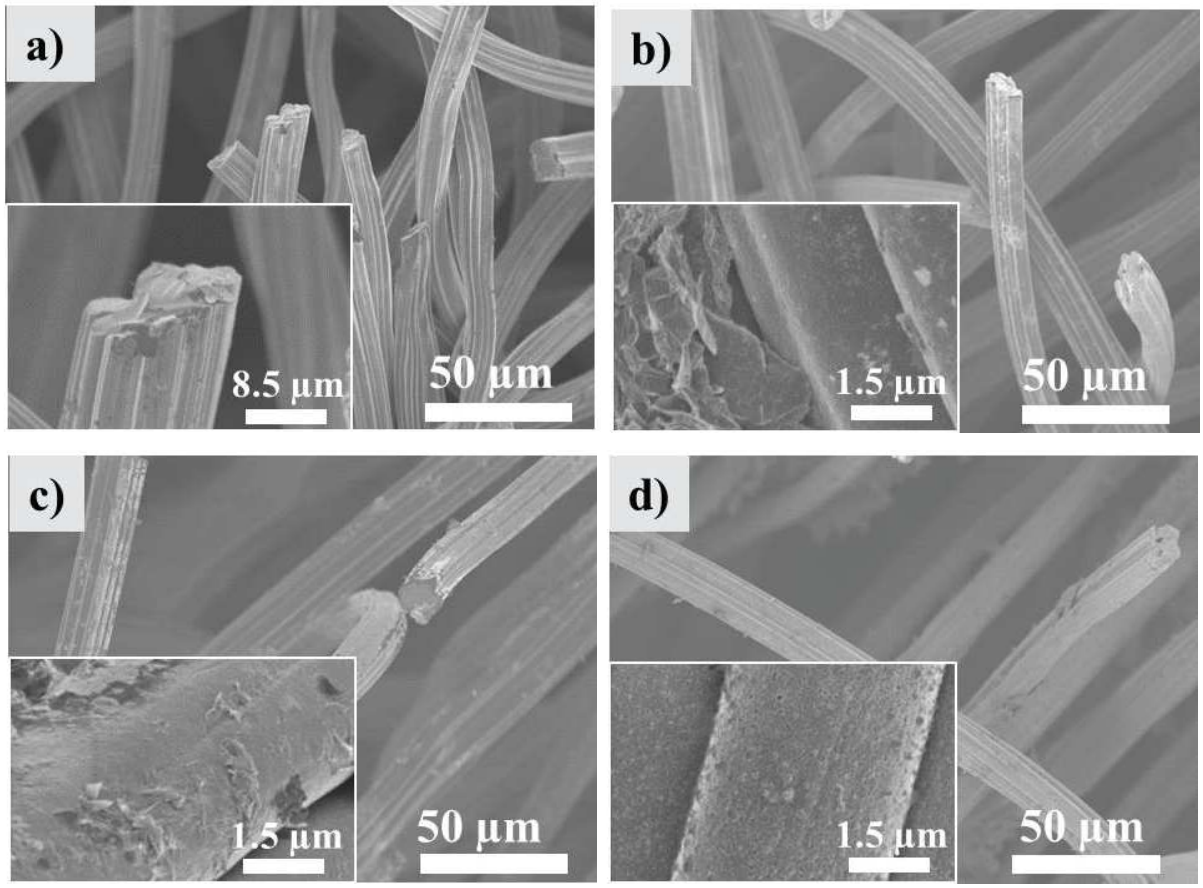

Figure 4-1. SEM images of (a) raw CF, (b) CR-CF, (c) CPR-CF, and (d) TR-CF electrodes.

The XRD patterns of graphite powder and GO are shown in Figure 4-2 a. A strong and sharp diffraction peak (002) at $2\theta = 26.5^0$ was attributed to the high ordered structure of graphite powder. On the other hand, XRD of GO exhibited a reflection at approximately 12.5^0 attesting of the high degree of oxidation of the obtained GO materials dispersed in the GO solution. The XRD shows as well the absence of a peak at around 26° confirming that all the graphite powders have been converted into GO with the modified hummers method [331]. Moreover, the much higher d-spacing of GO compared to graphite powder demonstrated the formation of oxygenated functional groups such as hydroxyl, epoxy and carboxyl after oxidation. This can be clearly seen on XPS spectrum with the appearance of carbon-oxygen bonds like C-O (286.79 eV), C=O (287.81 eV), O-C=O (288.89 eV) (Figure 4-2 b). These peaks were still observed in GO-CF sample, proving the successful EPD of GO on the surface of CF (Figure 4-3 a).

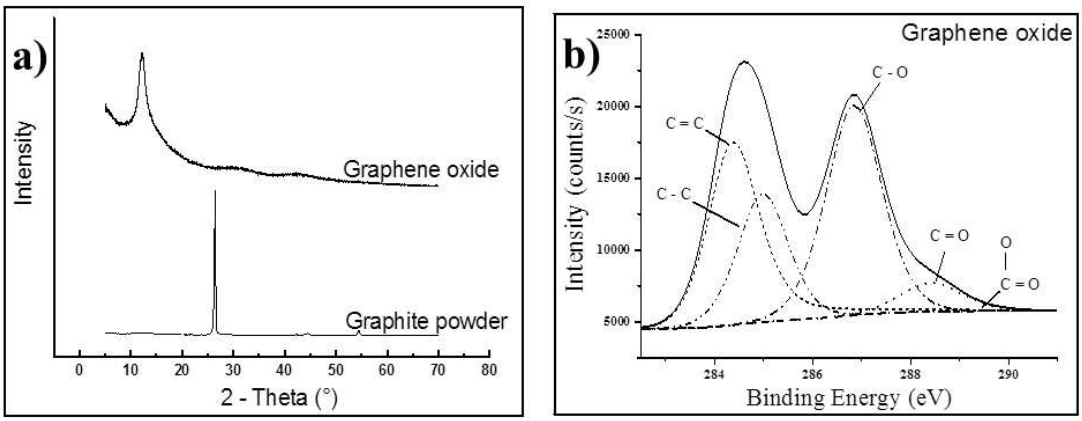

Figure 4-2. (a) XRD of graphite powder and GO; (b) XPS of GO.

The analysis of the C_{1s} spectra from Figure 4-3 a to Figure 4-3 d showed that peaks evolution of these oxygen-containing groups was different depending on the reduction methods applied: the C/O ratio changed from 4.66, 7.72, to 15.39 for CR-CF (Figure 4-3 b), CPR-CF (Figure 4-3 d), and TR-CF (Figure 4-3 c), respectively, compared to 2.56 for GO (Figure 4-3 a). In the case of CR-CF, hydrazine used as reducing agent is not a suitable choice because of electrode soaking in hot solution (~95^0) during long time reduction (1h) leaded to the flaking of the thin layer graphene. Moreover, the rGO in the liquid phase also tended to agglomerate upon reduction [320, 332]. On the contrary, the thermal reduction presented the best characteristics, with only 5.63% of oxygen remaining in sample TR-CF, indicating that nearly all the oxygen functionalities were removed from GO at high temperature (around 1000 ^{0}C) [322, 333]. This result demonstrates that thermal reduction is an efficient way for the modification. However, the high production cost as well as tedious control of the required experimental conditions caused a limitation for TR-CF development [320]. In addition, quantity of nitrogen was also different for each sample when the highest was TR-CF, 5.47 %, following CR-CF at 3.41 % because the thermal reduction (TR-CF) was happened in N_2 medium and the chemical reduction (CR-CF) was in ammonia solution. Despite more incomplete reduction of GO deposited on the surface of CPR-CF (11.15% of residual oxygen) compared to TR-CF material (5.63%), the constant potential technique used is quite simple, cheap and experimental conditions are easy to control.

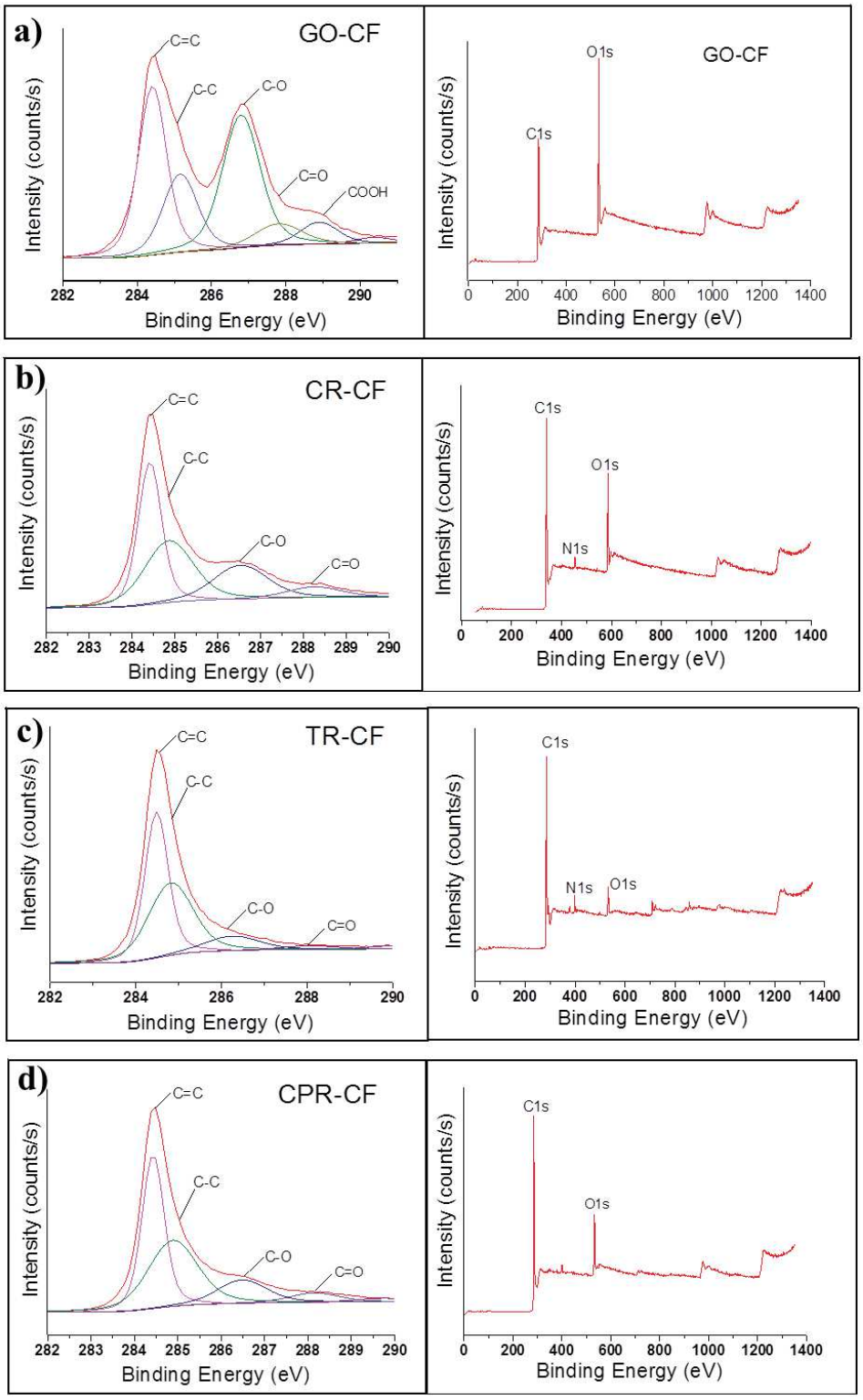

Figure 4-3. XPS of (a) GO-CF, (b) CR-CF, (c) TR-CF and (d) CPR-CF electrodes.

4.5.2. Effect of current and time for GO deposition on CF

In order to optimize GO electrochemical deposition on CF, parameters like current and time were investigated. The redox wave $[Fe(CN)_6]^{3-}/[Fe(CN)_6]^{4-}$ is sensitive to surface chemistry of carbon-based electrodes [86], so it was used to optimize the conditions for the deposition of GO on CF as shown in Figure 4-4. The current response toward $[Fe(CN)_6]^{3-/4-}$ of the modified electrode increased strongly as the current density deposition changed from 0.75 to 1.5 mA cm^{-2} or time deposition climbed from 5 min up to 10 min. In fact the higher current either time was, the more quantity of GO came and reduced on the surface of CF, forming an homogeneous graphene-layer which induced the acceleration of the electrochemical action as a consequence of the excellent electrical property of graphene [73]. Nevertheless a slight decline was observed continuously from 3.0 to 6.0 mA cm^{-2} which results from the agglomeration of the GO sheets, and uncompleted reduction. This decreased phenomenon was also observed if the time of deposition was extended over 10 min (*i.e.* 40 min) with the similar reason as too much rGO overlapped on CF. Therefore, we suggest choosing the best deposition condition at 1.5 mA cm^{-2} for 10 min.

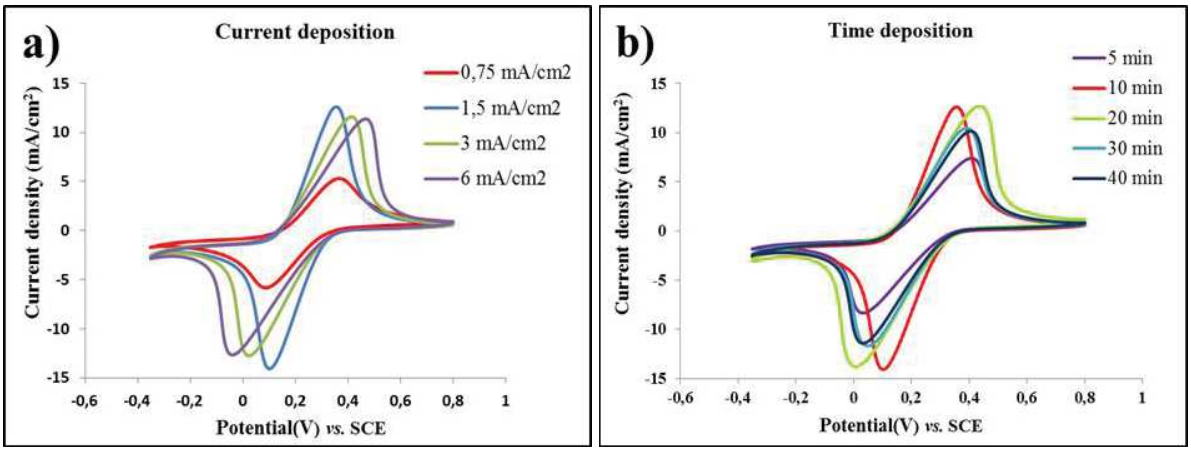

Figure 4-4. Effect of current and time for GO deposition on CF. (a) CVs of ECR-CF at different currents deposition, (b) at different times deposition, in 10mM $K_3[Fe(CN)_6]$ + 1M KNO_3 solution. Scan rate 10 mV s^{-1}.

4.5.3. Effect of the electrochemical conditions on the GO reduction

The characterization of GO reduction was carried out by CVs and results were shown in Figure 4-5. The reduced peak area of GO was identified to be in the range of -0.15 V to -0.65 V, performed before the reduction step and this agree with that obtained by Dogan *et al.* [334]. This peak disappeared almost totally after the reduction method applied (Figure 4-5 a).

The influence of operating potential value on the reduction rate was also studied. It was found that a more negative applied potential gave a faster reduction rate. Actually, on CVs, the reduction peak current density which was characteristic of GO reduction reaction significantly increased as the applied reduction potential decreased from -0.15 V/SCE to -0.45 V/SCE. However, when the applied potential was more negative than -0.55 V/ SCE, the reduction efficiency decreased (smaller reduction peak observed). This was proved by the investigation of redox reactions of the couple $[Fe(CN)_6]^{3-}/[Fe(CN)_6]^{4-}$ (Figure 4-5 b), which confirmed that a faster electrochemical reduction rate could create defects in the resulting rGO, as already noticed by Guo *et al* [335]. Additionally, applying a too highly reduction potential could also lead to too many H_2 gas bubbles produced from the reduction of water, creating a physical barrier that affected the capture of electrons of GO sheets, and thereby, limited the completion of the electrochemical reduction process [320, 330]. This clearly indicated that the selection of the appropriate cathodic reduction potential is crucial for the complete reduction of GO to rGO.

Another key parameter affecting the efficiency of the reduction is pH: The control of the pH of the solution is necessary to create an appreciate medium for efficient reduction while ensuring good adherence of the rGO onto the electrode substrate. Figure 4-5 c illustrated that GO could be reduced over a wide pH range of 3 to 11, but a slight decline of the electrochemical performances of the modified electrode was observed at extreme pH values: A low pH medium accelerated side-reactions (reduction of protons into H_2) which competed with the electrochemical reduction of GO [336]. Additionally, the formation of H_2 gas bubbles on the surface of the working electrode could induce the peeling of rGO film from the surface of CF [320]. In strongly basic media, the produced rGO films could be solubilized from the residual hydroxyl, epoxy and carboxylic groups that still existed in the structure of rGO, as previously noticed by Liu *et al.* [122]. Therefore, the modification should be preferably performed at neutral pH.

The reduction degree of GO could be monitored as a function of time, applying a fixed potential of -0.45 V/SCE (characteristic of the reduction peak). Peak currents observed on the CVs significantly increased with time from 5 min to 40 min (Figure 4-5 d), and this was attributed to an enhanced reduction of GO with time. From 40 minutes, current peak values kept almost stable. This means that highest reduction rate was reached.

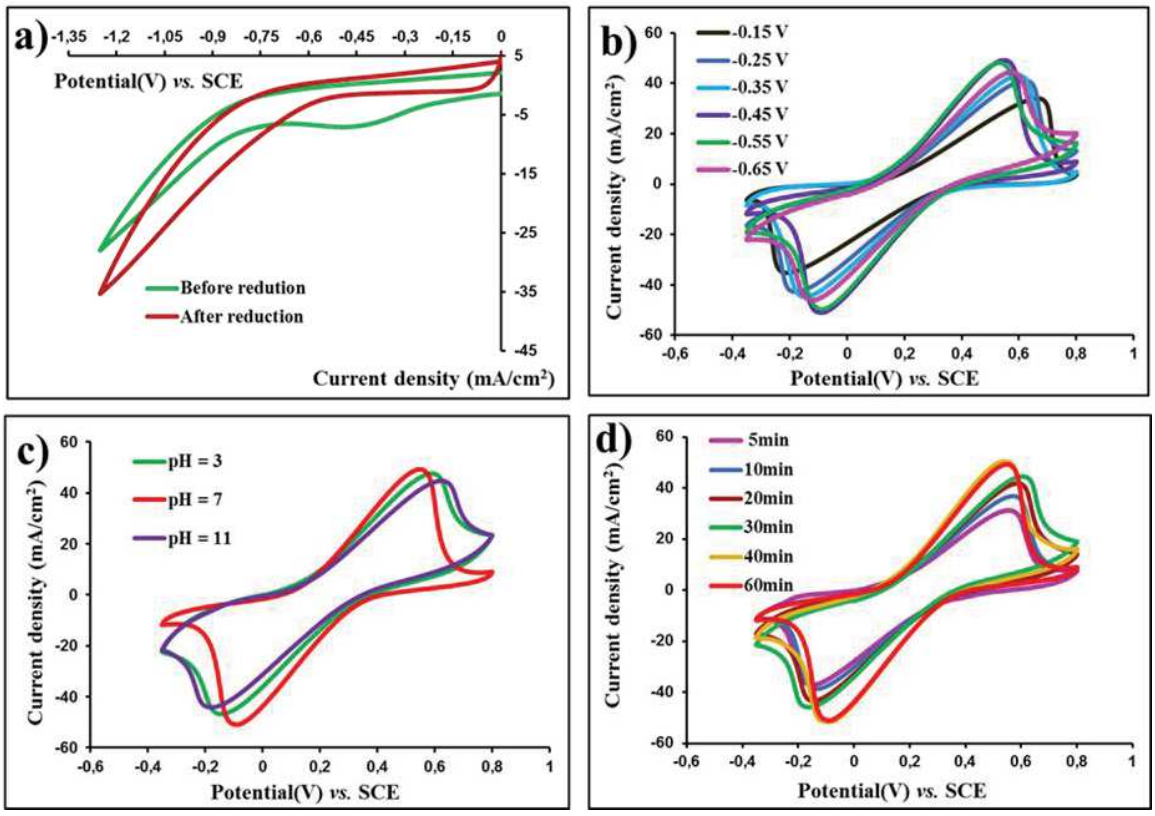

Figure 4-5. Effect of the GO reduction conditions. (a) CVs of CPR-CF before and after reduction in a N_2 saturated Na_2SO_4 solution (pH = 3), (b) CVs of CPR-CF in 10 mM $K_3[Fe(CN)_6]$ + 1M KNO_3 solution at different reduction potentials, (c) Different reduction pHs, and (d) Different reduction times at –0.45V/SCE. Scan rate 10 mV s^{-1}.

4.5.4. Electrochemical behavior of the modified electrodes

The electrochemical performance of electrodes was evaluated thanks to three indicators: electroactive surface area (EASA), charge transfer resistance of the interface electrode/electrolyte and H_2O_2 production efficiency.

4.5.4.1. Electroactive surface area characterization

The electrochemical properties of different cathodes were investigated using the redox reactions of the couple Fe^{III}/Fe^{II} which were illustrated in Figure 4-6 a. CVs of the ferrocyanide system is an effective and facile method to monitor the characteristics of the modified electrode surface as the higher electroactive surface area of electrode is, the higher the peak current of $Fe(CN)_6^{3-/4-}$ is [337]. From our CVs, it could be seen that the peak current density of CPR-CF was much higher than that of the substrate material, revealing that the deposited rGO significantly increased the electroactive surface area (due to the large surface area and good conductivity of graphene), as previously mentioned in studies dealing with graphene-modification [338]. Moreover, we could calculate the electroactive surface area according to the Eq. (2-5). From that, the electroactive surface area of CPR-CF, TR-CF, CR-CF were as 137.97 cm^2, 124.17 cm^2, 27.59 cm^2 respectively and 13.79 cm^2 for raw CF. These results agreed with the specific area identified by BET method where CPR-CF was nearly 20 times higher than 0.0915 $m^2\ g^{-1}$ for raw CF.

4.5.4.2. Charge transfer resistance of the interface

EIS is an efficient and facile tool for studying the interface properties and capability of electron transfer between the electroactive substance and electrode. The charge-transfer resistance (Rct) at the electrode surface was determined by EIS and deduced from the intercept of the semicircle with the real axis in the Nyquist representation shown. The decrease of the intercept in the Nyquist plot was due tothe decrease of the interfacial resistance relative to the increase of electrode conductivity [121]. The interfacial charge-transfer resistance (R_{ct}) measurement was 0.21 and 2.38 Ω for CPR-CF and raw CF, respectively (Figure 4-6 b). This result suggested that the modified electrodes caused a remarkable decrease in the charge transfer resistance compared to the unmodified cathode, indicating the much higher electron transfer efficiency, which is similar to that reported in other studies [105, 337], such as Jing Liu proved that with the graphene modification on carbon cloth, R_{ct} was four times lower than the plain one (2.5 Ω), exposing the excellent electrocatalytic behavior of modified electrode. The CPR-CF exhibited a very low charge transfer resistance, confirming that this cathode was favorable to catalyze electrochemical reaction like EF process. These results contributed to create a stable rGO film on the surface of CF cathode.

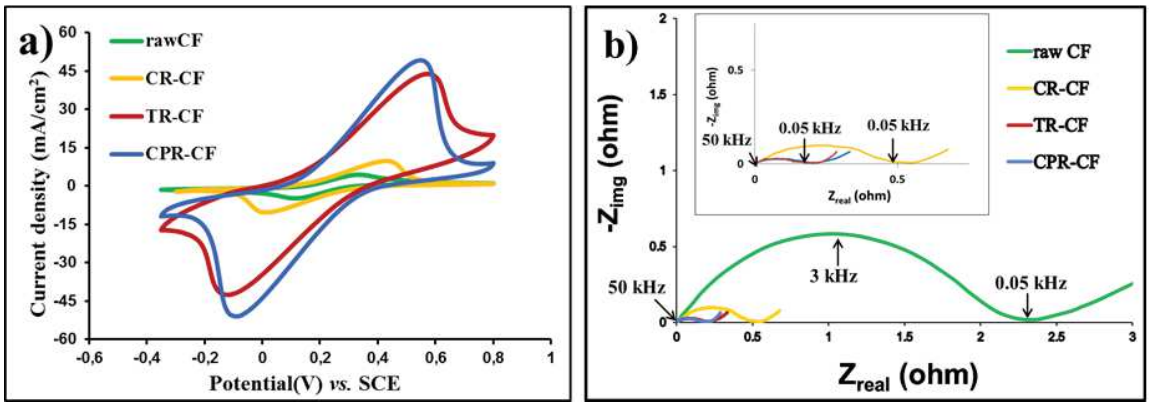

Figure 4-6. Electrochemical characterization of raw_CF, CR-CF, TR-CF and CPR-CF electrode. (a) CVs and (b) EIS of modified and unmodified electrodes in 10 mM $K_3[Fe(CN)_6]$ + 1M KNO_3 solution (after substration of the liquid electrolyte resistance).

Based on the physico-chemical characterizations, it is clear that best properties are obtained from GO reduction under thermal treatment or at constant potential. Then, because of the easiness of this latter, it has been chosen to get the best compromise between electrode efficiency and low cost. Therefore, CPR-CF was used as a cathode for EF process in the next section.

4.5.5. Removal of azo dye by electro-Fenton process

To evaluate the efficiency of the modified cathode in azo dye mineralization, the TOC of the solution was controlled during EF process. Within the first 2 h, a faster mineralization was obtained, compared to raw CF, which could be accounted for a higher production of $^{\bullet}OH$ in the system and by the way faster degradation of AO7 intermediate products. TOC removal after 2 h treatment reached 73.9% on the modified electrode, and this was 18.3% higher than on the raw CF. After 8 h electrolysis (Figure 4-7 a), 94.3% of mineralization could be obtained. In addition, the apparent rate constants for the degradation of AO7 were determined by plotting the $Ln([AO7_0]/[AO7])$ against time [173, 176, 178]. The values of 0.7846 min^{-1} was obtained for CPR-CF, more than nearly 3 times of the pristine one (Table 4-1). To conclude, these efficient AO7 degradation and mineralization results obtained on the CPR-CF electrode was definitively ascribed to its original surface structure developed by electro-reduction method and thereby

enhanced electrochemical properties acquired, compared to raw CF. This modification method could provide an effective solution to improve EF process performance.

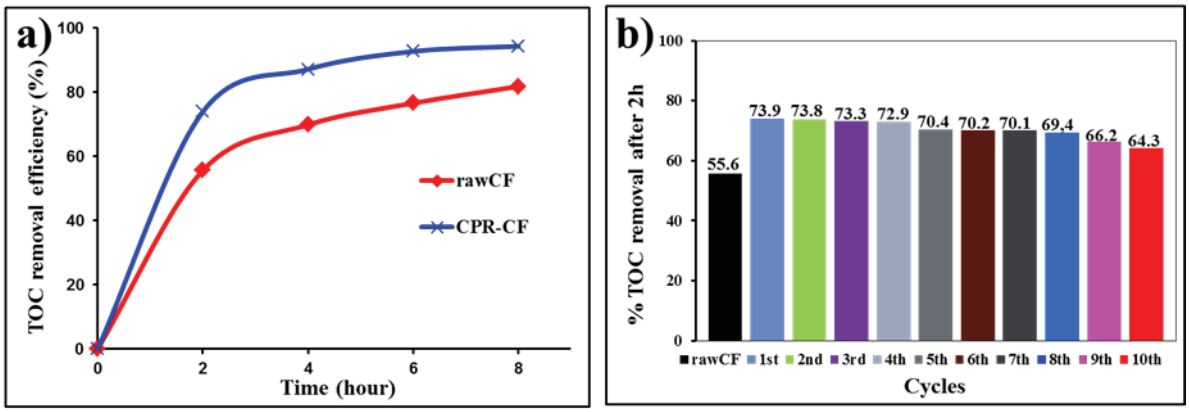

Figure 4-7. TOC removal following electrolysis time. (a) 8 h and (b) 2 h treatment. Conditions: Pt anode; V=30 mL, [AO7]=0.1 mM; [Fe^{2+}]=0.2 mM; pH=3; [Na_2SO_4]=50 mM, I = 40 mA, using the cathode: raw CF and CPR-CF used for 10 cycles.

Table 4-1. Apparent first order rate constants and abatements for the degradation kinetics of AO7 on raw CF and CPR-CF.

Cathode	k_{app} (min^{-1})	R^2	Abatement (%) after 3 min
rawCF	0.2596	0.9961	54.2
CPR-CF	0.7846	0.9987	89.7

For environmental applications in the future, the long-term stability of cathode materials is also a key property. After 10 cycles of use (80 h), the mineralization ratio of the modified cathode was only decreased by 9.6%, caused by small loss amount of rGO on the surface electrode during long time degradation (Figure 4-7 b).

4.6. Conclusion

In this study, we investigated different modification methods of CF (2 cm^2) electrode with rGO, in order to enhance the performance of EF process. Newly structured electrodes with optimized electrochemical properties could be obtained, according to the reduction method applied: constant potential reduction (CPR-CF electrode), chemical reduction (CR-CF electrode) and thermal reduction (TR-CF electrode).

Thermal reduction method (TR-CF) gave the best results in terms of electrochemical properties developed but this method appears less economic. Therefore, the CPR-CF was chosen as the best way for the modification because of its simplicity, low cost, more ecologic (no chemical addition) and its effective performance to mineralize azo dye by EF process. It was fabricated by an EPD of GO followed by a constant potential reduction at -0.45 V/SCE for 40 min. This new cathode exhibited remarkable electrochemical properties identified by CVs and impedance analyses: a 10 times higher peak area current could be obtained on this material compared to the redox probe $[Fe(CN)_6]^{3-}/[Fe(CN)_6]^{4-}$; a 2.17 Ω charge-transfer resistance lower than that obtained on raw CF.

The significantly higher production of H_2O_2 on CPR-CF could increase the degradation rate of AO7 by EF process, compared to raw CF. Moreover, the mineralization of AO7 was almost complete (94.3% TOC removal) after 8 h treatment. Furthermore, the good stability of the modified cathode was also controlled and showed that after 10 cycles of use, only 9,4% of performance decline was observed. This has been linked to small release of GO from the electrode surface.

From all the results obtained, this work could emphasize that easy and simple modification method of CF material can optimize the performance of EF processes dedicated to wastewater pollution problematics in relation to POPs.

4.7. General conclusions and perspectives

The modified CF proved its benefits when improving remarkably the treatment efficiency of AO7 by EF process mainly thanks to an increase of electroactive surface area and electronic properties of the CF substrate modified by rGO. Consequently the degradation kinetics of pollutants was greatly enhanced compare to raw CF but without affecting the thermodynamic properties of the electrode. That means we do not observed a shift of the oxygen reduction

potential related to an improvement of the electrocatalytic properties of the electrode material. To continue upgrading the EF technology, it is then also necessary to decrease the operating cost of the process. Hence, the idea about using cheap green power from FC for EF system instead of traditional generators was investigated through the development of electrocatalytic electrodes as well as the construction of an original zero energy depollution system in the next chapters.

CHAPTER V

GROWTH OF GOLD PARTICLES ON CARBON FELT FOR EFFICIENT HYBRID BIOFUEL CELL FOR MICROPOWER GENERATION

This chapter has been published in ***Electrochimica Acta*** as:

Thi Xuan Huong Le, Mikhael Bechelany, Adriana Both Engel, Marc Cretin, Sophie Tingry, *Growth of gold particles on carbon felt for efficient hybrid biofuel cell for micropower generation*, Electrochimica Acta, 2016,219, 121–129.

CHAPTER 5. GOLD PARTICLES GROWTH ON CARBON FELT FOR EFFICIENT MICROPOWER GENERATION IN A HYBRID BIOFUEL CELL

5.1. General introduction

This chapter gave out a concept about a BFC using CF material. This BFC was implemented by connecting an abiotic anode and a biocathode based on CF modified by gold particles (CF@Au) in a two-chamber cell separated by a Nafion® membrane. At the anode, gold particles on CF catalyzed for glucose oxidation to produce electron which was transfer to cathodic compartment. Three main contents were needed to solve in this chapter, including: (1) Deposition of gold particles on the surface of CF by electrodeposition and thermal treatment; (2) The CF@Au electrode was tested for enzymatic O_2 reduction and glucose electrooxidation and (3) The performance of hybrid glucose/O_2 BFC was evaluated via monitoring the generated power and its stability.

5.2. Abstract

In this study, homogeneously dispersed gold particles growth onto CF were fabricated by electrodeposition method followed by a thermal treatment at 1000 °C under nitrogen. The thermal treatment induced the dewetting of gold and the formation of well-crystallized gold particles. The structural properties of the resulted CF@Au material were evaluated by SEM, XRD and Thermal Gravimetric Analysis (TGA). We studied the electrocatalytic properties of this new gold material through the abiotic glucose oxidation in alkaline medium and the enzymatic dioxygen electroreduction by the enzyme bilirubin oxidase. Finally, we showed the potentiality of the resulting CF@Au material to build a 3-dimensional glucose hybrid BFC by assembling an abiotic anode with an enzymatic cathode. The system exhibited high electrochemical performance with an OCV of 0.71 V and a maximum power density of 310 µW cm^{-2} at 352 mV, in spite of a low gold loading (0.2 wt%).

Keywords: gold particles, electrodeposition, dewetting, glucose, enzyme, hybrid biofuel cell.

5.3. Introduction

Gold nanoparticles (AuNPs) and nanoporous gold, as well as metallic nanostructured films are becoming popular as electrode materials for electrocatalysis. These electrodes are attractive due to their large electrochemical surface area, excellent chemical stability, high conductivity and biocompatibility [243, 339]. Several techniques are used to prepare three-dimensional gold electrodes mainly based on (i) the immobilization of already synthesized nanoparticles by drop-casting, layer-by-layer methods and entrapment in a sol gel matrix [218, 223-226, 340], or (ii) the direct preparation of nanoparticles on electrode surface by electrochemical deposition, sputtering followed by dealloying, chemical reduction, seed-mediated growth and ion implantation [341-345]. Thanks to their catalytic efficiency and biocompatibility, AuNPs can be used either co-immobilized with redox enzymes or as the main catalyst. Three-dimensional gold nanoparticles electrodes have been widely applied to direct electron transfer reactions of redox enzymes [346-351], which can afford higher enzyme loading, better orientation by chemical modification and more efficient electrical contact. From examples found in the literature, AuNPs electrodes have shown to improve BFC performance [352, 353] and glucose biosensors detection [349, 354] compared to planar electrodes. Additionally, AuNPs exhibit good activity toward glucose oxidation (with typical current values ranging from some hundreds of µA to a few mA) due to their large surface area and high number of active sites [226, 355, 356].

Hybrid BFC, unlike fully enzymatic ones, present only one enzymatic electrode (bioanode or biocathode), while the other is catalyzed by metallic catalysts. In enzymatic BFCs, the enzymes offer high reactant specificity and high reaction rate. Glucose oxidase has been widely studied in glucose BFC through MET-type catalysis (Mediated Electron Transfer) with the use of mediators such as ferrocene [357] or osmium complexes [358, 359] or through DET-type catalysis (Direct Electron Transfer) with the introduction of nanomaterials including CNTs, graphene or gold particles [351]. However, the limited stability and regeneration of the enzymes hinder the potential use of enzymatic glucose BFC for long-term operation. An alternative option is thus the use of abiotic catalysts with high catalytic activity toward glucose oxidation and efficient stability that makes them more suitable for long-term applications. The non-selectivity of abiotic glucose catalysts can be easily overcome by the addition of a separation membrane. In our previous studies, we reported the construction of hybrid BFC involving an abiotic anode and an enzymatic cathode that can potentially convert chemical energy into electricity [360, 361]. The

devices were made of self-standing electrospun carbon electrodes modified by Au NPs at the anode for the electrocatalytic oxidation of glucose and by the enzyme bilirubin oxidase (BOD) at the cathode for the electrocatalytic reduction of dioxygen. The abiotic anodes were obtained either by the direct synthesis of the nanoparticles supported on carbon Vulcan® and deposited on the electrode surface [360], or by the formation *in situ* of the nanoparticles embedded in electrospun carbon fibers [361]. The electrodes were characterized by gold loadings of 21 and 12.2 wt.%, respectively, determined by thermogravimetric analysis. These results clearly showed the advantage to prepare *in situ* the nanoparticles to form very stable carbon-gold bonding with well dispersed AuNPs on the electrode surface to enhance the long-term stability of our devices.

Considering the importance of the bonding stability between the metallic particles and the electrode material, the aim of this work is to propose a new simple method to prepare gold particles attached on a commercial CF template that affords conformal coating and homogeneous dispersion of the gold onto the electrode surface. The technique is applied to prepare CF@Au material with the objective of using a very low gold loading (0.2 wt%). Besides, compared to our previous studies, the bioelectrode is prepared by connecting gold particles directly to the enzymes instead of using MWCNTs to establish electrical contact. The CF@Au material is obtained from the electrodeposition of gold salts on a CF followed by a subsequent thermal treatment at 1000°C under nitrogen gas flow to induce the dewetting of gold [362].

To our knowledge, this is the first time that this synthesis approach is used to confine gold particles in a three-dimensional electrode applied to the development of hybrid BFC. Structural properties of the new CF@Au material are characterized by SEM, XRD, and TGA. We focus on the electrocatalyic properties of this new material regarding both the abiotic glucose oxidation in alkaline medium and the enzymatic dioxygen electroreduction. The enzyme BOD, known to promote the four-electron reduction of oxygen directly to water [363], was chosen to perform DET (direct electron transfer). DET allows avoiding the problems associated with the use of redox mediators like limited stability, potential toxicity and lower electrode potential. As DET depends significantly on the distance between the redox active center of the enzyme and the electrode surface, we expect that the gold nanoparticles will promote DET between the BOD and the CF electrode. BOD is entrapped within chitosan matrix which provides favorable microenvironment and high stability for multicopper oxidases [364], and further immobilized within the CF@Au by simple immersion in solutions. Finally, the potentiality of the resulting CF@Au electrodes to assemble a glucose hybrid BFC is shown by using bare CF@Au at the

anode, and BOD-modified CF@Au at the cathode. In spite of low gold loading (0.2 wt%), this hybrid device exhibits higher electrochemical performance than the previous hybrid glucose BFC, proving the efficiency of the synthesis technique to form gold electrodes with high active surface for electrocatalysis.

5.4. Experimental

5.4.1. Materials

The CF was purchased from A Johnson Matthey Co., Germany. Chloroauric acid trihydrate ($HAuCl_4 \cdot 3H_2O$, 99.99 %), 2,2'-azino-bis(3-ethylbenzothiazoline-6-sulphonic acid) (ABTS) were obtained from Sigma Aldrich. Potassium hexacyanoferrate (≥ 99%) and potassium nitrate (≥ 99%) were bought from Fluka, enzyme bilirubin oxidase (BOD, 2.51 U mg^{-1} solid) from Amano Enzyme Inc., Japan; potassium hydroxide (KOH pellets pure) from Merck; D-(+)-glucose monohydrate, chitosan and acid sulfuric (98%) from Sigma-Aldrich, and used without further purification. Dihydrogen phosphate monohydrate ($NaH_2PO_4.H_2O$) and di-sodium hydrogen phosphate (Na_2HPO_4) salts from Merck were employed for preparation of the buffer phosphate (0.1 M) pH 7.0 (PBS). The aqueous solutions were prepared using 18.2 MΩ cm MilliQ water (Millipore). Glucose solution was stirred for 24 h prior to use.

5.4.2. Preparation of gold nanoparticles-modified CF (CF@Au)

The commercial CF was firstly cleaned in an ultrasonic bath with acetone for 2h to remove adsorbed contaminations, followed by thorough rinse with deionized water and drying at 60 ^{0}C for 24h. This pretreated CF was denoted as raw CF. After that, the gold layer was deposited on the surface of the CF by CVs technique running 70 scans from -0.9 to 0 V versus SCE (Saturated Calomel Electrode) at a scan rate of 10 mV s^{-1} in a N_2-saturated solution containing 0.05 mg mL^{-1} chloroauric acid. The process was recorded on a μ3AUT70466 Autolab system (Eco Chemie BV, Netherlands) at a scan rate of 10 mV s^{-1} using a three-electrode system with the CF as working electrode, a SCE as reference electrode and Pt foil as counter electrode. Aiming to form the gold particles by dewetting, an additional thermal treatment was realized in a tubular furnace (Vecstar Ltd) fed by nitrogen gas at the flow rate of 200 mL min^{-1} with heating rate of 5 ^{0}C min^{-1} and temperature ranging from 20 to 1200 ^{0}C. The parameters affecting the deposition of gold nanoparticles on the surface of the CF were investigated, such as the

concentration of chloroauric acid and treatment temperature. One electrode was prepared for each chloroauric acid trihydrate concentrations and for each treatment temperature from 600 to 1000 °C. The sample at the best state was noted as gold CF (CF@Au).

5.4.3. Preparation of enzyme-immobilized electrode

The biocathode consisted of an CF@Au electrode modified with BOD enzyme entrapped in a chitosan film. First the CF@Au material was immersed in a solution (300 µL) of BOD (19.5 mg mL^{-1}) in PBS (0.1 M) pH 7 until complete absorption of the liquid inside the felt electrode. More concentrated solutions of BOD did not yield higher catalytic currents. After drying, the modified electrode was covered by a chitosan solution, also by immersion. The solution was prepared by dissolving 1 wt.% of chitosan in 1 mL of acetic acid solution (1 vol.%) until complete dissolution, followed by the addition of 50 µL glutaraldehyde. The resulting electrode was let to dry at 5°C for 48 h.

5.4.4. Material characterization

Chemical and structural characterizations were performed by SEM (Hitachi S-4800), TGA using a TA instruments SDT 2960 under air atmosphere in the temperature range 25-800°C, and by XRD (PANAlytical Xpert-PRO diffractometer equipped with a X'celerator detector using Ni-filtered Cu-radiation).

5.4.5. Electrochemical characterizations

CVs experiments were conducted in a solution of 10 mM $K_3[Fe(CN)_6]$ in 1.0 M KNO_3 by using a µ3AUT70466 Autolab system (Eco Chemie BV, Netherlands) and a three-electrode cell with CF@Au or CF as working electrode, Pt foil as counter electrode, and a SCE as reference.

Glucose electrooxidation was investigated with CF@Au and raw CF electrodes by CVs in 0.1 M KOH containing 10 mM glucose. Dioxygen reduction was performed by linear scan voltammetry measurements at scan rate of 3 mV s^{-1} in dioxygen-saturated phosphate buffer (pH 7.0, 0.1 M) after stabilization of the BOD-modified CF@Au open circuit potential.

For hybrid BFC tests, the electrochemical performance was evaluated by the constant resistance discharge (CRD) technique with a variable external resistance applied to the cell, ranging from 10 MΩ to 100 Ω. The current and power were derived from the resistance and the

cell voltage. The tests were performed in a two-chamber cell, with a Nafion® 117 perfluorinated membrane (3.5 cm × 5 cm) separating the anode and cathode compartments. The cathode compartment contained 25 mL PBS (pH 7.0, 0.1 M) at 30 °C saturated with O_2. The anode compartment consisted in 25 mL of glucose (10 mM) in 0.1 M KOH (pH 11.0). The evolution of the anode and cathode potentials was monitored individually by inserting a reference electrode in each compartment of the two-chambers cell. Three gold particle-based electrodes were tested in the hybrid BFC device and the electrochemical performance resulted from averages values.

5.5. Results and discussion

5.5.1. Characterization of the structural properties of gold particles on CF

Gold particles were deposited on a CF by CVs from a solution of chloroauric acid trihydrate followed by a thermal treatment at 1000 °C under nitrogen gas for 1 hour. Regarding the SEM graphs in Figure 5-1 a, it could be seen that the raw CF presented a smooth surface, while the surface morphology of CF@Au without thermal treatment was quite rough because of the envelopment of the carbon fibers by a thin gold layer (Figure 5-1 b). After a thermal treatment at 1000 °C, hexagon-shaped gold particles with an average size of 300 nm are formed by dewetting and are homogeneously distributed on the surface of the CF (Figure 5-1 c, d). From TGA analysis (Figure 5-1 e), the gold loading is 0.2 % wt. in the CF@Au samples which corresponds to the gold amount in the initial solution of chloroauric acid trihydrate (0.05 mg mL^{-1}).

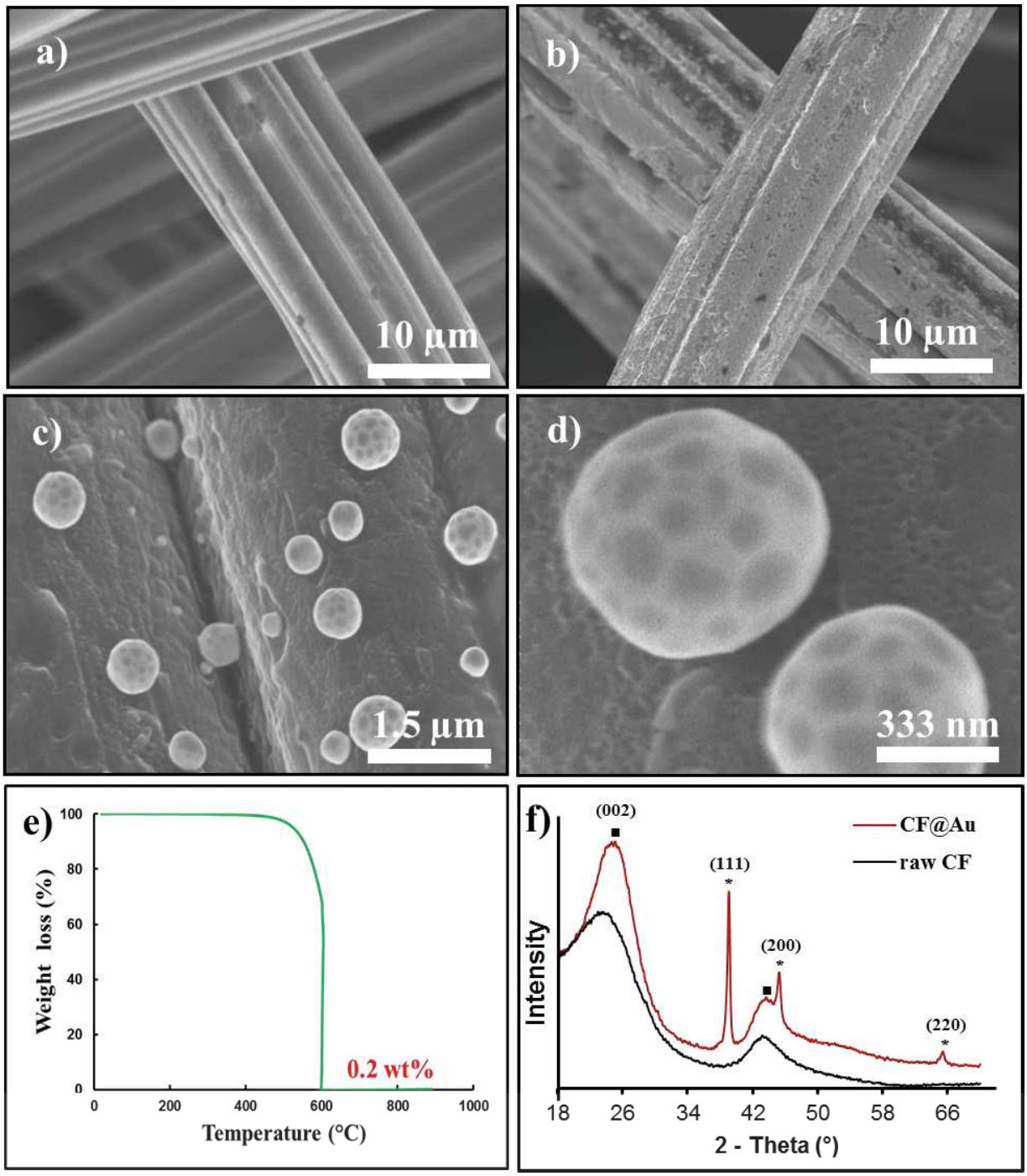

Figure 5-1. Characterization of CF@Au anode. SEM images of (a) raw CF, (b) CF@Au without thermal treatment, (c, d) CF@Au after heating treatment at 1000 °C for 1h, (e) TGA curve of CF@Au, and (f) XRD patterns of raw CF and CF@Au. Au (*), C (■).

The CF@Au material was characterized by XRD (Figure 5-1 f). The broad diffraction peak at around 23°, defined for hexagonal graphite structures (002) and the smaller peak at 43° are characteristic of the raw CF sample. Crystal gold on the surface of CF is proved through the emergence of the sharp peaks at 38.2° (111), 44.2° (200) and 64.6° (220), which are specific for cubic gold [365, 366]. This analysis confirmed that gold particles were successfully obtained from the reduction of the chloroauric anions by electrodeposition that formed a gold layer on the CF surface, subsequently transformed into particles by thermal treatment. The mechanism of formation of the gold particles by heat treatment will be discussed in details later in this manuscript.

5.5.1.1. Effect of the gold loading quantity

To maximize the gold particles loading, its dependence on $HAuCl_4$ concentration was studied. After the electrodeposition of the gold layer on the CF by scanning potentials, the resulting material was characterized by CVs in 0.5 M H_2SO_4. As shown in Figure 5-2 a, the curves present the typical peaks ascribed to the formation of Au surface oxides (around 1.1 V) and its reduction (0.9 V) [367]. From CVs of the redox probe potassium ferricyanide $Fe(CN)_6^{3-}$ (Figure 5-2 b), the increase in $HAuCl_4$ concentration contributes to a slight rise in the current response toward the redox waves of $[Fe(CN)_6]^{3-/4-}$ at the gold-modified CF, and to smaller anodic and cathodic peaks separation indicating that fast electron transfer kinetics predominantly occurred at the outermost plane of the gold particles. The increase in gold salt concentration to 0.1 mg mL^{-1} did not lead to detectable improvement. Therefore, 0.05 mg mL^{-1} of chloroauric acid trihydrate was chosen as optimal concentration for the electrodeposition step.

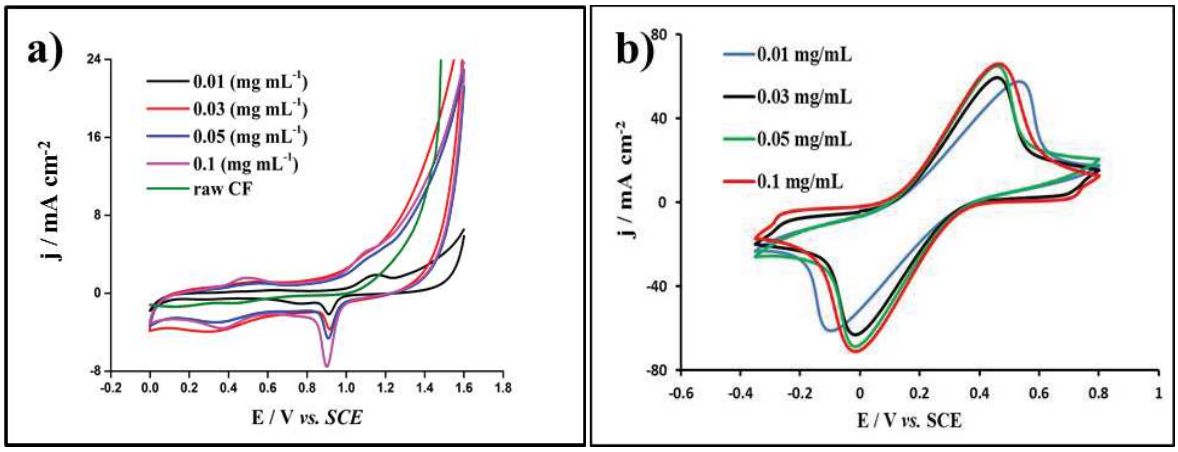

Figure 5-2. Effect of the gold loading quantity on CF@Au anode. CVs of raw CF and CF@Au electrodes at different chloroauric acid trihydrate concentrations in (a) 0.5 M H_2SO_4, and (b) potassium hexacyanoferrate solution (10 mM) in 1 M KNO_3. Scan rate 10 mV s^{-1}.

5.5.1.2. Effect of the heating temperature

The thermal treatment played an important role in the transformation of the gold layer to gold particles and in the elimination of contaminants. Consequently, the electrochemical behavior of the modified electrodes changes with the applied temperature treatment when the temperature rises from 600 to 1000 °C, as shown by the continuous increase in the anodic peak j_a of $[Fe(CN)_6]^{3-/4-}$ at the CF@Au electrodes (Figure 5-3 a), determined from the CVs of $Fe(CN)_6^{3-}$ at scan rate 10 mV s^{-1}. Higher temperature was not beneficial, as will be explained later.

In order to understand the gold particles growth with heating treatment, CF@Au was characterized by XRD, as shown in Figure 5-3 b. In the absence of thermal treatment, a small peak around 37° was assigned to complexes between Au and Cl coming from the uncompleted reduction of chloroauric acid by CV method. This peak disappeared by heating at higher temperature. The thermal treatment involved multiple and competitive mechanisms for the formation of gold particles: first, at low temperature (< 600°C) dewetting related to different expansion coefficients between the gold and the CF support [368, 369] induce the formation of the first Au droplets (Figure 5-3 c). This step was followed by the coalescence of the gold particles to form larger particles in order to reduce the total interfacial energy of the system. Gold particles tended to aggregate through coalescence [370]. Thus, gold was seen in the form of a rugged layer of Au droplets covering the surface of carbon fibers (Figure 5-3 d).

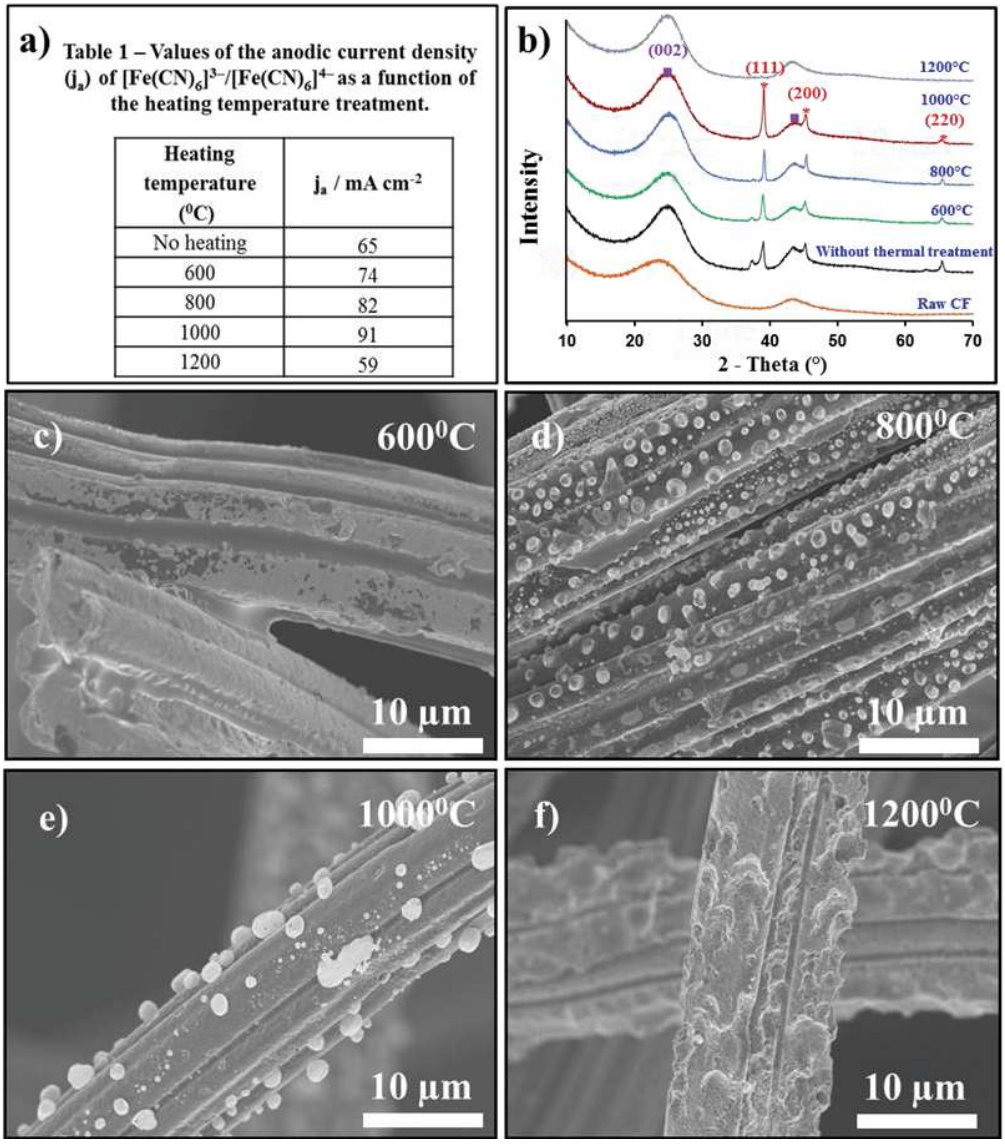

Figure 5-3. Effect of heating temperature on CF@Au anode. (a) Table 1 – Values of the anodic current density (j_a) of $[Fe(CN)_6]^{3-}/[Fe(CN)_6]^{4-}$ as a function of the heating temperature treatment. (b) XRD patterns of CF@Au (0.05 mg mL^{-1} $HAuCl_4.3H_2O$) electrodes at different treatment temperatures: Au (*), carbon (■). SEM images of CF@Au (0.05 mg mL^{-1} $HAuCl_4.3H_2O$) electrodes at different treatment temperatures: (c) 600 °C, (d) 800 °C, (e) 1000 °C, (f) 1200 °C.

At higher temperature, the Ostwald ripening process occurred by diffusion of the atoms (*via* evaporation or surface diffusion) from one particle to another [371] [362] to form the hexagon-shaped gold particles with an average size of 300 nm (Figure 5-3 e). At this temperature the XRD peak Au (111) at 38.2° was increased relying on the crystallization of Au during the

heat treatment [365, 370]. However, applying too high annealing temperature of 1200°C led to a decrease of the anodic current density of the redox wave $[Fe(CN)_6]^{3-}/[Fe(CN)_6]^{4-}$ (Figure 5-3 a). This came from the fact that at this temperature gold nanoparticles were evaporated. No more peaks of Au are observed on the XRD diffraction (Figure 5-3 b) and a rough surface without gold on SEM image (Figure 5-3 f) was noticed. This indicated that the selection of the appropriate treatment temperature was crucial for the formation of gold nanoparticles on CF.

5.5.2. CF@Au as support for electrocatalysis

5.5.2.1. Enzymatic O_2 reduction on CF@Au

The electrochemical response of the BOD-immobilized CF@Au electrode was shown in Figure 5-4 a, compared to a control biocathode prepared by the same immobilization technique on a raw CF electrode. The polarization curves were performed in oxygen saturated PBS pH 7.0. The oxygen reduction current began at around 0.45 V (vs Ag/AgCl), which is in good agreement with the reported values in the literature for the T1 site of BOD from *Myrothecium verrucaria* [348]. No catalytic current was observed in nitrogen saturated solution. The delivered current shows an almost linear potential dependence and the absence of a semi-plateau. This phenomenon was also observed for non-mediated system with some structure like carbonaceous foams [372] and carbon aerogel [373]. In such 3-dimensional materials, the enzymes are randomly oriented on the support, which induces a wide distribution in interfacial electron transfer rates and thus larger over potentials to electrically connect all the enzymes.

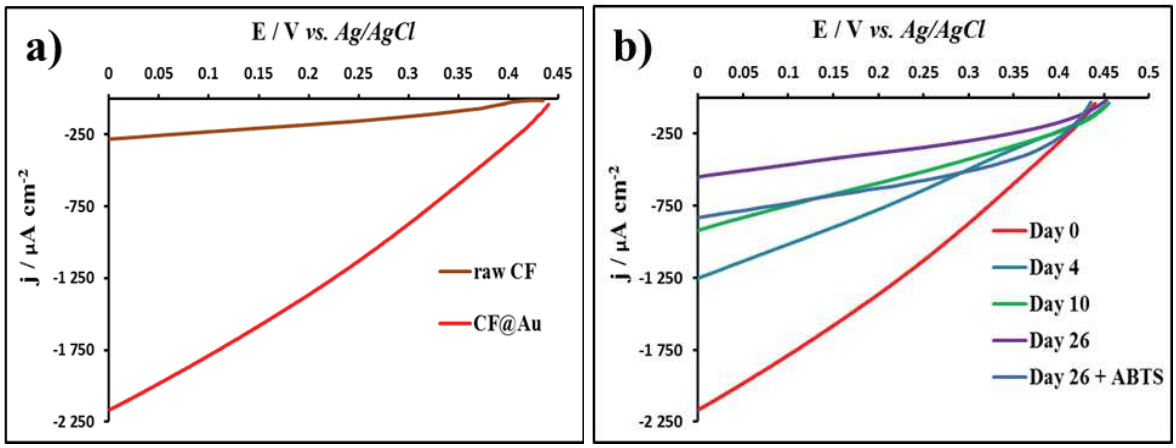

Figure 5-4. Enzymatic O_2 reduction on. (a) Polarization curves of O_2 electroreduction on the CF@Au and the raw CF biocathodes modified with the enzyme BOD. (b) Stability of the BOD-immobilized CF@Au electrode with time. Scan rate of 3 mV s^{-1}, O_2-saturated PBS 0.1 M, pH 7.0 at 30 °C.

The CF@Au biocathode showed the highest performance 2.160 mA cm^{-2} at 0 V (*vs* Ag/AgCl), which corresponded to an increase by 8-folds compared to the raw electrode. This outstanding performance came from the presence of the gold particles that enhanced the electronic conductivity of the electrode and the surface area. The stability of the electrode was investigated periodically (Figure 5-4 b) and between each testing time, the electrode was stored at 5 °C in a humid environment. For a 26 day-period, a significant reducing activity of the biocathode (-75 %) was observed, explained by several reasons such as enzyme inactivation, loss of electrical connection and desorption. The addition of 3 mM of ABTS (molecular mediator to transfer electron from enzyme to electrode) in the solution at the 26th day (Figure 5-4 b) gave rise to a noticeable increase in the current density, indicating that some enzymes have kept their activity but are no longer properly electrically connected to the electrode surface.

5.5.2.2. Glucose electrooxidation on CF@Au

In the following studies, the most promising CF@Au electrode obtained from the 0.05 mg mL^{-1} concentration of chloroauric acid trihydrate and the thermal treatment at 1000 °C under nitrogen was employed. The direct electro-oxidation of glucose was monitored by running CVs in 0.1 M KOH solution in the presence and absence of glucose 10 mM on CF@Au and raw CF electrodes for comparison. In the absence of glucose (Figure 5-5 a), the CVs of the CF@Au

electrode exhibited the two small electrochemical processes relative to gold surface oxides formation and reduction, respectively, in alkaline media [252, 374]. In the presence of glucose, raw CF was not active for glucose electrooxidation in the potential range investigated, whereas, the CF@Au electrode showed the typical voltammetric behavior characterized by three electrochemical processes: (1) formation of an adsorbed glucose layer on the gold electrode surface through the dehydrogenation of anomeric carbon of glucose molecules [249, 250], (2) oxidation of the previously adsorbed glucose intermediates to gluconolactone species, leading to the appearance of a large left shoulder pick around 0.3 V *vs* Ag/AgCl, and (3) re-adsorption and oxidation of glucose [255]. Figure 5-5 b showed that the positions of the peaks were dislocated when varying the scan rate, which is a point to consider when comparing different works. Compared to the literature on glucose oxidation by materials decorated with gold particles [266, 375-377], the CF@Au delivered very competitive values with a peak intensity around 9 mA cm^{-2} for the glucose oxidation to gluconolactone species, although comparison depended on the preparation methods, amount and form of active gold particles on the electrodes.

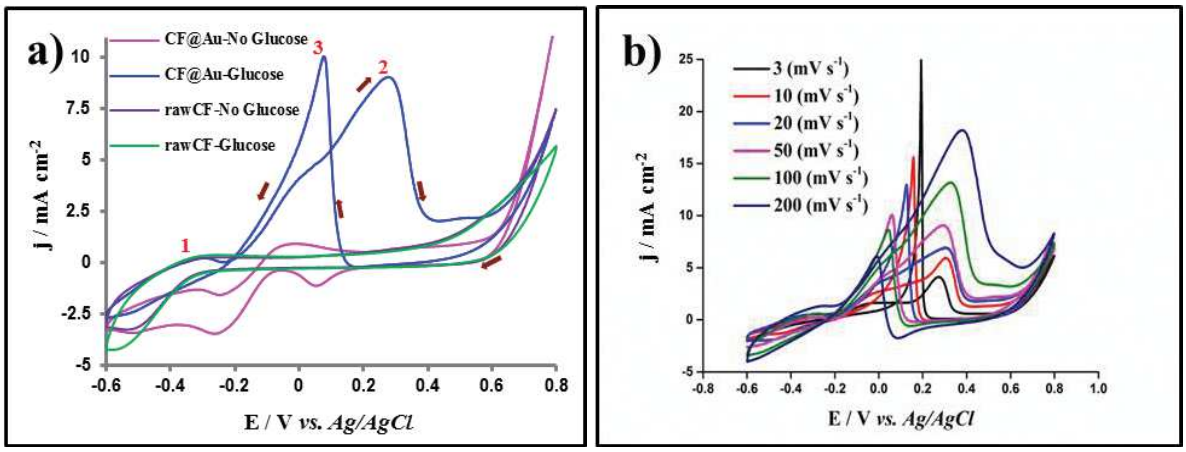

Figure 5-5. Glucose electrooxidation on CF@Au anode. CVs in 10 mM glucose in 0.1 M KOH (pH = 11) of (a) CF@Au and raw CF anodes in the presence and absence of 10 mM glucose at 50 mV s^{-1}, and of (b) CF@Au anode at various scan rates.

5.5.3. Glucose/O_2 hybrid BFC

A complete hybrid glucose/O_2 BFC was implemented by connecting the abiotic anode and the biocathode based on CF@Au in a two-chambers cell separated by a Nafion® membrane. Steady-state measurements were performed by applying various external resistances (ERs)

values. The evolution of the potential of each electrode was measured independently by introducing a reference electrode (Ag/AgCl) in each compartment (Figure 5-6 a). The output potential and current of the hybrid BFC were read on multimeter devices at the same time (Figure 5-6 b). The hybrid BFC delivered an OCV of 0.707 V. Figure 5-6 a displays the anodic and cathodic polarization curves. The anode potential starts at -220 mV and varies to -112 mV *vs* Ag/AgCl, corresponding to ΔE_{anode} = 108 mV. On the contrary, the variation of the cathode potential is more important, from 461 mV to 130 mV *vs* Ag/AgCl, meaning $\Delta E_{cathode}$ = 331 mV. The long-term stability of the electrodes was studied by recording the polarization curves after one week and after 2 months. As observed in Figure 5-6 a, the stability of the cathode decreased with time, as already observed in Figure 5-6 b. The cell performance was thus limited by the cathodic reaction, which performance relied on the enzyme stability and electrical connection. This result points out the well-established stability of abiotic materials as anode for glucose electrooxidation to construct hybrid devices. In Figure 5-6 b, the typical power profile of the hybrid device showed a maximum power density of 310 µW cm^{-2} at 352 mV. The performance was significantly enhanced compared to our previous devices fabricated from carbon electrospun fibers: 35 µW cm^{-2} with gold loading 20 % [25] and 65 µW cm^{-2} with gold loading 22% [26].

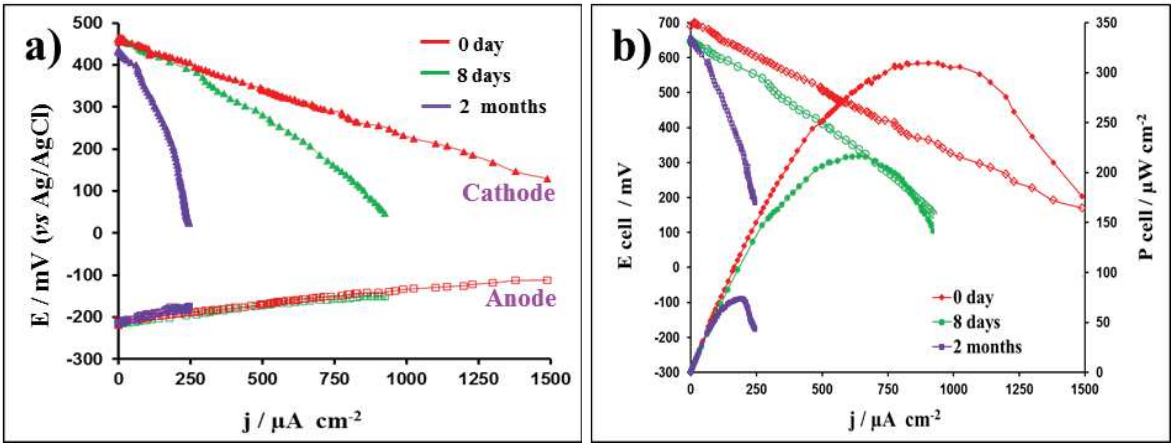

Figure 5-6. Electrical performance of the hybrid BFC at 30 °C with BOD-immobilized CF@Au cathode in O_2-saturated PBS (0.1 M, pH = 7.0) and CF@Au anode in 0.1 M KOH (pH = 11.0) containing 10 mM glucose. a) Monitoring of the potentials E_{anode} and $E_{cathode}$ with an Ag/AgCl reference electrode immersed in each compartment, (▲) $E_{cathode}$, (□) E_{anode}. b) Profile of the delivered E_{cell} potentials and power density of the hybrid BFC recorded from day 0 until 2 months. The biocathode was stored at 5 °C between each test.

5.6. Conclusions

A synthetic route of a gold particles-modified felt was performed by electrodeposition of gold salts on a CF template followed by a subsequent thermal treatment at 1000 °C. This method allowed for the dewetting of Au covering the surface of the CF to form hexagon-shaped gold particles homogeneously distributed with an average size of 300 nm. The presence of the Au particles enhanced the electroactivity of the CF@Au compared to the raw CF. A complete hybrid glucose/O_2 BFC was implemented by connecting the abiotic anode and the biocathode based on Au@CF. The BFC exhibited higher electrochemical performance than other reported hybrid glucose BFC, despite a low gold loading (0.2 wt%). It proved the efficient electrochemical activity of the CF@Au toward glucose oxidation in alkaline medium and toward enzymatic dioxygen electroreduction by the enzyme BOD in neutral pH.

5.7. General conclusions

The hybrid glucose/O_2 BFC could generate a maximum power density of 310 μW cm^{-2} at 352 mV from glucose oxidation at CF@Au anode. From that and based of the high stability of the abiotic anode for glucose oxidation, a new idea to develop EF system was born by using power produced from abiotic glucose oxidation to drive electrons for cathodic EF process for biorefractory pollutants degradation in a FC Fenton system. This was the content discussed in detail in the next chapter.

CHAPTER VI

DESIGN OF NOVEL FUEL CELL-FENTON SYSTEM: A SMART APPROACH TO ZERO ENERGY DEPOLLUTION

This chapter has been published in ***Journal of Materials Chemistry A*** as:

Thi Xuan Huong Le, Roseline Esmilaire, Martin Drobek, Mikhael Bechelany, Cyril Vallicari, Duy Linh Nguyen, Anne Julbe, Sophie Tingry, Marc Cretin, *Design of novel Fuel Cell-Fenton system: a smart approach to zero-energy depollution*, Journal of Materials Chemistry A, 2016, 4, 17686-17693.

CHAPTER 6. DESIGN OF NOVEL FUEL CELL-FENTON SYSTEM: A SMART APPROACH TO ZERO ENERGY DEPOLLUTION

6.1. General introduction

As discuss above, to decrease the operating cost for EF process, the power could be supplied from glucose oxidation at CF@Au anode without using input source from generators. In fact the glucose oxidation at anode takes place at -0.46 V *vs.* Ag/AgCl, which would make impossible to employ a combination of the CF@Au anode and either raw CF or CF modified by rGO cathode in the experimental set-up. Because the ORR for both of them happened at around -0.67 V, it was necessary to create a new cathode which could be combined with CF@Au anode to create an abiotic FC-Fenton system. Therefore there were two main missions given out for this chapter, including: (1) Preparing a novel cathode by modification CF with porous carbon layer coming from Metal Organic Framework to modify (i.e. to increase) the potential of ORR and (2) Construction of FC-Fenton system to treat AO7.

6.2. Abstract

A model azo dye pollutant, AO7, was removed efficiently from aqueous medium by a smart eco-friendly FC-Fenton system without any external power supply. In this approach, AO7 was degraded by EF process at a designed cathode (CF/porous Carbon (pC)) supplied by direct clean electrical energy from abiotic glucose oxidation at a CF/gold anode (CF@Au). The highly active cathode was fabricated by an attractive route combining Atomic Layer Deposition (ALD) of Zinc Oxide (ZnO) on commercial CF (CF) followed by subsequent solvothermal conversion of the metal oxide to a Metal Organic Framework (here Zeolitic Imidazolate Framework (ZIF-8)). The as-prepared composite material was further calcinated at high temperature under controlled nitrogen atmosphere. A porous carbon-based (pC) support with high specific surface area and containing nitrogen as a dopant was thus obtained, enhancing both conductivity and electrocatalytic properties toward H_2O_2 production from oxygen reduction. Degradation kinetics of AO7 (0.1 mM initial concentration) at the CF@pC cathode was monitored by UV-vis spectrophotometry and High-Performance Liquid Chromatography (HPLC) to prove the

efficiency of the composite material for the degradation of such a bio-refractory model molecule. Benefited from the H_2O_2 production rate (9.2 mg L^{-1} h^{-1}) by the carbon porous layer, AO7 (35.0 mg/L) was degraded by EF process in acidic medium (pH=3) with removal efficiency reaching 90 % in 10 h. The durability of the system was extended for more than 2 months with an average power output of 170 mW m^{-2}, confirming this abiotic FC-Fenton system as a green promising future technology for both environmental and energy-related areas.

Key words: Fuel cell – Fenton system, Electro-Fenton process, Atomic Layer Deposition, Metal Organic Framework, porous carbon, gold nanoparticles, glucose oxidation.

6.3. Introduction

Scarcity of pure water worldwide is dramatically affecting the economic development of Third Countries but also the industrial growth of others. When considering water recycling and reuse, new technologies such as EAOPs currently deserve strong attention. Indeed, such processes are of high interest since they are very efficient for the degradation of refractory pollutants that cannot be eliminated by conventional techniques. Among EAOPs, the EF process allows *in-situ* generation of highly reactive and non-selective $^{\bullet}OH$ radicals through oxygen reduction to hydrogen peroxide (Eq. (2-11)) and its further reduction to $^{\bullet}OH$ in the Fenton reaction (Eq. (2-12)) in the presence of Fe^{2+}, that induces the total mineralization of pollutants.

In EF process, the efficiency of pollutant degradation strongly depends on the cathode material where •OH radicals have to be generated. Carbon-based electrodes like vitreous carbon [221], CF [378], and carbon sponge [5] are commonly used as cathodes in oxygen dissolved solution to produce hydrogen peroxide, crucial species for the effective destruction of POPs. The enhancement of cathode material performances for the electrogeneration of H2O2 has thus received increasing interest through the development of composite electrodes prepared with PAN [220], ethanol/hydrazine hydrate [63], nitrogen-functionalized CNTs [309], multi-walled CNTs/surfactant [192], PPy/AQDS composite films [310]. Enhanced performance is mainly due to an increase of both the electronic conductivity of materials and the electrochemical active surface area in the developed microporous nanostructures.

In order to drive the electrons required for the ORR, an electric generator is generally required [379, 380]. To overcome this issue, innovative solutions were proposed. It was previously shown that MFC can be used for wastewater treatment as sustainable alternative energy sources [381]. The anode side contained electroactive biofilm working as a biocatalyst to

produce electrons while the EF process took place at the cathode. The biocatalyst was grew up on graphite rods [381], porous GF [209], granular graphite [382], carbon fiber brush [213] or CF [203]. In spite of their very promising performance for both energy savings and wastewater treatment, these processes still suffer from some restrictions associated to complex experimental conditions, limited bacteria durability and low electrocatalytic property of the electrodes.

An attractive alternative to MFC-driven EF process is the direct production of electrons through glucose oxidation process. Glucose FC can be classified into three types according to the nature of the catalyst: (i) enzymatic catalyst [383] (ii) microbial catalyst [384], and (iii) metal catalyst [385]. The electro-oxidation of non-enzymatic glucose with metallic nanoparticles displays long-term stability and can be performed on electrode materials containing Ni [386], Pt [387], Pd–Rh [388], Pt-Ru [389], Au [389], or Au-Pt-Pd [390].

In order to move forward towards a clean electrical energy system, we propose in this study a smart system whose working principle is based on abiotic glucose oxidation to drive the EF process. We focused our work on the development of relevant electrodes with electrocatalytic properties resulting from modifications of commercial CF. In order for the system to operate efficiently, the electric potential difference between the two electrodes must be large enough and the redox reactions must be sufficiently fast at the electrodes to limit kinetic losses. At the anode, the glucose oxidation reaction was performed on gold particles deposited on commercial CF (CF@Au), whereas at the cathode, a novel porous based-carbon material (CF@pC) was prepared with relevant catalytic properties to facilitate H_2O_2 production, to extend the system durability and to ensure an easy and fast procedure unlike MFC-Fenton.

According to our best knowledge such a concept of an abiotic FC-Fenton system has never been described in the literature and its application for efficient pollutants degradation represents an innovative green technology approach for both environment and energy-related areas.

6.4. Experimental

6.4.1. Materials

The CF was purchased from A Johnson Matthey Co., Germany. Diethyl zinc (DEZ), $Zn(CH_2CH_3)_2$ (95%), 2-methyl imidazole (2-mim, purity-97 %), chloroauric acid trihydrate ($HAuCl_4 \cdot 3H_2O$, 99.99 %), AO7 (Orange II sodium salt), D-(+)-Glucose monohydrate, sodium

sulphate (anhydrous, 99.0 – 100.5%), iron (II) sulphate hepta-hydrate (99%), methanol (99.8%), and acid sulfuric (98%) were bought from Sigma-Aldrich; potassium hexacyanoferrate (≥ 99%) and potassium nitrate (≥ 99%) from Fluka; potassium hydroxide (KOH pellets pure) from Merck, and used without further purification.

6.4.2. Fabrication of porous carbon/CF (CF@pC) cathode

Cathodes have been prepared by an original strategy combining 3 steps: i) ALD of a metal oxide (MO), ii) solvothermal conversion of MO to a metal organic framework (MOF) and finally iii) MOF carbonization, forming porous carbon with high specific surface area.

i) A home-made ALD set-up [391, 392] was used for depositing ZnO thin layers on the commercial CF (1 cm × 4 cm) at 100°C using sequential exposures of diethyl zinc (DEZ) and deionized water, separated by a purge with dry argon (Ar flow rate of 100 sccm). The deposition protocol was as follows : a) 0.5 s pulse of DEZ, 30 s exposure and 50 s purge with dry Ar ; b) 2 s pulse of H_2O, 40 s of exposure, and 60 s purge with dry Ar. The selected pulse, exposure and purge times were chosen both to ensure completion of the ALD surface reactions and to prevent any mixing of the reactive species. The characteristics of the ZnO ALD deposits (thickness, crystalline phase, grain/crystallite sizes) were found to be insensitive to both support morphology and composition. The growth rate per cycle of the ZnO layers was controlled by measuring the films thickness deposited on Si-wafer companion substrates placed in the ALD reaction chamber.

ii) The ZnO-coated CF were submitted to a solvothermal treatment in a closed pressure vessel (Teflon–lined stainless-steel autoclave - 45 mL) containing a solution of 2-methyl imidazole in methanol (10 wt% 2-min.). The autoclave was heated at 100 °C for 5 h in a conventional oven. After this solvothermal treatment, the resulting material was washed five times with methanol and dried for 2 h at 70°C.

iii) The as-modified CF were further carbonized at 1000^0C for 10 h under nitrogen atmosphere in order to obtain a porous carbon (pC) layer deposited on the commercial CF. The resulting CF@pC cathode was expected to offer a high specific surface area, enhanced conductivity and electrocatalytic properties toward H_2O_2 production from oxygen reduction.

6.4.3. The Fuel Cell – Fenton system

The FC-Fenton system was composed of two compartments separated by a Nafion® 117 perfluorinated membrane (3.5 cm × 5 cm) as depicted in Figure 6-1. The anode electrode consisted of CF@Au, while the cathodic electrode consisted of porous carbon deposited on commercial CF CF@pC. The anode compartment consisted in 90 mL of glucose (0.5 M) in 0.1 M KOH (pH 11.0), saturated by N_2 under magnetic stirring, whereas the cathode compartment contained 90 mL aqueous solution of AO7 (Azo dye AO7, 0.1 mM), with $FeSO_4.7H_2O$ (0.2 mM) as the catalyst and Na_2SO_4 (50 mM) as supporting electrolyte adjusted at pH=3 and saturated by oxygen. The pH of each compartment was maintained by adding either H_2SO_4 (1 M) or KOH (1 M). The decomposition of AO7 was monitored by measuring the dye absorbance at the selected single wavelength 485 nm, specific for azo bonds [390], with a Spectrophotometer Jenway 6300 (Barioworld Scientific Ltd, Dunmow UK). Concentrations of AO7 during the experiments were measured in parallel by a HPLC system (Waters 717 Autosampler and Waters 616 Pump) with a Photodiode Array Detector (Waters 2996 Photodiode Array Detector) fitted with a reverse phase (RP) Thermo Scientific C18 column (L = 250 mm, I.D = 4.6 mm, and 5 µm particles).

The electrochemical performance of the FC-Fenton system was evaluated by connecting the abiotic anode and the electro Fenton cathode under a discharge resistor of 5 ohms. The evolution of the potential of each electrode was measured independently by introducing a reference electrode (Ag/AgCl) in each compartment. The delivered current density and the output power density were derived from the resistance and the cell voltage (U), with P (mW m^{-2}) = U (V).j (mA m^{-2}).

PAN (Mw=150 000) and dimethylformamide (ACS reagent, ⩾99.8%) were purchased from Sigma Aldrich. Diethyl zinc (DEZ) ($Zn(CH_2CH_3)_2$, 95% purity, CAS: 557-20-0) was purchased from Sterm Chemical.

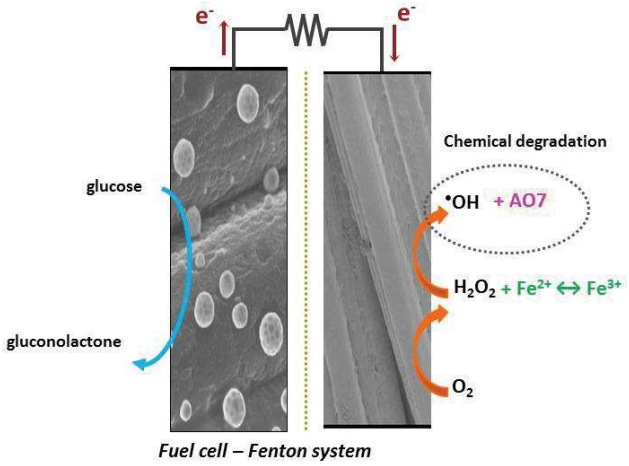

Figure 6-1. Schematic diagram of the FC-Fenton based system.

6.4.4. Material characterization

Chemical and structural characterizations of the prepared materials have been performed by SEM (Hitachi S-4800), XRD (PANAlytical Xpert-PRO diffractometer equipped with a X'celerator detector using Ni-filtered Cu-radiation), EDX analysis (Silicon Drift Detector (SDD), X-MaxN, Oxford Instrument) coupled to a Zeiss EVO HD15 SEM analyzer. The XPS measurements have been conducted using ESCALAB 250 Thermal Electron with AlKα (1486.6 eV). Binding energies were calibrated by using the containment carbon (C1s = 284.4 eV).

6.4.5. Electrocatalytic activity measurements

Electrochemical analysis was performed with a μ3AUT70466 Autolab system (Eco Chemie BV, Netherlands) with a conventional three-electrodes assembly composed of a saturated calomel reference electrode, a Pt foil counter electrode, and the developed electrodes as working electrode. To evaluate the catalytic activity of the CF@pC cathode toward H_2O_2 electrogeneration, linear sweep voltammetry (LSV) measurements were performed in Na_2SO_4 (50 mM) solution at pH=3.0. Before measurements, the solution was saturated by oxygen for 10 min and the potential was scanned from the open circuit potential to -1.2 V versus Ag/AgCl at 5 mV s^{-1} in a three-electrodes system. The electrogeneration of H_2O_2 was carried out at the potential of -0.21 V *vs.* Ag/AgCl by chronopotentiometry and the resulting H_2O_2 concentrations were determined by spectrophotometry using potassium titanium (IV) oxalate as a colored indicator. The absorbance of the yellow pertitanic acid complex between H_2O_2 and potassium titanium

oxalate in acidic solution was measured by a Spectrophotometer Jenway 6300 (Barioworld Scientific Ltd, Dunmow UK) at λ = 400 nm through a 1 cm polystyrene cuvette. The calibration curve was contributed from standard H_2O_2 solution which was titrated by potassium permanganate solution (0.1N).

6.5. Results and discussion

To develop an efficient FC-Fenton system, the innovation proposed in this work involves relevant modifications of commercial CF according to two different strategies: *i)* preparation of a cathode from the modification of CF with a porous carbon layer and *ii)* preparation of an anode by electrodeposition of gold particles on CF. The key parameters of both steps were examined through a description of the deposits (location, quantity, physico-chemical characteristics) and investigation of the electro-catalytic activity of the as-prepared materials assembled in a FC-Fenton cell. The electrodes were assembled in a FC-Fenton cell whose characteristics were described and discussed in relation with the electrodes structure and morphology, and with the degradation kinetics of the pollutant AO7 in aqueous solution.

6.5.1. Characterization of the CF@pC cathode

The active cathode was fabricated by combining ALD of metal oxide on CF followed by its solvothermal conversion to ZIF-8, and a subsequent calcination under controlled atmosphere forming porous carbon-based (pC) deposits. The presence of ZnO was highlighted with the diffraction peaks at 2Θ = 31.7°, 34.4° and 36.2° corresponding to the diffraction lines (100), (002) and (101) of the wurtzite hexagonal ZnO phase. After 250 ALD cycles, the thickness of the ZnO layer was ~ 50 nm and the mean size of crystallites in the ZnO layer was typically 18 nm, calculated by using the Debye–Scherrer equation as reported elsewhere [393]. The solvothermal conversion of the as-modified CF resulted in a ZIF-8-based composite material with ZIF-8 crystals (0.1-1 μm in size), homogeneously covering the carbon fibers (Figure 6-2 a). Both ZIF-8 and ZnO were found to co-exist on the carbon fibers, as confirmed in Figure 6-2 d by the characteristic XRD peaks of both ZIF-8 (2Θ = 7.3° (011), 10.4° (200), 12.7° (112), 18.0° (222)) and ZnO (2Θ = 31.7° (100), 34.4° (002), 36.2° (101)). Hence, under the selected reaction conditions, the synthesis resulted in CF/ZnO/ZIF-8 composites in which a thin ZnO nanolayer was locally dissolved by the 2-methyl imidazole linker and directly converted to ZIF-8 with a yield > 60%. The above composite was further carbonized under controlled atmosphere leading

to the formation of porous carbon (pC) thin layers homogeneously covering the surface of CF (Figure 6-2 b, c). XRD analysis (Figure 6-2 d) confirmed the full carbonization of both ZIF-8 and ZnO in the CF@pC material after thermal treatment.

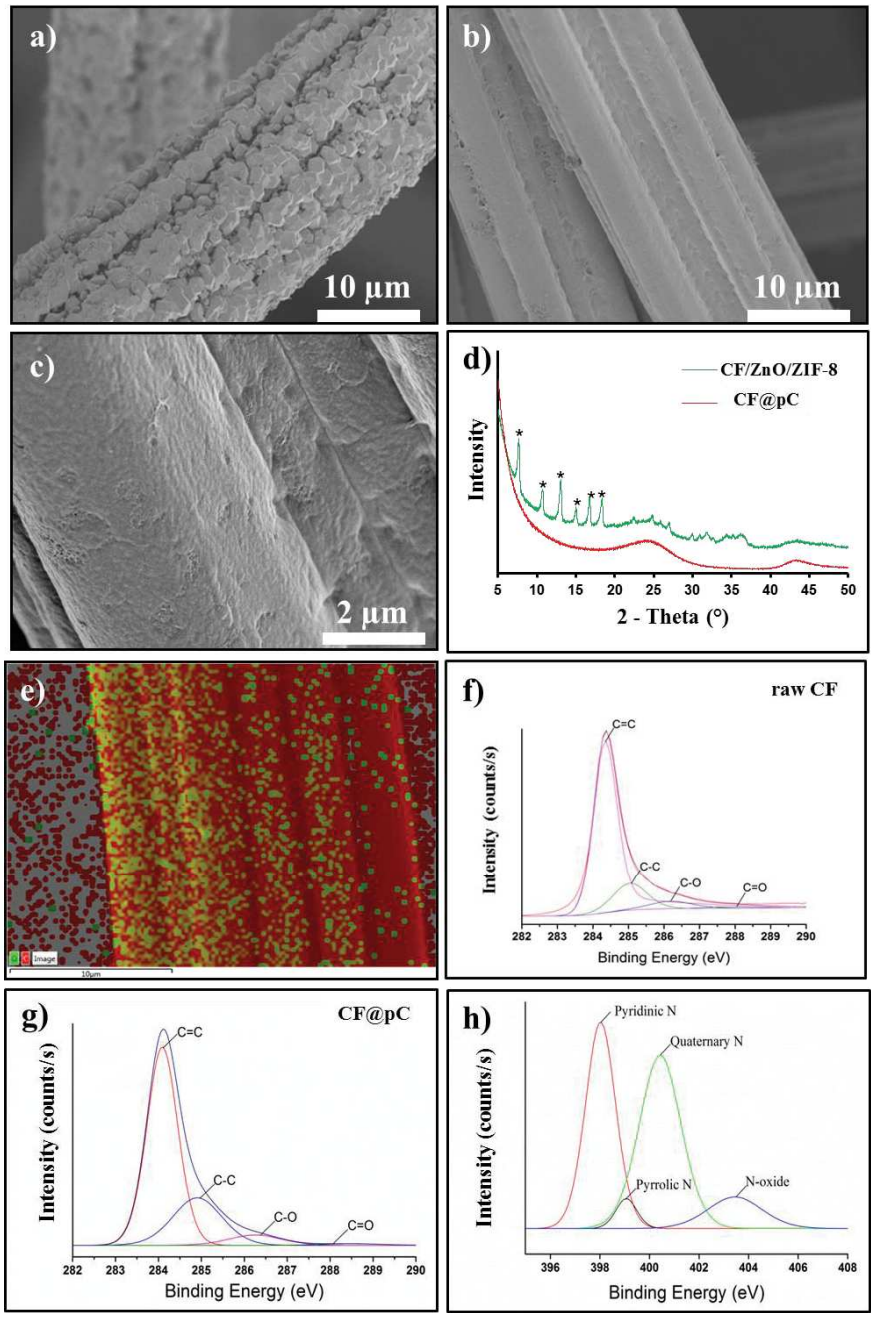

Figure 6-2. Characterization of CF@pC cathode. SEM images of CF/ZnO/ZIF-8 (a) and CF@pC samples (b,c); XRD patterns of both CF/ZnO/ZIF-8 and CF@pC samples, ZIF-8(*) (d); EDX of CF@pC electrode (e); C1s spectrum of raw CF (f) , and CF@pC (g), N1s spectrum of CF@pC (h).

The EDX mapping (Figure 6-2 e) clearly evidenced the presence of C and O atoms (~96 and ~4 at.%, respectively) that corresponded to the porous carbon on the surface that tended to be partially oxidized, as pointed out by XPS analysis. In Figure 6-2 (f, g), the presence of C=C and C-C carbonaceous structures were evidenced by the binding energies of 284.3 eV and 285 eV, respectively. The oxygen contamination in both materials was attested by the presence of the carbon-oxygen bonds C-O (286.79 eV) and C=O (287.81 eV). The presence of carbonaceous structures and the absence of ZnO in the resulting CF@pC material confirmed that a metal-free carbon material was successfully synthesized. Besides, the elemental analysis of CF@pC by XPS indicated as well the presence of nitrogen (1.73 %) on the porous carbon that could be attributed to N-containing functional groups like pyridinic-N (398.2 eV), pyrrolic-N (399.8 eV), quaternary-N (400.8 eV) and N-oxide (403 eV) (Figure 6-2 h) as reported elsewhere [394, 395]. These nitrogen-containing groups partly improve hydrophilic characteristics which promoted both electron transport and mass transfer, and thus electrochemical performance toward ORR during EF process [64, 396]. The improved hydrophilicity was proved by measuring the contact angles of raw CF which was 89.9°, meanwhile droplets of water disappeared immediately when it contacted with the surface of CF@pC (Figure 6-3).

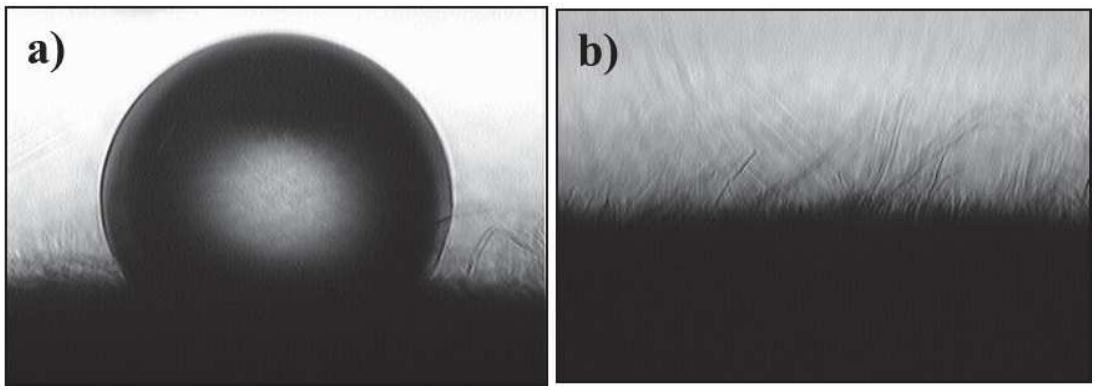

Figure 6-3. Shapes of water droplets formed on (a) raw CF, and (b) CF@pC surface.

According to N_2 physisorption measurements, it was apparent that the carbon layer on the CF generated a porous structure consisting mainly of micropores (pore volume =0.082 $cm^2\ g^{-1}$) increasing the specific surface area of the CF material from 0.0915 $m^2\ g^{-1}$to 64 $m^2\ g^{-1}$, corresponding to 700 times higher. As previously mentioned [397, 398], the microstructure of such a cathode material could facilitate the diffusion and transformation of oxygen to H_2O_2 on the

surface, and thus the CF@pC material was explored for the *in-situ* electrochemical production of H_2O_2.

Figure 6-4 a showed the LSV of H_2O_2 production, by running the potential of the CF@pC and raw CF electrodes from the open circuit potential to -1.2 V *vs.* Ag/AgCl. The production of H_2O_2 started at +0.2 V on the CF@pC electrode, whereas it started at -0.3 V on raw CF electrode with high overvoltage. This observation and the higher current densities delivered by the CF@pC electrode pointed out the faster electron transfer kinetics for ORR on the modified cathode [64]. This came from the reason that the porous structure with very high specific surface area combining with super hydrophilic property helped dissolved oxygen in aqueous medium move easily and quickly to be reduced at the whole active sites of cathode. Therefore, abundant amount of H_2O_2 was then generated rapidly. The electrocatalytic ability of CF@pC electrode to O_2 reduction was investigated by measuring the H_2O_2 production at a constant potential of -0.21 V *vs.* Ag/AgCl. After 60 min, a stable concentration of H_2O_2 (9.2 mg L^{-1}) was obtained at pH=3, whereas no H_2O_2 generation was detected at the raw CF electrode, revealing the outstanding performance of the newly designed CF@pC cathode.

Besides, as observed in Figure 6-4 a, glucose oxidation at CF@Au anode started at -0.46 V *vs.* Ag/AgCl. For efficient operation, it was thus obvious that raw CF cathode could not be combined to CF@Au anode to build a FC-Fenton system due to the low electric potential difference between the two electrodes. Briefly, the CF@pC electrode had great promise as an efficient cathode to generate H_2O_2 at low potential in EF process for pollutants degradation.

6.5.2. FC– Fenton system efficiency

The FC-Fenton system was operated by connecting both the abiotic CF@Au anode and the CF@pC cathode in a two-chambers cell separated by a Nafion membrane. Figure 6-4 presented the operation feature of the FC- Fenton system where direct electrical energy from abiotic glucose oxidation at CF@Au electrode in anodic compartment was transferred to cathodic one for oxygen reduction at CF@pC electrode.

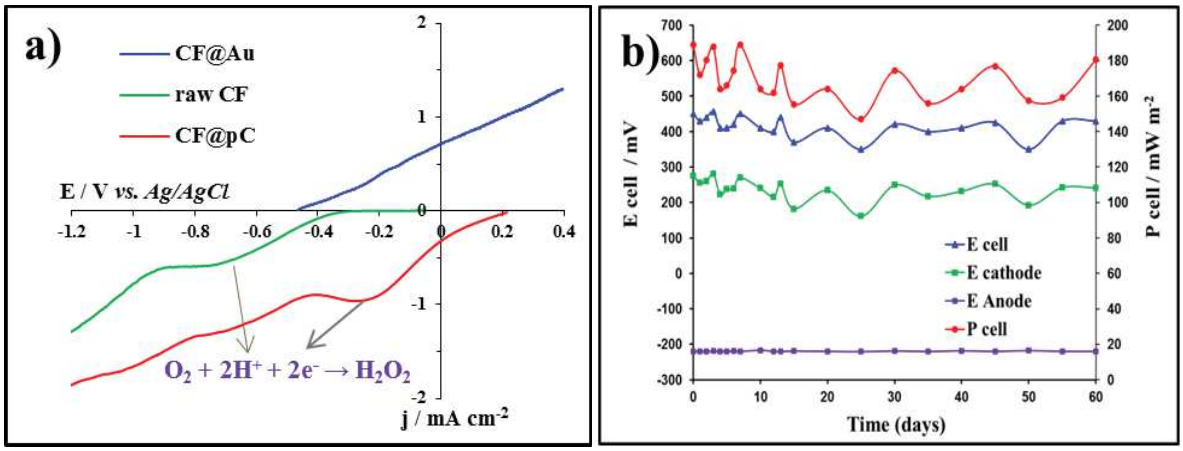

Figure 6-4. Acitivity of FC-Fenton system. (a) LSV of raw CF, CF@pC cathodes obtained in 50 mM Na_2SO_4, O_2 saturated solution, pH = 3. Scan rate 5 mV s^{-1}; and CF@Au anode in 0.1M KOH solution with 0.5 M glucose (pH =11.0). (b) Electrical performance of the FC-Fenton cell at 30°C with the CF@pC cathode in O_2-saturated solution (0.1 mM of AO7, 50 mM Na_2SO_4, 0.20 mM Fe^{2+}, pH =3.0) and the CF@Au anode in 0.1M KOH (pH =11.0) containing 0.5 M glucose.

An average output current density of 360.3 ± 51.5 mA m^{-2} at 400 ± 50 mV was generated providing electrons for the ORR at the cathode where the hydroxyl radical (•OH) were formed. Figure 6-4 b clearly demonstrated that an average power output of 170 mW m^{-2} was continuously produced for at least two months. The CF@Au electrode exhibited stable electroactivity toward glucose oxidation at around -220 mV due to the presence of the gold nanoparticles. In the cathodic compartment, regular potential oscillation took place due to both proton consumption in ORR (Eq. 1) and exchange through Nafion membrane, leading to pH variations affecting the cathodic potential values. As a result, pH adjustment played a key role to maintain a stable performance of the FC-Fenton system. The characterization of both CF@Au anode and CF@pC cathode after two months use in FC-Fenton system has been performed by SEM observations (Figure 6-5 a, b), EDX analysis (Figure 6-5 e, f), XPS analysis (Figure 6-5 c, d), in order to prove the durability of both fabricated electrodes. As observed from Figure 6-5 a, the gold particles were still steadily deposited on CF@Au anode after two months use in FC-Fenton system. In the case of CF@pC cathode, some additional impurities (F, Si, S) at very low quantities (Figure 6-5 f) occurred after two months of system operation. This contamination coming from the dye solution continuously supplied into the cathodic compartment had however no negative impact

on the FC-Fenton efficiency. These results thus clearly confirmed the robustness of both cathode and anode electrodes attesting their long-term stability in the proposed FC system.

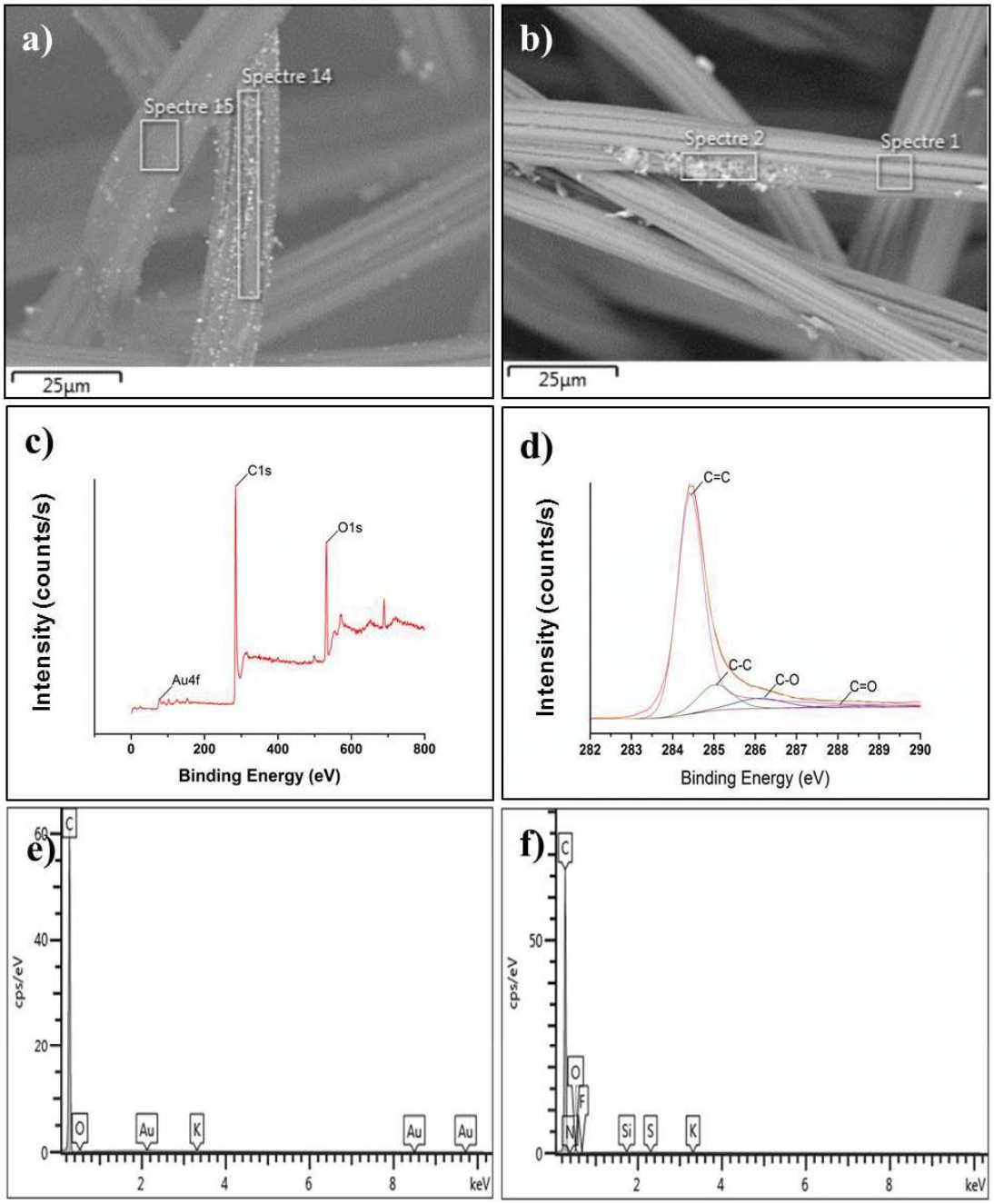

Figure 6-5. Characterization of electrodes after two months use in FC-Fenton system. (a,b) SEM image of CF@Au anode and CF@pC cathode; (c,d) XPS spectra of CF@Au anode and CF@pC cathode; (e,f) EDX analysis of CF@Au anode and CF@pC cathode.

The AO7 degradation was followed by HPLC analysis during electrolysis. As shown in Figure 6-6 b, the concentration of AO7 decreased rapidly at the early stage of electrolysis with approximately 70 % conversion within 3 hours. Subsequently, degradation decelerated because the decomposition of AO7 by EF process led to the formation of various aromatic compounds, short-chain carboxylic acids or their complexes, which were difficult to remove. Hence, the AO7 decomposition increased by only ~20 % in the seven following hours, resulting in about 90% elimination of AO7 after 10 h of the electro-catalytic process. On the other hand, the absorption peaks at 254 and 310 nm (spectrophotometry), attributed to aromatic amines and naphthalene in the initial mother solution, were also weakened as a result of the increased treatment time (elimination of the aromatic ring structure by $^{\bullet}OH$ - Figure 6-6 c). In order to evaluate the durability of the studied FC-Fenton system, the decay kinetics of AO7 was monitored during two months. The cathodic compartment was weekly replenished with fresh AO7 0.1 mM solution with 50 mM Na_2SO_4 and 0.20 mM Fe^{2+} at pH = 3, while in the anodic compartment the abiotic anode and the solution were kept unchanged. The breaking of the azo bond in AO7 structure (Figure 6-6 a) by $^{\bullet}OH$ was identified by measuring the absorbance of the solution at λ = 485 nm. As a result of the high consistency of both gold nanoparticles and porous carbon layer at anode and cathode electrodes respectively, the cell current output remained stable during at least two months and led to steady degradation of AO7 from water environment (Figure 6-6 d). From Figure 6-4 a, it could be clearly noticed that the ORR occurred at less negative potentials after modification (-0.21 V *vs.* Ag/AgCl on CF@pC instead of -0.67 V on the bare CF). This observation was of an utmost importance when applying such cathode in the proposed FC-Fenton system. In fact the glucose oxidation at anode takes place at -0.46 V *vs.* Ag/AgCl, which would make impossible to employ a combination of the CF@Au anode and raw CF cathode in the experimental set-up. Therefore, we could not have the AO7 degradation using the non-modified CF in this FC system. These results proved the promising efficiency of the proposed FC-Fenton cell for the zero-energy depollution systems of acidic solutions and could be further extended to other energy systems.

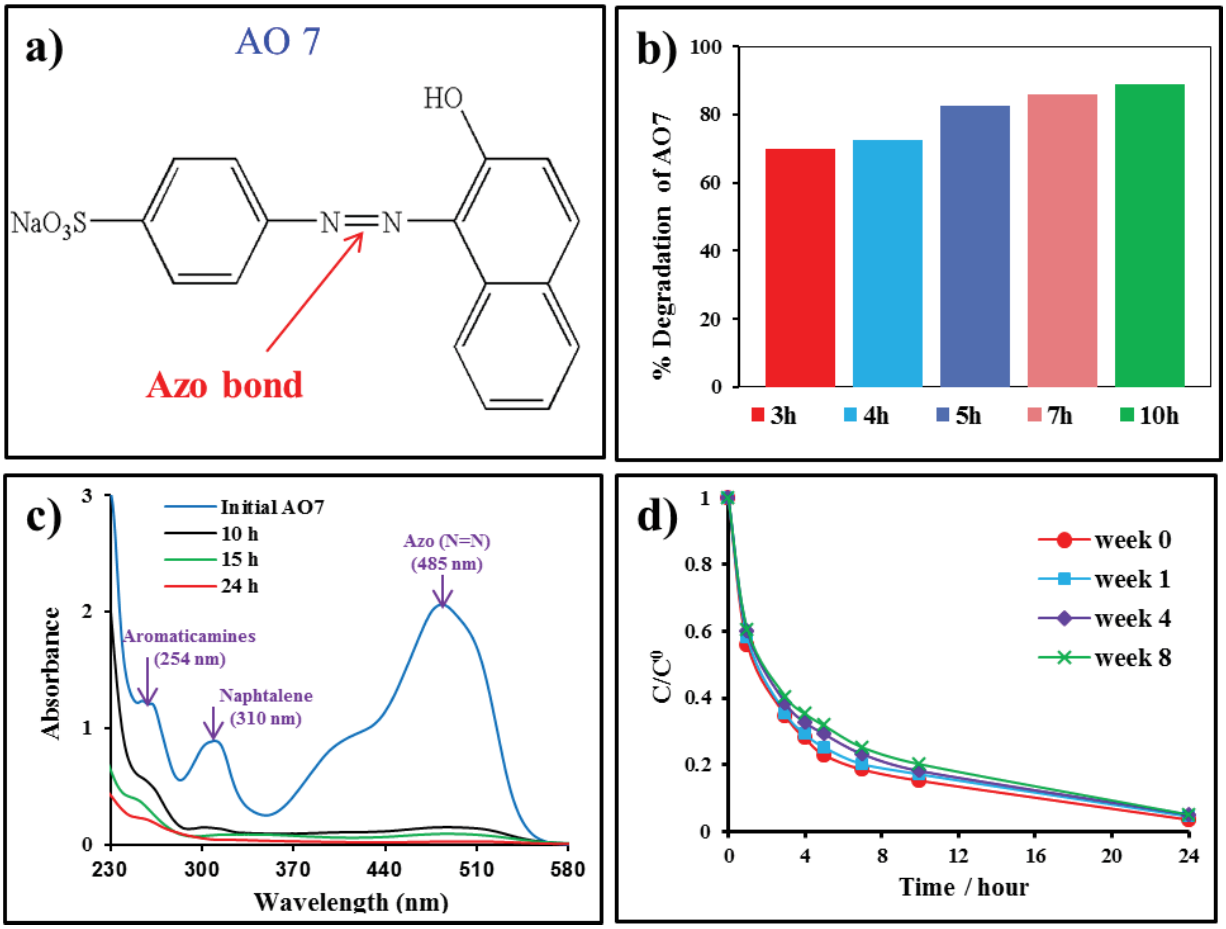

Figure 6-6. AO7 degradation by FC-Fenton system. (a) Molecular structure of AO7; (b) % removal of AO7 concentration as a function of treatment time; (c) Evolution of UV–Vis spectra of AO7with treatment time. d) Degradation kinetics of AO7 recorded on 24 h from a fresh solution at week 0, week 1, week 4 and week 8. Conditions: 90 mL AO7 (0.1 mM) aqueous solution in 50 mM Na_2SO_4 with 0.20 mM Fe^{2+} at pH 3.0.

Compared with other studies from the literature [203, 209, 382], the present FC-Fenton system showed remarkable advantages such as *i)* virtually zero energy costs (no need of any external power generator), *ii)* simple and fast operating cell at ambient temperature with no need of an anaerobic medium (contrary to bacterial electrodes and biofilms), *iii)* accelerated ORR leading to H_2O_2 production at higher potential, *iv)* low negative potentials leading to more efficient pollutants removal and finally *v)* long-term stability enabling multiple degradation cycles without decreasing the catalytic activity in time.

6.6. Conclusions

The present work demonstrated the potential of a smart eco-friendly approach for the removal of POPs from water media without using any external power input. The proposed green technology relied upon a FC - Fenton system composed of an originally designed carbon porous felt (CF@pC) cathode and CF@Au anode placed in a cell with two-chambers separated by a protonic exchange membrane (Nafion). The original synthesis of the cathode electrode, based on ALD of ZnO and its subsequent solvothermal conversion to ZIF-8 and pyrolysis, produced a porous carbon material with beneficial electrocatalytic properties for the diffusion and the reduction of oxygen into H_2O_2. The presence of gold particles on the CF anode allowed the direct electro-oxidation of glucose to supply green electrons for the ORR. The catalytic properties of both anode and cathode induced a stable output current density of 360.3 ± 51.5 mA m^{-2} at 400 ± 50 mV, maintained for long-term period. As a consequence, 90 % of the initial concentration of the azo dye pollutant AO7, identified by HPLC analysis, was eliminated upon extended EF degradation for 10 h, and the cell power output of 170 mW m^{-2} was stable at least for two months. Hence, this first proof of concept of an abiotic FC – Fenton system demonstrated a high efficiency towards pollutant degradation with a huge potential in both energy-related areas and environmental protection.

6.7. General conclusion

Our idea about EF technology without using input power was realized using the abiotic FC- Fenton system which combined between carbon porous felt (CF@pC) cathode and CF@Au anode. It is necessary to develop more this system by using other less expensive catalysts at the anodes instead of using gold particles. At the moment, we just developed a lab scale cell, so it will be more practical if the FC-Fenton system can be enlarged to larger reactors with higher volumes. Parallels, the performance of cathode should be more improved by applying other modification methods towards a low cost and efficient technology which can be used in industrial fields. They will be interesting perspectives of this thesis.

CHAPTER VII

CONCLUSION and PERSPECTIVES

CHAPTER 7. CONCLUSION and PERSPECTIVES

7.1. Conclusion

Improving the properties of CF electrode by different modification methods as well as its application for wastewater treatment containing POPs by EF process towards zero energy depollution is still a fertile land for future studies in energy and environmental field. In this study, we solved many important problems and brought to a huge number of interesting results relevant to CF based electrodes for EF process that was listed as following:

(i) Finding the optimal conditions for removal of AO7 and ACE in aqueous medium by EF treatment using commercial CF cathode (60 cm^2). These parameters were corresponding to 500 mA and 0.2 mM for applied current density and catalyst concentration. At these values, the mineralization of 200 mL of 0.1 mM ACE and AO7 was 86.9% and 96.2%, respectively. The identification and the evolution of intermediate compounds, as well as the toxicity of the solution, were also examined carefully along the EF process. In order to characterize and quantify as accurately as possible the formation of by-products, both the volume of solutions (500mL) and initial concentrations of pollutants (1mM) were extended. Twelve aromatic by-products could be revealed by HPLC and LC/MS techniques during the decomposition of AO7 and 4 ones during ACE degradation. In both cases, the early formation of toxic aromatic products like 1,2-naphtoquinone or 1,4-benzoquinone was correlated to the increase in solution toxicity reaching 100% for 60 minutes of the EF treatment of PCM and for 100 min for AO7. The subsequent decomposition of these intermediates led to the formation of short-chain carboxylic acids and thereby to a drastic decrease of the bacteria luminescence inhibition ratio. Consequently the total detoxification of the solution was accomplished after 120 minutes and 270 minutes for ACE and AO7, respectively. The sequential degradation of pollutants and their intermediates produced inorganic ions such as ammonium, nitrate and sulfate which could be quantified at the end of the electrolysis. Finally two complete pathways of AO7 and ACE degradation by the EF process could be built and presented. Moreover the innovative point of this approach was to identify sub-products at the different stages of the EF treatment and more especially to link sub-products formation with effluent toxicity toward *Vibria Fischeri* bacteria strain. We have then identified the most toxic subproducts of AO7 and ACE degradation and shown the possibility to control treatment duration thank to the monitoring of effluents toxicity.

(ii) The commercial CF (1 cm x 2 cm) was modified by rGO, applying three various reduction ways: constant potential reduction (CPR-CF electrode), chemical reduction (CR-CF electrode) and thermal reduction (TR-CF electrode). The CPR-CF was chosen as the best way for the modification because of its simplicity, low cost, and high efficiency. The parameters affecting the conversion of GO to rGO, such as pH, applied potential and duration of the reduction process, were investigated. This new cathode upgraded significantly the electrochemical properties identified by CVs and impedance analyses: a 10 times higher peak current could be obtained on this material with the redox probe $[Fe(CN)_6]^{3-}/[Fe(CN)_6]^{4-}$; a 2.17 Ω charge-transfer resistance lower than that obtained on raw CF. The modified electrode was served as cathode for AO7 degradation by EF process in acidic medium. TOC removal after 2 h treatment reached 73.9% on the CPR-CF, and this was 18.3% higher than on the raw CF. 94.3% of mineralization could be obtained for 8 h electrolysis. After 10 cycles of use (80 h), the mineralization ratio of the modified cathode was only decreased by 9.6%, showing that this rGO-CF is a powerful and promising electrode for improving the removal efficiency of dye pollutants using EF technology.

(iii) A Fuel-cell Fenton system towards zero energy depollution without using input power like traditional EF treatment was successfully contributed. This FC-Fenton system was composed of two compartments separated by a Nafion® 117 perfluorinated membrane. The gold particles-modified CF anode was obtained by electrodeposition of gold salts on a commercial CF (1 cm x 4 cm) followed by a subsequent thermal treatment at 1000 °C. This method allowed for the diffusion of Au droplets covering the surface of the CF to form larger hexagon-shaped gold particles homogeneously distributed with an average size of 300 nm. The affect of gold loading as well as thermal treatment were studied for Au deposition and transfer to gold particles. The active cathode was fabricated by combining ALD of metal oxide on CF followed by its solvothermal conversion to ZIF-8, and a subsequent calcination under nitrogen atmosphere forming porous carbon-based (pC) deposits. The ORR occurred on CF@pC cathode at less negative potential (-0.21 V *vs.* Ag/AgCl on CF@pC instead of -0.67 V on the bare CF). This observation was of an utmost importance when applying such cathode in the proposed FC-Fenton system. In fact the glucose oxidation at anode takes place at -0.46 V *vs.* Ag/AgCl, which would make impossible to employ a combination of the CF@Au anode and raw CF cathode in the experimental set-up. The characterization of both CF@Au anode and CF@pC cathode after two months use in FC -Fenton system has been performed by SEM observations, EDX analysis, XPS analysis, in order to prove the durability of both fabricated electrodes. This new FC-Fenton

system showed a long-term stability enabling multiple degradation cycles without decreasing the catalytic activity in time. Particularly, 90 % of the initial concentration of the azo dye pollutant AO7, identified by HPLC analysis, was eliminated upon extended EF degradation for 10 h, and the cell power output of 170 mW m^{-2} was stable at least for two months.

The results presented in this study are hoped to be the first of other scientific contribution to the development of green & clean systems using EAOPs technology for wastewater treatment in nearly future.

7.2. Perspectives

The works in this thesis manuscript can be continued developing according to many different directions as following:

- Because of friendly environmental feature of EF treatment that can remove remarkably the high toxic contaminants to non-toxic compounds, the future studies focusing on correlation between degradation pathway and toxicity of new emerging POPs by EF process on CF are actually useful.
- The benefits from graphene or porous carbon modification on CF were very impressive. This brings to interesting ideas for combination of two kind materials for CF modification, from that promotes maximum their efficiencies including hydrophilic, electrochemical properties, specific surface area, and conductivities.
- Concerning the Fuel-cell Fenton system, it is necessary to continue decreasing the cost preparation by using other less expensive catalysts at anodes instead of using gold particles. At the moment, our study have just stopped at lab scale, so it will be more practical if the FC-Fenton system can be enlarged to big reactors with higher volumes. Parallels, the performance of cathode should be more improved by applying other modification methods towards a low cost and efficient technology which can be used in industrial fields.
- It is also interesting to upgrade the EF treatment by coupling this process with other advanced technologies like ultra- and nano-filtration.

SCIENTIFIC CONTRIBUTIONS

Publications

- **Thi Xuan Huong Le**, Mikhael Bechelany, Joffrey Champavert and Marc Cretin, *A Highly Active Based Graphene Cathode for Electro-Fenton Reaction*, RSC Advances, 2015, 5, 42536 – 42539.

  URL: http://pubs.rsc.org/EN/content/articlehtml/2015/ra/c5ra04811g

- Marc Cretin, **Thi Xuan Huong Le**, *•OH Radicals Production*, Chapter in book: Encyclopedia of Membranes, pp.1423-1424, 2016.

  URL: http://www.springer.com/us/book/9783662443231

- **Thi Xuan Huong Le**, Thi Van Nguyen, Amadou Yacouba Zoulkifli, Zoungrana Laetitia, Avril Florent, Eddy Petit, Julie Mendret, Valerie Bonniol, Mikhael Bechelany, Stella Lacour, Geoffroy Lesage, Marc Cretin, *Toxicity removal assessments related to degradation pathways of azo dyes: toward an optimization of electro-Fenton treatment*, Chemosphere, 2016,161, 308–318.

  URL: https://www.ncbi.nlm.nih.gov/pubmed/27441990

- **Thi Xuan Huong Le**, Mikhael Bechelany, Adriana Both Engel, Marc Cretin, Sophie Tingry, *Growth of gold particles on carbon felt for efficient hybrid biofuel cell for micropower generation*, Electrochimica Acta, 2016 , 219, 121–129.

  URL: http://dx.doi.org/10.1016/j.electacta.2016.09.135

- **Thi Xuan Huong Le**, Mikhael Bechelany, Stella Lacour, Nihal Oturan, Mehmet A. Oturan, Marc Cretin, *High removal efficiency of dye pollutants by electro-Fenton process using a graphene based cathode*, CARBON 94, 2015, 1003–1011.

  URL: http://www.sciencedirect.com/science/article/pii/S0008622315301093

- **Thi Xuan Huong Le**, Roseline Esmilaire, Martin Drobek, Mikhael Bechelany, Cyril Vallicari, Duy Linh Nguyen, Anne Julbe, Sophie Tingry, Marc Cretin, *Design of novel Fuel Cell-Fenton system: a smart approach to zero-energy depollution*, Journal of Materials Chemistry A, 2016, 4, 17686-17693.

  URL: http://pubs.rsc.org/en/journals/journalissues/ta

- **Thi Xuan Huong Le**, Christophe Charmette, Mikhael Bechelany, Marc Cretin, *Facile Preparation of Porous Carbon Cathode to Eliminate Paracetamol in Aqueous Medium Using Electro-Fenton System*, Electrochimica Acta, 2016, 188, 378–384.

  URL: http://www.sciencedirect.com/science/article/pii/S0013468615309294

- Soliu O. Ganiyu; **Thi Xuan Huong Le**; Mikhael Bechelany; Giovanni, Esposito; Eric D. van Hullebusch; Mehmet A.Oturan; Marc Cretin, *Hierarchical CoFe-Layered Double Hydroxide Modified Carbon-felt Cathode for Heterogeneous Electro-Fenton process,* Journal of Materials Chemistry A, 2016, DOI: 10.1039/C6TA09100H.

  URL: http://pubs.rsc.org/en/content/articlelanding/2016/ta/c6ta09100h#!divAbstract

- **Thi Xuan Huong Le**, Thi Van Nguyen, Amadou Yacouba Zoulkifli, Zoungrana Laetitia, Avril Florent, Eddy Petit, Julie Mendret, Valerie Bonniol, Mikhael Bechelany, Stella Lacour, Geoffroy Lesage, Marc Cretin, *Correlation between degradation pathway and toxicity of acetaminophen and its by-products, using electro-Fenton process in aqueous media,* Chemosphere, 2017, 172, 1-9.

  URL: http://www.sciencedirect.com/science/article/pii/S0045653516317805

- **Thi Xuan Huong Le**, Mikhael Bechelany, Marc Cretin, Sophie Tingry, *Optimal direct electron transfer between MWCNTs@COOH/BOD /chitosan layer and porous carbon felt for dioxygen reduction*, 2016. Electrochimica Acta, Revision (EO16-2823).

- **Thi Xuan Huong Le**, Mikhael Bechelany, Marc Cretin, *Carbon felt -based electrodes for environmental and energy applications: A Review*, Energy & Environmental Science, Submission.

- **Thi Xuan Huong Le**, Roseline Esmilaire, Martin Drobek, Mikhael Bechelany, Cyril Vallicari, Anne Julbe, Sophie Cerneaux, Marc Cretin, *Elaboration of highly porous carbon layer of carbon on carbon felt for application in Electrochemical Advanced Oxidation Process,* Electrochimica Acta , Prepare for submission.

Participation in conferences

❖ Oral communications

- **Thi Xuan Huong Le**, Roseline Esmilaire, Mikhael Bechelany, Martin. Drobek, Cyril Vallicari, Anne Julbe, Sophie Tingry, Marc Cretin, *Fuel Cell-Fenton system: a smart approach for water depollution***,** The 3rd International Conference on Bioinspired and Biobased Chemistry & Materials**,** October 16-19, 2016, Nice, France.
- **Thi Xuan Huong Le**, Mikhael Bechelany, Adriana Both Engel, Marc Cretin, Sophie Tingry, *Growth of gold particles on carbon felt for efficient micropower generation in a hybrid biofuel cell*, MRS Fall Meeting & Exhibit, September 19-22, 2016, Poland.
- **Thi Xuan Huong Le**, Mikhael Bechelany, Marc Cretin, *Graphene-based material in advanced oxidation process for mineralization of persistent organic pollutants (POPs) by electro-Fenton*, Oral presentation, MRS Fall Meeting & Exhibit, September 19-22, 2016, Poland.
- **X. H. LE Thi**, M. Bechelany, M. cretin, *A highly active cathode for electro-Fenton reaction based on Graphene*, Advances in Functional Materials, 2015, Stony Brook University, USA.
- Soliu O. Ganiyu, **Thi Xuan Huong Le**, Mikhael Bechelany, Mehmet A. Oturan, Eric D. van Hullebusch, Marc Cretin, *Synthesis, characterization and application of self-catalyzed layered double hydroxide coated carbon-felt cathode in Electro-Fenton's degradation of organic pollutants,* 67th annual meeting of the International Society of Electrochemistry, Netherlands, 2016.

❖ Poster

- **Thi Xuan Huong Le**, Mikhael Bechelany, Marc Cretin, *Graphene modified carbon felt electrode: A highly active cathode for electro-Fenton reaction*, 2nd Journées Méditerranéennes des Jeunes Chercheurs, 2014, Marseille, France.

- **Thi Xuan Huong Le**, Mikhael Bechelany, Marc Cretin, *Mineralization of biorefactory pollutants by the electro-Fenton reaction on a highly active cathode based on graphene*, Journées d'Electrochimie, 2015, Rome, Italie.
- **Thi Xuan Huong Le**, Roseline Esmilaire, Sophie Cerneaux, Martin Drobek, Anne Julbe, Mikhael Bechelany, Marc Cretin, *Design of attractive carbon-based membrane for application in advanced oxidation process by electro-Fenton*, ICIM 2016, July 10-13, 2016, Atlanta, USA.

References

[1] Enric Brillas, Ignasi Sirés, and M. A. Oturan, "Electro-Fenton Process and Related Electrochemical Technologies Based on Fenton's Reaction Chemistry," *Chem. Rev. ,* vol. 109 pp. 6570–6631, 2009.

[2] C. T. Wang, J. L. Hu, W. L. Chou, and Y. M. Kuo, "Removal of color from real dyeing wastewater by Electro-Fenton technology using a three-dimensional graphite cathode," *Journal of hazardous materials,* vol. 152, pp. 601-6, Apr 1 2008.

[3] C. Ponce de León and D. Pletcher, "Removal of formaldehyde from aqueous solutions via oxygen reduction using a reticulated vitreous carbon cathode cell," *J. Appl. Electrochem.,* vol. 25, pp. 307-313, 1995

[4] Y. B. Xie and X. Z. Li, "Interactive oxidation of photoelectrocatalysis and electro-Fenton for azo dye degradation using TiO2–Ti mesh and reticulated vitreous carbon electrodes," *Materials Chemistry and Physics,* vol. 95, pp. 39-50, 2006.

[5] A. Özcan, Y. Şahin, A. Savaş Koparal, and M. A. Oturan, "Carbon sponge as a new cathode material for the electro-Fenton process: Comparison with carbon felt cathode and application to degradation of synthetic dye basic blue 3 in aqueous medium," *Journal of Electroanalytical Chemistry,* vol. 616, pp. 71-78, 2008.

[6] M. Panizza and M. A. Oturan, "Degradation of Alizarin Red by electro-Fenton process using a graphite-felt cathode," *Electrochimica Acta,* vol. 56, pp. 7084-7087, 2011.

[7] A. Wang, J. Qu, J. Ru, H. Liu, and J. Ge, "Mineralization of an azo dye Acid Red 14 by electro-Fenton's reagent using an activated carbon fiber cathode," *Dyes and Pigments,* vol. 65, pp. 227-233, 2005.

[8] H. Lei, H. Li, Z. Li, Z. Li, K. Chen, X. Zhang, and H. Wang, "Electro-Fenton degradation of cationic red X-GRL using an activated carbon fiber cathode," *Process Safety and Environmental Protection,* vol. 88, pp. 431-438, 2010.

[9] I. Sirés, N. Oturan, M. A. Oturan, R. M. Rodríguez, J. A. Garrido, and E. Brillas, "Electro-Fenton degradation of antimicrobials triclosan and triclocarban," *Electrochimica Acta,* vol. 52, pp. 5493-5503, 2007.

[10] Jean Jacques Aaron and M. A. Oturan, "New photochemical and electrochemical methods for the degradation of pesticides in aqueous media. Environmental applications.," *Turk. J. Chem. ,* vol. 25, pp. 509–520, 2001.

[11] M. A. Oturan, "An ecologically effective water treatment technique using electrochemically generated hydroxyl radicals for in situ destruction of organic pollutants: Application to herbicide 2,4-D," *Journal of Applied Electrochemistry* vol. 30, pp. 475-482, 2000.

[12] Mehmet A Oturan, Jean-Jacques Aaron, Nihal Oturan, and J. Pinson, "Degradation of chlorophenoxyacid herbicides in aqueous media, using a novel electrochemical method," *Pestic. Sci. ,* vol. 55, pp. 558–562, 1999.

[13] H. Lin, H. Zhang, X. Wang, L. Wang, and J. Wu, "Electro-Fenton removal of Orange II in a divided cell: Reaction mechanism, degradation pathway and toxicity evolution," *Separation and Purification Technology,* vol. 122, pp. 533-540, 2014.

[14] R. E. G. Smith, T. J. Davies, N. d. B. Baynes, and R. J. Nichols, "The electrochemical characterisation of graphite felts," *Journal of Electroanalytical Chemistry,* vol. 747, pp. 29-38, 2015.

[15] A. Di Blasi, O. Di Blasi, N. Briguglio, A. S. Aricò, D. Sebastián, M. J. Lázaro, G. Monforte, and V. Antonucci, "Investigation of several graphite-based electrodes for vanadium redox flow cell," *Journal of Power Sources,* vol. 227, pp. 15-23, 2013.

[16] Y. Wang and Y. Hasebe, "Carbon felt-based biocatalytic enzymatic flow-through detectors: chemical modification of tyrosinase onto amino-functionalized carbon felt using various coupling reagents," *Talanta,* vol. 79, pp. 1135-41, Sep 15 2009.

[17] L. Han, S. Tricard, J. Fang, J. Zhao, and W. Shen, "Prussian blue @ platinum nanoparticles/graphite felt nanocomposite electrodes: application as hydrogen peroxide sensor," *Biosensors & bioelectronics,* vol. 43, pp. 120-4, May 15 2013.

[18] K. J. Kim, Y.-J. Kim, J.-H. Kim, and M.-S. Park, "The effects of surface modification on carbon felt electrodes for use in vanadium redox flow batteries," *Materials Chemistry and Physics,* vol. 131, pp. 547-553, 2011.

[19] Z. González, A. Sánchez, C. Blanco, M. Granda, R. Menéndez, and R. Santamaría, "Enhanced performance of a Bi-modified graphite felt as the positive electrode of a vanadium redox flow battery," *Electrochemistry Communications,* vol. 13, pp. 1379-1382, 2011.

[20] B. Sun and M. S. Kazacos, "Modification of graphite electrode materials for vanadium redox flow battery application—I. Thermal treatment," *Electrochim. Acta,* vol. 37, pp. 1253-1260, 1992.

[21] M.H. Chakrabarti, N.P. Brandon, S.A. Hajimolana, F. Tariq, V. Yufit, M.A. Hashim, M.A. Hussain, C.T.J. Lowd, and P. V. Aravind, "Application of carbon materials in redox flow batteries," *Journal of Power Sources* vol. 253, pp. 150-166, 2014.

[22] Ki Jae Kim, Min-Sik Park, Young-Jun Kim, Jung Ho Kim, Shi Xue Dou, and M. Skyllas-Kazacos, "A technology review of electrodes and reaction mechanisms in vanadium redox flow batteries," *J. Mater. Chem. A,* vol. 3, pp. 16913-16933 2015.

[23] A. Parasuraman, T. M. Lim, C. Menictas, and M. Skyllas-Kazacos, "Review of material research and development for vanadium redox flow battery applications," *Electrochimica Acta,* vol. 101, pp. 27-40, 2013.

[24] P. V. Nidheesh and R. Gandhimathi, "Trends in electro-Fenton process for water and wastewater treatment: An overview," *Desalination,* vol. 299, pp. 1-15, 2012.

[25] E. Rosales, M. Pazos, and M. A. Sanromán, "Advances in the Electro-Fenton Process for Remediation of Recalcitrant Organic Compounds," *Chemical Engineering & Technology,* vol. 35, pp. 609-617, 2012.

[26] I. Sires and E. Brillas, "Remediation of water pollution caused by pharmaceutical residues based on electrochemical separation and degradation technologies: a review," *Environment international,* vol. 40, pp. 212-29, Apr 2012.

[27] P. A. Thrower, "Proc. Workshop Electrochemistry of Carbon, Cleveland, OH, Vol. 84-5, Proc. Vol. 84-5, The Electrochemical Society, Pennington, NJ," p. 40, 1983.

[28] Z. He, L. Shi, J. Shen, Z. He, and S. Liu, "Effects of nitrogen doping on the electrochemical performance of graphite felts for vanadium redox flow batteries," *International Journal of Energy Research,* vol. 39, pp. 709-716, 2015.

[29] S. Zhong, C. Padeste, M. Kazacos, and M. S. Kazacos, "Comparison of the physical, chemical and electrochemical properties of rayon- and polyacrylonitrile-based graphite felt electrodes," *Journal of Power Sources,* vol. 45, pp. 29-41, 1993.

[30] T. Liu, X. Li, H. Nie, C. Xu, and H. Zhang, "Investigation on the effect of catalyst on the electrochemical performance of carbon felt and graphite felt for vanadium flow batteries," *Journal of Power Sources,* vol. 286, pp. 73-81, 2015.

[31] CeraMaterials. (2016). http://www.ceramaterials.com/contactinformation.html.

[32] I. HP Materials Solutions. (2016). http://www.hpmsgraphite.com/graphite-felt.html.
[33] J. González-García, P. Bonete, E. Expósito, V. Montiel, A. Aldaz, and R. Torregrosa-Maciá, "Characterization of a carbon felt electrode structural and physical properties," *Journal of Materials Chemistry,* vol. 9, pp. 419-426, 1999.
[34] R. Carta, S. Palmas, A. M. Polcaro, and G. Tola, "Behaviour of a carbon felt flow by electrodes Part I: Mass transfer characteristics," *Journal of Applied Electrochemistry,* vol. 21, pp. 793-798, 1991.
[35] S. Langlois and F. Coeuret, "Flow-through and flow-by porous electrodes of nickel foam. I. Material characterization," *Journal of Applied Electrochemistry,* vol. 19, pp. 43-50, 1989.
[36] Jan Olek, MenashiI D. Cohen, and C. Lobo, "Determination of Surface Area of Portland Cement and Silica Fume by Mercury Intrusion Porosimetry," *ACI. Mater. J.,* vol. 87, pp. 473-478, 1990.
[37] C. J. Brown, D. Pletcher, F. C. Walsh, J. K. Hammond, and D. Robinson, "Studies of three-dimensional electrodes in the FMO1-LC laboratory electrolyser," *Journal of Applied Electrochemistry,* vol. 24, pp. 95-106, 1994.
[38] N. Vatistas, P. F. Marconi, and M. Bartolozzi, "Mass-transfer study of the carbon felt electrode," *Electrochim. Acta,* vol. 36, pp. 339-343, 1991.
[39] J. M. Rosolen, E. Y. Matsubara, M. S. Marchesin, S. M. Lala, L. A. Montoro, and S. Tronto, "Carbon nanotube/felt composite electrodes without polymer binders," *Journal of Power Sources,* vol. 162, pp. 620-628, 2006.
[40] A. J. Bard and L. R. Faulkner, "Electrochemical Methods: Fundamentals and Applications. ," *John Wiley and Sons: New York,* 2000.
[41] M. Wen, H. Liu, F. Zhang, Y. Zhu, D. Liu, Y. Tian, and Q. Wu, "Amorphous FeNiPt nanoparticles with tunable length for electrocatalysis and electrochemical determination of thiols," *Chemical communications,* pp. 4530-2, Aug 14 2009.
[42] G. Dogu, " Chemical Engineering, Volume 1: Fluid Flow Heat Transfer And Mass Transfer, ed. J. M. Coulson, J. F. Richardson, J. R. Backhurst and J. H. Harker," *Pergamon Press, Oxford,* vol. ch. 4, p. 125, 1978.
[43] D. A. C. Brownson, L. C. S. Figueiredo-Filho, X. Ji, M. Gómez-Mingot, J. Iniesta, O. Fatibello-Filho, D. K. Kampouris, and C. E. Banks, "Freestanding three-dimensional graphene foam gives rise to beneficial electrochemical signatures within non-aqueous media," *Journal of Materials Chemistry A,* vol. 1, p. 5962, 2013.
[44] B. Delanghe, S. Tellier, and M. Astruc, "Mass transfer to a carbon or graphite felt electrode," *Electrochimica Acta,* vol. 35, pp. 1369-1376, 1990.
[45] R. Y. Bek and A. P. Zamyatin, "Mass-transfer cofficient and area accessible to electrolysis in flow-through graphitic-carbon-fiber electrodes," *Sov. Electrochem.,* vol. 14, p. 1034, 1978.
[46] K. Kinoshita and S. C. Leach, "Mass-transfer study of carbon felt, Flow-through electrode," *J. electrochem. Sot.,* vol. 129, p. 1993, 1982.
[47] D. Schmal, J. Van Erkel, and P. J. V. Duin, "Mass transfer at carbon fibre electrodes," *Journal of Applied Electrochemistry,* vol. 16, pp. 422-430, 1986.
[48] K. Wang, K. Chizari, Y. Liu, I. Janowska, S. M. Moldovan, O. Ersen, A. Bonnefont, E. R. Savinova, L. D. Nguyen, and C. Pham-Huu, "Catalytic synthesis of a high aspect ratio carbon nanotubes bridging carbon felt composite with improved electrical conductivity and effective surface area," *Applied Catalysis A: General,* vol. 392, pp. 238-247, 2011.
[49] Y. Oren and A. Soffer, "Graphite felt as an efficient porous electrode for impurity removal and recovery of metals," *Electrochimica Acta,* vol. 28, pp. 1649-1654, 1983.

[50] D. Dixon, D. J. Babu, J. Langner, M. Bruns, L. Pfaffmann, A. Bhaskar, J. J. Schneider, F. Scheiba, and H. Ehrenberg, "Effect of oxygen plasma treatment on the electrochemical performance of the rayon and polyacrylonitrile based carbon felt for the vanadium redox flow battery application," *Journal of Power Sources,* vol. 332, pp. 240-248, 2016.

[51] J.-Z. Chen, W.-Y. Liao, W.-Y. Hsieh, C.-C. Hsu, and Y.-S. Chen, "All-vanadium redox flow batteries with graphite felt electrodes treated by atmospheric pressure plasma jets," *Journal of Power Sources,* vol. 274, pp. 894-898, 2015.

[52] Y. Shao, X. Wang, M. Engelhard, C. Wang, S. Dai, J. Liu, Z. Yang, and Y. Lin, "Nitrogen-doped mesoporous carbon for energy storage in vanadium redox flow batteries," *Journal of Power Sources,* vol. 195, pp. 4375-4379, 2010.

[53] K. Ma, J. P. Cheng, F. Liu, and X. Zhang, "Co-Fe layered double hydroxides nanosheets vertically grown on carbon fiber cloth for electrochemical capacitors," *Journal of Alloys and Compounds,* vol. 679, pp. 277-284, 2016.

[54] B. Sun and M. S. Kazacos, "Modification of graphite electrode materials for vanadium redox flow battery application—I. Thermal treatment.," *Electrochim. Acta,* vol. 37, pp. 1253-1260, 1992.

[55] T. Wu, K. Huang, S. Liu, S. Zhuang, D. Fang, S. Li, D. Lu, and A. Su, "Hydrothermal ammoniated treatment of PAN-graphite felt for vanadium redox flow battery," *Journal of Solid State Electrochemistry,* vol. 16, pp. 579-585, 2011.

[56] Z. Zhang, J. Xi, H. Zhou, and X. Qiu, "KOH etched graphite felt with improved wettability and activity for vanadium flow batteries," *Electrochimica Acta,* vol. 218, pp. 15-23, 2016.

[57] C. Ding, H. Zhang, X. Li, T. Liu, and F. Xing, "Vanadium Flow Battery for Energy Storage: Prospects and Challenges," *The journal of physical chemistry letters,* vol. 4, pp. 1281-94, Apr 18 2013.

[58] D. Hidalgo, T. Tommasi, S. Bocchini, A. Chiolerio, A. Chiodoni, I. Mazzarino, and B. Ruggeri, "Surface modification of commercial carbon felt used as anode for Microbial Fuel Cells," *Energy,* vol. 99, pp. 193-201, 2016.

[59] Bianting Sun and M. S. Kazacos, "Chemical modification of graphite electrode materials for vanadium redox flow battery application—part II. Acid treatments," *Electrochim. Acta,* vol. 37, pp. 2459-2465, 1992.

[60] C. Flox, J. Rubio-García, M. Skoumal, T. Andreu, and J. R. Morante, "Thermo–chemical treatments based on NH3/O2 for improved graphite-based fiber electrodes in vanadium redox flow batteries," *Carbon,* vol. 60, pp. 280-288, 2013.

[61] X.-g. Li, K.-l. Huang, S.-q. Liu, N. Tan, and L.-q. Chen, "Characteristics of graphite felt electrode electrochemically oxidized for vanadium redox battery application," *Transactions of Nonferrous Metals Society of China,* vol. 17, pp. 195-199, 2007.

[62] X. Tang, K. Guo, H. Li, Z. Du, and J. Tian, "Electrochemical treatment of graphite to enhance electron transfer from bacteria to electrodes," *Bioresource technology,* vol. 102, pp. 3558-60, Feb 2011.

[63] L. Zhou, Z. Hu, C. Zhang, Z. Bi, T. Jin, and M. Zhou, "Electrogeneration of hydrogen peroxide for electro-Fenton system by oxygen reduction using chemically modified graphite felt cathode," *Separation and Purification Technology,* vol. 111, pp. 131-136, 2013.

[64] L. Zhou, M. Zhou, Z. Hu, Z. Bi, and K. G. Serrano, "Chemically modified graphite felt as an efficient cathode in electro-Fenton for p-nitrophenol degradation," *Electrochimica Acta,* vol. 140, pp. 376-383, 2014.

[65] B. Sun and M. Skyllas-Kazacos, "Chemical modification and electrochemical behaviour of graphite fibre in acidic vanadium solution," *Electrochim. Acta,* vol. 36, pp. 513-517, 1991.

[66] W. H. Wang and X. D. Wang, "Investigation of Ir-modified carbon felt as the positive electrode of an all-vanadium redox flow battery," *Electrochimica Acta,* vol. 52, pp. 6755-6762, 2007.

[67] Z. Lv, D. Xie, X. Yue, C. Feng, and C. Wei, "Ruthenium oxide-coated carbon felt electrode: A highly active anode for microbial fuel cell applications," *Journal of Power Sources,* vol. 210, pp. 26-31, 2012.

[68] R. Solmaz, A. Gündoğdu, A. Döner, and G. Kardaş, "The Ni-deposited carbon felt as substrate for preparation of Pt-modified electrocatalysts: Application for alkaline water electrolysis," *International Journal of Hydrogen Energy,* vol. 37, pp. 8917-8922, 2012.

[69] S. Chen, W. Hu, J. Hong, and S. Sandoe, "Electrochemical disinfection of simulated ballast water on PbO2/graphite felt electrode," *Marine pollution bulletin,* vol. 105, pp. 319-23, Apr 15 2016.

[70] C. Zhang, P. Liang, X. Yang, Y. Jiang, Y. Bian, C. Chen, X. Zhang, and X. Huang, "Binder-free graphene and manganese oxide coated carbon felt anode for high-performance microbial fuel cell," *Biosensors & bioelectronics,* vol. 81, pp. 32-8, Jul 15 2016.

[71] P. Wang, B. Lai, H. Li, and Z. Du, "Deposition of Fe on graphite felt by thermal decomposition of Fe(CO)5 for effective cathodic preparation of microbial fuel cells," *Bioresource technology,* vol. 134, pp. 30-5, Apr 2013.

[72] C. N. Rao, A. K. Sood, K. S. Subrahmanyam, and A. Govindaraj, "Graphene: the new two-dimensional nanomaterial," *Angewandte Chemie,* vol. 48, pp. 7752-77, 2009.

[73] S. K. Jang, J. Jeon, S. M. Jeon, Y. J. Song, and S. Lee, "Effects of dielectric material properties on graphene transistor performance," *Solid-State Electronics,* vol. 109, pp. 8-11, 2015.

[74] D. Chen, L. Tang, and J. Li, "Graphene-based materials in electrochemistry," *Chemical Society reviews,* vol. 39, pp. 3157-80, Aug 2010.

[75] Z. González, C. Flox, C. Blanco, M. Granda, J. R. Morante, R. Menéndez, and R. Santamaría, "Outstanding electrochemical performance of a graphene-modified graphite felt for vanadium redox flow battery application," *Journal of Power Sources,* 2016.

[76] A. Chavez-Valdez, M. S. Shaffer, and A. R. Boccaccini, "Applications of graphene electrophoretic deposition. A review," *The journal of physical chemistry. B,* vol. 117, pp. 1502-15, Feb 14 2013.

[77] P. Sehrawat, C. Julien, and S. S. Islam, "Carbon nanotubes in Li-ion batteries: A review," *Materials Science and Engineering: B,* vol. 213, pp. 12-40, 2016.

[78] W. Li, J. Liu, and C. Yan, "The electrochemical catalytic activity of single-walled carbon nanotubes towards VO2+/VO2+ and V3+/V2+ redox pairs for an all vanadium redox flow battery," *Electrochimica Acta,* vol. 79, pp. 102-108, 2012.

[79] S. Wang, X. Zhao, T. Cochell, and A. Manthiram, "Nitrogen-Doped Carbon Nanotube/Graphite Felts as Advanced Electrode Materials for Vanadium Redox Flow Batteries," *The journal of physical chemistry letters,* vol. 3, pp. 2164-7, Aug 16 2012.

[80] J. Mauricio Rosolen, C. H. Patrick Poá, S. Tronto, M. S. Marchesin, and S. R. P. Silva, "Electron field emission of carbon nanotubes on carbon felt," *Chemical Physics Letters,* vol. 424, pp. 151-155, 2006.

[81] K.-z. Li, L. Li, H.-j. Li, Q. Song, J.-h. Lu, and Q.-g. Fu, "Electrophoretic deposition of carbon nanotubes onto carbon fiber felt for production of carbon/carbon composites with improved mechanical and thermal properties," *Vacuum,* vol. 104, pp. 105-110, 2014.

[82] J. M. Rosolen, S. Tronto, M. S. Marchesin, E. C. Almeida, N. G. Ferreira, C. H. Patrick Poá, and S. R. P. Silva, "Electron field emission from composite electrodes of carbon nanotubes-boron-doped diamond and carbon felts," *Applied Physics Letters,* vol. 88, p. 083116, 2006.

[83] Q. Song, K. Li, H. Li, and Q. Fu, "Increasing the Tensile Property of Unidirectional Carbon/Carbon Composites by Grafting Carbon Nanotubes onto Carbon Fibers by Electrophoretic Deposition," *Journal of Materials Science & Technology,* vol. 29, pp. 711-714, 2013.

[84] Q. An, A. N. Rider, and E. T. Thostenson, "Electrophoretic deposition of carbon nanotubes onto carbon-fiber fabric for production of carbon/epoxy composites with improved mechanical properties," *Carbon,* vol. 50, pp. 4130-4143, 2012.

[85] G. Wei, C. Jia, J. Liu, and C. Yan, "Carbon felt supported carbon nanotubes catalysts composite electrode for vanadium redox flow battery application," *Journal of Power Sources,* vol. 220, pp. 185-192, 2012.

[86] W. Li, J. Liu, and C. Yan, "Multi-walled carbon nanotubes used as an electrode reaction catalyst for /VO2+ for a vanadium redox flow battery," *Carbon,* vol. 49, pp. 3463-3470, 2011.

[87] P. Serp, "Carbon nanotubes and nanofibers in catalysis," *Applied Catalysis A: General,* vol. 253, pp. 337-358, 2003.

[88] M.-J. Ledoux and C. Pham-Huu, "Carbon nanostructures with macroscopic shaping for catalytic applications," *Catalysis Today,* vol. 102-103, pp. 2-14, 2005.

[89] P. Li, T. Li, J.-H. Zhou, Z.-J. Sui, Y.-C. Dai, W.-K. Yuan, and D. Chen, "Synthesis of carbon nanofiber/graphite-felt composite as a catalyst," *Microporous and Mesoporous Materials,* vol. 95, pp. 1-7, 2006.

[90] J. H. Zhou, M. G. Zhang, L. Zhao, P. Li, X. G. Zhou, and W. K. Yuan, "Carbon nanofiber/graphite-felt composite supported Ru catalysts for hydrogenolysis of sorbitol," *Catalysis Today,* vol. 147, pp. S225-S229, 2009.

[91] R. Vieira, C. Pham-Huu, N. Keller, and M. J. Ledoux, "New carbon nanofiber/graphite felt composite for use as a catalyst support for hydrazine catalytic decomposition," *Chemical Communications,* pp. 954-955, 2002.

[92] J. Menéndez, E. Menéndez, A. García, J. Parra, and J. Pis, "Thermal treatment of active carbons: a comparison between microwave and electrical heating," *J. Microw. Power Electromagn. Energy,* vol. 34, pp. 137–143, 1999.

[93] A.M. Schwenke, S. Hoeppener, and U. S. Schubert, "Microwave synthesis of carbon nanofibers – the influence of MW irradiation power, time, and the amount of catalyst," *J. Mater. Chem. A,* vol. 3, pp. 23778–23787, 2015.

[94] T. Druzhinina, S. Hoeppener, and U. S. Schubert, "On the Synthesis of Carbon Nanofibers and Nanotubes by Microwave Irradiation: Parameters, Catalysts, and Substrates," *Advanced Functional Materials,* vol. 19, pp. 2819-2825, 2009.

[95] A. M. Schwenke, T. Janoschka, C. Stolze, N. Martin, S. Hoeppener, and U. S. Schubert, "Microwave-assisted preparation of carbon nanofiber-functionalized graphite felts as electrodes for polymer-based redox-flow batteries," *Journal of Power Sources,* vol. 335, pp. 155-161, 2016.

[96] P. Chandrasekhar and K. Naishadham, "Broadband microwave absorption and shielding properties of a poly(aniline)," *Synthetic Metals,* vol. 105, pp. 115–120, 1999.

[97] Yuehe Lin, Xiaoli Cui, and J. Bontha, "Electrically controlled anion exchange based on polypyrrole and carbon nanotubes nanocomposite for perchlorate removal," *Environ. Sci. Technol.,* vol. 40, pp. 4004–4009, 2006.

[98] Guoquan Zhang, Fenglin Yang, Mingming Gao, and L. Liu, "Electrocatalytic behavior of the bareand anthraquinonedisuldonatepolypyrrole composite film modified graphitecathodes in the electro-Fenton system," *J. Phys. Chem. C,* vol. 112, pp. 8957-8962, 2008.

[99] Y. Hasebe, Y. Wang, and K. Fukuoka, "Electropolymerized poly(Toluidine Blue)-modified carbon felt for highly sensitive amperometric determination of NADH in flow injection analysis," *Journal of Environmental Sciences,* vol. 23, pp. 1050-1056, 2011.

[100] C. Feng, F. Li, H. Liu, X. Lang, and S. Fan, "A dual-chamber microbial fuel cell with conductive film-modified anode and cathode and its application for the neutral electro-Fenton process," *Electrochimica Acta,* vol. 55, pp. 2048-2054, 2010.

[101] C. Li, L. Ding, H. Cui, L. Zhang, K. Xu, and H. Ren, "Application of conductive polymers in biocathode of microbial fuel cells and microbial community," *Bioresource technology,* vol. 116, pp. 459-65, Jul 2012.

[102] X. Jiang, S. Lou, D. Chen, J. Shen, W. Han, X. Sun, J. Li, and L. Wang, "Fabrication of polyaniline/graphene oxide composite for graphite felt electrode modification and its performance in the bioelectrochemical system," *Journal of Electroanalytical Chemistry,* vol. 744, pp. 95-100, 2015.

[103] S. Mu, "Electrochemical copolymerization of aniline and o-aminophenol," *Synthetic Metals,* vol. 143, pp. 259-268, 2004.

[104] H. Cui, Y. Qian, H. An, C. Sun, J. Zhai, and Q. Li, "Electrochemical removal of fluoride from water by PAOA-modified carbon felt electrodes in a continuous flow reactor," *Water research,* vol. 46, pp. 3943-50, Aug 2012.

[105] Z. Lv, Y. Chen, H. Wei, F. Li, Y. Hu, C. Wei, and C. Feng, "One-step electrosynthesis of polypyrrole/graphene oxide composites for microbial fuel cell application," *Electrochimica Acta,* vol. 111, pp. 366-373, 2013.

[106] J. Hui, X. Jiang, H. Xie, D. Chen, J. Shen, X. Sun, W. Han, J. Li, and L. Wang, "Laccase-catalyzed electrochemical fabrication of polyaniline/graphene oxide composite onto graphite felt electrode and its application in bioelectrochemical system," *Electrochimica Acta,* vol. 190, pp. 16-24, 2016.

[107] H.-F. Cui, L. Du, P.-B. Guo, B. Zhu, and J. H. T. Luong, "Controlled modification of carbon nanotubes and polyaniline on macroporous graphite felt for high-performance microbial fuel cell anode," *Journal of Power Sources,* vol. 283, pp. 46-53, 2015.

[108] A. Walcarius, "Zeolite-modifed electrodes in electroanalytical chemistry," *Analytica Chimica Acta* vol. 384, pp. 1-16, 1999.

[109] X. Wu, F. Tong, X. Yong, J. Zhou, L. Zhang, H. Jia, and P. Wei, "Effect of NaX zeolite-modified graphite felts on hexavalent chromium removal in biocathode microbial fuel cells," *Journal of hazardous materials,* vol. 308, pp. 303-11, May 5 2016.

[110] X.-y. Wu, F. Tong, T.-s. Song, X.-y. Gao, J.-j. Xie, C. C. Zhou, L.-x. Zhang, and P. Wei, "Effect of zeolite-coated anode on the performance of microbial fuel cells," *Journal of Chemical Technology & Biotechnology,* vol. 90, pp. 87-92, 2015.

[111] B. Haghighi, H. Hamidi, and L. Gorton, "Electrochemical behavior and application of Prussian blue nanoparticle modified graphite electrode," *Sensors and Actuators B: Chemical,* vol. 147, pp. 270-276, 2010.

[112] F. Ricci and G. Palleschi, "Sensor and biosensor preparation, optimisation and applications of Prussian Blue modified electrodes," *Biosensors & bioelectronics,* vol. 21, pp. 389-407, Sep 15 2005.
[113] D. Ellis, M. Eckhoff, and V. D. Neff, "Electrochromism in the mixed-valence hexacyanides. 1. Voltammetric and spectral studies of the oxidation and reduction of thin films of Prussian Blue," *J. Phys. Chem.,* vol. 85, pp. 1225-1231, 1981.
[114] F Ricci, A Amine, G Palleschi, and D. Moscone, "Prussian Blue based screen printed biosensors with improved characteristics of long-term lifetime and pH stability," *Biosensors and Bioelectronics,* vol. 18, pp. 165-174, 2003.
[115] V. D. Neff, "Electrochemical Oxidation and Reduction of Thin Films of Prussian Blue," *J. Electrochem. Soc.,* vol. 125 pp. 886–887, 1978.
[116] D.M. DeLongchamp and P. T. Hammond, "High-contrast electrochromism and controllable dissolution of assembled Prussian blue/polymer nanocomposites," *Adv. Funct. Mater.,* vol. 14, pp. 224–232, 2004.
[117] K. Itaya, I. Uchida, and V. D. Neff, "Electrochemistry of polynuclear transition metal cyanides: Prussian blue and its analogues," *Acc. Chem. Res.,* vol. 19, pp. 162–168, 1986.
[118] M. Pyrasch and B. Tieke, "Electro- and photoresponsive films of Prussian blue prepared upon multiple sequential adsorption," *Langmuir,* vol. 17, pp. 7706–7709, 2001.
[119] P. Zhou, D. Xue, H. Luo, and X. Chen, "Fabrication, structure, and magnetic properties of highly ordered Prussian blue nanowire arrays," *Nano. Lett.,* vol. 2, pp. 845–847, 2002.
[120] L. Wang, S. Tricard, L. Cao, Y. Liang, J. Zhao, J. Fang, and W. Shen, "Prussian blue/1-butyl-3-methylimidazolium tetrafluoroborate – Graphite felt electrodes for efficient electrocatalytic determination of nitrite," *Sensors and Actuators B: Chemical,* vol. 214, pp. 70-75, 2015.
[121] Chunyan Wang, Fucheng Ye, Hongfu Wu, and Y. Qian, "Depositing Au Nanoparticles onto Graphene Sheets for Simultaneous Electrochemical Detection Ascorbic Acid, Dopamine and Uric Acid," *Int. J. Electrochem. Sci.,* vol. 8, pp. 2440 - 2448, 2013.
[122] C. Liu, K. Wang, S. Luo, Y. Tang, and L. Chen, "Direct electrodeposition of graphene enabling the one-step synthesis of graphene-metal nanocomposite films," *Small,* vol. 7, pp. 1203-6, May 9 2011.
[123] D. S. Aaron, Q. Liu, Z. Tang, G. M. Grim, A. B. Papandrew, A. Turhan, T. A. Zawodzinski, and M. M. Mench, "Dramatic performance gains in vanadium redox flow batteries through modified cell architecture," *Journal of Power Sources,* vol. 206, pp. 450-453, 2012.
[124] M. Skyllas Kazacos, D. Kasherman, D.R. Hong, and M. Kazacos, "Characteristics and performance of 1 kW UNSW vanadium redox battery," *Journal of Power Sources* vol. 35 p. 399, 1991.
[125] M. Skyllas Kazacos and F. Grossmith, "Efficient Vanadium Redox Flow Cell," *Journal of the Electrochemical Society* vol. 134 p. 2950, 1987.
[126] M.H. Chakrabarti, N.P. Brandon, S.A. Hajimolana, F. Tariq, V.Yufit, M.A. Hashim, M.A. Hussain, C.T.J. Low, and P. V. Aravind, "Application of carbon materials in redox flow batteries," *Journal of Power Sources,* vol. 253, pp. 150-166, 2014.
[127] H. Vafiadis and M. Skyllas-Kazacos, "Evaluation of membranes for the novel vanadium bromine redox flow cell," *Journal of Membrane Science,* vol. 279, pp. 394-402, 2006.
[128] W. Zhang, J. Xi, Z. Li, H. Zhou, L. Liu, Z. Wu, and X. Qiu, "Electrochemical activation of graphite felt electrode for VO2+/VO2+ redox couple application," *Electrochimica Acta,* vol. 89, pp. 429-435, 2013.

[129] C. Gao, N. Wang, S. Peng, S. Liu, Y. Lei, X. Liang, S. Zeng, and H. Zi, "Influence of Fenton's reagent treatment on electrochemical properties of graphite felt for all vanadium redox flow battery," *Electrochimica Acta,* vol. 88, pp. 193-202, 2013.

[130] C. Flox, M. Skoumal, J. Rubio-Garcia, T. Andreu, and J. R. Morante, "Strategies for enhancing electrochemical activity of carbon-based electrodes for all-vanadium redox flow batteries," *Applied Energy,* vol. 109, pp. 344-351, 2013.

[131] Q. Xu, T. S. Zhao, and C. Zhang, "Performance of a vanadium redox flow battery with and without flow fields," *Electrochimica Acta,* vol. 142, pp. 61-67, 2014.

[132] S.C. Barton, J. Gallaway, and P. Atanassov, "Enzymatic biofuel cells for implantable and microscale devices," *Chem. Rev.,* vol. 104 pp. 4867–4886, 2004.

[133] R. A. Bullen, T. C. Arnot, J. B. Lakeman, and F. C. Walsh, "Biofuel cells and their development," *Biosensors & bioelectronics,* vol. 21, pp. 2015-45, May 15 2006.

[134] V. Coman, R. Ludwig, W. Harreither, D. Haltrich, L. Gorton, T. Ruzgas, and a. S. Shleev, "A Direct Electron Transfer-Based Glucose/Oxygen Biofuel Cell Operating in Human Serum," *Fuel Cells,* pp. NA-NA, 2009.

[135] F. Gao, L. Viry, M. Maugey, P. Poulin, and N. Mano, "Engineering hybrid nanotube wires for high-power biofuel cells," *Nature communications,* vol. 1, p. 2, Apr 12 2010.

[136] M. H. Osman, A. A. Shah, and F. C. Walsh, "Recent progress and continuing challenges in bio-fuel cells. Part I: enzymatic cells," *Biosensors & bioelectronics,* vol. 26, pp. 3087-102, Mar 15 2011.

[137] S. Rubenwolf, O. Strohmeier, A. Kloke, S. Kerzenmacher, R. Zengerle, and F. von Stetten, "Carbon electrodes for direct electron transfer type laccase cathodes investigated by current density-cathode potential behavior," *Biosensors & bioelectronics,* vol. 26, pp. 841-5, Oct 15 2010.

[138] L. Deng, L. Shang, D. Wen, J. Zhai, and S. Dong, "A membraneless biofuel cell powered by ethanol and alcoholic beverage," *Biosensors & bioelectronics,* vol. 26, pp. 70-3, Sep 15 2010.

[139] Y. Handa, K. Yamagiwa, Y. Ikeda, Y. Yanagisawa, S. Watanabe, N. Yabuuchi, and S. Komaba, "Fabrication of carbon-felt-based multi-enzyme immobilized anodes to oxidize sucrose for biofuel cells," *Chemphyschem : a European journal of chemical physics and physical chemistry,* vol. 15, pp. 2145-51, Jul 21 2014.

[140] S. Tsujimura, M. Fujita, H. Tatsumi, K. Kano, and T. Ikeda, "Bioelectrocatalysis-based dihydrogen/dioxygen fuel cell operating at physiological pH," *Physical Chemistry Chemical Physics,* vol. 3, pp. 1331-1335, 2001.

[141] N. L. Akers, C. M. Moore, and S. D. Minteer, "Development of alcohol/O2 biofuel cells using salt-extracted tetrabutylammonium bromide/Nafion membranes to immobilize dehydrogenase enzymes," *Electrochimica Acta,* vol. 50, pp. 2521-2525, 2005.

[142] B. E. Logan, C. Murano, K. Scott, N. D. Gray, and I. M. Head, "Electricity generation from cysteine in a microbial fuel cell," *Water research,* vol. 39, pp. 942-52, Mar 2005.

[143] M. Ghasemi, W. R. W. Daud, S. H. A. Hassan, S.-E. Oh, M. Ismail, M. Rahimnejad, and J. M. Jahim, "Nano-structured carbon as electrode material in microbial fuel cells: A comprehensive review," *Journal of Alloys and Compounds,* vol. 580, pp. 245-255, 2013.

[144] Peter Clauwaert, David van der Ha, Nico Boon, Kim Verbeken, Marc Verhaege, Korneel Rabaey, and W. Verstraete, "Open Air Biocathode Enables Effective Electricity Generation with Microbial Fuel Cells," *Environ. Sci. Technol.,* vol. 41, pp. 7564–7569, 2007.

[145] G. Zhen, X. Lu, T. Kobayashi, G. Kumar, and K. Xu, "Promoted electromethanosynthesis in a two-chamber microbial electrolysis cells (MECs) containing a hybrid biocathode

covered with graphite felt (GF)," *Chemical Engineering Journal,* vol. 284, pp. 1146-1155, 2016.

[146] B. Cercado-Quezada, M.-L. Delia, and A. Bergel, "Electrochemical micro-structuring of graphite felt electrodes for accelerated formation of electroactive biofilms on microbial anodes," *Electrochemistry Communications,* vol. 13, pp. 440-443, 2011.

[147] C. Li, L. Zhang, L. Ding, H. Ren, and H. Cui, "Effect of conductive polymers coated anode on the performance of microbial fuel cells (MFCs) and its biodiversity analysis," *Biosensors & bioelectronics,* vol. 26, pp. 4169-76, Jun 15 2011.

[148] Y. Zhang, J. Sun, Y. Hu, S. Li, and Q. Xu, "Bio-cathode materials evaluation in microbial fuel cells: A comparison of graphite felt, carbon paper and stainless steel mesh materials," *International Journal of Hydrogen Energy,* vol. 37, pp. 16935-16942, 2012.

[149] M. Rahimnejad, A. Adhami, S. Darvari, A. Zirepour, and S.-E. Oh, "Microbial fuel cell as new technology for bioelectricity generation: A review," *Alexandria Engineering Journal,* vol. 54, pp. 745-756, 2015.

[150] C. Feng, L. Ma, F. Li, H. Mai, X. Lang, and S. Fan, "A polypyrrole/anthraquinone-2,6-disulphonic disodium salt (PPy/AQDS)-modified anode to improve performance of microbial fuel cells," *Biosensors & bioelectronics,* vol. 25, pp. 1516-20, Feb 15 2010.

[151] E. C. Almeida, A. F. Azevedo, M. R. Baldan, N. A. Braga, J. M. Rosolen, and N. G. Ferreira, "Nanocrystalline diamond/carbon felt as a novel composite for electrochemical storage energy in capacitor," *Chemical Physics Letters,* vol. 438, pp. 47-52, 2007.

[152] Qian Yang, Liubing Dong, Chengjun Xu, and F. Kang, "High-performance supercapacitors based on graphene/MnO2/activated carbon fiber felt composite electrodes in different neutral electrolytes," *RSC Advances,* vol. 6, p. 12525, 2016.

[153] M. He, Y. Zheng, and Q. Du, "Three-dimensional polypyrrole/MnO2 composite networks deposited on graphite felt as free-standing electrode for supercapacitors," *Materials Letters,* vol. 104, pp. 48-52, 2013.

[154] H. T. Tan, X. Rui, W. Shi, C. Xu, H. Yu, H. E. Hoster, and Q. Yan, "Controlled Synthesis of Manganese Oxyhydroxide Nanotubes: Implications for High-Efficiency Supercapacitors," *ChemPlusChem,* vol. 78, pp. 554-560, 2013.

[155] I. Dincer, "Renewable energy and sustainable development: a crucial review," *Renewable and Sustainable Energy Reviews,* vol. 4, pp. 157-175, 2000.

[156] H. Hanaei, M. K. Assadi, and R. Saidur, "Highly efficient antireflective and self-cleaning coatings that incorporate carbon nanotubes (CNTs) into solar cells: A review," *Renewable and Sustainable Energy Reviews,* vol. 59, pp. 620-635, 2016.

[157] M. Torimura, A. Miki, A. Wadano, K. Kano, and T. Ikeda, "Electrochemical investigation of cyanobacteria Synechococcus sp. PCC7942-catalyzed photoreduction of exogenous quinones and photoelectrochemical oxidation of water," *J Electroanal Chem,* vol. 496, pp. 21–28, 2001.

[158] K. Tanaka, R. Tamamushi, and T. Ogawa, "Bioelectrochemical fuel-cells operated by the cyanobacterium, Anabaena variabilis," *J. Chem. Tech. Biotechnol.,* vol. 35B, pp. 191-197, 1985.

[159] T. Yagishita, S. Sawayama, K. Tsukahara, and T. Ogi, "Performance of Photosynthetic Electrochemical Cells Using Immobilized Anabaena variabilis M-3 in Discharge/Culture Cycles " *Journal of Fermantation and Bioengineering,* vol. 85, pp. 546-549, 1998.

[160] Seiya Tsujimura, Akira Wadano, Kenji Kano, and T. Ikeda, "Photosynthetic bioelectrochemical cell utilizing cyanobacteria and water-generating oxidase," *Enzyme and Microbial Technology,* vol. 29, pp. 225–231, 2001.

[161] J.M. Tarascon and M. Armand, "Issues and challenges facing rechargeable lithium batteries," *Nature,* vol. 414, pp. 359–367, 2001.
[162] Andy Fiedler, Andrew P. Vogt, Lukas Pfaffmann, Vanessa Trouillet, Jorg T. Breukelgen, Ralf Koppe, Christopher Barner-Kowollik, Helmut Ehrenberg, and F. Scheiba, "Lithium–air battery cathode modification via an unconventional thermal method employing borax," *RSC Advances,* vol. 6, pp. 66307-66310, 2016.
[163] E.O.Vilar, E.B.Cavalcanti, H.R.Carvalho, and F.B.Sousa, "Cr (VI) electromechimal reduction using RVG 4OOO graphite felt as the electrode," *Braz. J. Chem. Eng.,* vol. 20, pp. 291-303, 2003.
[164] G. Chen, "Electrochemical technologies in wastewater treatment," *Separation and Purification Technology,* vol. 38, pp. 11-41, 2004.
[165] K.-K. Park, J.-B. Lee, P.-Y. Park, S.-W. Yoon, J.-S. Moon, H.-M. Eum, and C.-W. Lee, "Development of a carbon sheet electrode for electrosorption desalination," *Desalination,* vol. 206, pp. 86-91, 2007.
[166] A. K. Abdessalem, N. Oturan, N. Bellakhal, M. Dachraoui, and M. A. Oturan, "Experimental design methodology applied to electro-Fenton treatment for degradation of herbicide chlortoluron," *Applied Catalysis B: Environmental,* vol. 78, pp. 334-341, 2008.
[167] Mehmet A. Oturan, Nihal Oturan, Claude Lahitte, and S. Trevin, "Production of hydroxyl radicals by electrochemically assisted Fenton's reagent Application to the mineralization of an organic micropollutant, pentachlorophenol," *Journal of Electroanalytical Chemistry* vol. 507 pp. 96–102, 2001.
[168] E. Petrucci, A. Da Pozzo, and L. Di Palma, "On the ability to electrogenerate hydrogen peroxide and to regenerate ferrous ions of three selected carbon-based cathodes for electro-Fenton processes," *Chemical Engineering Journal,* vol. 283, pp. 750-758, 2016.
[169] S. Hammami, N. Oturan, N. Bellakhal, M. Dachraoui, and M. A. Oturan, "Oxidative degradation of direct orange 61 by electro-Fenton process using a carbon felt electrode: Application of the experimental design methodology," *Journal of Electroanalytical Chemistry,* vol. 610, pp. 75-84, 2007.
[170] M. A. Oturan, E. Guivarch, N. Oturan, and I. Sirés, "Oxidation pathways of malachite green by Fe3+-catalyzed electro-Fenton process," *Applied Catalysis B: Environmental,* vol. 82, pp. 244-254, 2008.
[171] Mohamed C. Edelahi, Nihal Oturan, Mehmet A. Oturan, Y. Padellec, A. Bermond, and K. E. Kacemi, "Degradation of diuron by the electro-Fenton process " *Environmental Chemistry Letters,* vol. 1, pp. 233-236., 2003.
[172] K. Hanna, S. Chiron, and M. A. Oturan, "Coupling enhanced water solubilization with cyclodextrin to indirect electrochemical treatment for pentachlorophenol contaminated soil remediation," *Water research,* vol. 39, pp. 2763-73, Jul 2005.
[173] M. Diagne, N. Oturan, and M. A. Oturan, "Removal of methyl parathion from water by electrochemically generated Fenton's reagent," *Chemosphere,* vol. 66, pp. 841-8, Jan 2007.
[174] I. Sirés, J. A. Garrido, R. M. Rodríguez, E. Brillas, N. Oturan, and M. A. Oturan, "Catalytic behavior of the Fe3+/Fe2+ system in the electro-Fenton degradation of the antimicrobial chlorophene," *Applied Catalysis B: Environmental,* vol. 72, pp. 382-394, 2007.
[175] M. Pimentel, N. Oturan, M. Dezotti, and M. A. Oturan, "Phenol degradation by advanced electrochemical oxidation process electro-Fenton using a carbon felt cathode," *Applied Catalysis B: Environmental,* vol. 83, pp. 140-149, 2008.

[176] S. Hammami, N. Bellakhal, N. Oturan, M. A. Oturan, and M. Dachraoui, "Degradation of Acid Orange 7 by electrochemically generated (*)OH radicals in acidic aqueous medium using a boron-doped diamond or platinum anode: a mechanistic study," *Chemosphere,* vol. 73, pp. 678-84, Oct 2008.

[177] I. Sires, E. Guivarch, N. Oturan, and M. A. Oturan, "Efficient removal of triphenylmethane dyes from aqueous medium by in situ electrogenerated Fenton's reagent at carbon-felt cathode," *Chemosphere,* vol. 72, pp. 592-600, Jun 2008.

[178] A. Ozcan, M. A. Oturan, N. Oturan, and Y. Sahin, "Removal of Acid Orange 7 from water by electrochemically generated Fenton's reagent," *Journal of hazardous materials,* vol. 163, pp. 1213-20, Apr 30 2009.

[179] E. Rosales, O. Iglesias, M. Pazos, and M. A. Sanroman, "Decolourisation of dyes under electro-Fenton process using Fe alginate gel beads," *Journal of hazardous materials,* vol. 213-214, pp. 369-77, Apr 30 2012.

[180] S. C. Elaoud, M. Panizza, G. Cerisola, and T. Mhiri, "Coumaric acid degradation by electro-Fenton process," *Journal of Electroanalytical Chemistry,* vol. 667, pp. 19-23, 2012.

[181] O. Iglesias, J. Gómez, M. Pazos, and M. Á. Sanromán, "Electro-Fenton oxidation of imidacloprid by Fe alginate gel beads," *Applied Catalysis B: Environmental,* vol. 144, pp. 416-424, 2014.

[182] L. Labiadh, M. A. Oturan, M. Panizza, N. B. Hamadi, and S. Ammar, "Complete removal of AHPS synthetic dye from water using new electro-fenton oxidation catalyzed by natural pyrite as heterogeneous catalyst," *Journal of hazardous materials,* vol. 297, pp. 34-41, Oct 30 2015.

[183] S. Ammar, M. A. Oturan, L. Labiadh, A. Guersalli, R. Abdelhedi, N. Oturan, and E. Brillas, "Degradation of tyrosol by a novel electro-Fenton process using pyrite as heterogeneous source of iron catalyst," *Water research,* vol. 74, pp. 77-87, May 1 2015.

[184] N. Barhoumi, L. Labiadh, M. A. Oturan, N. Oturan, A. Gadri, S. Ammar, and E. Brillas, "Electrochemical mineralization of the antibiotic levofloxacin by electro-Fenton-pyrite process," *Chemosphere,* vol. 141, pp. 250-7, Dec 2015.

[185] F. Sopaj, N. Oturan, J. Pinson, F. Podvorica, and M. A. Oturan, "Effect of the anode materials on the efficiency of the electro-Fenton process for the mineralization of the antibiotic sulfamethazine," *Applied Catalysis B: Environmental,* vol. 199, pp. 331-341, 2016.

[186] A. Özcan, A. Atılır Özcan, and Y. Demirci, "Evaluation of mineralization kinetics and pathway of norfloxacin removal from water by electro-Fenton treatment," *Chemical Engineering Journal,* vol. 304, pp. 518-526, 2016.

[187] H. Lin, N. Oturan, J. Wu, H. Zhang, and M. A. Oturan, "Cold incineration of sucralose in aqueous solution by electro-Fenton process," *Separation and Purification Technology,* vol. 173, pp. 218-225, 2017.

[188] A. Özcan, A. Atılır Özcan, Y. Demirci, and E. Şener, "Preparation of Fe2O3 modified kaolin and application in heterogeneous electro-catalytic oxidation of enoxacin," *Applied Catalysis B: Environmental,* vol. 200, pp. 361-371, 2017.

[189] Belgin Gözmen, Mehmet A. Oturan, Nihal Oturan, and O. Erbatur, "Indirect Electrochemical Treatment of Bisphenol A in Water via Electrochemically Generated Fenton's Reagent," *Environ. Sci. Technol.,* vol. 37 pp. 3716-3723, 2003.

[190] S. Irmak, H. I. Yavuz, and O. Erbatur, "Degradation of 4-chloro-2-methylphenol in aqueous solution by electro-Fenton and photoelectro-Fenton processes," *Applied Catalysis B: Environmental,* vol. 63, pp. 243-248, 2006.

[191] E. J. Ruiz, A. Hernández-Ramírez, J. M. Peralta-Hernández, C. Arias, and E. Brillas, "Application of solar photoelectro-Fenton technology to azo dyes mineralization: Effect of current density, Fe2+ and dye concentrations," *Chemical Engineering Journal,* vol. 171, pp. 385-392, 2011.
[192] E. Pajootan, M. Arami, and M. Rahimdokht, "Discoloration of wastewater in a continuous electro-Fenton process using modified graphite electrode with multi-walled carbon nanotubes/surfactant," *Separation and Purification Technology,* vol. 130, pp. 34-44, 2014.
[193] J. Miao, H. Zhu, Y. Tang, Y. Chen, and P. Wan, "Graphite felt electrochemically modified in H2SO4 solution used as a cathode to produce H2O2 for pre-oxidation of drinking water," *Chemical Engineering Journal,* vol. 250, pp. 312-318, 2014.
[194] S. R. Popuri, C.-Y. Chang, and J. Xu, "A study on different addition approach of Fenton's reagent for DCOD removal from ABS wastewater," *Desalination,* vol. 277, pp. 141-146, 2011.
[195] S. Guo, G. Zhang, and J. Wang, "Photo-Fenton degradation of rhodamine B using Fe2O3-Kaolin as heterogeneous catalyst: characterization, process optimization and mechanism," *Journal of colloid and interface science,* vol. 433, pp. 1-8, Nov 1 2014.
[196] H. Hassan and B. H. Hameed, "Fe–clay as effective heterogeneous Fenton catalyst for the decolorization of Reactive Blue 4," *Chemical Engineering Journal,* vol. 171, pp. 912-918, 2011.
[197] C. M. Sánchez-Sánchez, E. Expósito, J. Casado, and V. Montiel, "Goethite as a more effective iron dosage source for mineralization of organic pollutants by electro-Fenton process," *Electrochemistry Communications,* vol. 9, pp. 19-24, 2007.
[198] N. Xu, Y. Zhang, H. Tao, S. Zhou, and Y. Zeng, "Bio-electro-Fenton system for enhanced estrogens degradation," *Bioresource technology,* vol. 138, pp. 136-40, Jun 2013.
[199] N. Birjandi, H. Younesi, A. A. Ghoreyshi, and M. Rahimnejad, "Electricity generation through degradation of organic matters in medicinal herbs wastewater using bio-electro-Fenton system," *Journal of environmental management,* vol. 180, pp. 390-400, Sep 15 2016.
[200] L. Zhuang, S. Zhou, Y. Yuan, M. Liu, and Y. Wang, "A novel bioelectro-Fenton system for coupling anodic COD removal with cathodic dye degradation," *Chemical Engineering Journal,* vol. 163, pp. 160-163, 2010.
[201] Y. Li, A. Lu, H. Ding, X. Wang, C. Wang, C. Zeng, and Y. Yan, "Microbial fuel cells using natural pyrrhotite as the cathodic heterogeneous Fenton catalyst towards the degradation of biorefractory organics in landfill leachate," *Electrochemistry Communications,* vol. 12, pp. 944-947, 2010.
[202] X. Q. Wang, C. P. Liu, Y. Yuan, and F. B. Li, "Arsenite oxidation and removal driven by a bio-electro-Fenton process under neutral pH conditions," *Journal of hazardous materials,* vol. 275, pp. 200-9, Jun 30 2014.
[203] Chun-Hua Feng, Fang-Bai Li, Hong-Jian Mai, and X.-Z. Li, "Bio-Electro-Fenton Process Driven by Microbial Fuel Cell for Wastewater Treatment," *Environ. Sci. Technol.,* vol. 44, pp. 1875–1880, 2010.
[204] K. V. Plakas, S. D. Sklari, D. A. Yiankakis, G. T. Sideropoulos, V. T. Zaspalis, and A. J. Karabelas, "Removal of organic micropollutants from drinking water by a novel electro-Fenton filter: Pilot-scale studies," *Water research,* vol. 91, pp. 183-94, Mar 15 2016.
[205] G. Ren, M. Zhou, M. Liu, L. Ma, and H. Yang, "A novel vertical-flow electro-Fenton reactor for organic wastewater treatment," *Chemical Engineering Journal,* vol. 298, pp. 55-67, 2016.

[206] N. A. S. Smith, K. Knoerzer, and Á. M. Ramos, "Evaluation of the differences of process variables in vertical and horizontal configurations of High Pressure Thermal (HPT) processing systems through numerical modelling," *Innovative Food Science & Emerging Technologies,* vol. 22, pp. 51-62, 2014.

[207] E. Rosales, M. Pazos, M. A. Longo, and M. A. Sanromán, "Electro-Fenton decoloration of dyes in a continuous reactor: A promising technology in colored wastewater treatment," *Chemical Engineering Journal,* vol. 155, pp. 62-67, 2009.

[208] F. Yu, M. Zhou, L. Zhou, and R. Peng, "A Novel Electro-Fenton Process with H2O2Generation in a Rotating Disk Reactor for Organic Pollutant Degradation," *Environmental Science & Technology Letters,* vol. 1, pp. 320-324, 2014.

[209] L. Zhang, X. Yin, and S. F. Y. Li, "Bio-electrochemical degradation of paracetamol in a microbial fuel cell-Fenton system," *Chemical Engineering Journal,* vol. 276, pp. 185-192, 2015.

[210] L. Zhuang, S. Zhou, Y. Li, T. Liu, and D. Huang, "In situ Fenton-enhanced cathodic reaction for sustainable increased electricity generation in microbial fuel cells," *Journal of Power Sources,* vol. 195, pp. 1379-1382, 2010.

[211] X. Zhu and J. Ni, "Simultaneous processes of electricity generation and p-nitrophenol degradation in a microbial fuel cell," *Electrochemistry Communications,* vol. 11, pp. 274-277, 2009.

[212] Y. Luo, R. Zhang, G. Liu, J. Li, B. Qin, M. Li, and S. Chen, "Simultaneous degradation of refractory contaminants in both the anode and cathode chambers of the microbial fuel cell," *Bioresource technology,* vol. 102, pp. 3827-32, Feb 2011.

[213] X. Zhu and B. E. Logan, "Using single-chamber microbial fuel cells as renewable power sources of electro-Fenton reactors for organic pollutant treatment," *Journal of hazardous materials,* vol. 252-253, pp. 198-203, May 15 2013.

[214] C. Espinoza, J. Romero, L. Villegas, L. Cornejo-Ponce, and R. Salazar, "Mineralization of the textile dye acid yellow 42 by solar photoelectro-Fenton in a lab-pilot plant," *Journal of hazardous materials,* vol. 319, pp. 24-33, Dec 5 2016.

[215] S. Garcia-Segura and E. Brillas, "Advances in solar photoelectro-Fenton: Decolorization and mineralization of the Direct Yellow 4 diazo dye using an autonomous solar pre-pilot plant," *Electrochimica Acta,* vol. 140, pp. 384-395, 2014.

[216] S. Garcia-Segura, E. B. Cavalcanti, and E. Brillas, "Mineralization of the antibiotic chloramphenicol by solar photoelectro-Fenton," *Applied Catalysis B: Environmental,* vol. 144, pp. 588-598, 2014.

[217] A. El-Ghenymy, P. L. Cabot, F. Centellas, J. A. Garrido, R. M. Rodriguez, C. Arias, and E. Brillas, "Mineralization of sulfanilamide by electro-Fenton and solar photoelectro-Fenton in a pre-pilot plant with a Pt/air-diffusion cell," *Chemosphere,* vol. 91, pp. 1324-31, May 2013.

[218] V. Andoralov, M. Falk, D. B. Suyatin, M. Granmo, J. Sotres, R. Ludwig, V. O. Popov, J. Schouenborg, Z. Blum, and S. Shleev, "Biofuel cell based on microscale nanostructured electrodes with inductive coupling to rat brain neurons," *Scientific reports,* vol. 3, p. 3270, 2013.

[219] P. Venkatesan and J. Santhanalakshmi, "Core-Shell Bimetallic Au-Pd Nanoparticles: Synthesis, Structure, Optical and Catalytic Properties," *Nanoscience and Nanotechnology,* vol. 1, pp. 43-47, 2012.

[220] G. Xia, Y. Lu, and H. Xu, "Electrogeneration of hydrogen peroxide for electro-Fenton via oxygen reduction using polyacrylonitrile-based carbon fiber brush cathode," *Electrochimica Acta,* vol. 158, pp. 390-396, 2015.

[221] H. C. Arredondo Valdez, G. Garcia Jimenez, S. Gutierrez Granados, and C. Ponce de Leon, "Degradation of paracetamol by advance oxidation processes using modified reticulated vitreous carbon electrodes with TiO(2) and CuO/TiO(2)/Al(2)O(3)," *Chemosphere,* vol. 89, pp. 1195-201, Nov 2012.

[222] X. Yu, M. Zhou, G. Ren, and L. Ma, "A novel dual gas diffusion electrodes system for efficient hydrogen peroxide generation used in electro-Fenton," *Chemical Engineering Journal,* vol. 263, pp. 92-100, 2015.

[223] S. Aquino Neto, T. S. Almeida, L. M. Palma, S. D. Minteer, and A. R. de Andrade, "Hybrid nanocatalysts containing enzymes and metallic nanoparticles for ethanol/O2 biofuel cell," *Journal of Power Sources,* vol. 259, pp. 25-32, 2014.

[224] K. Murata, K. Kajiya, N. Nakamura, and H. Ohno, "Direct electrochemistry of bilirubin oxidase on three-dimensional gold nanoparticle electrodes and its application in a biofuel cell," *Energy & Environmental Science,* vol. 2, p. 1280, 2009.

[225] F. N. Crespilho, M. Emilia Ghica, M. Florescu, F. C. Nart, O. N. Oliveira, and C. M. A. Brett, "A strategy for enzyme immobilization on layer-by-layer dendrimer–gold nanoparticle electrocatalytic membrane incorporating redox mediator," *Electrochemistry Communications,* vol. 8, pp. 1665-1670, 2006.

[226] A. Karczmarczyk, A. Celebanska, W. Nogala, V. Sashuk, O. Chernyaeva, and M. Opallo, "Electrocatalytic glucose oxidation at gold and gold-carbon nanoparticulate film prepared from oppositely charged nanoparticles," *Electrochimica Acta,* vol. 117, pp. 211-216, 2014.

[227] E. Brillas and C. A. Martinez-Huitle, "Decontamination of wastewaters containing synthetic organic dyes by electrochemical methods. An updated review. ," *Applied Catalysis B-Environmental* vol. 166, pp. 603-643, 2015.

[228] M. A. Oturan and J. J. Aaron, "Advanced oxidation processes in water/wastewater treatment: Principles and applications. A review," *Critical Reviews in Environmental Science and Technology,* vol. 44, pp. 2577-2641, 2014.

[229] M. A. Oturan, J. Pinson, J. Bizot, D. Deprez, and B. Terlain, "An International Journal Devoted to all Aspects of Electrode Kinetics, Interfacial Structure, Properties of Electrolytes, Colloid and Biological ElectrochemistryReaction of inflammation inhibitors with chemically and electrochemically generated hydroxyl radicals," *Journal of Electroanalytical Chemistry,* vol. 334, pp. 103-109, 1992/09/04 1992.

[230] E. Brillas, B. Boye, I. Sirés, J. A. Garrido, R. M. a. Rodríguez, C. Arias, P.-L. s. Cabot, and C. Comninellis, "Electrochemical destruction of chlorophenoxy herbicides by anodic oxidation and electro-Fenton using a boron-doped diamond electrode," *Electrochimica Acta,* vol. 49, pp. 4487-4496, 2004.

[231] A. Özcan, Y. Şahin, A. Savaş Koparal, and M. A. Oturan, "Carbon sponge as a new cathode material for the electro-Fenton process: Comparison with carbon felt cathode and application to degradation of synthetic dye basic blue 3 in aqueous medium," *Journal of Electroanalytical Chemistry,* vol. 616, pp. 71-78, 2008.

[232] K. Hanna, S. Chiron, and M. A. Oturan, "Coupling enhanced water solubilization with cyclodextrin to indirect electrochemical treatment for pentachlorophenol contaminated soil remediation," *Water Research,* vol. 39, pp. 2763-2773, 2005.

[233] B. Boye, M. Morième Dieng, and E. Brillas, "Anodic oxidation, electro-Fenton and photoelectro-Fenton treatments of 2,4,5-trichlorophenoxyacetic acid," *Journal of Electroanalytical Chemistry,* vol. 557, pp. 135-146, 2003.

[234] E. Brillas, E. Mur, R. Sauleda, L. Sànchez, J. Peral, X. Domènech, and J. Casado, "Aniline mineralization by AOP's: anodic oxidation, photocatalysis, electro-Fenton and

photoelectro-Fenton processes," *Applied Catalysis B: Environmental,* vol. 16, pp. 31-42, 1998.

[235] M. A. Oturan, J. Peiroten, P. Chartrin, and A. J. Acher, "Complete Destruction of p-Nitrophenol in Aqueous Medium by Electro-Fenton Method," *Environmental Science & Technology,* vol. 34, pp. 3474-3479, 2000/08/01 2000.

[236] M. Skoumal, P.-L. Cabot, F. Centellas, C. Arias, R. M. Rodríguez, J. A. Garrido, and E. Brillas, "Mineralization of paracetamol by ozonation catalyzed with Fe2+, Cu2+ and UVA light," *Applied Catalysis B: Environmental,* vol. 66, pp. 228-240, 2006.

[237] A. Özcan, M. A. Oturan, N. Oturan, and Y. Şahin, "Removal of Acid Orange 7 from water by electrochemically generated Fenton's reagent," *Journal of Hazardous Materials,* vol. 163, pp. 1213-1220, 2009.

[238] Y. Kumagai, Y. Shinkai, T. Miura, and A. K. Cho, "The chemical biology of naphthoquinones and its environmental implications," *Annual review of pharmacology and toxicology,* vol. 52, pp. 221-47, 2012.

[239] A. Das, S. Chakrabarty, D. Choudhury, and G. Chakrabarti, "1,4-Benzoquinone (PBQ) induced toxicity in lung epithelial cells is mediated by the disruption of the microtubule network and activation of caspase-3," *Chemical research in toxicology,* vol. 23, pp. 1054-66, Jun 21 2010.

[240] A. Dirany, I. Sires, N. Oturan, A. Ozcan, and M. A. Oturan, "Electrochemical treatment of the antibiotic sulfachloropyridazine: kinetics, reaction pathways, and toxicity evolution," *Environmental science & technology,* vol. 46, pp. 4074-82, Apr 3 2012.

[241] J.Devillers, P.Boule, P.Vasseur, P.Prevot, R.Steiman, F.Seigle-Murandi, J.L.Benoit-Guyod, M.Nendza, C.Grioni, D.Dive, and P.Chambon, "Environmental and health risks of Hydroquinone," *Ecotoxicology and Environmental Safety,* vol. 19, pp. 327-354, 1990.

[242] J. A. Zazo, J. A. Casas, C. B. Molina, A. Quintanilla, and J. J. Rodriguez, "Evolution of Ecotoxicity upon Fenton's Oxidation of Phenol in Water," *Environmental science & technology,* vol. 41, pp. 7164-7170, 2007.

[243] E. Seker, M. L. Reed, and M. R. Begley, "Nanoporous Gold: Fabrication, Characterization, and Applications," *Materials,* vol. 2, pp. 2188-2215, 2009.

[244] P. Bansal, D. Singh, and D. Sud, "Photocatalytic degradation of azo dye in aqueous TiO2 suspension: Reaction pathway and identification of intermediates products by LC/MS," *Separation and Purification Technology,* vol. 72, pp. 357-365, 2010.

[245] T. Velegraki, I. Poulios, M. Charalabaki, N. Kalogerakis, P. Samaras, and D. Mantzavinos, "Photocatalytic and sonolytic oxidation of acid orange 7 in aqueous solution," *Applied Catalysis B: Environmental,* vol. 62, pp. 159-168, 2006.

[246] H.-Z. Zhao, Y. Sun, L.-N. Xu, and J.-R. Ni, "Removal of Acid Orange 7 in simulated wastewater using a three-dimensional electrode reactor: Removal mechanisms and dye degradation pathway," *Chemosphere,* vol. 78, pp. 46-51, 2010.

[247] R. P. Schwarzenbach, B. I. Escher, K. Fenner, T. B. Hofstetter, C. A. Johnson, U. von Gunten, and B. Wehrli, "The challenge of micropollutants in aquatic systems," *Science,* vol. 313, pp. 1072-7, Aug 25 2006.

[248] R. Andreozzi, V. Caprio, R. Marotta, and A. Radovnikovic, "Ozonation and H2O2/UV treatment of clofibric acid in water: a kinetic investigation," *Journal of hazardous materials,* vol. 103, pp. 233-246, 2003.

[249] Leónidas A. Pérez-Estrada , Sixto Malato , Wolfgang Gernjak , Ana Agüera , E. Michael Thurman , Imma Ferrer , and A. R. Fernández-Alba, "Photo-Fenton Degradation of Diclofenac: Identification of Main Intermediates and Degradation Pathway," *Environmental Science & Technology,* vol. 39, pp. 8300-06, 2005.

[250] Thomas A. Ternes , Martin Meisenheimer , Derek McDowell , Frank Sacher , Heinz-Jürgen Brauch , Brigitte Haist-Gulde , Gudrun Preuss , Uwe Wilme , and N. Zulei-Seibert, "Removal of pharmaceuticals during drinking water treatment," *Environmental Science & Technology,* vol. 36, pp. 3855-63, 2002.

[251] T. E. Doll and F. H. Frimmel, "Fate of pharmaceuticals—photodegradation by simulated solar UV-light," *Chemosphere,* vol. 52, pp. 1757-1769, 2003.

[252] B. Halling-Sørensen, S. Nors Nielsen, P.F. Lanzky, F. Ingerslev, H.C. Holten Lützhøft, and S. E. Jørgensen, "Occurrence, fate and effects of pharmaceutical substances in the environment- A review," *Chemosphere,* vol. 36, pp. 357-93, 1998.

[253] T. A. Ternes, "Occurrence of drugs in German sewage treatment plants and rivers," *Water Research,* vol. 32, pp. 3245-3260, 1998.

[254] M. Huerta-Fontela, M. T. Galceran, and F. Ventura, "Occurrence and removal of pharmaceuticals and hormones through drinking water treatment," *Water Research,* vol. 45, pp. 1432-42, Jan 2011.

[255] B. Huerta, S. Rodriguez-Mozaz, C. Nannou, L. Nakis, A. Ruhi, V. Acuna, S. Sabater, and D. Barcelo, "Determination of a broad spectrum of pharmaceuticals and endocrine disruptors in biofilm from a waste water treatment plant-impacted river," *The Science of the total environment,* vol. 540, pp. 241-9, Jan 1 2016.

[256] F.J. García-Mateos, R. Ruiz-Rosas, M.D. Marqués, L.M. Cotoruelo, J. Rodríguez-Mirasol, and T. Cordero, "Removal of paracetamol on biomass-derived activated carbon: Modeling the fixed bed breakthrough curves using batch adsorption experiments," *Chemical Engineering Journal* vol. 279, pp. 18–30, 2015.

[257] E. Zuccato, D. Calamari, M. Natangelo, and R. Fanelli, "Presence of therapeutic drugs in the environment," *The Lancet,* vol. 355, pp. 1789-1790, 2000.

[258] Işıl Akmehmet Balcıoğlu and M. Ötker, "Treatment of pharmaceutical wastewater containing antibiotics by O3 and O3/H2O2 processes," *Chemosphere,* vol. 50, pp. 85–95, 2003.

[259] F. J. García-Mateos, R. Ruiz-Rosas, M. D. Marqués, L. M. Cotoruelo, J. Rodríguez-Mirasol, and T. Cordero, "Removal of paracetamol on biomass-derived activated carbon: Modeling the fixed bed breakthrough curves using batch adsorption experiments," *Chemical Engineering Journal,* vol. 279, pp. 18-30, 2015.

[260] D. W. Kolpin, E. T. Furlong, M. T. Meyer, E. M. Thurman, S. D. Zaugg, L. B. Barber, and H. T. Buxton, "Pharmaceuticals, Hormones, and Other Organic Wastewater Contaminants in U.S. Streams, 1999 - 2000: A National Reconnaissance," *Environ. Sci. Technol.,* vol. 36, pp. 1202–1211, 2002.

[261] I. Kabdaşli, M. Gürel, and O. Tünay, "Pollution prevention and waste treatment in chemical synthesis processes for pharmaceutical industry," *Water Science and Technology,* vol. 39, pp. 265–271, 1999.

[262] P. H. Roberts and K. V. Thomas, "The occurrence of selected pharmaceuticals in wastewater effluent and surface waters of the lower Tyne catchment," *The Science of the total environment,* vol. 356, pp. 143-53, Mar 1 2006.

[263] J. Reungoat, M. Macova, B. I. Escher, S. Carswell, J. F. Mueller, and J. Keller, "Removal of micropollutants and reduction of biological activity in a full scale reclamation plant using ozonation and activated carbon filtration," *Water Research,* vol. 44, pp. 625-37, Jan 2010.

[264] J. Reungoat, B. I. Escher, M. Macova, F. X. Argaud, W. Gernjak, and J. Keller, "Ozonation and biological activated carbon filtration of wastewater treatment plant effluents," *Water Research,* vol. 46, pp. 863-72, Mar 1 2012.

[265] R. I. Eggen, J. Hollender, A. Joss, M. Scharer, and C. Stamm, "Reducing the discharge of micropollutants in the aquatic environment: the benefits of upgrading wastewater treatment plants," *Environmental science & technology,* vol. 48, pp. 7683-9, Jul 15 2014.

[266] I. Sirés, E. Brillas, M. A. Oturan, M. A. Rodrigo, and M. Panizza, "Electrochemical advanced oxidation processes: today and tomorrow. A review," *Environmental science and pollution research international,* vol. 21, pp. 8336-67, 2014.

[267] F. C. Moreira, R. A. R. Boaventura, E. Brillas, and V. J. P. Vilar, "Electrochemical advanced oxidation processes: A review on their application to synthetic and real wastewaters," *Applied Catalysis B: Environmental,* vol. 202, pp. 217-261, 2017.

[268] S. Giannakis, F. A. Gamarra Vives, D. Grandjean, A. Magnet, L. F. De Alencastro, and C. Pulgarin, "Effect of advanced oxidation processes on the micropollutants and the effluent organic matter contained in municipal wastewater previously treated by three different secondary methods," *Water Research,* vol. 84, pp. 295-306, Nov 1 2015.

[269] D. Gerrity, S. Gamage, J. C. Holady, D. B. Mawhinney, O. Quinones, R. A. Trenholm, and S. A. Snyder, "Pilot-scale evaluation of ozone and biological activated carbon for trace organic contaminant mitigation and disinfection," *Water Research,* vol. 45, pp. 2155-65, Feb 2011.

[270] Z. Frontistis, V. M. Daskalaki, E. Hapeshi, C. Drosou, D. Fatta-Kassinos, N. P. Xekoukoulotakis, and D. Mantzavinos, "Photocatalytic (UV-A/TiO2) degradation of 17α-ethynylestradiol in environmental matrices: Experimental studies and artificial neural network modeling," *Journal of Photochemistry and Photobiology A: Chemistry,* vol. 240, pp. 33-41, 2012.

[271] Y. Lee, D. Gerrity, M. Lee, S. Gamage, A. Pisarenko, R. A. Trenholm, S. Canonica, S. A. Snyder, and U. von Gunten, "Organic Contaminant Abatement in Reclaimed Water by UV/HO and a Combined Process Consisting of O/HO Followed by UV/HO: Prediction of Abatement Efficiency, Energy Consumption, and Byproduct Formation," *Environmental science & technology,* Mar 17 2016.

[272] Marc M. Huber , Anke GÖbel , Adriano Joss , Nadine Hermann , Dirk LÖffler , Christa S. McArdell , Achim Ried , Hansruedi Siegrist , Thomas A. Ternes , and U. v. Gunten, "Oxidation of Pharmaceuticals during Ozonation of Municipal Wastewater Effluents: A Pilot Study," *Environmental Science & Technology,* vol. 39, pp. 4290-99, 2005.

[273] S. G. Zimmermann, M. Wittenwiler, J. Hollender, M. Krauss, C. Ort, H. Siegrist, and U. von Gunten, "Kinetic assessment and modeling of an ozonation step for full-scale municipal wastewater treatment: micropollutant oxidation, by-product formation and disinfection," *Water Research,* vol. 45, pp. 605-17, Jan 2011.

[274] J. Margot, C. Kienle, A. Magnet, M. Weil, L. Rossi, L. F. de Alencastro, C. Abegglen, D. Thonney, N. Chevre, M. Scharer, and D. A. Barry, "Treatment of micropollutants in municipal wastewater: ozone or powdered activated carbon?," *The Science of the total environment,* vol. 461-462, pp. 480-98, Sep 1 2013.

[275] H. Tekin, O. Bilkay, S. S. Ataberk, T. H. Balta, I. H. Ceribasi, F. D. Sanin, F. B. Dilek, and U. Yetis, "Use of Fenton oxidation to improve the biodegradability of a pharmaceutical wastewater," *Journal of hazardous materials,* vol. 136, pp. 258-65, Aug 21 2006.

[276] N. Kulik, M. Trapido, A. Goi, Y. Veressinina, and R. Munter, "Combined chemical treatment of pharmaceutical effluents from medical ointment production," *Chemosphere,* vol. 70, pp. 1525-31, Feb 2008.

[277] R. Molinari, F. Pirillo, V. Loddo, and L. Palmisano, "Heterogeneous photocatalytic degradation of pharmaceuticals in water by using polycrystalline TiO2 and a nanofiltration membrane reactor," *Catalysis Today,* vol. 118, pp. 205-213, 2006.
[278] M. N. Abellán, B. Bayarri, J. Giménez, and J. Costa, "Photocatalytic degradation of sulfamethoxazole in aqueous suspension of TiO2," *Applied Catalysis B: Environmental,* vol. 74, pp. 233-241, 2007.
[279] I. Sirés and E. Brillas, "Remediation of water pollution caused by pharmaceutical residues based on electrochemical separation and degradation technologies: a review," *Environment international,* vol. 40, pp. 212-29, Apr 2012.
[280] M. D. de Luna, M. L. Veciana, C. C. Su, and M. C. Lu, "Acetaminophen degradation by electro-Fenton and photoelectro-Fenton using a double cathode electrochemical cell," *Journal of hazardous materials,* vol. 217-218, pp. 200-7, May 30 2012.
[281] M. Irani, L. R. Rad, H. Pourahmad, and I. Haririan, "Optimization of the combined adsorption/photo-Fenton method for the simultaneous removal of phenol and paracetamol in a binary system," *Microporous and Mesoporous Materials,* vol. 206, pp. 1-7, 2015.
[282] A. G. Trovó, S. A. S. Melo, and R. F. P. Nogueira, "Photodegradation of the pharmaceuticals amoxicillin, bezafibrate and paracetamol by the photo-Fenton process—Application to sewage treatment plant effluent," *Journal of Photochemistry and Photobiology A: Chemistry,* vol. 198, pp. 215-220, 2008.
[283] L. R. Rad, M. Irani, F. divsar, H. Pourahmad, M. S. Sayyafan, and I. Haririan, "Simultaneous degradation of phenol and paracetamol during photo-Fenton process: Design and optimization," *Journal of the Taiwan Institute of Chemical Engineers,* vol. 47, pp. 190-196, 2015.
[284] A. Cabrera Reina, L. Santos-Juanes, J. L. García Sánchez, J. L. Casas López, M. I. Maldonado Rubio, G. Li Puma, and J. A. Sánchez Pérez, "Modelling the photo-Fenton oxidation of the pharmaceutical paracetamol in water including the effect of photon absorption (VRPA)," *Applied Catalysis B: Environmental,* vol. 166-167, pp. 295-301, 2015.
[285] A. G. Trovo, R. F. Pupo Nogueira, A. Aguera, A. R. Fernandez-Alba, and S. Malato, "Paracetamol degradation intermediates and toxicity during photo-Fenton treatment using different iron species," *Water Research,* vol. 46, pp. 5374-80, Oct 15 2012.
[286] I. Sirés, J. A. Garrido, R. M. Rodríguez, P. L. Cabot, F. Centellas, C. Arias, and E. Brillas, "Electrochemical Degradation of Paracetamol from Water by Catalytic Action of Fe[sup 2+], Cu[sup 2+], and UVA Light on Electrogenerated Hydrogen Peroxide," *Journal of The Electrochemical Society,* vol. 153, p. DOI: 10.1149/1.2130568, 2006.
[287] L. Yang, L. E. Yu, and M. B. Ray, "Degradation of paracetamol in aqueous solutions by TiO2 photocatalysis," *Water Research,* vol. 42, pp. 3480-8, Jul 2008.
[288] E. Brillas, I. Sirés, C. Arias, P. L. Cabot, F. Centellas, R. M. Rodriguez, and J. A. Garrido, "Mineralization of paracetamol in aqueous medium by anodic oxidation with a boron-doped diamond electrode," *Chemosphere,* vol. 58, pp. 399-406, Jan 2005.
[289] M. Skoumal, P. L. Cabot, F. Centellas, C. Arias, R. M. Rodríguez, J. A. Garrido, and E. Brillas, "Mineralization of paracetamol by ozonation catalyzed with Fe2+, Cu2+ and UVA light," *Applied Catalysis B: Environmental,* vol. 66, pp. 228-240, 2006.
[290] Roberto Andreozzia, Vincenzo Caprioa, Raffaele Marottaa, and D. Vogna, "Paracetamol oxidation from aqueous solutions by means of ozonation andH 2O2/UV system," *Water Research* vol. 37, pp. 993–1004, 2003.
[291] U. von Gunten, "Ozonation of drinking water: Part I. Oxidation kinetics and product formation," *Water Research,* vol. 37, pp. 1443-1467, 2003.

[292] N. Hamdi El Najjar, A. Touffet, M. Deborde, R. Journel, and N. Karpel Vel Leitner, "Kinetics of paracetamol oxidation by ozone and hydroxyl radicals, formation of transformation products and toxicity," *Separation and Purification Technology,* vol. 136, pp. 137-143, 2014.

[293] Enric Brillas, Ignasi Sirés, and M. A. Oturan, "Electro-Fenton Process and Related Electrochemical Technologies Based on Fenton's Reaction Chemistry," *Chem. Rev.,* vol. 109, pp. 6570–6631, 2009.

[294] L. Yang, L. E. Yu, and M. B. Ray, "Degradation of paracetamol in aqueous solutions by TiO2 photocatalysis," *Water Research,* vol. 42, pp. 3480-3488, 2008.

[295] A. Dirany, I. Sirés, N. Oturan, A. Ozcan, and M. A. Oturan, "Electrochemical treatment of the antibiotic sulfachloropyridazine: kinetics, reaction pathways, and toxicity evolution," *Environmental science & technology,* vol. 46, pp. 4074-82, Apr 3 2012.

[296] P. Y. Lee and C. Y. Chen, "Toxicity and quantitative structure-activity relationships of benzoic acids to Pseudokirchneriella subcapitata," *Journal of hazardous materials,* vol. 165, pp. 156-61, Jun 15 2009.

[297] T. Velegraki, G. Balayiannis, E. Diamadopoulos, A. Katsaounis, and D. Mantzavinos, "Electrochemical oxidation of benzoic acid in water over boron-doped diamond electrodes: Statistical analysis of key operating parameters, kinetic modeling, reaction by-products and ecotoxicity," *Chemical Engineering Journal,* vol. 160, pp. 538-548, 2010.

[298] M. G. Paulraj, A. D. Reegan, and S. Ignacimuthu, "Toxicity of Benzaldehyde and Propionic Acid against Immature and Adult Stages of Aedes aegypti (Linn.) and Culex quinquefasciatus (Say) (Diptera: Culicidae)," *Journal of Entomology* vol. 8, pp. 539-547, 2011.

[299] V. Rubio, J. Zhang, M. Valverde, E. Rojas, and Z. Z. Shi, "Essential role of Nrf2 in protection against hydroquinone- and benzoquinone-induced cytotoxicity," *Toxicology in vitro : an international journal published in association with BIBRA,* vol. 25, pp. 521-9, Mar 2011.

[300] Z. Liu, B. Zhao, C. Guo, Y. Sun, Y. Shi, H. Yang, and Z. Li, "Carbon nanotube/raspberry hollow Pd nanosphere hybrids for methanol, ethanol, and formic acid electro-oxidation in alkaline media," *Journal of colloid and interface science,* vol. 351, pp. 233-8, Nov 1 2010.

[301] T. G. Bulc and A. Ojstrsek, "The use of constructed wetland for dye-rich textile wastewater treatment," *Journal of hazardous materials,* vol. 155, pp. 76-82, Jun 30 2008.

[302] M. Faouzi, P. Cañizares, A. Gadri, J. Lobato, B. Nasr, R. Paz, M. A. Rodrigo, and C. Saez, "Advanced oxidation processes for the treatment of wastes polluted with azoic dyes," *Electrochimica Acta,* vol. 52, pp. 325-331, 2006.

[303] P. Banerjee, S. Dasgupta, and S. De, "Removal of dye from aqueous solution using a combination of advanced oxidation process and nanofiltration," *Journal of hazardous materials,* vol. 140, pp. 95-103, Feb 9 2007.

[304] E. Brillas and C. A. Martinez-Huitle, "Decontamination of wastewaters containing synthetic organic dyes by electrochemical methods. An updated review. ," *Applied Catalysis B-Environmental,* vol. 166, pp. 603-643, 2015.

[305] I. A. B. Idil Arslan, Detlef W. Bahnemann, "Advanced chemical oxidation of reactive dyes in simulated dyehouse effluents by ferrioxalate-Fenton/UV-A and TiO2/UV-A processes," *Dyes and Pigments,* vol. 47, pp. 207-218, 2000.

[306] P. V. Reddy and K. H. Kim, "A review of photochemical approaches for the treatment of a wide range of pesticides," *Journal of hazardous materials,* vol. 285C, pp. 325-335, Mar 21 2015.

[307] H. T. Madsen, E. G. Sogaard, and J. Muff, "Study of degradation intermediates formed during electrochemical oxidation of pesticide residue 2,6-dichlorobenzamide (BAM) in chloride medium at boron doped diamond (BDD) and platinum anodes," *Chemosphere,* vol. 120, pp. 756-63, Feb 2015.

[308] E. Brillas, I. Sire´s, and M. A. Oturan, "Electro-Fenton Process and Related Electrochemical Technologies Based on Fenton's Reaction Chemistry," *Chem. Rev.,* vol. 109, pp. 6570–6631, 2009.

[309] X. Zhang, J. Fu, Y. Zhang, and L. Lei, "A nitrogen functionalized carbon nanotube cathode for highly efficient electrocatalytic generation of H2O2 in Electro-Fenton system," *Separation and Purification Technology,* vol. 64, pp. 116-123, 2008.

[310] G. Zhang, F. Yang, M. Gao, X. Fang, and L. Liu, "Electro-Fenton degradation of azo dye using polypyrrole/anthraquinonedisulphonate composite film modified graphite cathode in acidic aqueous solutions," *Electrochimica Acta,* vol. 53, pp. 5155-5161, 2008.

[311] K. S. Novoselov, A. K. G. , S. V. M. , D. J. , Y. Z. , S. V. D. , I. V. G. , and A. A. F. , "Electric Field Effect in Atomically Thin Carbon Films," *Science,* vol. 306, pp. 666–669, 2004.

[312] C. Berger, Z. Song, X. Li, X. Wu, N. Brown, C. Naud, D. Mayou, T. Li, J. Hass, A. N. Marchenkov, E. H. Conrad, P. N. First, and W. A. de Heer, "Electronic confinement and coherence in patterned epitaxial graphene," *Science,* vol. 312, pp. 1191-6, May 26 2006.

[313] W. C. X. Li, S. K. J. An, D. Y. J. Nah, R. Piner, A. Velamakanni, I. Jung, E. Tutuc, S.K. Banerjee, and R. S. R. L. Colombo, "Large-area synthesis of highquality and uniform graphene films on copper foils," *Science,* vol. 324, p. 1312, 2009.

[314] K. S. Kim, Y. Zhao, H. Jang, S. Y. Lee, J. M. Kim, J. H. Ahn, P. Kim, J. Y. Choi, and B. H. Hong, "Large-scale pattern growth of graphene films for stretchable transparent electrodes," *Nature,* vol. 457, pp. 706-10, Feb 5 2009.

[315] T. Choi, H. Jung, C. W. Lee, K.-Y. Mun, S.-H. Kim, J. Park, and H. Kim, "Growth characteristics of graphene synthesized via chemical vapor deposition using carbon tetrabromide precursor," *Applied Surface Science,* vol. 343, pp. 128-132, 2015.

[316] B. Qi, L. He, X. Bo, H. Yang, and L. Guo, "Electrochemical preparation of free-standing few-layer graphene through oxidation–reduction cycling," *Chemical Engineering Journal,* vol. 171, pp. 340-344, 2011.

[317] G. Wang, B. Wang, J. Park, Y. Wang, B. Sun, and J. Yao, "Highly efficient and large-scale synthesis of graphene by electrolytic exfoliation," *Carbon,* vol. 47, pp. 3242-3246, 2009.

[318] Jiong Lu, Jia-xiang Yang, Junzhong Wang, Ailian Lim, Shuai Wang, and K. P. Loh, "One-Pot Synthesis of Fluorescent Carbon Nanoribbons, Nanoparticles, and Graphene by the Exfoliation of Graphite in Ionic Liquids," *CS Nano,* vol. 3, pp. 2367–2375, 2009.

[319] Owen C. Compton, Bonny Jain, Dmitriy A. Dikin, Ali Abouimrane, Khalil Amine, and S. T. Nguyen, "Chemically active reduced graphene oxide with tunable C/O ratios," *ACS Nano,* vol. 5, p. 4380, 2011.

[320] S. Y. Toh, K. S. Loh, S. K. Kamarudin, and W. R. W. Daud, "Graphene production via electrochemical reduction of graphene oxide: Synthesis and characterisation," *Chemical Engineering Journal,* vol. 251, pp. 422-434, 2014.

[321] S. Stankovich, D. A. Dikin, R. D. Piner, K. A. Kohlhaas, A. Kleinhammes, Y. Jia, Y. Wu, S. T. Nguyen, and R. S. Ruoff, "Synthesis of graphene-based nanosheets via chemical reduction of exfoliated graphite oxide," *Carbon,* vol. 45, pp. 1558-1565, 2007.

[322] X. Liu, H. Kim, and L. J. Guo, "Optimization of thermally reduced graphene oxide for an efficient hole transport layer in polymer solar cells," *Organic Electronics,* vol. 14, pp. 591-598, 2013.
[323] P. Afzali, Y. Abdi, and E. Arzi, "Directional reduction of graphene oxide sheets using photocatalytic activity of ZnO nanowires for the fabrication of a high sensitive oxygen sensor," *Sensors and Actuators B: Chemical,* vol. 195, pp. 92-97, 2014.
[324] D. Huang, B. Zhang, Y. Zhang, F. Zhan, X. Xu, Y. Shen, and M. Wang, "Electrochemically reduced graphene oxide multilayer films as metal-free electrocatalysts for oxygen reduction," *Journal of Materials Chemistry A,* vol. 1, p. 1415, 2013.
[325] M. Pumera, "Graphene-based nanomaterials for energy storage," *Energy & Environmental Science,* vol. 4, p. 668, 2011.
[326] Xiaochen Xu, Jie Chen, Guoquan Zhang, Yan Song, and F. Yang, "Homogeneous Electro-Fenton Oxidative Degradation of Reactive Brilliant Blue Using a Graphene Doped Gas-Diffusion Cathode," *Int. J. Electrochem. Sci.,* vol. 9, pp. 569 - 579, 2014.
[327] B. Yang, Z. Tian, L. Zhang, Y. Guo, and S. Yan, "Enhanced heterogeneous Fenton degradation of Methylene Blue by nanoscale zero valent iron (nZVI) assembled on magnetic Fe3O4/reduced graphene oxide," *Journal of Water Process Engineering,* vol. 5, pp. 101-111, 2015.
[328] N. I. Kovtyukhova, P. J. Ollivier, B. R. Martin, T. E. Mallouk, S. A. Chizhik, E. V. Buzaneva, and A. D. Gorchinskiy, "Layer-by-Layer Assembly of Ultrathin Composite Films from Micron-Sized Graphite Oxide Sheets and Polycations," *Chem. Mater,* vol. 11, pp. 771-778, 1999.
[329] D. Li, Muller, M. B., Gilje, S., Kaner, R. B. & Wallace, G. G., "Processable aqueous dispersions of graphene nanosheets. ," *Nature Nanotechnology,* vol. 3 (2), pp. 101-105, 2008.
[330] LEILA SHAHRIARY and A. A. ATHAWALE, "Graphene Oxide Synthesized by using Modified Hummers Approach," *International Journal of Renewable Energy and Environmental Engineering,* vol. Vol. 02, No. 01, pp. 58-63, 2014.
[331] Y. Shao, J. Wang, M. Engelhard, C. Wang, and Y. Lin, "Facile and controllable electrochemical reduction of graphene oxide and its applications," *Journal of Materials Chemistry,* vol. 20, p. 743, 2010.
[332] L. Chen, Y. Tang, K. Wang, C. Liu, and S. Luo, "Direct electrodeposition of reduced graphene oxide on glassy carbon electrode and its electrochemical application," *Electrochemistry Communications,* vol. 13, pp. 133-137, 2011.
[333] Xingfa Gao, Joonkyung Jang, and S. Nagase, "Hydrazine and Thermal Reduction of Graphene Oxide: Reaction Mechanisms, Product Structures, and Reaction Design," *J. Phys. Chem. C,* vol. 114, pp. 832–842, 2010.
[334] H. Ö. Doğan, D. Ekinci, and Ü. Demir, "Atomic scale imaging and spectroscopic characterization of electrochemically reduced graphene oxide," *Surface Science,* vol. 611, pp. 54-59, 2013.
[335] A. G. A. t. t. S. of, G. Nanosheets, Hui-Lin Guo, Xian-Fei Wang, Qing-Yun Qian, Feng-Bin Wang, and X.-H. Xia, "A Green Approach to the Synthesis of Graphene Nanosheets," *ACS Nano,* vol. 3, pp. 2653-2659, 2009.
[336] M. Hilder, B. Winther-Jensen, D. Li, M. Forsyth, and D. R. MacFarlane, "Direct electro-deposition of graphene from aqueous suspensions," *Physical chemistry chemical physics : PCCP,* vol. 13, pp. 9187-93, May 28 2011.

[337] J. Liu, Y. Qiao, C. X. Guo, S. Lim, H. Song, and C. M. Li, "Graphene/carbon cloth anode for high-performance mediatorless microbial fuel cells," *Bioresource technology,* vol. 114, pp. 275-80, Jun 2012.
[338] Q. Li, N. Mahmood, J. Zhu, Y. Hou, and S. Sun, "Graphene and its composites with nanoparticles for electrochemical energy applications," *Nano Today,* vol. 9, pp. 668-683, 2014.
[339] J. Erlebacher, "An Atomistic Description of Dealloying Porosity Evolution, the Critical Potential, and Rate-Limiting Behavior," *J. Electrochem. Soc.,* vol. 151, pp. C614-C626, 2004.
[340] L. Wang and E. Wang, "Direct electron transfer between cytochrome c and a gold nanoparticles modified electrode," *Electrochemistry Communications,* vol. 6, pp. 49-54, 2004.
[341] Q. Kang, L. Yang, and Q. Cai, "An electro-catalytic biosensor fabricated with Pt-Au nanoparticle-decorated titania nanotube array," *Bioelectrochemistry,* vol. 74, pp. 62-5, Nov 2008.
[342] V. G. Praig, G. Piret, M. Manesse, X. Castel, R. Boukherroub, and S. Szunerits, "Seed-mediated electrochemical growth of gold nanostructures on indium tin oxide thin films," *Electrochimica Acta,* vol. 53, pp. 7838-7844, 2008.
[343] M. D. Scanlon, U. Salaj-Kosla, S. Belochapkine, D. MacAodha, D. Leech, Y. Ding, and E. Magner, "Characterization of nanoporous gold electrodes for bioelectrochemical applications," *Langmuir : the ACS journal of surfaces and colloids,* vol. 28, pp. 2251-61, Jan 31 2012.
[344] S. Tuncagil, C. Ozdemir, D. O. Demirkol, S. Timur, and L. Toppare, "Gold nanoparticle modified conducting polymer of 4-(2,5-di(thiophen-2-yl)-1H-pyrrole-1-l) benzenamine for potential use as a biosensing material," *Food chemistry,* vol. 127, pp. 1317-22, Aug 1 2011.
[345] Y. Fu, F. Liang, H. Tian, and J. Hu, "Nonenzymatic glucose sensor based on ITO electrode modified with gold nanoparticles by ion implantation," *Electrochimica Acta,* vol. 120, pp. 314-318, 2014.
[346] W. Putzbach and N. J. Ronkainen, "Immobilization techniques in the fabrication of nanomaterial-based electrochemical biosensors: a review," *Sensors,* vol. 13, pp. 4811-40, 2013.
[347] K. Murata, K. Kajiya, M. Nukaga, Y. Suga, T. Watanabe, N. Nakamura, and H. Ohno, "A Simple Fabrication Method for Three-Dimensional Gold Nanoparticle Electrodes and Their Application to the Study of the Direct Electrochemistry of Cytochromec," *Electroanalysis,* vol. 22, pp. 185-190, 2010.
[348] U. Salaj-Kosla, S. Pöller, Y. Beyl, M. D. Scanlon, S. Beloshapkin, S. Shleev, W. Schuhmann, and E. Magner, "Direct electron transfer of bilirubin oxidase (Myrothecium verrucaria) at an unmodified nanoporous gold biocathode," *Electrochemistry Communications,* vol. 16, pp. 92-95, 2012.
[349] M. Tominaga, T. Shimazoe, M. Nagashima, and I. Taniguchi, "Electrocatalytic oxidation of glucose at gold nanoparticle-modified carbon electrodes in alkaline and neutral solutions," *Electrochemistry Communications,* vol. 7, pp. 189-193, 2005.
[350] M. Falk, V. Andoralov, Z. Blum, J. Sotres, D. B. Suyatin, T. Ruzgas, T. Arnebrant, and S. Shleev, "Biofuel cell as a power source for electronic contact lenses," *Biosensors & bioelectronics,* vol. 37, pp. 38-45, Aug-Sep 2012.
[351] S. Aquino Neto, R. D. Milton, L. B. Crepaldi, D. P. Hickey, A. R. de Andrade, and S. D. Minteer, "Co-immobilization of gold nanoparticles with glucose oxidase to improve

bioelectrocatalytic glucose oxidation," *Journal of Power Sources,* vol. 285, pp. 493-498, 2015.

[352] S. Boland and D. Leech, "A glucose/oxygen enzymatic fuel cell based on redox polymer and enzyme immobilisation at highly-ordered macroporous gold electrodes," *The Analyst,* vol. 137, pp. 113-7, Jan 7 2012.

[353] X. Wang, M. Falk, R. Ortiz, H. Matsumura, J. Bobacka, R. Ludwig, M. Bergelin, L. Gorton, and S. Shleev, "Mediatorless sugar/oxygen enzymatic fuel cells based on gold nanoparticle-modified electrodes," *Biosensors & bioelectronics,* vol. 31, pp. 219-25, Jan 15 2012.

[354] Jianbo Jia, Bingquan Wang, G. C. Aiguo Wu, Zhuang Li, and S. Dong, "A Method to Construct a Third-Generation Horseradish Peroxidase Biosensor Self-Assembling Gold Nanoparticles to Three-Dimensional Sol−Gel Network," *Analytical Chemistry,* vol. 74, pp. 2217-2223, 2002.

[355] V. Matveeva, A. Bykov, V. Doluda, M. Sulman, N. Kumar, S. Dzwigaj, E. Marceau, L. Kustov, O. Tkachenko, and E. Sulman, "Direct d-Glucose Oxidation over Noble Metal Nanoparticles Introduced on Polymer and Inorganic Supports," *Topics in Catalysis,* vol. 52, pp. 387-393, 2009.

[356] M. Pasta, R. Ruffo, E. Falletta, C. M. Mari, and C. D. Pina, "Alkaline glucose oxidation on nanostructured gold electrodes," *Gold Bull,* vol. 43, pp. 57-64, 2010.

[357] Matthew T. Meredith, Der-You Kao, David Hickey, David W. Schmidtke, and D. T. Glatzhofer, "High Current Density Ferrocene-Modified Linear Poly(ethylenimine) Bioanodes and Their Use in Biofuel Cells," *Electrochem. Soc. ,* vol. 158, pp. B166-B174, 2011.

[358] Nicolas Mano, Fei Mao, and A. Heller, "Characteristics of a Miniature Compartment-less Glucose−O2 Biofuel Cell and Its Operation in a Living Plant," *JACS,* vol. 125, pp. 6588-6594, 2003.

[359] Minling Shao, Muhammad Nadeem Zafar, Magnus Falk, Roland Ludwig, Christoph Sygmund, Clemens K. Peterbauer, Dmitrii A. Guschin, Domhnall MacAodha, Peter Ó Conghaile, Dónal Leech, Miguel D. Toscano, Sergey Shleev, Wolfgang Schuhmann, and Lo Gorton, "Optimization of a Membraneless Glucose/Oxygen Enzymatic Fuel Cell Based on a Bioanode with High Coulombic Efficiency and Current Density," *ChemPhysChem,* vol. 14, pp. 2260–2269, 2013.

[360] Y. Holade, A. Both Engel, S. Tingry, A. Cherifi, D. Cornu, K. Servat, T. W. Napporn, and K. B. Kokoh, "Insights on Hybrid Glucose Biofuel Cells Based on Bilirubin Oxidase Cathode and Gold-Based Anode Nanomaterials," *ChemElectroChem,* vol. 1, pp. 1976-1987, 2014.

[361] A. Both Engel, M. Bechelany, O. Fontaine, A. Cherifi, D. Cornu, and S. Tingry, "One-Pot Route to Gold Nanoparticles Embedded in Electrospun Carbon Fibers as an Efficient Catalyst Material for Hybrid Alkaline Glucose Biofuel Cells," *ChemElectrochem,* vol. 3, pp. 629–637 2016.

[362] M. Bechelany, X. Maeder, J. Riesterer, J. Hankache, D. Lerose, S. Christiansen, J. Michler, and L. Philippe, "Synthesis Mechanisms of Organized Gold Nanoparticles: Influence of Annealing Temperature and Atmosphere," *Crystal Growth & Design,* vol. 10, pp. 587-596, 2010.

[363] Scott Calabrese Barton, Josh Gallaway, and P. Atanassov, "Enzymatic Biofuel Cells for Implantable and Microscale Devices," *Chemical Reviews,* vol. 104, p. 4867−4886, 2004.

[364] S. El Ichi, A. Zebda, J.-P. Alcaraz, A. Laaroussi, F. Boucher, J. Boutonnat, N. Reverdy-Bruas, D. Chaussy, M. N. Belgacem, P. Cinquin, and D. K. Martin, "Bioelectrodes

modified with chitosan for long-term energy supply from the body," *Energy & Environmental Science,* vol. 8, p. 1017, 2015.

[365] WEIMIN HUANG and J. SHI, "Synthesis and Properties of ZrO2 Films Dispersed With Au Nanoparticles," *Journal of Sol-Gel Science and Technology,* vol. 20, pp. 145–151, 2001.

[366] R. P. Ramasamy and S. M. Maliyekkal, "Formation of gold nanoparticles upon chitosan leading to formation and collapse of gels," *New J. Chem.,* vol. 38, pp. 63-69, 2014.

[367] Bikash Kumar Jena, Stephen J. Percival, and B. Zhang, "Au Disk Nanoelectrode by Electrochemical Deposition in a Nanopore," *Analytical Chemistry,* vol. 82, pp. 6737–6743, 2010.

[368] C. M. Muller, F. C. Mornaghini, and R. Spolenak, "Ordered arrays of faceted gold nanoparticles obtained by dewetting and nanosphere lithography," *Nanotechnology,* vol. 19, p. 485306, Dec 3 2008.

[369] S. Namsani and J. K. Singh, "Dewetting dynamics of a gold film on graphene: implications for nanoparticle formation," *Faraday discussions,* vol. 186, pp. 153-70, 2016.

[370] M. I. Ali Umar, C. C. Yap, R. Awang, A. Ali Umar, M. Mat Salleh, and M. Yahaya, "Formation of gold-coated multilayer graphene via thermal reduction," *Materials Letters,* vol. 106, pp. 200-203, 2013.

[371] R. S. Goeke and A. K. Datye, "Model oxide supports for studies of catalyst sintering at elevated temperatures," *Topics in Catalysis,* vol. 46, pp. 3-9, 2007.

[372] V. Flexer, N. Brun, O. Courjean, R. Backov, and N. Mano, "Porous mediator-free enzyme carbonaceous electrodes obtained through Integrative Chemistry for biofuel cells," *Energy Environ. Sci.,* vol. 4, pp. 2097-2106, 2011.

[373] S. Tsujimura, Y. Kamitaka, and K. Kano, "Diffusion-Controlled Oxygen Reduction on Multi-Copper Oxidase-Adsorbed Carbon Aerogel Electrodes without Mediator," *Fuel Cells,* vol. 7, pp. 463-469, 2007.

[374] M. Pasta, F. La Mantia, and Y. Cui, "Mechanism of glucose electrochemical oxidation on gold surface," *Electrochimica Acta,* vol. 55, pp. 5561-5568, 2010.

[375] J. Zhao, X. Kong, W. Shi, M. Shao, J. Han, M. Wei, D. G. Evans, and X. Duan, "Self-assembly of layered double hydroxide nanosheets/Au nanoparticles ultrathin films for enzyme-free electrocatalysis of glucose," *Journal of Materials Chemistry,* vol. 21, p. 13926, 2011.

[376] C. Zhu, S. Guo, and S. Dong, "PdM (M = Pt, Au) bimetallic alloy nanowires with enhanced electrocatalytic activity for electro-oxidation of small molecules," *Advanced materials,* vol. 24, pp. 2326-31, May 2 2012.

[377] S. Biella and M. Rossi, "Gas phase oxidation of alcohols to aldehydes or ketones catalysed by supported gold," *Chemical Communications,* pp. 378-379, 2003.

[378] L. Thi Xuan Huong, B. Mikhael, C. Joffrey, and C. Marc, "A highly active based graphene cathode for the electro-fenton reaction " *RSC Adv.,* vol. 5, pp. 42536-42539 2015

[379] A. Ozcan and M. Gencten, "Investigation of acid red 88 oxidation in water by means of electro-Fenton method for water purification," *Chemosphere,* vol. 146, pp. 245-52, Mar 2016.

[380] S. Garcia-Segura, E. Brillas, L. Cornejo-Ponce, and R. Salazar, "Effect of the Fe3+/Cu2+ ratio on the removal of the recalcitrant oxalic and oxamic acids by electro-Fenton and solar photoelectro-Fenton," *Solar Energy,* vol. 124, pp. 242-253, 2016.

[381] M. A. Fernandez de Dios, A. G. del Campo, F. J. Fernandez, M. Rodrigo, M. Pazos, and M. A. Sanroman, "Bacterial-fungal interactions enhance power generation in microbial fuel cells and drive dye decolourisation by an ex situ and in situ electro-Fenton process," *Bioresource technology,* vol. 148, pp. 39-46, Nov 2013.

[382] X. W. Liu, X. F. Sun, D. B. Li, W. W. Li, Y. X. Huang, G. P. Sheng, and H. Q. Yu, "Anodic Fenton process assisted by a microbial fuel cell for enhanced degradation of organic pollutants," *Water research,* vol. 46, pp. 4371-8, Sep 15 2012.

[383] Y. Gong, C. Zhang, Q. Yan, W. He, W. Xiao, J. Lin, and Z. Liu, "Enhanced enzymatic hydrolysis of sugarcane bagasse hemicellulose using recombinant glucose oxidase expressed by Pichia pastoris," *Industrial Crops and Products,* vol. 77, pp. 458-466, 2015.

[384] M. G. Hosseini and I. Ahadzadeh, "Electrochemical impedance study on methyl orange and methyl red as power enhancing electron mediators in glucose fed microbial fuel cell," *Journal of the Taiwan Institute of Chemical Engineers,* vol. 44, pp. 617-621, 2013.

[385] C.-C. Chen, C.-L. Lin, and L.-C. Chen, "Functionalized Carbon Nanomaterial Supported Palladium Nano-Catalysts for Electrocatalytic Glucose Oxidation Reaction," *Electrochimica Acta,* vol. 152, pp. 408-416, 2015.

[386] A. M. Ghonim, B. E. El-Anadouli, and M. M. Saleh, "Electrocatalytic glucose oxidation on electrochemically oxidized glassy carbon modified with nickel oxide nanoparticles," *Electrochimica Acta,* vol. 114, pp. 713-719, 2013.

[387] J.-S. Ye, Z.-T. Liu, C.-C. Lai, C.-T. Lo, and C.-L. Lee, "Diameter effect of electrospun carbon fiber support for the catalysis of Pt nanoparticles in glucose oxidation," *Chemical Engineering Journal,* vol. 283, pp. 304-312, 2016.

[388] C.-T. Hsieh, Y.-F. Chen, and P.-Y. Yu, "Deposition of binary Pd–Rh catalysts on nanostructured carbon supports for non-enzymatic glucose oxidation," *International Journal of Hydrogen Energy,* vol. 40, pp. 14857-14865, 2015.

[389] D. Basu and S. Basu, "A study on direct glucose and fructose alkaline fuel cell," *Electrochimica Acta,* vol. 55, pp. 5775-5779, 2010.

[390] K. W. Jung, D. S. Park, M. J. Hwang, and K. H. Ahn, "Decolorization of Acid Orange 7 by an electric field-assisted modified orifice plate hydrodynamic cavitation system: Optimization of operational parameters," *Ultrasonics sonochemistry,* vol. 26, pp. 22-9, Sep 2015.

[391] A. Abou Chaaya, R. Viter, I. Baleviciute, M. Bechelany, A. Ramanavicius, Z. Gertnere, D. Erts, V. Smyntyna, and P. Miele, "Tuning Optical Properties of Al2O3/ZnO Nanolaminates Synthesized by Atomic Layer Deposition," *Journal of Physical Chemistry C,* vol. 118, pp. 3811-3819, Feb 20 2014.

[392] A. Abou Chaaya, R. Viter, M. Bechelany, Z. Alute, D. Erts, A. Zalesskaya, K. Kovalevskis, V. Rouessac, V. Smyntyna, and P. Miele, "Evolution of microstructure and related optical properties of ZnO grown by atomic layer deposition," *Beilstein Journal of Nanotechnology,* vol. 4, pp. 690-698, Oct 28 2013.

[393] Adib Abou Chaaya, Mikhael Bechelany, Sebastien Balme, and P. Miele, "ZnO 1D nanostructures designed by combining atomic layer deposition and electrospinning for UV sensor applications," *Journal of Materials Chemistry A,* vol. 2, p. 20650, 2014.

[394] M. Jiang, X. Cao, D. Zhu, Y. Duan, and J. Zhang, "Hierarchically Porous N-doped Carbon Derived from ZIF-8 Nanocomposites for Electrochemical Applications," *Electrochimica Acta,* vol. 196, pp. 699-707, 2016.

[395] X. Ma, L. Li, S. Wang, M. Lu, H. Li, W. Ma, and T. C. Keener, "Ammonia-treated porous carbon derived from ZIF-8 for enhanced CO2 adsorption," *Applied Surface Science,* vol. 369, pp. 390-397, 2016.

[396] N. Alexeyeva, E. Shulga, V. Kisand, I. Kink, and K. Tammeveski, "Electroreduction of oxygen on nitrogen-doped carbon nanotube modified glassy carbon electrodes in acid and alkaline solutions," *Journal of Electroanalytical Chemistry,* vol. 648, pp. 169-175, 2010.
[397] Y. Liu, S. Chen, X. Quan, H. Yu, H. Zhao, and Y. Zhang, "Efficient Mineralization of Perfluorooctanoate by Electro-Fenton with H2O2 Electro-generated on Hierarchically Porous Carbon," *Environmental science & technology,* vol. 49, pp. 13528-33, Nov 17 2015.
[398] W. Ren, Q. Peng, Z. a. Huang, Z. Zhang, W. Zhan, K. Lv, and J. Sun, "Effect of Pore Structure on the Electro-Fenton Activity of ACF@OMC Cathode," *Industrial & Engineering Chemistry Research,* vol. 54, pp. 8492-8499, 2015.

Appendix

The thesis summary in French

Résumé en français

Ce manuscrit de thèse est consacré à la modification de feutres de carbone pour la préparation de matériaux d'électrodes hautement performants pour le procédé électro-Fenton (EF), appliqué aux traitements des eaux chargées en polluants bioréfractaires. Dans un premier temps, des feutres de carbone commerciaux (CF) ont été mis en œuvre pour optimiser l'élimination de colorants (Acide Orange) et de produits pharmaceutiques (Paracétamol, Amoxicilline). Les chemins réactionnels conduisant à la minéralisation de ces polluants bioréfractaires ont été élucidés et la toxicité des sous-produits identifiés a été déterminée à différents temps d'électrolyse. Dans la suite du travail, une nouvelle cathode a été préparée par dépôt électrochimique d'oxyde de graphène réduit (rGO) sur la surface des feutres de carbone commerciaux. Divers moyens de réduction ont été étudiés et les propriétés structurales et texturales de l'électrode modifiée ont été déterminées par SEM, XRD, XPS, BET et mesure d'angle de contact. La cathode élaborée présente une bonne stabilité et une grande efficacité de traitement lorsqu'elle est appliquée pour décomposer l'Acide Orange 7 (AO7), la molécule de colorant azoïque modèle choisie. Dans une dernière partie du travail, nous avons proposé un système original de traitement électrochimique de type EF à base d'une pile à glucose. Dans ce système, l'énergie nécessaire est fournie par l'oxydation du glucose à l'anode, sur feutre de carbone décoré de nanoparticules d'or alors que la cathode est constituée du feutre modifié par un carbone microporeux dopé en azote présentant des propriétés d'électrocatalyse compatibles à la réduction de l'oxygène en peroxyde d'hydrogène dans la cellule de type pile à combustible. Le manuscrit présente la synthèse et la caractérisation de ces deux électrodes. L'originalité du travail réside en la quantité particulièrement faible d'or nécessaire à l'anode et au potentiel de réduction de l'oxygène particulièrement bas obtenus sur les carbones microporeux dopés à l'azote. Les propriétés catalytiques de l'anode et de la cathode ont induit une densité de courant de sortie stable (360,3 ± 51,5 $mA.m^{-2}$ à 400 ± 50 mV) et maintenue à long terme. En conséquence, 90% de la concentration initiale du polluant (AO7) a été éliminée après une dégradation prolongée de 10 h. La puissance de la cellule est faible (170 $mW.m^{-2}$) mais stable au moins pendant deux mois. Cette première preuve de concept d'un système abiotique de type pile à combustible - Fenton a démontré une efficacité élevée vis-à-vis de la dégradation des polluants bioréfractaires avec un énorme potentiel dans les domaines liés à l'énergie et la protection de l'environnement.

1. Introduction

1.1. Problématique

L'industrialisation des sociétés a été identifiée de longue date comme une cause majeure de la contamination de l'environnement *via* entre autres les rejets d'eaux usées. Les eaux usées contenant des polluants organiques persistants (POP) constituent toujours une menace pour les écosystèmes en raison de leur toxicité élevée et de leur difficulté à être traitées par les méthodes classiques physiques et chimiques. Les processus d'oxydation avancée (AOP) sont largement étudiés pour l'élimination des polluants organiques bioréfractaires. Au cours de la dernière décennie, les AOPs ont suscité un intérêt croissant pour éliminer efficacement de nombreux polluants, comme les colorants de l'industrie textile. Les AOPs sont des méthodes chimiques, photochimiques ou électrochimiques respectueuses de l'environnement dont la caractéristique commune est la production in situ de radicaux hydroxyle (OH°) en tant qu'agent oxydant. L'un des AOP chimique les plus populaires est le procédé de Fenton, où le mélange Fe^{2+} / H_2O_2 (réactif de Fenton) est utilisé pour dégrader les composés organiques. Pour éviter d'utiliser des réactifs chimiques, le peroxyde d'hydrogène peut être également produit par l'électroréduction d'O_2 dissous sur électrode à base de graphite. Lorsque cette réduction est réalisée en présence de Fe^{2+}, le procédé mis en place est appelé électro-Fenton. Il est globalement plus efficace que le processus basique de Fenton et plus facile à gérer [1]. Dans ce procédé, les matériaux carbonés sont généralement utilisés comme cathode, tels que le graphite tridimensionnel [2], le carbone vitreux réticulé (RVC) [3, 4], l'éponge de carbone [5], le feutre de graphite [6] ou la fibre de charbon actif (ACF) [7, 8]. Le processus d'électro-Fenton utilisant des cathodes à feutres de carbone et de graphite a été appliqué pour éliminer avec succès de nombreux types de POPs : des colorants [6], des composés pharmaceutiques [9], des herbicides et des pesticides [10-12]. Il a été prouvé qu'il peut dégrader efficacement les contaminants initiaux très toxiques en des composés non toxiques comme le CO_2, l'eau et des acides carboxyliques à chaîne courte [13]. En raison des potentiels prometteurs de traitement des eaux usées par le procédé EF, il sera utile et nécessaire d'améliorer son efficacité pour une tendre vers une technologie à faible coût, propre et verte. C'est le but principal de ce travail de thèse.

1.2. Objectifs de recherche

Les objectifs de cette étude sont les suivants :

• Optimiser la minéralisation de polluants bioréfractaires modèles de type colorants et résidus pharmaceutiques par le procédé EF ; Les paramètres importants affectant directement les résultats tels que le courant appliqué, la concentration de catalyseur seront étudiés en utilisant des feutres de carbone commerciaux. En outre, la corrélation entre les voies de dégradation et la toxicité des POPs et de leurs sous-produits seront soigneusement étudiés en vue de la connaissance globale de l'ensemble du procédé de traitement.

• Modifier les feutres de carbone commerciaux pour améliorer l'efficacité du processus EF ; pour cela les feutres seront modifiés par du graphène selon différents processus. Une corrélation entre les propriétés physico-chimiques et électrochimiques des cathodes et leurs propriétés d'usage sera recherchée.

• Diminuer le coût du traitement EF en proposant un nouveau type de système de traitement auto-généré sur la base du fonctionnement d'une pile à combustible, alimentée dans notre cas en glucose à l'anode et en oxygène de l'air à la cathode.

1.3. Plan du manuscrit

Les objectifs détaillés ci-dessus, ont été traités dans le manuscrit selon le plan suivant :

• Chapitre 1 : Introduction générale

• Chapitre 2 : Revue de la littérature. Dans cette partie d'état de l'art, les propriétés des matériaux à base de feutres de carbone et de graphite ainsi que les méthodes de modification et les applications de ces matériaux ont été détaillés.

• Chapitre 3 : Il est consacré à la détermination des corrélations entre la dégradation électrochimique des polluants bioréfractaires dans des conditions optimisées, les voies de minéralisation et la toxicité des effluents au cours du traitement. Deux types de polluants sont étudiés, un colorant azoïque, l'Acide Orange 7 et une molécule pharmaceutique, l'acétaminophène ou paracétamol.

• Chapitre 4 : Les modifications de feutres de carbone commerciaux par de l'oxyde de graphène réduit (rGO) sont présentées. Les matériaux sont caractérisés d'un point de vue physico-chimique et électrochimique et enfin utilisés comme cathode dans le procédé électro-Fenton appliqué à la minéralisation du colorant Acide Orange 7.

• Chapitre 5 : Il est dédié à la préparation d'une anode par modification de feutre de carbone commerciaux par des nanoparticules d'or électrogénérées. Le matériau obtenu est caractérisé et ses propriétés d'électrocatalyse du glucose démontrée. Cette anode est alors associée à une cathode enzymatique pour la réalisation d'une biopile hybride alimentée en glucose et oxygène de l'air.

• Chapitre 6 : Il est consacré à la préparation d'une nouvelle cathode obtenue par le dépôt sur le feutre de carbone d'une couche de carbone microporeux dopé à l'azote qui va permettre de baisser le potentiel de réduction de l'oxygène en peroxyde d'hydrogène. Dans ce chapitre, cette cathode est associée à l'anode décorée de nanoparticules d'or préparée au chapitre 5, pour réaliser une cellule électrochimique permettant la dégradation des polluants bioréfractaires dans un système de type pile à combustible.

2. Revue de la littérature

Les feutres de carbone et de graphite sont couramment utilisés comme électrodes en raison de leur bonne conduction électronique, une structure 3D avec une surface et une porosité élevées pour fournir de nombreux sites de réaction redox, une excellente efficacité électrolytique, une stabilité mécanique et un coût relativement faible [14-17]. Cependant, il est intéressant d'améliorer leur mouillabilité peu adaptée à une utilisation en milieu aqueux et leur activité électrochimique en raison de leur hydrophobicité de surface et de la faible cinétique vis-à-vis des réactions de réduction et d'oxydation [18, 19]. Dans le but de rendre ces électrodes plus actives, différentes techniques de modification ont donc été présentées et discutée de manière à corréler méthodes de modification, propriétés physico-chimiques et propriétés d'usage dans le domaine de l'énergie et du traitement des eaux usées.

3. Feutre de carbone commercial pour l'élimination de l'acide orange 7 et de l'acétaminophène par le procédé Electro-Fenton

Ce chapitre a porté sur l'utilisation de feutres de carbone commerciaux comme cathode pour éliminer l'acide orange 7 (AO7) et l'acétaminophène (ACE) par le procédé électro-Fenton. Dans la partie consacrée à la dégradation de l'AO7, nous avons résolu les problèmes suivants: (1) Trouver les conditions optimales (courant appliqué et concentration de catalyseur de fer) pour le

traitement de 200 mL d'AO7 (0,1 mM), (2) Utiliser différentes méthodes analytiques comme HPLC-UV, LC-MS, IC pour déterminer la voie de dégradation de l'AO7 et (3) Déterminer la toxicité de la solution traitée ainsi que celle des sous-produits pris individuellement et en mélange par la méthode Microtox utilisant les bactéries marines Vibrio fischeri. Les expériences de dégradation et de toxicité ont été effectuées sur 500 mL d'AO7 (1 mM) avec les paramètres optimaux qui ont été trouvés dans la première étape. De même, les conditions optimales de courant appliqué et de concentration en catalyseur au fer ont été utilisées pour traiter l'ACE. La corrélation entre la voie de dégradation et la toxicité de l'ACE ainsi que leurs sous-composés a également été étudiée.

3.1. Partie expérimentale

Les expériences d'Electro-Fenton ont été effectuées à température ambiante dans une cellule de verre cylindrique à un compartiment de 500 ml avec un système à deux électrodes (Figure 3.1). Le courant appliqué a été contrôlé grâce à une alimentation électrique (Lambda Electronic, USA) en mode galvanostatique. La cathode à feutre de carbone (60 cm2) a été utilisée comme électrode de travail et une grille cylindrique en platine comme contre-électrode. L'anode est centrée dans la cellule électrolytique, entourée par la cathode, qui couvre la paroi intérieure de la cellule. La distance entre les électrodes est de 1,5 cm. Une solution aqueuse d'AO7, Na2S04 (50 mM) est utilisée en tant qu'électrolyte support et FeSO4.7H2O en tant que catalyseur en ajustant le pH à 3,0 avec de l'acide sulfurique (H2SO4). Des conditions différentes de concentration de catalyseur à 0,05, 0,1, 0,2, 1 et 2 mM et des courants appliqués à 60, 100, 300, 500 et 700 mA ont d'abord été étudiées afin de déterminer les conditions optimales pour la minéralisation de 200 mL de solutions d'AO7 à 0,1 mM. Ensuite, la mise en évidence des sous-produits intermédiaires de dégradation a été effectuée dans 500 mL de solution d'AO7 / ACE (1 mM), de FeSO4.7H2O (0,2 mM) avec un courant appliqué de 500 mA pendant l'expérience. Avant l'électrolyse, un bullage d'oxygène a été effectué pendant 5 minutes pour saturer les solutions et maintenu pendant l'expérience sous agitation magnétique continue à une vitesse de 800 tr / min.

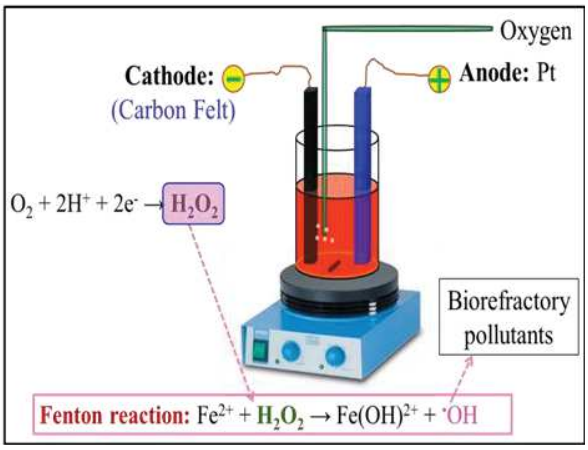

Figure 3.1. Schéma de la cellule électrochimique de dégradation par le processus EF.

3.2. Résultats

3.2.1. Évaluation de l'élimination de la toxicité du colorant azoïque AO7 : vers une optimisation du traitement électro-Fenton

3.2.1.1. Effet du courant appliqué sur la cinétique de dégradation

Dans le procédé EF, le courant appliqué est un paramètre important pour le coût opérationnel et l'efficacité du processus [20]. Pour évaluer l'effet du courant appliqué sur la cinétique de décomposition de l'AO7, des courants différents ont été étudiés comme suit: à 60, 100, 300, 500 et 700 mA. Le taux de minéralisation a augmenté rapidement avec l'augmentation du courant cathodique de 60 mA à 500 mA. A partir de 500 mA, le procédé conduit à une élimination stable et quasi complète des colorants de la solution de colorant après seulement 3 min.

3.2.1.2. Effet de la concentration du catalyseur sur l'efficacité de la minéralisation

Le taux de minéralisation augmente avec une augmentation de la concentration de Fe^{2+} de 0,05 à 0,2 mM, car une concentration de catalyseur plus élevée entraîne une production plus élevée de radicaux hydroxyle à la cathode. Cependant, pour des concentrations plus importantes de catalyseur (jusqu'à 2 mM), une diminution de l'élimination du COT a été observée. Ceci est caractéristique d'une réaction secondaire qui se déroule entre l'excès de radicaux produit et les espèces de fer, comme mentionné dans des études antérieures concernant le processus EF [21, 22]. Par conséquent, la concentration optimale en catalyseur est de 0,2 mM, valeur de concentration fixée dans la suite du travail.

3.2.1.3. Voie de dégradation de l'Acide Orange 7 lors du processus EF

À partir de l'identification des sous-produits par les méthodes HPLC-UV et LC-MS, des voies possible pour la dégradation du colorant AO7 par le procédé électro-Fenton sont proposée figure 3.2. Le processus a été initié par une attaque du nradical OH] entraînant la formation de deux molécules hydroxylées, c'est-à-dire le 4-[(2,3-dihydroxy-1-naphthyl)diazenly]-benzenesulfonate (m/z = 346) (XI) et le 4-[(2,3,4-trihydroxy-1-naphthyl)diazenly]-benzenesulfonate (m/z = 362) (XII) qui ont été identifiés dans les premières minutes de la réaction EF. Ces intermédiaires hydroxylés ont rarement été observés dans les études antérieures traitant de la dégradation du colorant AO7. La formation de ces intermédiaires a toutefois été rapportée lors de la dégradation photocatalytique du colorant azoïque dans une solution aqueuse en présence du catalyseur TiO_2 [23]. Le processus se poursuit avec l'attaque de la liaison azoïque pour former les intermédiaires suivants: 1,2-naphtoquinone (IV) et l'acide 4-hydroxybenzènesulfonique (VI). Ensuite, l'acide 4-hydroxylbenzènesulfonique a subi une autre désulfonation pour former la 1,4-benzoquinone (II) qui a ensuite été oxydée en hydroquinone hydroxylée (I) et potentiellement la 1,2,4-benzentriol. Ce dernier produit pouvant difficilement être identifié car il est instable et rapidement transformé en acides carboxyliques par des réactions d'ouverture de cycles. L'intermédiaire (IV) est oxydé pour former des composés du type naphtalène bien identifiés, tels que la 2-hydroxy-1,4-naphtalènedione (V), la 2,3-dihydroxy-1,4-naphtalènedione (VIII), le 1,2-naphtalènedol (IX) et le 2-naphtol (VII). La formation de ces produits de type naphtalène a également été rapportée dans plusieurs études antérieures portant sur la dégradation de l'AO7 [24, 25]. Par action des radicaux, les sous-produits de naphtalène ont été décomposés en 1 (3H) -isobenzofuranone (X) et en 2-formyl-benzoïque (III). Ces derniers sous-produits aromatiques ont encore été dégradés pour générer des acides carboxyliques à chaîne courte comprenant l'acide fumarique, l'acide maléique, l'acide oxalique et l'acide oxamique. Enfin, ces acides organiques ont été décomposés en CO_2, H_2O et ions inorganiques.

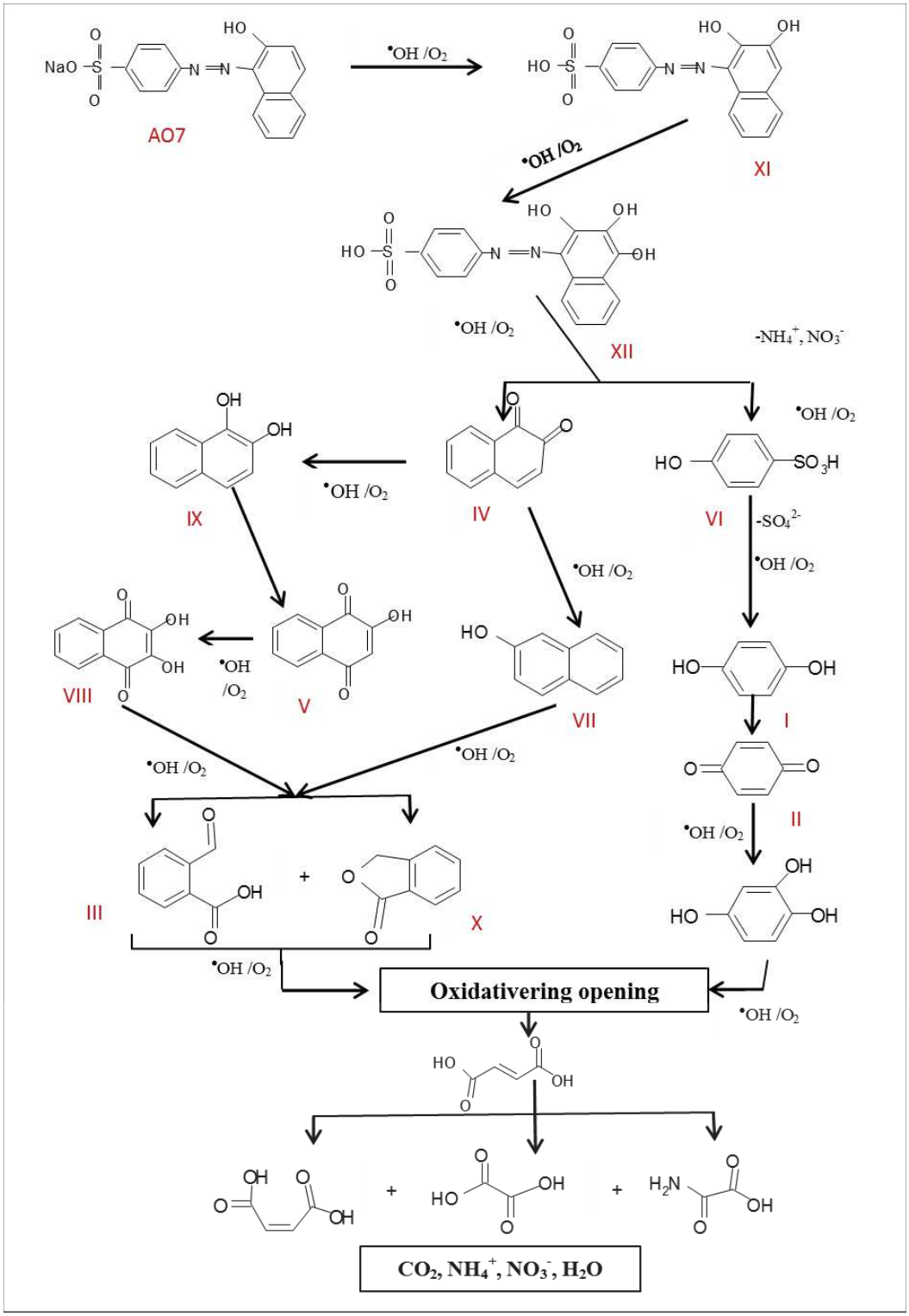

Figure 3.2. : Voies de dégradation de l'acide orange 7 par le procédé EF

La toxicité des solutions traitée a été mesurée en déterminant l'inhibition des bactéries marines Vibrio fischeri après 5 min et 15 minutes d'exposition. Au début de processus EF, l'inhibition de la luminescence qui reflète la toxicité de la solution augmente immédiatement jusqu'à 100% et reste à cette valeur pendant 20 minutes pour 200 ml d'AO7 0,1 mM et 100 minutes pour 500 ml d'AO7 1 mM. Cela est très certainement lié à la formation de composés très toxiques comme le 2-naphtol (NOL); 2-hydro-1,4naphtoquinone (HNQ); 1,2-naphtoquinone (NAPQ) et 1,4-benzoquinone (BZQ) (Figure 5a), comme l'ont déjà montré d'autres études [26-30]. Après cela, la décomposition de ces produits et l'émergence d'acides carboxyliques à chaîne courte ont conduit à la forte baisse de la toxicité de la solution, confirmée par l'évolution du taux d'inhibition, qui tend rapidement vers zéro après 80 min et 270 min pour 200 mL de 0,1 mM AO7 et 500 mL d'AO7 1 mM respectivement.

3.2.2. Corrélation entre la voie de dégradation et la toxicité de l'acétaminophène et de ses sous-produits, lors de la minéralisation par le procédé électro-Fenton

L'évolution des sous-produits de dégradation d'une solution d'acétaminophène (ACE) a été suivie par HPLC-UV / MS et IC parallèlement à son écotoxicité (tests de dépistage Microtox® Vibrio Fischeri 81,9%) lors de son oxydation par électro-Fenton (EF). Les composés aromatiques 2-hydroxy-4- (N-acétyl) aminophénol, 1,4-benzoquinone, benzaldéhyde et acide benzoïque ont été identifiés comme sous-produits toxiques lors de la première étape du traitement électrochimique alors que les acides carboxyliques aliphatiques à chaîne courte (oxalique, maléique, oxamique, formique, acétique, fumarique) et les ions inorganiques (ammonium, nitrate) ont été bien identifiés comme sous-produits terminaux non toxiques. La toxicité de chaque produit intermédiaire produit lors de la minéralisation de l'ACE a été quantifiée et une relation a été établie entre la voie de dégradation de l'ACE et l'évolution globale de la toxicité de la solution. Après deux heures de traitement seulement (volume solution 500 mL, concentration ACE 1 mM), la solution ne présente plus de toxicité selon le test Microtox®. Après 8 heures de traitement, une élimination de TOC de 86,9% a pu être atteinte pour ACE 0,1 mM à un courant appliqué de 500 mA avec 0,2 mM de Fe^{2+} utilisé comme catalyseur.

4. Minéralisation du colorant Acide Orange 7 par procédé Electron-Fenton sur feutres de carbone modifié par du graphène

L'objectif de ce chapitre est de réaliser la modification de feutres de carbone commerciaux (CF) par dépôt d'oxyde de graphène réduit (rGO) pour augmenter la production de peroxyde d'hydrogène (H_2O_2). Dans le procédé EF, H_2O_2 joue un rôle important pour la génération des radicaux hydroxyle (OH°), qui est le principal agent oxydant pour attaquer les POPs. Il y a deux objectifs principaux dans ce chapitre: (1) modification de CF par différentes méthodes de réduction de l'oxyde de graphène. Les propriétés du feutre de carbone modifié ont été caractérisées par diverses techniques physiques et électrochimiques et (2) application du feutre fabriqué (2 cm2) comme cathode pour éliminer l'AO7 en milieu acide. Pour les applications environnementales, la stabilité à long terme des matériaux cathodiques étant une propriété clé, les expériences EF ont été répétées après dix cycles, et l'efficacité de dégradation a été identifiée par mesure de TOC après 2 h d'électrolyse.

4.1. Résultats

Une nouvelle cathode pour le procédé électro-Fenton a été mise en place par dépôt électrochimique d'oxyde de graphène réduit (rGO) à la surface du feutre de carbone (CF). Les propriétés structurales de l'électrode modifiée ont été étudiées. Parmi les différentes méthodes de réduction utilisées, la réduction à potentiel constant a démontré une performance considérable. Les paramètres affectant la conversion de GO en rGO, tels que le pH, le potentiel appliqué et la durée du processus de réduction, ont été étudiés. La cathode modifiée rGO présente des propriétés électrochimiques améliorées comme une augmentation du courant redox et une diminution de la résistance au transfert de charge en présence de la sonde redox $[Fe(CN)_6]^{3-}$ /$[Fe(CN)_6]^{4-}$. Cette amélioration a considérablement augmenté le taux de production du peroxyde d'hydrogène comme confirmé par une analyse en voltamétrie de balayage linéaire (LSV) et une quantification par colorimétrie de la concentration en peroxyde dans le milieu. Cette nouvelle cathode présente en outre une bonne stabilité après 10 cycles d'utilisation (Fig. 4.1.b) ce qui montre que cette rGO-CF est une électrode puissante et prometteuse pour améliorer l'efficacité vis à vis de la dégradation des polluants émergents.

Tableau 4 1. Constantes apparentes de première ordre et abattements pour la cinétique de dégradation de l'AO7 sur les CF brutes et les CF modifiés par l'oxyde de graphène réduit (CPR-CF).

Cathode	k_{app} (min^{-1})	R^2	Abattement (%) après 3 min
CF non modifié	0.2596	0.9961	54.2
CPR-CF	0.7846	0.9987	89.7

En particulier, au cours des 2 premières heures, une minéralisation plus rapide a été obtenue avec les feutres modifiés au graphène, par rapport aux CF brutes, ce qui peut s'expliquer par une production plus élevée de •OH dans le système et, d'une manière générale, une dégradation plus rapide des produits intermédiaires de l'AO7. L'élimination du TOC après 2 h de traitement a atteint 73,9% sur l'électrode modifiée, ce qui est 18,3% supérieur à celui des CF brutes. Après 8 h d'électrolyse (Figure 4.1 a), on peut obtenir 94,3% de minéralisation. En outre, les constantes de vitesse apparentes pour la dégradation de l'AO7 ont été déterminées [20, 31, 32]. Une valeur de 0,7846 min^{-1} a été obtenue pour CPR-CF, soit plus de près de 3 fois la valeur obtenue pour le feutre non modifié (tableau 4 1). Pour conclure, ces bons résultats de dégradation et de minéralisation obtenus sur l'électrode CPR-CF ont été attribués à une structuration de surface conduisant à une augmentation de la surface électroactive par la méthode d'électro-réduction et, par conséquent, à des propriétés électrochimiques améliorées par rapport aux CF brutes. Cette méthode de modification pourrait fournir une solution efficace pour améliorer les performances du processus d'autant plus qu'après 10 cycles d'utilisation (80 h), le taux de minéralisation de la cathode modifiée n'a diminué que de 9,6%, certainement en raison d'une perte de matière électroactive (Figure 4.1 b).

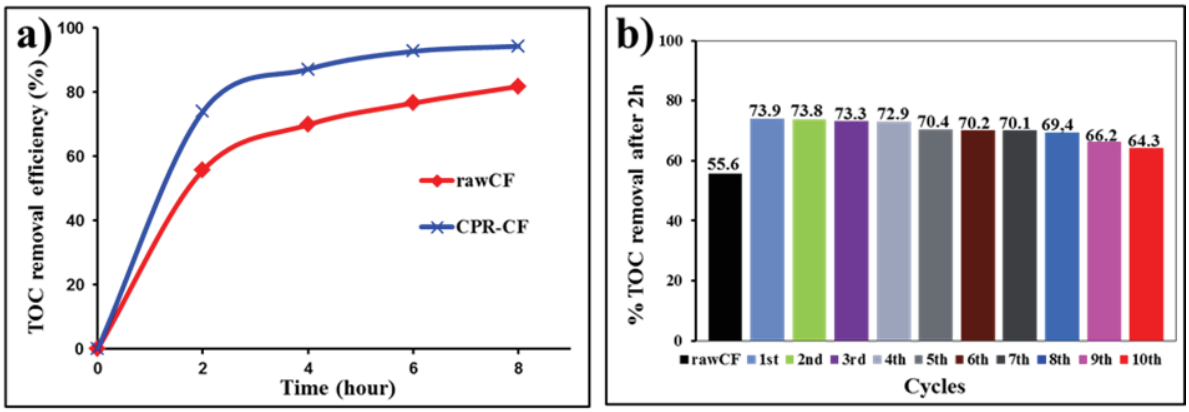

Figure 4.1. Suivi de la minéralisation de l'AO7 avec le temps d'électrolyse (a) 8 h and (b) 2 h de traitement. Conditions: Pt anode; V=30 mL, [AO7]=0.1 mM; [Fe2+]=0.2 mM; pH=3; [Na2SO4]=50 mM, I = 40 mA, cathode: CF non modifié et CF modifié oxyde de graphène réduit (CPR-CF) 10 cycles.

5. Croissance de nanoparticules d'or sur feutre de carbone pour une utilisation comme matériau d'anode dans une biopile hybride

Ce chapitre a pour but de réaliser une biopile à combustible (BFC) hybride en associant une anode abiotique à base de feutre de carbone modifié par des particules d'or (CF@Au) et une biocathode enzymatique, dans une cellule à deux compartiments séparée par une membrane Nafion®. À l'anode, des particules d'or sur feutre de carbone catalysent l'oxydation du glucose pour produire les électrons qui sont transférés dans le compartiment cathodique où l'oxygène est réduit par catalyse enzymatique. Trois éléments principaux ont été nécessaires pour résoudre ce chapitre, notamment: (1) Dépôt de particules d'or à la surface du feutre de carbone par électrodéposition et traitement thermique; (2) Tests de l'électrode CF@Au pour l'électrooxydation du glucose et (3) Evaluation des performances du système hybride via l'enregistrement de la puissance générée et de la stabilité du système.

5.1. Résultats

Dans cette étude, une croissance de particules d'or dispersées de manière homogène sur des feutres de carbone (CF@Au) a été réalisée par électrodéposition suivie d'un traitement thermique à 1000 °C sous azote. Le traitement thermique a induit la formation de nanoparticules d'or bien cristallisées de grande surface spécifique. Les propriétés structurales du matériau CF@Au résultant ont été évaluées par SEM, XRD et TGA. Nous avons étudié les propriétés

électrocatalytiques de ce nouveau matériau vis-à-vis de l'oxydation abiotique du glucose en milieu alcalin et montré la potentialité du matériau CF@Au associé à une cathode enzymatique pour construire une cellule électrochimique. Cette cellule présente des performances électrochimiques élevées avec une tension de circuit ouvert de 0,71 V et une densité de puissance maximale de 310 μW cm^{-2} à 352 mV, malgré une très faible charge d'or (0,2% en poids).

6. Conception d'un nouveau système de piles à combustible-Fenton: une approche permettant un traitement autonome de la pollution bioréfractaire

Pour diminuer le coût d'exploitation du processus EF, la puissance nécessaire au fonctionnement de l'électrolyseur pourrait être fournie par l'oxydation spontanée du glucose à l'anode CF@Au en fonctionnement pile à combustible. Néanmoins, cette oxydation a lieu à un potentiel (-0,46 V vs Ag/AgCl) ne permettant pas d'utiliser une combinaison de l'anode CF@Au avec les CF brutes ou modifiés par rGO utilisés à la cathode puisque la réaction de réduction de l'oxygène (ORR) se produit à environ 0,67 V vs Ag/AgCl pour ces deux types de feutre de carbone. Par conséquent, deux objectifs ont été ciblés dans ce chapitre notamment: (1) Préparer une nouvelle cathode par modification de feutre de carbone par une couche de carbone microporeuse dopée à l'azote pour améliorer la catalyse de réduction de l'oxygène (2) Réaliser le couplage anode CF@Au et cathode en carbone microporeux dopés à l'azote pour traiter le colorant acide orange 7 dans ce nouveau système Fuel Cell - Fenton (FC-Fenton).

6.1. Le système Fuel Cell - Fenton

Le système FC-Fenton est composé de deux compartiments séparés par une membrane perfluorée Nafion® 117 (3,5 cm × 5 cm), comme le montre la figure 6.1. L'anode est constituée de l'électrode CF@Au, tandis que l'électrode cathodique est constituée de carbone microporeux déposé sur un feutre de carbone Commercial CF@pC. Le compartiment anodique est constitué de 90 mL de glucose (0,5 M) dans KOH 0,1 M (pH 11,0), saturé par N_2 sous agitation magnétique, tandis que le compartiment cathodique contient 90 mL de solution aqueuse d'AO7 (Azo Dye acid Orange 7, 0,1 mM) , Avec $FeSO_4.7H_2O$ (0,2 mM) en tant que catalyseur et Na_2S0_4 (50 mM) comme électrolyte support ajusté à pH = 3 et saturé par de l'oxygène. Le pH de chaque compartiment a été maintenu en ajoutant H_2SO_4 (1 M) ou KOH (1 M). La décomposition de AO7 a été surveillée en mesurant l'absorbance du colorant à la longueur d'onde unique de 485 nm, spécifique aux liaisons azoïques [33], avec un Spectrophotomètre Jenway 6300 (Barioworld

Scientific Ltd, Dunmow UK). Les concentrations d'AO7 au cours des expériences ont été mesurées en parallèle par un système HPLC (Waters 717 Autosampler et Waters 616 Pump) avec un Photodiode Array Detector (Waters 2996 Photodiode Array Detector) équipé d'une colonne de phase inversée (RP) Thermo Scientific C18 (L = 250 mm, ID = 4,6 mm et particules de 5 µm).

Les performances électrochimiques du système FC-Fenton ont été évaluées en reliant l'anode abiotique et la cathode électro-Fenton sous une résistance de décharge de 5 ohms. L'évolution du potentiel de chaque électrode a été mesurée indépendamment en introduisant une électrode de référence (Ag/AgCl) dans chaque compartiment. La densité de courant délivrée et la densité de puissance de sortie ont été déduites de la résistance et de la tension de la cellule (U), avec P ($mW.m^{-2}$) = U (V) .j ($mA.m^{-2}$).

Figure 6.1. Schéma de principe du système Fuel Cell-Fenton.

6.2. Résultats

Le polluant modèle Acide Orange 7 (AO7) a été éliminé efficacement en milieu aqueux par un système de pile à combustible Fenton (FC-Fenton) sans alimentation externe. Dans cette approche, l'AO7 a été dégradé par le procédé électro-Fenton grâce à l'association de la cathode microporeuse alimentée en oxygène dissous et de l'anode à base de nanoparticules d'or alimentée en glucose. La cathode a été fabriquée par une voie combinant dépôt par couches atomiques (ALD) de ZnO sur des feutres de carbone commerciaux (CF) suivie d'une conversion solvothermale ultérieure de l'oxyde métallique en un MOF (ici ZIF-8). Le matériau composite préparé a été finalement calciné à haute température sous atmosphère d'azote pour obtenir une couche microporeuse à base de carbone (pC) avec une surface spécifique élevée et contenant de l'azote en tant que dopant. A la fois la conductivité et les propriétés électrocatalytiques vis-à-vis

de la production de H_2O_2 à partir de la réduction de l'oxygène ont été améliorées grâce à ce nouveau matériau d'électrode. La cinétique de dégradation de l'AO7 (concentration initiale 0,1 mM) à la cathode CF@pC a été enregistrée par spectrophotométrie UV-vis et Chromatographie liquide haute performance (HPLC) pour prouver l'efficacité du matériau composite pour la dégradation d'un tel modèle bio-réfractaire de molécule. Grâce à un taux de production d'H_2O_2 élevé (9,2 mg L^{-1} h^{-1}) au sein de la couche microporeuse de carbone, l'AO7 (35,0 mg/L) a été dégradé par le procédé électro-Fenton dans un milieu acide (pH = 3) avec une efficacité d'élimination atteignant 90% en 10 h. La durabilité du système a été prolongée pendant plus de 2 mois avec une puissance moyenne de 170 mW m^{-2}, ce qui confirme que ce système abiotique FC-Fenton peut avoir une potentialité comme future technologie prometteuse pour les domaines de l'environnement et de l'énergie.

7. Conclusion

L'amélioration des propriétés de l'électrode de feutre de carbone par différentes méthodes de modification ainsi que son application pour le traitement des eaux usées contenant des polluants organiques persistants par le procédé électro-Fenton vers une dépollution d'énergie nulle est encore une terre fertile pour les études futures dans le domaine de l'énergie et de l'environnement. Dans cette étude, nous avons résolu de nombreux problèmes importants et apporté un grand nombre de résultats intéressants concernant les électrodes à base de feutre au carbone pour les processus EF qui ont été répertoriés comme suit:

(i) Trouver les conditions optimales pour l'élimination de AO7 et d'ACE en milieu aqueux par traitement EF en utilisant une cathode commerciale à feutre de carbone (60 cm2). Ces paramètres correspondaient à 500 mA et 0,2 mM pour la densité de courant appliquée et la concentration du catalyseur. A ces valeurs, la minéralisation de 200 ml d'ACE 0,1 mM et AO7 était respectivement de 86,9% et 96,2%. L'identification et l'évolution des composés intermédiaires, ainsi que la toxicité de la solution, ont également été examinées attentivement le long du procédé EF. Afin de caractériser et de quantifier aussi précisément que possible la formation de sous-produits, le volume de solutions (500 mL) et les concentrations initiales de polluants (1mM) ont été étendus. Douze sous-produits aromatiques pourraient être révélés par des techniques HPLC et LC / MS pendant la décomposition de AO7 et 4 pendant la dégradation de l'ACE. Dans les deux cas, la formation précoce de produits aromatiques toxiques comme la 1,2-naphtoquinone ou la 1,4-benzoquinone a été corrélée à l'augmentation de la toxicité de la solution

atteignant 100% pendant 60 minutes du traitement EF de PCM et pendant 100 minutes pour AO7. La décomposition ultérieure de ces intermédiaires a conduit à la formation d'acides carboxyliques à chaîne courte et donc à une diminution drastique du taux d'inhibition de la luminescence bactérienne. Par conséquent, la désintoxication totale de la solution a été réalisée après 120 minutes et 270 minutes pour ACE et AO7, respectivement. La dégradation séquentielle des polluants et de leurs intermédiaires a produit des ions inorganiques tels que l'ammonium, le nitrate et le sulfate qui pourraient être quantifiés à la fin de l'électrolyse. Enfin, deux chemins complets de la dégradation AO7 et ACE par le processus Electro-Fenton pourraient être construits et présentés.

(ii) Le feutre de carbone commercial (1cm x 2cm) a été modifié par réduction de l'oxyde de graphène (rGO), en appliquant trois méthodes différentes de réduction: réduction à potentiel constant (électrode CPR-CF), réduction chimique (électrode CR-CF) et Réduction thermique (électrode TR-CF). Le CPR-CF a été choisi comme le meilleur moyen pour la modification en raison de sa simplicité, son faible coût et sa grande efficacité. Les paramètres affectant la conversion de GO en rGO, tels que le pH, le potentiel appliqué et la durée du processus de réduction, ont été étudiés. Cette nouvelle cathode a amélioré de manière significative les propriétés électrochimiques identifiées par voltamétrie cyclique et analyses d'impédance : un courant rédox 10 fois plus élevé a été obtenu sur ce matériau avec la sonde $[Fe(CN)_6]^{3-}$ /$[Fe(CN)_6]^{4-}$; une résistance au transfert de charge de 2,17 Ω inférieure à celle obtenue sur les FC brutes a été nregistrrée. L'électrode modifiée a été utilisée en cathode pour la dégradation d'AO7 par EF en milieu acide. L'élimination du TOC après 2 h de traitement a atteint 73,9% sur le CPR-CF soit une augmentation de 18,3% par rapport aux feutres commerciaux. Une minéralisation à 94% peut être obtenue pour une électrolyse de 8 h. Après 10 cycles d'utilisation (80 h), la stabilité de la cathode modifiée est bonne (perte de moins de 10% de performance) ce qui montre que cette rGO-CF est une électrode puissante et prometteuse pour améliorer l'efficacité du procédé EF. De plus, le point innovant de cette approche était d'identifier les sous-produits aux différents stades du traitement EF et plus particulièrement de lier la formation de sous-produits et la toxicité des effluents. Nous avons ainsi identifié les sous-produits les plus toxiques de la dégradation de l'AO7 et de l'ACE et avons montré la possibilité de contrôler la durée du traitement grâce à la surveillance de la toxicité des effluents.

(iii) Un système de type Fenton / pile à combustible pour une dépollution sans le recours à un générateur d'électrolyse a été initié avec succès. Ce système FC-Fenton est composé de

deux compartiments séparés par une membrane perfluorée Nafion® 117. L'anode de feutre de carbone modifiée par des particules d'or a été obtenue par électrodéposition de sels d'or sur un CF commercial (1 cm x 4 cm) suivi d'un traitement thermique à 1000 °C. Cette méthode a permis de couvrir la surface du feutre carbone par des nanoparticules d'or hexagonales réparties de manière homogène avec une taille moyenne de 300 nm. L'effet du chargement de l'or ainsi que le traitement thermique ont été étudiés. Par ailleurs une nouvelle cathode a été fabriquée en combinant dépôt en couche atomique (ALD) d'oxyde métallique (ZnO) sur CF, puis conversion solvothermale en ZIF-8 et enfin calcination sous atmosphère d'azote pour former des dépôts poreux à base de carbone (nommés CF@pC). L'ORR s'est produite sur la cathode CF@pC à un potentiel moins négatif (-0,21 V vs Ag/AgCl sur CF@pC au lieu de -0,7V sur le CF commercial). Ce point clé a permis de combiner anode à base de nanoparticules d'or et cathode en carboen microporeux dopés à l'azote pour réaliser le système FC-Fenton proposé. Ce système a montré une stabilité à long terme permettant de multiples cycles de dégradation sans diminuer l'activité catalytique dans le temps. En particulier, 90% de la concentration initiale du polluant AO7 a été éliminée lors de la dégradation EF prolongée pendant 10 h et la puissance de sortie de 170 mW m^{-2} est stable au moins pendant deux mois.

Les résultats présentés dans cette étude permettront très certainement de développer des systèmes propres, autonomes en énergie utilisant la technologie EAOP pour le traitement des eaux usées dans un avenir proche.

[1] Enric Brillas, Ignasi Sirés, and M. A. Oturan, "Electro-Fenton Process and Related Electrochemical Technologies Based on Fenton's Reaction Chemistry," Chem. Rev. , vol. 109 pp. 6570–6631, 2009.

[2] C. T. Wang, J. L. Hu, W. L. Chou, and Y. M. Kuo, "Removal of color from real dyeing wastewater by Electro-Fenton technology using a three-dimensional graphite cathode," Journal of hazardous materials, vol. 152, pp. 601-6, Apr 1 2008.

[3] C. Ponce de León and D. Pletcher, "Removal of formaldehyde from aqueous solutions via oxygen reduction using a reticulated vitreous carbon cathode cell," J. Appl. Electrochem., vol. 25, pp. 307-313, 1995

[4] Y. B. Xie and X. Z. Li, "Interactive oxidation of photoelectrocatalysis and electro-Fenton for azo dye degradation using TiO2–Ti mesh and reticulated vitreous carbon electrodes," Materials Chemistry and Physics, vol. 95, pp. 39-50, 2006.

[5] A. Özcan, Y. Şahin, A. Savaş Koparal, and M. A. Oturan, "Carbon sponge as a new cathode material for the electro-Fenton process: Comparison with carbon felt cathode and application to degradation of synthetic dye basic blue 3 in aqueous medium," Journal of Electroanalytical Chemistry, vol. 616, pp. 71-78, 2008.

[6] M. Panizza and M. A. Oturan, "Degradation of Alizarin Red by electro-Fenton process using a graphite-felt cathode," Electrochimica Acta, vol. 56, pp. 7084-7087, 2011.

[7] A. Wang, J. Qu, J. Ru, H. Liu, and J. Ge, "Mineralization of an azo dye Acid Red 14 by electro-Fenton's reagent using an activated carbon fiber cathode," Dyes and Pigments, vol. 65, pp. 227-233, 2005.

[8] H. Lei, H. Li, Z. Li, Z. Li, K. Chen, X. Zhang, and H. Wang, "Electro-Fenton degradation of cationic red X-GRL using an activated carbon fiber cathode," Process Safety and Environmental Protection, vol. 88, pp. 431-438, 2010.

[9] I. Sirés, N. Oturan, M. A. Oturan, R. M. Rodríguez, J. A. Garrido, and E. Brillas, "Electro-Fenton degradation of antimicrobials triclosan and triclocarban," Electrochimica Acta, vol. 52, pp. 5493-5503, 2007.

[10] Jean Jacques Aaron and M. A. Oturan, "New photochemical and electrochemical methods for the degradation of pesticides in aqueous media. Environmental applications.," Turk. J. Chem. , vol. 25, pp. 509–520, 2001.

[11] M. A. Oturan, "An ecologically effective water treatment technique using electrochemically generated hydroxyl radicals for in situ destruction of organic pollutants: Application to herbicide 2,4-D," Journal of Applied Electrochemistry vol. 30, pp. 475-482, 2000.

[12] Mehmet A Oturan, Jean-Jacques Aaron, Nihal Oturan, and J. Pinson, "Degradation of chlorophenoxyacid herbicides in aqueous media, using a novel electrochemical method," Pestic. Sci. , vol. 55, pp. 558–562, 1999.

[13] H. Lin, H. Zhang, X. Wang, L. Wang, and J. Wu, "Electro-Fenton removal of Orange II in a divided cell: Reaction mechanism, degradation pathway and toxicity evolution," Separation and Purification Technology, vol. 122, pp. 533-540, 2014.

[14] R. E. G. Smith, T. J. Davies, N. d. B. Baynes, and R. J. Nichols, "The electrochemical characterisation of graphite felts," Journal of Electroanalytical Chemistry, vol. 747, pp. 29-38, 2015.

[15] A. Di Blasi, O. Di Blasi, N. Briguglio, A. S. Aricò, D. Sebastián, M. J. Lázaro, G. Monforte, and V. Antonucci, "Investigation of several graphite-based electrodes for vanadium redox flow cell," Journal of Power Sources, vol. 227, pp. 15-23, 2013.

[16] Y. Wang and Y. Hasebe, "Carbon felt-based biocatalytic enzymatic flow-through detectors: chemical modification of tyrosinase onto amino-functionalized carbon felt using various coupling reagents," Talanta, vol. 79, pp. 1135-41, Sep 15 2009.

[17] L. Han, S. Tricard, J. Fang, J. Zhao, and W. Shen, "Prussian blue @ platinum nanoparticles/graphite felt nanocomposite electrodes: application as hydrogen peroxide sensor," Biosensors & bioelectronics, vol. 43, pp. 120-4, May 15 2013.

[18] K. J. Kim, Y.-J. Kim, J.-H. Kim, and M.-S. Park, "The effects of surface modification on carbon felt electrodes for use in vanadium redox flow batteries," Materials Chemistry and Physics, vol. 131, pp. 547-553, 2011.

[19] Z. González, A. Sánchez, C. Blanco, M. Granda, R. Menéndez, and R. Santamaría, "Enhanced performance of a Bi-modified graphite felt as the positive electrode of a vanadium redox flow battery," Electrochemistry Communications, vol. 13, pp. 1379-1382, 2011.

[20] S. Hammami, N. Bellakhal, N. Oturan, M. A. Oturan, and M. Dachraoui, "Degradation of Acid Orange 7 by electrochemically generated (*)OH radicals in acidic aqueous medium using a boron-doped diamond or platinum anode: a mechanistic study," Chemosphere, vol. 73, pp. 678-84, Oct 2008.

[21] E. Brillas and C. A. Martinez-Huitle, "Decontamination of wastewaters containing synthetic organic dyes by electrochemical methods. An updated review. ," Applied Catalysis B-Environmental vol. 166, pp. 603-643, 2015.

[22] M. A. Oturan and J. J. Aaron, "Advanced oxidation processes in water/wastewater treatment: Principles and applications. A review," Critical Reviews in Environmental Science and Technology, vol. 44, pp. 2577-2641, 2014.

[23] P. Bansal, D. Singh, and D. Sud, "Photocatalytic degradation of azo dye in aqueous TiO2 suspension: Reaction pathway and identification of intermediates products by LC/MS," Separation and Purification Technology, vol. 72, pp. 357-365, 2010.

[24] T. Velegraki, I. Poulios, M. Charalabaki, N. Kalogerakis, P. Samaras, and D. Mantzavinos, "Photocatalytic and sonolytic oxidation of acid orange 7 in aqueous solution," Applied Catalysis B: Environmental, vol. 62, pp. 159-168, 2006.

[25] H.-Z. Zhao, Y. Sun, L.-N. Xu, and J.-R. Ni, "Removal of Acid Orange 7 in simulated wastewater using a three-dimensional electrode reactor: Removal mechanisms and dye degradation pathway," Chemosphere, vol. 78, pp. 46-51, 2010.

[26] Y. Kumagai, Y. Shinkai, T. Miura, and A. K. Cho, "The chemical biology of naphthoquinones and its environmental implications," Annual review of pharmacology and toxicology, vol. 52, pp. 221-47, 2012.

[27] A. Das, S. Chakrabarty, D. Choudhury, and G. Chakrabarti, "1,4-Benzoquinone (PBQ) induced toxicity in lung epithelial cells is mediated by the disruption of the microtubule network and activation of caspase-3," Chemical research in toxicology, vol. 23, pp. 1054-66, Jun 21 2010.

[28] A. Dirany, I. Sires, N. Oturan, A. Ozcan, and M. A. Oturan, "Electrochemical treatment of the antibiotic sulfachloropyridazine: kinetics, reaction pathways, and toxicity evolution," Environmental science & technology, vol. 46, pp. 4074-82, Apr 3 2012.

[29] J.Devillers, P.Boule, P.Vasseur, P.Prevot, R.Steiman, F.Seigle-Murandi, J.L.Benoit-Guyod, M.Nendza, C.Grioni, D.Dive, and P.Chambon, "Environmental and health risks of Hydroquinone," Ecotoxicology and Environmental Safety, vol. 19, pp. 327-354, 1990.

[30] J. A. Zazo, J. A. Casas, C. B. Molina, A. Quintanilla, and J. J. Rodriguez, "Evolution of Ecotoxicity upon Fenton's Oxidation of Phenol in Water," Environmental science & technology, vol. 41, pp. 7164-7170, 2007.

[31] M. Diagne, N. Oturan, and M. A. Oturan, "Removal of methyl parathion from water by electrochemically generated Fenton's reagent," Chemosphere, vol. 66, pp. 841-8, Jan 2007.

[32] A. Ozcan, M. A. Oturan, N. Oturan, and Y. Sahin, "Removal of Acid Orange 7 from water by electrochemically generated Fenton's reagent," Journal of hazardous materials, vol. 163, pp. 1213-20, Apr 30 2009.

[33] K. W. Jung, D. S. Park, M. J. Hwang, and K. H. Ahn, "Decolorization of Acid Orange 7 by an electric field-assisted modified orifice plate hydrodynamic cavitation system: Optimization of operational parameters," Ultrasonics sonochemistry, vol. 26, pp. 22-9, Sep 2015.